SAPIENZA
UNIVERSITÀ DI ROMA

Safety Analyses with uncertainty quantification for fusion and fission nuclear power plants. Applications to EU DEMO fusion reactor and BWRs.

Facoltà di Ingegneria Civile e Industriale
Dottorato di Ricerca in Energia e Ambiente - Scuola di Dottorato in Scienze e Tecnologie per l'Innovazione Industriale – XXXII Ciclo

Candidate

Matteo D'Onorio

ID Number: 1420584

Thesis Advisor

Prof. Gianfranco Caruso

February 2020

To Obertino

Abstract

The EUropean DEMOnstrating fusion power reactor (DEMO) Water Cooled Lithium Lead (WCLL) breeding blanket concept is currently in its pre-conceptual design phase by the EUROfusion consortium members. It aims to be the first tokamak fusion reactor to demonstrate the capability for net electricity production, tritium-self-sufficiency, and a lifetime plasma operation of several full-power years. The WCLL breeding blanket is one of the two concepts being studied for implementation in the EU DEMO reactor. This concept relies on the separate-cooled architecture, where the liquid metal is utilized exclusively as tritium breeder and neutron multiplier, whereas the role of coolant is fulfilled by pressurized water.

Following the previous experience of the experimental International Thermonuclear Experimental Reactor (ITER), the design project of the DEMO reactor is constantly supported by safety studies for all the different breeding blanket concepts under investigation, so that best performance within safety requirements are achieved. The basic goal of safety is to ensure that a nuclear reactor will not contribute significantly to individual and societal health risks. These risks stem mainly from the radioactive inventory inside the reactor, so this basic goal translates into the prevention of radioactive material releases toward the environment. A secondary, but fundamental, objective is to prevent damage of fusion power plant main components. To deal with safety requirements within the DEMO project, a widely use of passive safety systems (a smart mix with active safety systems) will be made together with established safety principles, such as defense in depth and maintaining doses as low as reasonably achievable (ALARA).

The research activity described in this Ph.D. dissertation has the main objective to characterize and quantify the safety and environmental aspects of the EU DEMO WCLL concept design, studying the reactor response to some of the most severe possible accident scenarios. Safety analyses are performed with the fusion adapted versions of MELCOR code, to investigate the thermal hydraulic behavior of DEMO main components and radioactive source term mobilization. Moreover, the performed safety analyses, supported by sensitivity studies, could be useful to provide insight into physics and technology issues that need addressing to develop fusion as an optimal electricity generation alternative in the near future.

In this early development phase of the DEMO design, in the frame of the EUROfusion safety working project (WPSAE), a list of initiating events, which could start an accident sequence, has been identified through a Functional Failure Mode and Effect Analysis (FFMEA). Many accident sequences enveloping from these initiating events have been investigated comprehensively.

The dissertation is divided in three main parts. The first part concerns a general description of the principal safety issues associated with fusion reactors and provides an overview description of main EU DEMO components from a safety perspective. The second part contains preliminary safety studies relating to design basis accidents, beyond design basis situations and hydrogen mitigation systems. The progression of design basis accidents has

been simulated following a conservative approach taking into consideration the passive and active accident mitigation capabilities of the plant. Four different loss of coolant accident (LOCA) scenarios have been studied: in-vessel LOCA; ex-vessel LOCA; single in-vessel LOCA; and an in-box LOCA.

Concerning the multiple in-vessel LOCA, parametric analyses have been performed to determine the minimum flow area required by the suppression system pipework to limit the vacuum vessel (VV) pressure below the limit of 2 bar imposed as requirement by safety. Moreover, because limiters could be introduced in future design of the EU DEMO reactor to prevent the plasma to touch the breeding blankets plasma facing components (PFC), the same parametric study has been performed to evaluate their accident mitigation effects. In this framework, a new vacuum vessel suppression system (VVPSS) concept has been proposed following the ITER experience. It is based on six separated suppression tanks located in the containment basement, one of them is dedicated to retaining small leakages. The pipework consists mainly of six bleed lines connecting the VV to the small leakage tank, and five rupture disks line one for each suppression tank. To avoid steam and radioactive flows inside neutral beam ports, pipework connecting the vacuum vessel to the suppression system has been attached to the upper port. This last choice caused the necessity of a detailed nodalization of in-vessel volumes to model correctly steam flow path from VV to VVPSS and relative convective heat transfer effects between the modules' back supporting structure (BSS) and the steam flowing at high velocity in the interspace volume between the BSS and the VV.

Relatively to a simple in-vessel event involving the rupture of 10 first wall cooling pipes, two different simulations have been performed to evaluate downstream isolation valves' effects in terms of radioactive releases and thermal hydraulic behavior of main DEMO components. In fact, the large number of downstream valves (isolation and Safety Relief Valves (SRV) to be installed, could give rise to safety and reliability constraints.

Concerning ex-vessel LOCA events, a very unlikely double-ended pipe rupture is postulated in a coolant distributor ring of the EU DEMO reactor. The fusion power termination system is assumed to terminate the plasma burn with a mitigated disruption. Two different simulations have been performed related to failure in FW-PHTS and BZ-PHTS, respectively. However, due to its similarity, only the results of the former are described. The objective of these analyses is to show that the accident consequences are within the safety requirements for tokamak building structures which must withstand large internal pressures as well as avoiding significant leak rate into the environment. Because the tokamak building layout of the EU DEMO is currently in a preliminary design phase, parametric studies have been performed to support design activities. A preliminary, but quite detailed, model of the TCR was made to take into account steam condensation phenomena on TCR walls, being the only available effect for mitigating the overpressure in the TCR. In fact, no active systems for containment cooling are currently foreseen for DEMO.

To complete the wide range of DBA performed for the EU DEMO WCLL concept, a preliminary analysis of an in-box LOCA has been carried out. This kind of accident has not

been yet deeply investigated for fusion reactors because of the lack of multi-phase safety-related system codes able to deal with water and liquid metals. To overcome this code limitation, a Python script has been developed for an external coupling of two MELCOR input decks working with different fluids. At each user-imposed time step the information of one MELCOR run are extracted and used as feedback for the other input deck.

In the framework of BDBA an ex-vessel LOCA and a Loss of Flow Accident (LOFA) have been studied with the objective to show the robustness of the defense in depth approach and demonstrating that no cliff edge effects occur in the safety analysis. In both the simulations the failure of active plasma shutdown system has been assumed as aggravating event. Differently from DBA these accident analyses should be performed using best estimate assumptions and not conservative ones. At this purpose, the failure temperature of FW structure is increased from 1273 K to 1598 K. However, this parameter results very correlated, in particular for the ex-vessel LOCA simulation, with the amount of tritiated water and other radioactive aerosols that could be released toward the external environment. Instead, preliminary safety analyses for the LOFA beyond event, highlighted that the major safety concern is not related to radiological releases, but to the huge pressurization of in-vessel components, for such a reason this accident has been simulated using a lower pressure setpoint for safety relief valves. Three different simulations have been performed, by changing the number of FW channels affected by the rupture.

In-box LOCAs, as well as other accidents involving a chemical reaction between hot steam and lead lithium, could led to the production of large amounts of hydrogen inside the tokamak vacuum chamber. In order to avoid that flammable concentrations could be achieved, the production of hydrogen must be limited and properly monitored. In particular, the simultaneous presence of hydrogen and dust in the VV volume enhances the risk of explosion. After a short description of possible technical solutions suitable for EU DEMO to mitigate hydrogen concentration, preliminary accident study involving the use of passive autocatalytic recombiners (PARs) are reported. The MELCOR ESF package has been activated to simulate the presence of PARs directly installed in the atmosphere of the VVPSS suppression tanks.

Successively, in the third part, sensitivity and uncertainty analyses are reported. Because severe accidents in both fission and fusion power plants involve a wide range of uncertain phenomena and parameters, sensitivity and uncertainty analysis have to be performed to evaluate the influence of input parameters on selected figures-of-merit (FoMs). At this purpose a Python interface has been developed to allow the interaction between RAVEN and MELCOR. The Python interface allows to perturb all the parameters accessible through the MELCOR input deck. In such a way RAVEN is capable to investigate the system response as well as the input space using sampling schemes. Two sensitivity and uncertainty analyses have been performed, with applications to EU DEMO reactor and to the unit 3 of the Fukushima Daiichi power plant.

Table of Contents

List of Tables

List of Figures

Acronyms and nomenclature

ACP	*Activation Corrosion Product*
ADS	*Automatic Depressurization System*
AL	*Axial Level*
ALARA	*As Low As Reasonably Achievable*
ASD	*Accident Selection and Description*
BB	*Breeding Blanket*
BDBA	*Beyond Design Basis Accident*
BL	*Bleed Line*
BMs	*Blanket Modules*
BSS	*Back Supporting Structure*
BWR	*Boiling Water Reactor*
BZ	*Breeding Zone*
CB	*Cassette Body*
CF	*Control Function*
CSS	*Containment Spray System*
CST	*Cooling Storage Tank*
CV	*Control Volume*
CVH	*Control Volume Hydrodynamics*
D	*Deuterium*
DBA	*Design Basis Accident*
DCLL	*Dual Coolant Lithium Lead*
DDD	*Design Description Document*
DDFPs	*Diesel Driven Fire Pumps*
DEGB	*Double-Ended Guillotine Break*
DEMO	*Demonstrating fusion power reactor*
DHRS	*Decay Heat Removal System*
DW	*DryWell*
DWT	*Double-Wall tube*
EDF	*External Data File*
EDG	*Emergency Diesel Generator*
ESS	*Energy storage system*
EV	*Expansion Volume*
FMEA	*Failure Mode and Effect Analysis*
FFMEA	*Functional Failure Mode and Effect Analysis*
FL	*Flow Path*
FoMs	*Figure of Merits*
FSP	*Fusion Safety Program*
FU-3	*Fukushima Daiichi Unit 3*
FW	*First Wall*
GSSR	*Generic Site Safety Report*
HCLL	*Helium Cooled Lithium Lead*
HCPB	*Helium Cooled Pebble Bed*
He	*Helium*
HPCI	*High-Pressure Coolant Injection*
HS	*Heat Structure*
HX	*Heat Exchanger*
IB	*Inboard*
IHTS	*Intermediate Heat Storage System*
INL	*Idaho National Laboratory*

IWL	*Inner Wall Limiter*
ITER	*International Thermonuclear Experimental Reactor*
IVT	*Inner vertical Target*
LiPb	*lithium-lead*
LOCA	*Loss of Coolant Accident*
LOFA	*Loss of Flow Accident*
LPC	*Lower Pipe Chase*
MMS	*Multi Module Segment*
MP	*Molten Pool*
MSIV	*Main Steam Line Isolation Valve*
NWL	*Neutron Wall Load*
NPP	*Nuclear Power Plant*
OB	*Outboard*
OTSG	*Once Through Steam Generators*
OVT	*Outer Vertical Target*
PAR	*Passive Autocatalytic Recombiner*
PbLi	*Lithium-Lead*
PCS	*Power Conversion System*
PFC	*Plasma Facing Component*
PHTS	*Primary Heat Transfer System*
PIE	*Postulated Initiating Event*
PRZ	*Pressurizer*
PWR	*Pressurized Water Reactor*
RAVEN	*Reactor Analysis and Virtual control ENVironment*
RISMC	*Risk Informed Safety Margin Characterization*
RD	*Rupture Disc*
ROM	*Reduced Order Model*
RN	*RadioNuclide*
SADL	*Safety Analysis Data List*
SAE	*Safety and Environment*
SBO	*Station Black Out*
SC	*Suppression Chamber*
SDL	*Safety Data List*
SEAFP	*Safety and Environmental Assessment of Fusion Power*
SG	*Steam Generator*
SMS	*Single Module Segment*
SNL	*Sandia National Laboratories*
SRV	*Safety relief valves*
ST	*Suppression Tank*
TCR	*Tokamak Cooling Room*
TCWS	*Tokamak Cooling Water System*
TEPCO	*Tokyo Electronic Power Company*
TF	*Tabular Function*
UPC	*Upper Pipe Chase*
U.S.NRC	*United States Nuclear Regulatory Commission*
TF	*Toroidal Field*
VDE	*Vertical Displacement Event*
VS	*Vertical Shaft*
VV	*Vacuum Vessel*
VVDHRS	*Vacuum Vessel Decay Heat Removal System*
VVPSS	*Vacuum Vessel Pressure Suppression System*
W	*Tungsten*
WCLL	*Water Cooled Lithium Lead*
WF	*Working fluid*
WP	*Working Package*

WPBB	*WP Breeding Blanket*
WPSAE	*WP Safety and Environment project*
WW	*WetWell*

1 Introduction

The progress of human civilization is strictly related to man's ability to exploit natural resources and to produce energy. In order to survive and develop mankind needs powerful and reliable sources of energy, for this reason, his future is inextricable from nuclear energy which may play an important role in achieving sustainable growth, reducing carbon dioxide emissions and thus relieving a global warming warning. Nowadays, scientific and technical efforts to develop alternative energy sources are attracting increasing attention. In this scenario nuclear fusion power represents an important option for the world's energy supply. Research and technological development are key ingredients to demonstrate that the production of power in fusion plants is possible. However, because of the quantities of radioactive the utilization of nuclear energy, either from fission or from fusion reactors, gives rise to special safety requirements which are not encountered in other areas of energy utilization. Nuclear fusion has several advantages over nuclear fission, if the technology will be successfully developed. In fact, reduced radioactivity due to the lack of production of fission products and long-lived high-level radioactive waste, no hazard caused by the super criticality, the availability and the easy transport of the fuel are some advantages of the fusion reactor [1]. However, efforts still need to be done to engineer a system that can sustain the plasma for a period of time sufficient to reach very high temperature and density and use materials that withstand to this particular environment [2].

The short-term goal of the ongoing fusion R&D is to create and control a burning plasma, which is a key requirement to net fusion power generation. The ITER project aims to build a research tokamak facility capable of generating the world's first sustained (300 seconds, self-heating) burning plasma.

Parallel to the ITER exploitation in the 2030s [3], the construction of the DEMO plant, a research reactor similar to a power reactor, needs to be prepared.

DEMO must demonstrate the possibility of generating electricity through nuclear fusion reactions, although not at the price and the quantities of commercial power plant. Moreover, it must show the necessary technologies not only for controlling a more powerful plasma but for safely generating electricity consistently and for rapid, regular and reliable maintenance of the plant [4]. The characteristics of the DEMO plasma must be different respect to the characteristic of the ITER plasma, to maintain the stability of the reaction for a longer time. DEMO project with the purpose of demonstrating the possibility to produce electric energy. DEMO's goal is to produce 25 times as much power compared to ITER [5].

These three year of research activities, mainly focused on evaluating the consequences, in terms of thermal hydraulic and radiological impact of the EU DEMO reactor, with a specific focus on the WCLL Breeding Blanket (BB) concept. Studies have been undertaken within EUROfusion Safety and Environment (SAE) working package to evaluate the maximum potential impact on the plant, workers and environment of accident sequences. Such analyses have been performed by following a deterministic approach, so conservative assumptions have been used to study the worst enveloping scenarios of each initiating event. Both design basis accident (DBA) and beyond design basis accident (BDBA) analyses have been investigated.

In parallel to these activities, safety studies have been performed with the MELCOR code to analyse severe accident progression in fission power plant. An external code interface has been developed to couple MELCOR with the open source RAVEN code (https://github.com/idaholab/raven). The code interface will allow MELCOR users to perform sensitivity and uncertainty quantification analyses and simulate the system evolution with a probabilistic approach by means of advanced statistics tool.

1.1 Document outline

This manuscript is structured in ten sections. The first section includes the framework of the Ph.D. research, while §10 presents conclusions and future perspectives.

An overview of the thermonuclear fusion technology is described in § 2, together with a short overview of the operating principles of tokamak reactors.

In § 3 an overview of the safety approach used in the nuclear fusion field is foreseen.

Then § 4 provides a description of the main components and systems of the EU DEMO reactor from a safety perspective, specifically addressed to the WCLL BB DEMO concept.

A detailed description of the EU MELCOR model developed to perform safety analyses is reported in § 5.

Preliminary safety analyses of DBA and BDBA performed for the EU DEMO WCLL blanket concept are reported in § 6 and § 7, respectively.

In § 8 results of some preliminary accident analyses to supply the development of hydrogen mitigation systems suitable for the EU DEMO reactor are reported.

Finally, § 9 presents the results of sensitivity analyses performed by using the external code interfaced developed for the coupling between MELCOR and RAVEN. Analyses have been performed for both fission and fusion reactors, using the version 2.1 and 1.86 of the MELCOR code, respectively.

2 Thermonuclear fusion reactor technology

Current nuclear power reactors produce energy by splitting heavy nuclei, mainly uranium, into lighter nuclei trough a chain process called nuclear fission. The opposite process, that allows two nuclei to collide and fuse together into a heavier nucleus is the nuclear fusion reaction. In both these nuclear processes, the missing mass is transformed into energy, in accordance with the famous mass-energy equivalence law formulated by Einstein in 1905.

To give rise to a fusion reaction the two nuclei must collide with enough energy to overcome repulsive Coulombian force acting between nuclei and approach each other sufficiently close that the short-range attractive nuclear force becomes dominant. The fusion reaction, in fact, has an activation energy, but it was shown that the Coulomb barrier could be overcome with much lower kinetic energies than the one corresponding to the Coulomb peak: the so-called tunnel effect allows the reaction at lower energies. The attractive nuclear forces, that are responsible for the fusion reaction, become predominant when the distance between nuclei is less than 10^{-13}cm (i.e. about the nucleus radius). In order to give enough energy to the nucleus to approach and fuse overcoming repulsive forces the kinetic energy of the nuclei is increased by heating to temperatures around 100 million degrees [6].

At much lower temperatures (about 10000 K), the electrons are stripped from the nuclei and create an ionized gas where positively and negatively charged particles move independently called plasma. Plasmas are also known as the fourth state of matter, together with solids, liquids, and gases.

There are many nuclear fusion reactions, however, the reaction chosen to be used for the fusion reactor is one based on the fusion of two heavy hydrogen isotopes, deuterium-tritium one:

$$D + T = {}^{4}He + n + 17.586\ MeV$$

which produces 17.6 MeV of energy which is the kinetic energy of neutron (14 MeV) and the alpha particle (3.5 MeV).

To obtain high reaction parameters and so a higher fusion power density with this reaction nuclei must be heated up to $5 \cdot 10^{-7}$ K.

The difficulty in producing fusion energy is the development of a device that can heat the fuel to a sufficiently high temperature and then confine it for a long enough time so that more energy is released through fusion reactions than is used for heating [2]. Various types of confinement have been evaluated [7], among which the two that have gathered the greatest interest are the inertial and the magnetic ones. The former consists of transferring large amounts of energy to the particles in such a way as to determine values of temperature and density giving a favorable fusion reaction rate. The latter, uses strong magnetic fields, produced by external sources, to confine the plasma.

The most promising of these approaches is magnetic confinement, which is the one used in tokamak machines.

2.1 Tokamak reactors

Since the discovery of fusion reaction in the ‘30s of the past century, the quest to realize a device able to sustain controlled fusion reactions has been one of the main goals pursued by the worldwide scientific community, for such a reason over 200 tokamaks have been developed around the world [8].

In a nuclear fusion facility using the tokamak magnetic confinement concept, fusion reactions take place inside a toroidal plasma.

A charged particle moving in a magnetic field follows a spiral path around the field line. By creating magnetic field lines in a closed toroidal shape, the particles could be confined, there is no "ends" from which to escape [9]. However, in practice, they tend to drift to the outer edge of the plasma and escape. A helical shaped magnetic field, spiraling around the surface of the toroidal plasma, reduces this loss of particles from the edges. Such a helical field can be generated by the combination of two separate magnetic fields: a toroidal magnetic field produced by toroidal field coils and a poloidal magnetic field produced by an electric current induced in the plasma. To induce this current a central solenoid is provided within the central hole of the Tokamak. Because there is a limit to the current swing in the central solenoid coil, this current induction is of limited duration. For steady-state operation of a Tokamak, the plasma current is not in itself enough to heat the plasma to reach the temperature conditions needed for the fusion of deuterium and tritium. For such a reason, it is necessary to provide additional plasma current by systems such as neutral beam injection or radiofrequency heating and current drive.

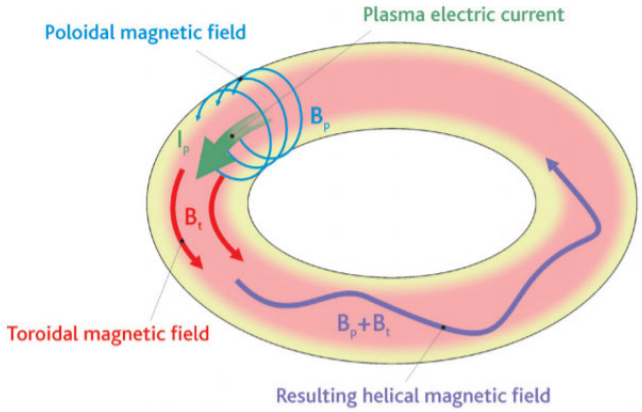

Figure 2.1.1 – Principle of magnetic confinement of a plasma in a tokamak [8]

As well as, the alpha produced in the D-T reaction remain in the plasma and transfer their energy to it; however, this energy is not sufficient to compensate thermal energy losses, for such a reason additional heating from external sources should be provided.

A schematic diagram showing the basic principles of a fusion power station, based on the "tokamak" magnetic configuration, is given in Figure 2.1.2. The hot plasma, where the D-T fusion reactions occur, is held thermally insulated from the material surroundings by magnetic fields. The energy carried away by the neutrons is absorbed in surrounding structures called breeding blanket. Blankets are filled with lithium compounds, which nuclei interact with the neutrons from the plasma to generate tritium, which is extracted from the blanket and injected, together with deuterium, into the plasma to sustain the fusion process. The energy is removed from the blanket, by a flow of coolant fluid to steam generators, and used to produce electricity in a conventional way. There are several basic concepts for the practical implementation of fusion power. Of these, the "tokamak" concept has been developed furthest and has produced 16 MW of fusion power in the European JET experiment [10][11]. The Safety and Environmental Assessment of Fusion Power (SEAFP) [12], power stations were based on the tokamak concept. In such a power station, the plasma is held by the magnetic fields in a torus-shaped vacuum chamber. Thus, the blanket surrounding the plasma is also toroidal. Between the blanket and the vacuum vessel is another toroidal structure, the shield. This serves to reduce the neutron flux to the vacuum vessel and the ex-vessel structures. The magnetic fields are created in part by electric currents in the plasma, and in part by currents in coils surrounding the vacuum vessel.

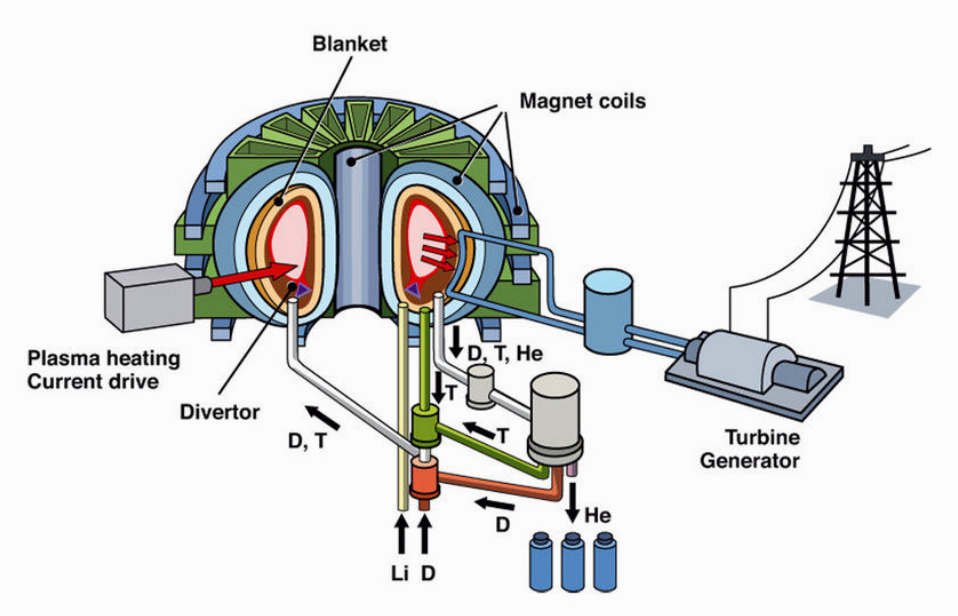

Figure 2.1.2 – Tokamak reactor

The main components of this type of reactor are [13]:

- Vacuum Vessel (VV): it represents the first confinement barrier, so its integrity must be maintained to avoid the dispersion of radionuclides outside the reactor. This vessel must withstand high temperatures and accident without losing its confinement;
- First Wall: it is the front part of the blanket segment, which must withstand the high flux of heat and high energy neutrons. Moreover, it must resist to radiation damage, creep, embrittlement and swelling during all the period of its operational life;
- Breeding blanket: it is located just behind the first wall and it is a very important part of the reactor because it has to: breed tritium fuel from 14 MeV neutron flux with sufficient efficiency in order to ensure tritium self-sufficiency; slow down fusion neutrons and to transform their kinetic energy into heat, so that it will be possible to extract and use it; shield the VV external vessel components and also superconducting coils from thermal and nuclear radiation; remove the heat generated in the tokamak plasma and the heat produced in the blanket to produce electricity;
- Thermal shielding: it attenuates gamma rays and neutrons in order to protect the magnet coils and other components. Its operational life covers the entire lifetime of the plant, so the shield must withstand to high temperature in order to guarantee the structural support for the first wall and the Blanket;
- Magnet coils: in order to confine plasma particles in the plasma chamber a system of magnets are present: toroidal field coils that provide the toroidal field, the central solenoid that induces a toroidal current in the plasma and the poloidal field coils that control the plasma shape and position;
- Cryostat: the vacuum vessel is contained in the cryostat, where very low temperatures are obtained to guarantee the thermal insulation of the superconductors;
- Divertor: is the region in the bottom of the reactor where plasma is neutralized and pumped away by the vacuum pumps. This component has multiple tasks such as reduce the heat flux on

the first wall, remove Helium ash from the outer layers of the plasma and provide a barrier to keep sputtered impurities out of the plasma.

3 Safety in fusion reactors

Safety studies related to fusion reactor have been started since the ’90s [8] together with the beginning of fusion reactor design studies. As in fission power, safety by design approach is fundamental to operate fusion power minimizing the potential health cost of fusion technology. However, a wide range of parameters such as the plasma power, masses of radioactive material, combination of different materials can affect safety characteristic of fusion devices [14]. Thus, as tokamaks develop, safety design must develop, but it is important to be aware of the safety implications of the various designs as they are developed so that safety aspects can be optimized.

Tokamak safety requirements are to protect the public and the workers against the environmental release of radioactivity and release of radiation from the facility during normal operation. At the same time, safety systems shall be used to mitigate the impact of accident scenarios which could lead to releases of radioactive materials from the facility [15]. The radioactivity source terms expected to be involved in a typical tokamak fusion reactor are [16]:

- Tritium within the vacuum vessel and the one permeated in the primary coolant system;
- The activity in structural materials including the first wall, blanket, structural material, limiter walls, shieldings, etc.;
- Radioactive tungsten dust originated from the erosion of plasma-facing structures;
- Gaseous activation products resulting from direct activation from nuclear reaction with neutrons of the gases in the building atmosphere (O^{16}, N^{17});
- Activated corrosion products circulating in the primary coolant system.

Because of this large inventory radioactive materials, a rigorous safety approach is needed to ensure that the safety and environmental advantages of fusion are fully realized. In pursuing the above safety requirement, use is made of well-established safety principles [17], in particular:

- ALARA: radiation exposure of personnel and releases of radioactive material toward the environment should be maintained as low as reasonably achievable (ALARA), during both normal operation and maintenance activities;
- Defence in depth: the approach is based on posing several successive barriers to prevent the release of radioactive material to the environment [18]. This principle is applied to the safety design of DEMO and tokamak in generals to prevent or reduce the occurrence of accident situations resulting from system and equipment failures, human errors and internal or external hazards.
- Passive safety: safety functions are to be provided passively, thus without any electrical power supply. Moreover, if cooling is required, a passive cooling system based for example on natural convection or other passive methods is always preferred as the ultimate heat removal method.

The defence in depth approach of confinement of the radioactive materials is based on fission reactors. In tokamak design double or triple confinement is implemented for in-vessel radioactive inventories, depending on the role of the cryostat. For example, in the preliminary design of DEMO concepts the PHTS cooling loops, which are a part of the first confinement barrier, are directly routed to heat exchangers outside the cryostat and inside the tokamak building. Thus, the first barrier will be the VV, its extensions and cooling loops for the in-vessel components; the second, and final barriers will be the reactor building, cleanup systems, and stack. While, in some fusion reactors safety design, such as ITER, the cryostat plays the role of second barrier.

Confinement structures must address two types of issues, radioactive mass transport hazards and energy-related or pressure/vacuum hazards.

3.1 Internal energies that can mobilize source terms

Tokamaks are very complex machines housing several potential high energy sources, which could cause accidents or have an impact during the accident sequence. These so called energy-related hazards come from the energy contained in different systems of the tokamak and that can lead to the failure of both first and second confinement barriers and mobilize radioactive materials in several forms during loss of coolant or loss of vacuum events. These energy sources include [8]:

- plasma stored thermal and magnetic energy;
- electromagnetic energies in superconducting magnets;
- structure decay heat from activation products;
- coolants internal energy;
- chemical energies and hydrogen production and possible combustion.

In the table below some of these energies are reported with reference to the EU DEMO [20] reactor and ITER [8].

Table 3.1-1 – Energy sources in EU DEMO and ITER

Parameter	Unit	DEMO	ITER
Plasma thermal energy	GJ	1.3	0.7
Plasma magnetic energy	GJ	0.9	
Magnets system magnetic energy	GJ	120	50
Enthalpy in the first wall/blanket cooling channel	GJ	1300	--
Enthalpy in the divertor cooling channel	GJ	230	--
Decay heat just after shut-down	MW	38	11
Decay heat one day after the shut-down	MW	8.3	0.6
Decay heat one month after the shut-down	MW	2.2	0.16
Chemical potential energy with tungsten (W-steam reaction)	GJ	200	
Chemical potential energy with tungsten (Be-steam reaction)	GJ	31000	

One of the main issues related to the plasma energy is the fact that up to now plasma is subject to multiple types of instability. Small-scale instabilities consist of mixing the hot ions and electrons from the center of the plasma with the colder ones nearer to the edges but does not destabilize the plasma enough to make it lose its magnetic confinement [7]. However, large-scale instabilities affect the plasma. These include oscillation, wave propagations and vertical displacements up or down. If the plasma touches the first wall of the blanket or the first wall of the divertor, it completely loses its magnetic confinement in a few milliseconds. This fast plasma termination is called disruption, system to mitigate this are being studied (for example by a large injection of gas or the use of limiters). Under the current operating conditions of a tokamak, disruptions are frequent, which is one of the reasons why operating sequences with plasma remain very short. Given the large amount of energy stored in the plasma, when a disruption occurs it causes physical phenomena such as thermal shocks in the first wall of the blanket, production of dust from erosion of the first wall of the blanket and the appearance of electromagnetic loads. In some cases, such a disruption can create an electron beam could potentially cause damage to the first wall and thereby initiate an in-vessel LOCA.

Concerning the magnetic energy of the field coils. In the event of loss of coil superconductivity (for example due to a leak of helium coolant), the drop in electric current in the coils could lead to the appearance of eddy currents and electromagnetic loads, which are taken into account in the design-basis used for the VV internal components and the vessel structure itself. Furthermore, a short circuit in a coil could cause local deformation of this coil. Finally, an electric arc could occur, causing local melting of the material structures of the coil and nearby equipment such as the VV or the cryostat. The integrity of the VV is not affected, unlike that of the cryostat.

In the WCLL concept of the EU DEMO reactor the BB coolant conditions are like those of PWRs [21], for the purpose of electricity generation. This suggests that a crucial issue is development of safety systems and confinement barrier strategies against the break of heat primary systems. Any water leak from a cooling system into the VV structures or into the tokamak building will cause vaporization and rising pressure phenomena. These amounts of water and steam flowing toward the tokamak environments cause the mobilization of radioactive materials. Typical solutions to optimize safety and provide mitigative capabilities are segmentation of inventories, and redundancy. In order to limit the inventory of primary coolant discharged in the event of an accident safety equipment (i.e. isolation valves) must be considered. However, these may have a significant impact on pressure drop on both WCLL and HCPB EU DEMO concept.

As reported in Table 3.1-1 for a high power DEMO reactor with high availability using the same materials, the residual heat to be removed could be one or two orders of magnitude greater than for the ITER facility. This is due to due to the longer operating times with plasma and to the greater fusion power of DEMO reactors. However, use of lower activation materials (martensitic steel, vanadium alloy, silicon carbide, composites etc.), which is planned for all DEMO reactor projects to limit risks of exposure to ionizing radiation, should also reduce the residual heat to be removed. In the ITER safety study [16] and the PPCS design [22], it was shown that under the extreme situation where all the coolants of the in-vessel components and vacuum vessel are completely and instantaneously lost, the temperature rise in the tokamak structures would be slow, especially since in this situation air would be introduced into the cryostat to further slow this rise in temperature. It would take about four months for the temperature of the divertor to become hot enough to cause failure of its cooling system and consequent water ingress into the vacuum vessel [8]. This intimates that the heat transfer characteristics of the DEMO are different from those of ITER and other reactor designs.

In tokamak devices, chemical energy will be potentially released by the beryllium and tungsten-steam reaction or lithium-steam reaction [23]. The formers can occur during an in-vessel loss of coolant accident; the latter is typical of a WCLL blanket concept and could occur because of an in-box LOCA, or during an in-vessel LOCA with an in-depth break of the FW. Of these reactions, the latter one could be more hazardous to the DEMO design because this reaction yields a bigger quantity of hydrogen, which causes an explosion hazard than the W-steam reaction. Lithium is very chemically reactive with water, air, and to some extent concrete. These reactions are exothermic and can result in lithium fires, hydrogen production and potential explosion, aerosol generation, and structural over-heating. Table 3.1-1 indicates that the energy potentially released by the Be-steam chemical reaction is 1 to 4 orders of magnitude larger than the other internal energies of the DEMO. It should be mentioned that unlike the primary coolant and decay heat, this type of energy manifests only in the case where the coolant water is leaked inside a blanket module.

3.2 Radioactive mobilizable sources

The principal hazards associated with the tokamaks are internal and external radiation doses arising the operation of the facility, principally tritium and mobile activation products.

The radioactivity source terms expected to be involved in a typical tokamak fusion reactor are:

- Tritium within the vacuum vessel and the one permeated in the primary coolant system;
- The activity in structural materials including the first wall, blanket, structural material, limiter walls, shielding etc.;
- Radioactive tungsten dust originated from the erosion of plasma facing structures;
- Gaseous activation products resulting from direct activation from nuclear reaction with neutrons of the gases in the building atmosphere (O^{16}, N^{17});
- Activated corrosion products circulating in the primary coolant system.

3.2.1 Tritium

Tritium is inherent in fusion reactors using the deuterium-tritium fusion reaction. DEMO will burn around 0.334 kg of tritium per full-power-day to generate a plasma power of 2037 MW. The minimization of tritium releases in accordance to the ALARA principle is one of the key safety issues for fusion reactors. In fact, for both safety and economic reasons, as much tritium as possible must be recovered inside the plant for reuse within the tritium fuel cycle.

Tritium decays via a beta emission with a peak energy of 18.6 keV and average energy of 5.7 keV to produce stable ^{3}He. Its half-life is 12.3 years. The specific activity of ^{3}H is approximately $3.6 \cdot 10^{14}$ Bq/g.

The most dangerous compound that tritium can form is the tritiated water (HTO), because of its high solubility into human body fluids. In case of intake, one microgram of HTO is enough to cause an internal exposure sufficient for a dose equivalent commitment equal to the annual limit defined by law [25].

Main sources of tritium in tokamak reactors results from [25]:

- Tritium produced by neutron reaction with nuclei of Lithium constituting breeding blanket;
- Fuel within the plasma chamber that has not undergone a fusion reaction can permeate materials surrounding the plasma and become implanted or form co-deposited layers;
- Tritium in the fuel cycle systems including the circulating tritium, tritium in storage, tritium in the isotope separation system and recovery systems. Tritium will also be present in the hot cell and waste treatment systems.

As an isotope of hydrogen, tritium is the most mobile of the significant radioactive source that will be present in tokamaks and requires special handling and confinement procedures to prevent its escape. Mobilization of tritium is either through diffusion or non-diffusive burst release. A concentration gradient of tritium within plasma facing components can cause tritium to diffuse into the bulk and eventually to the outer wall surfaces where it can enter the coolant.

Detritiation systems would be required to keep tritium concentrations and environmental releases within safe limits.

3.2.2 Dust and activated products

The fusion reactions produce high-energy neutrons (14 MeV) that leave the plasma, as they have no charge, and activate the surrounding materials. A large part of the activation products is bound in solid metal structures of the in-vessel components and thus they are not considered as mobile source terms. However, some activated products may become mobilized through mechanical (dust and plasma vaporization) or chemical (corrosion products) mechanisms. The amount of material that can become mobile is described by the mobilization fraction [20]. Activated products can be found also in gaseous forms, such as activated air from between the cryostat and bioshield and activated divertor exhaust gases.

In tokamak, reactor dust can be produced both in steady state normal operation and during transient events. The main process that led to dust production is the interaction between the energetic plasma and surrounding surfaces [26]. During normal operation, the formation of dust is associated with erosion through physical and chemical sputtering of plasma facing materials. The plasma interaction temperatures are in the range of 780-3500 K causing erosion phenomena. During off-normal events, such as plasma disruptions and vertical displacement events, enormous amounts of plasma energy can be deposited on a surface, generating particulates [27]. This rapid intense heating of material results in vaporization and melting. Dust particles may be created by in-flight condensation of the vaporized material, pressure-driven ejection of melt layer material, and explosive brittle destruction by heating of gas pockets near the material's surface.

The main hazard related to the dust its mobility. Dust can be mobilized and resuspended during in accident scenarios, such as LOCA or LOVA, but also during maintenance operation inside the plasma chamber [28]. Issues related to dust are; its chemical reaction with water and air that can produce several quantities of hydrogen; the degradation of heat transfer from a surface if layers of dust with poor thermal contact are deposited.

Corrosion phenomena in fusion reactors led to the production of activated corrosion products that can be transported into both the water coolant loop and the breeder loop especially if the breeder is liquid lithium lead [29]. The coolant can move the active nuclei toward the cooling system placed outside of the biological shield with potential for significant impact on the radiological dose received by personnel in the event of environment release (LOCA). Moreover, precipitation of activate corrosion products in the cold parts of systems (heat exchangers, cold legs, etc.) could lead to the creation of areas of high exposure to ionizing radiation.

4 Overview of EU DEMO plant and systems

The EU DEMOnstration Power Station (DEMO) will be the last research tokamak reactor before a commercial fusion power plant (Figure 4.1). It aims to demonstrate capability for net electricity production, tritium-self-sufficiency, and a lifetime plasma operation of several full-power years. For such reasons it also should achieve economic and environmental acceptability to become competitive with other energy sources. The EU DEMO reactor relies on the D-T thermonuclear fusion reaction to produce thermal energy. The reactor is currently designed to produce about 2 GW of plasma power, with a plant electricity output capability of 500 MW. The reference operational sequence is the pulsed operation, based on about eleven pulses per each day with a burn time of 2 hours (power pulse period; 100% of fusion power) and a dwell time of 10 minutes (1% of fusion power generated due to decay heat). The design has been built upon the experience of the licensing of the ITER experimental magnetic fusion reactor, taking on board a requirement for safety and environmental considerations to be taken into account from the very beginning of design activities right through to the end of life of the facility.

Currently, the EU DEMO is in the so called pre-conceptual design phase. Several outstanding technology and physics integration issues have still to be resolved before the development of a concrete DEMO plant project. To successfully develop and deploy an operational DEMO reactor in the 2050s-2060s, eight key issues must be addressed [5]:

- Demonstrate long-term and high power operation regimes of stable plasma;
- Demonstrate that is possible to extract the exhaust heat efficiently;
- Develop and extensively validate materials compatible with high plasma performance. In particular, structural materials must withstand large 14 MeV neutron fluence withstand without degrading their physical properties. Moreover, plasma Facing Materials must withdraw erosion and sputtering;
- Demonstrate plant tritium self-sufficiency;
- Demonstrate fusion intrinsic safety features in a power plant environment and develop passive safety system;
- Develop an integrated DEMO design with high reliability and availability;
- Demonstrate economic potential of fusion by reducing the DEMO capital costs and developing long-term technologies;
- Bring the stellarator concept to maturity

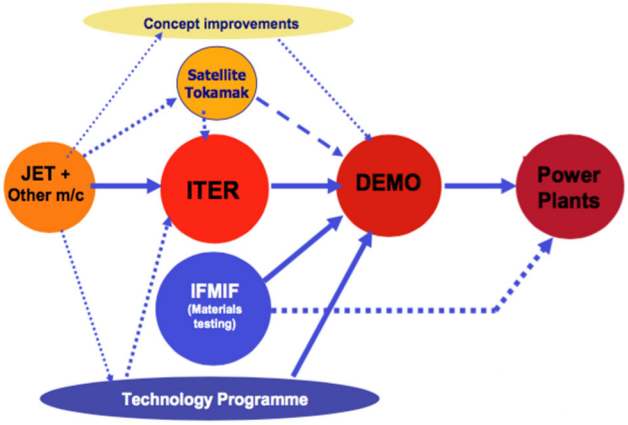

Figure 4.1 – DEMO roadmap [30]

Concerning the materials to be used in DEMO, reduced activation ferritic-martensitic steel (EUROFER) has been proposed as the structural material for the in-vessel components, because of its tolerance to high energy neutron irradiation. Tungsten is proposed as armour material for PFCs due to its refractory properties and low erosion rate.
In order to achieve the tritium self-sufficiency (differently from ITER in DEMO tritium is required only during plasma start-up), tritium breeding blanket with a minimum TBR of 1.05 have to be implemented in DEMO. Currently, in the framework of the R&D activities coordinated by the EUROfusion consortium, two different breeding blanket configurations are mainly investigated: the Water Cooled Lithium Lead (WCLL), based on liquid metal breeder technology and the Helium Cooled Pebble Bed (HCPB), based on solid breeder technology.

In the figure below the general layout of the integrated EU DEMO reactor is show. The tokamak is divided in 16 sectors (22.5°) in toroidal direction. A blanket sector comprises three segments in the outboard blanket (OB) and two segments in the inboard (IB). The segments are separated by a gap of 20 mm. Thus, there is a total of 48 segments in the outboard blanket and 32 on the inboard blanket along the toroidal direction.

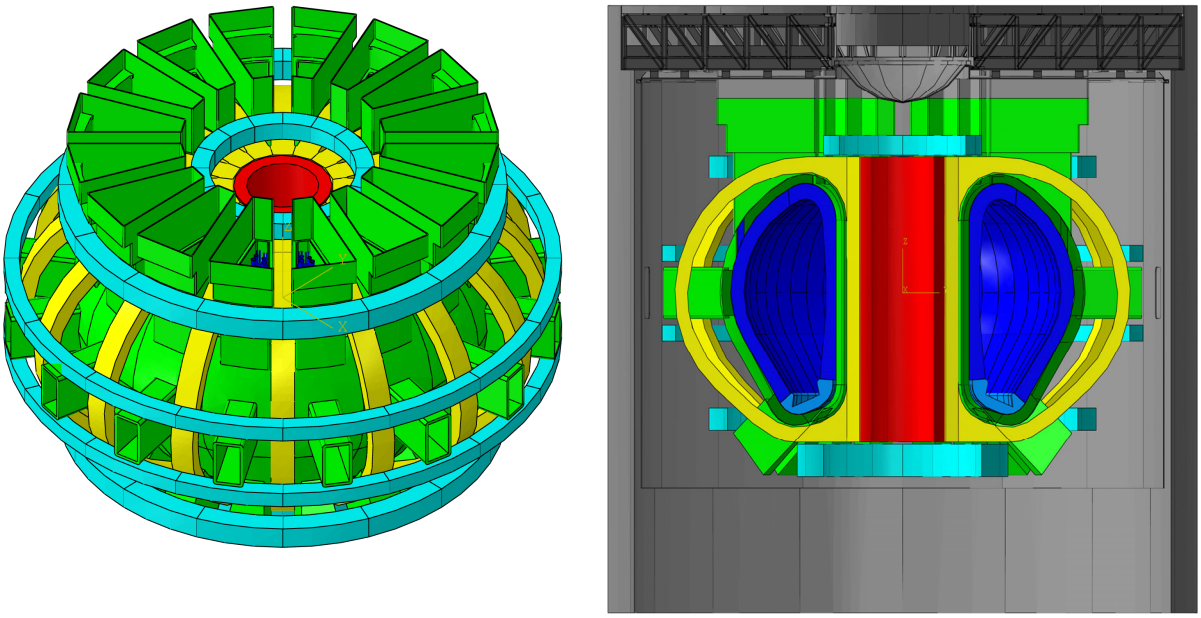

Figure 4.2 – EU DEMO CAD MODEL 2017 [31]

Table 3.2-1 - EU DEMO basic tokamak parameters [33]

Parameter	**Unit**	**Quantity**
Plasma power	MW	1998
Pulse length	h	2.0
Thermal power including n-multiplication in blanket (depending on blanket concept)	MW	2368-2607
Plant electricity output capability during flat top	MW	500
Lifetime neutron damage in steel in the FW	dpa	20+50
Number of full power years		5.98

Torus major radius (R0)	m	8.938
Torus minor radius	m	2.883
Plasma current	MA	19.07
Toroidal field at R0	T	4.89
Plasma volume	m^3	2466
Plasma chamber free volume (all IVCs installed, excl. ports)	m^3	3000
Plasma chamber free volume (all IVCs installed, incl. ports)	m^3	6400
Free primary vacuum volume inside upper ports with horizontal annexes	m^3	1500
Plasma surface area	m^2	1419
FW surface area (not considering BB penetrations)	m^2	1473

Regarding the dimensioning of the blanket structures of DEMO, an important role is represented by the plasma thermal loads. These loads are due to two contributes: the heat flux coming from the plasma and acting on the first wall and the volumetric power heating produced by the nuclear reactions inside the blanket caused by the neutron flux. EU DEMO power parameters are reported in Table 3.2-2. The total nuclear heating of 1739 MW represents the 87% of the total power and does not take into account the power deposited in the first wall, breeding zone, manifold structure, and shielding. The total FW heat flux, 318.21 MW, is calculated multiplying the average first wall heat flux (0.22 MW/m^2) and the total breeding blanket and first wall surface. Therefore, it is to consider that the total first wall power is composed from two contributes, the first due to the heat flux (318.21 MW) and second due to the neutron wall load (336.58 MW). The total FW power is 654.79 MW. Thus, the total power of the BB available for the thermal balance, which results from the total power of breeding zone and first wall: 1739.24 + 318.21 = 2057.45 MW. This power shall be removed by the first wall and the breeding zone cooling systems.

Table 3.2-2 - DEMO and WCLL BB power balance [32]

Description	**Unit**	**Power (WCLL 2017 design)**
Total nuclear heating	MW	1739.24
Total FW heat flux	MW	318.21
Total FW nuclear heat	MW	336.58
Total FW power	MW	654.79
Total BZ power	MW	1402.66
Total power	MW	2057.45

The main components of the EU DEMO are described below.

4.1 DEMO Vacuum Vessel

The fusion plasma is confined in a torus-shaped double-walled vacuum vessel by magnetic forces induced by the plasma current and the magnetic fields of the tokamak magnet system. The function of the VV is to provide the first confinement barrier, remove the nuclear heating, withstand accidents without losing confinement, and support in-vessel components. In its last configuration, the EU DEMO

vacuum vessel is made of austenitic stainless steel and consists of 16 prefabricated sectors supposed to be assembled on-site. The height of the EU DEMO Vacuum Vessel torus is 15.3 m, the inner diameter is 8.9 m and the outer diameter is 27.7 m. Its design pressure is 2.6 MPa and the design temperature is 200 °C [34].

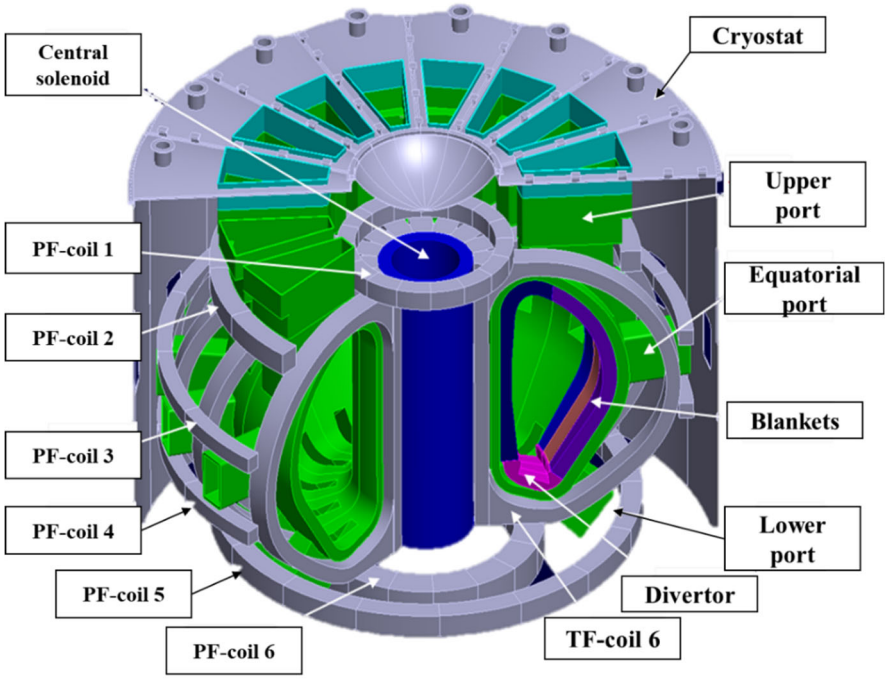

Figure 4.1.1 - Overview of the DEMO Tokamak Machine, Vacuum Vessel (in green) with main components [34]

However, being the size of the VV strictly related to the fusion plasma volume and so to the amount of power that can be produced, these dimensions may will change with different design configurations. But as the VV size increases, the design becomes more complicated and is confined by the more requirements such as withstanding the different kinds of loads.

The double-wall structure of the vacuum vessel principally consists of an inner shell, an outer shell, and ribs that connect the shell as support against the cooling pressure, magnetic forces and gravity. The inner shell is in contact with the vacuum of the plasma chamber on the one side and with the water cooling the VV on the other side. The outer shell faces the cooling water on one side and the vacuum of the cryostat on the other side. The VV structure can be divided into two regions, the inboard wall, and the outboard wall. The inboard wall is the closest to the central solenoid and is the highest loaded parts of the entire Vacuum Vessel because of high magnetic forces acting on the inboard wall and inboard blankets. The outboard wall is the curved double-walled part of the Vacuum Vessel. It is the region most distant from the central solenoid. It consists of the inner shell and the outer shell, which are connected via poloidal ribs. For thermal insulation of the superconducting toroidal and poloidal magnetic coils a thermal shield surrounds all external surfaces of the VV in the cryostat.

The vacuum vessel main structure is characterized by several openings for port structures whose main function is to build the linkages between the internal components and the external components. These opening are the upper, equatorial and lower ports. The port stubs are the interface on the Vacuum Vessel to which the ports are joined via splice plates in the tokamak pit. These stubs are connected to the inner and the outer shell of the Vacuum Vessel and provide a hydraulic connection of the ports to the cooling circuit of the vessel. Ports and double walls are cooled by the same water circuit [33].

The main safety function of the VV is to act as the first confinement barrier for radioactivity and as shielding of the magnet system. The confinement barrier is formed by the outer shell of the double-walled parts and inner shell of ports in single wall portions and the connection between ports and port plugs. To increase the neutron shielding capability for the VV, the spaces between the inner and outer shells are partially filled with stacked in-wall shielding plates made of steel and actively cooled by water supplied by inlet piping. Water acts also as a neutron moderator in such a way a high shielding efficiency can be achieved. The VV PHTS is designed as a two loop PHTS to remove 86.0 MW from the reactor during the plasma and 1 MW during the dwell.

A Decay heat removal system (DHRS) is required to remove decay heat generated in IVCs under emergency conditions[34]. The technical solution is to use a heat exchanger and a pump installed in both VV PHTS loops. The system is intended to be fully redundant so that, in case of loss of one of two independent VV PHTS loops, it is possible to rely on the operation of the DHRS portion pertaining to the intact VV PHTS loop. Two configurations are discussed:

- active DHRS which is characterized by high compactness but challenges HX design requirements;
- a partially passive configuration using water pools integrated in the tokamak building with a relatively easy HX design.

Another important safety function of the vacuum vessel is the support function to in-vessel components. The high forces acting on each blanket are distributed to several supports at different positions. The divertors are supported at the inboard and at the outboard. The support function requires the demonstration of structural integrity, which is important since the vessel is a major confinement boundary. To assure the structural integrity, the vessel (main vessel and ports) are designed and constructed with respect to allowable stress limits.

From a safety perspective the maximum allowable vacuum chamber pressure is 0.2 MPa. The neutron irradiation limit for the VV structure is defined as 2.75 dpa [34]. The most relevant postulated initiating events (PIE) for the VV are a LOVA in VV due to large ingress of air induced by a rupture in a VV penetration and an in-vessel LOCA from the VV primary cooling loop due to leak in the internal shell of the VV.

4.2 DEMO Cryostat

The function of the cryostat is to create a vacuum environment to operate the magnet system in cryogenic conditions, reduce external thermal loads (radiation from the VV and neutrons heat) from transferring to coil assembly, and supports the vacuum vessel structure The cryostat of the EU DEMO reactor is a single-walled, passively cooled Vacuum Vessel made of 304 steel. The Cryostat operational pressure is about 10^{-4} Pa [36]. The structures of the cryostat are designed to withstand an external pressure of about 1 bar and an internal pressure of 2.0 bar in case of an accident.

The cryostat is encased in a ~2m thick reinforced concrete bioshield [35]. This fulfills three main functions: it reduces the gamma radiation level to allow man access into the tokamak building during maintenance periods, provides access to the cryostat, and provides provide support to the equipment and building structures on top of the bioshield roof. Because of its design concept the cryostat transfers large part of the pressure load to the bioshield and bioshield roof through radial and vertical supports.

The cryostat cylinder is toroidally segmented into 16 segments and consists of the following components having a structural function [36]:

- Top lid (top head) with central lid: consists of radial beams that are supported by the bioshield roof. Curved steel plates in between the radial beams make up the cryostat top lid through which the tokamak could be assembled maintained. Top lid structures allow also the penetration of primary heat transfer system cooling pipes and magnet feeders.
- Main cylinder: is made up of vertical concave tube segments radially and axially supported by the bioshield [37]. The tube segments are adapted to the required penetrations of the lower ports and must provide flexibility in toroidal direction. The tube segments are toroidally aligned with the lower port to allow the required penetration.
- Skirt segments and pedestal rings: skirt is made up of 16 plates of steel circular segments allow the connection between the pedestal ring and main cylinder. The plates are welded together along their toroidal joints. Skirt segments provide flexibility in radial direction to allow the radial contraction of the pedestal ring while the skirt support remains radially fixed. The pedestal ring supports the tokamak structure and the magnet system but is not supporting the cryostat apart from its basement cylinder and plate. The thickness of the basement cylinder is 30 mm.

To operate a tokamak machine is required to thermally insulate the tokamak systems from one another. Thus, it is necessary to prevent convective heat transfer, decrease the heat transfer by radiation through low coefficients of emissivity, and design support structures that connect systems operating at different temperatures in such a way as to minimize conduction.

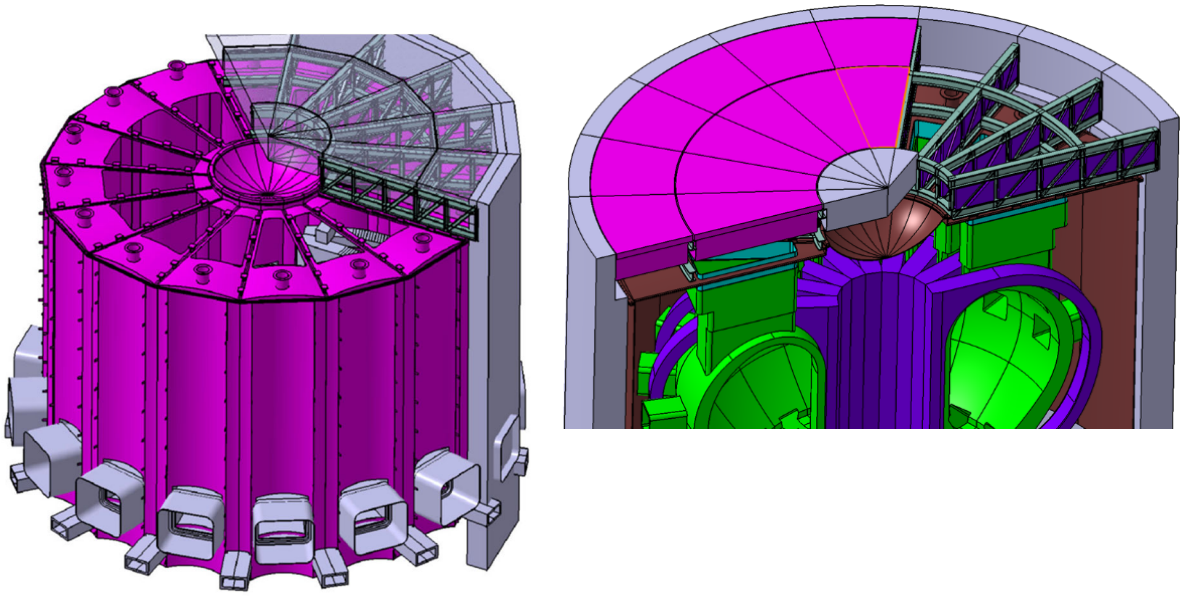

Figure 4.2.1 – General view of the final cryostat and bioshield design concept (DEMO 2017) [36]

The most significant conduction through support structures occurs between the cryostat pedestal ring and the TF coils, and between the magnet system and the VV thermal shield. To minimize the total and local heat loads from being transferred from hot in-vessel components to the structure and superconducting coils operated at 4.2 K, both vacuum vessel and cryostat structures are equipped with thermal shields.

Thermal shield panels consist of a single wall structure made of stainless steel and covered on both sides with a thin, low emissivity layer of silver to keep the emissivity value below 0.05 [38][39]. The VV thermal shield is a shell-like structure enclosed between magnets and main vessel supported by the TF coils that covers the VV and its port structures. The cryostat thermal shield shields the magnet system

from radiation loads from the cryostat and in-cryostat components. Both the systems are actively cooled by helium at about 80 K.

4.3 Divertor

The main function of the divertor is to extract the power conducted in the tokamak scrape-off layer (the plasma region characterized by open field lines) whilst maintaining the plasma purity. The design and the shape of the divertor is determined by the tokamak magnetic topology in a way that the field lines outside the last closed flux surface intersect the divertor targets, which collect most of the particles and energy exhausted by the plasma. Divertor is a component of prime importance for future tokamak reactors. Its components must withstand high heat flux (up to 20 MW/m^2) [40], contributing at the same time in providing neutron shielding for the Vacuum Vessel (VV) and magnet coils in the vicinity of the divertor region. Because of their position the huge particle fluxes arising from plasma contribute to the deterioration of divertor cassettes, which should be easily inserted, mounted, demounted and removed from the VV volume via the lower port [41].

Each DEMO sector contains three divertor cassettes, for a total of 48 cassettes. The structural element of the divertor cassette is named cassette body (CB). The CB supports the PFCs and the cooling pipes, and it contributes to provide neutron shielding for the VV and magnetic coils. It consists of an EUROFER steel box composed by an upper plate, a lower plate and an internal stiffening grid that provides mechanical resistance. Such grid is holed to allow the coolant transition along the whole CB. The diameter chosen for the holes is 70 mm, except in the small section at outboard where the diameter is 40 mm. Each cassette body supports three the divertor plasma facing components, made of tungsten, directly exposed to particle impact and heat radiation generated by the plasma: Inner Vertical Target (IVT), Outer Vertical Target (OVT) and liner. The overall nuclear power deposited into the PFCs is 115.2 MW. The vertical targets are inclined to intercept the magnetic field lines of the separatrix at an acute angle, giving deep inboard and outboard channels in which to establish a partially detached plasma regime. The plasma facing unit geometry is based on the “monoblocs” concept, which consists of tungsten blocks with a drilled hole in which it has inserted and fixed a CuCrZr pipe. Each monobloc has an axial length of 12 mm (or 12.5 considering the gap) and a constant toroidal width of 23 mm both at OVT and IVT. The IVT has a dimension of about 0.76 m high and 0.82 m wide. The OVT has a dimension of about 0.65 m high and 1.07 m wide. There are 158928 monoblocs in the whole supply of OVTs and 136896 monoblocs for IVTsv [42].

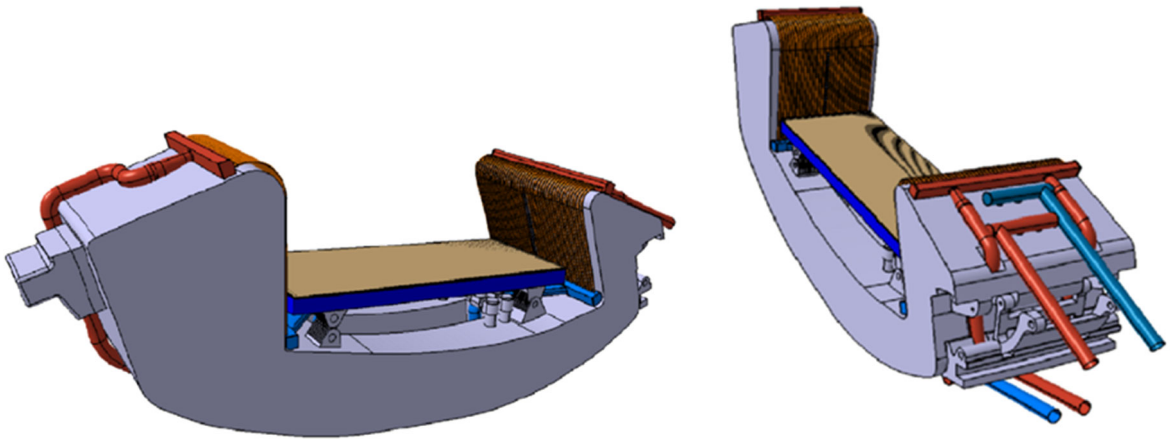

Figure 4.3.1 – 3D view of the DEMO Divertor [42]

The shielding liner consists in a plate with internal structure similar to the water cooled blanket First Wall (FW). It is composed by four distinct layers: a 90 mm thick EUROFER plate crossed by 6 semicircle-shaped slots where the coolant can flow through; two EUROFER plates joined together to form an array of 6 mm slots for cooling circuit to remove the surface heat load due to radiation; a layer of manifolds made of EUROFER which collect the coolant coming from the first layer; and a 2 mm in thickness plasma spray tungsten layer that covers the entire liner surface.

Each cassette body is connected to a Tokamak Cooling Water System (TCWS) [43] through two pair of radial pipes, one pair for cooling the CB and one pair for cooling the PFC. Due to the presence of accumulated dusts in the bottom of the VV, means that a LOCA, LOVA or LOFA from divertor cooling system enhances the risk of chemical reaction between steam and dust.

4.4 WCLL Breeding Blankets

In order to shield the VV and the superconducting coils from the high energy produced by the fusion reactions, the inner surface of the VV is covered with breeding blanket modules. The breeding blanket is a major system of a fusion reactor. It has to interface the plasma, to remove the heat generated in the tokamak and transfer it to the PHTS ensuring an efficient power conversion. Moreover, the breeding blanket shall also breed the tritium ensuring the self-sufficiency of the reactor.

The EU DEMO fusion reactor features big breeding blankets at the inboard and the outboard side. Since the blankets are wear parts due to the limited lifetime of their structural material in neutron-irradiated environment, they can be removed via the upper ports for maintenance operation and substitution. In the EUROfusion Breeding Blanket Project (WPBB) in 2014-2020, four different tritium breeder blanket concepts have been investigated for DEMO application: Helium Cooled Lithium Lead (HCLL), the Helium Cooled Pebble Bed (HCPB), the Dual Coolant Lithium Lead (DCLL) and the Water Cooled Lithium Lead [5].

An advantage of the use of lithium-lead eutectic alloy in fusion reactors is represented by the fact that breeder and neutron multiplier are combined in one and the same material [44]. Moreover, an important criterion in the choice of breeder materials is its chemical reactivity and compatibility with structural material. The lithium-lead reacts with air and water but not vigorously and has worse compatibility with steels due to the possible oxidation. The lithium-lead eutectic has been shown to react with concrete to produce hydrogen on a very small scale, so large-scale tests are necessary. Other disadvantages are due to its high density, tritium containment problems caused by its very low solubility and melting temperature [45]. The reaction of lithium-lead with neutrons produced a neutron multiplication reaction that results in an attractive neutronic performance for the lithium-lead blanket. When water is used as coolant, neutrons will be moderated, and this fact allows a reduction of the blanket thickness with positive effects for both volume and weight. tritium is produced mostly through the reaction so that enrichment is necessary [46].

$$^{6}Li + n \rightarrow {}^{4}He + T + 4.78\ MeV$$

$$^{7}Li + n \rightarrow {}^{4}He + T + n - 2.47\ MeV$$

The WCLL blanket is based on the use of reduced activation ferritic-martensitic steel (EUROFER) as structural material, liquid Lithium-Lead (PbLi) enriched at 90% in ^{6}Li as breeder, neutron multiplier and tritium carrier, and water at Pressurized Water Reactor (PWR) conditions as coolant (295-328 °C, 15.5 MPa).

Several improvements have been made to the WCLL breeding blanket design over the years, passing from a design based on Multi Module Segment (MMS) approach, which implied thermomechanical disadvantages due to segmentation, to a Single Module Segment (SMS) approach. Following the Single

Module Segment (SMS) approach, the inboard and outboard blanket are composed by a large continuous segment that is interrupted for the whole vertical extension of the component [21]. This approach facilitates the PbLi drainage and helium bubbles removal from the segment compared with the MMS approach and, moreover, it provides superior thermomechanical performances during both normal operation and central major disruption events

The whole WCLL blanket system covers the VV in an all-round toroidal direction. It is divided in 16 sectors. One DEMO sector is composed of two inboard segments and three outboard segments, thus there is a total of 36 and 54 segments, respectively. Each module is essentially formed by a directly cooled steel box performing the function of Lithium-Lead container and by a Double Walled C-shaped Tube (DWT) bundle, immersed in the liquid metal, in which the water coolant circulates. The module box is reinforced by radial and toroidal stiffeners to withstand the disruption-induced forces and the full water-pressure under faulted condition.

The modules are cooled by two independent system:

- The First Wall (FW) system having the main function of extracting heat due to the heat flux and Neutron Wall Load (NWL);
- The Breeding Zone (BZ) which function is to extract the heating due to nuclear reactions inside the blanket between neutron and PbLi.

4.4.1 First wall

The FW plasma facing area is two-layer structure named First Wall and placed in the front part of the breeding blanket unit. It is covered by a tungsten layer of 2 mm thickness, and a 25 mm thick layer of EUROFER. The coolant is water at 15.5 MPa flowing in counter current direction in square channels of 7×7 mm built inside the structural material, with a pitch of 13.5 mm. The position of FW channels is symmetrical with respect to the plane of TR and baffle plates in order to ensure the symmetry of the breeding units. In each breeding unit there are 10 coolant channels. Water enters at 295 °C and exits at 325 °C, at 15.5 MPa [48].

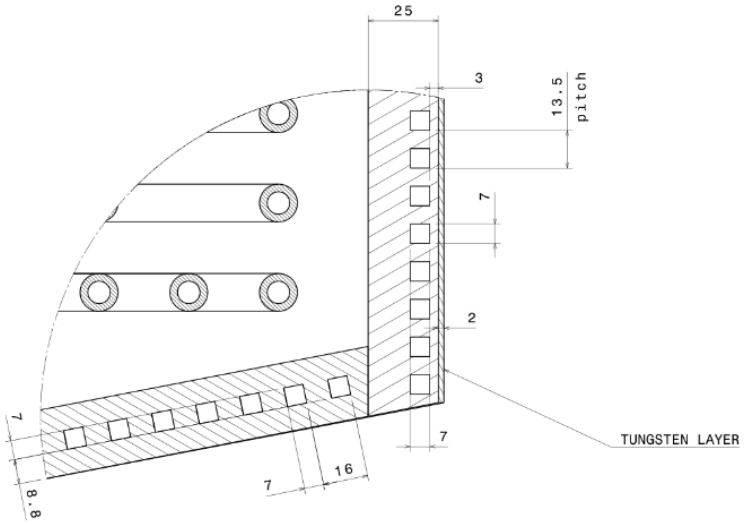

Figure 4.4.1 - Layout of FW cooling channels [47]

The first blanket set has to be designed for a lifetime corresponding to neutron damages of 20 dpa, with a second set aiming to 50 dpa; this means that one scheduled replacement of the whole blanket system is necessary in the life of the reactor (which will be sum up to about 70 dpa).

4.4.2 Breeding zone

The BZ cooling system is independent from the FW one. To minimize the risk of pipe rupture with consequent ingress of water into the breeding zone and violent chemical reactions occurring with the breeder, the BZ coolant pipe system consists of radial-toroidal Double Walled Tubes (DWTs), displaced in a horizontal plane. The DWTs have an external diameter of 13.5 mm, the internal one of 8 mm and a thickness of 1.375 mm [48]. An iron or copper interlayer of 0.1 mm is foreseen to be adopted among the two tubes. According to the last WCLL BB layout, the total number of BZ tubes of one breeding unit is 22. Several arrangements are possible for the pipes position that, however, must provide a symmetrical temperature in the breeder and the lowest amount of structural material, to affect the least the TBR. The Lead-Lithium enters in the breeding unit from the bottom of the elementary cell, flows from the back plate toward the first wall, then turns up in poloidal direction, and flows back in the outlet channel, which is separated from the inlet by a thin baffle plate. Since the PbLi is only employed as breeding medium and neutron multiplier, its velocity is minimized to avoid large pressure losses: the maximum PbLi velocity at inlet orifices is 5 mm/s, and the average velocity in the BZ is 0.1 mm/s.

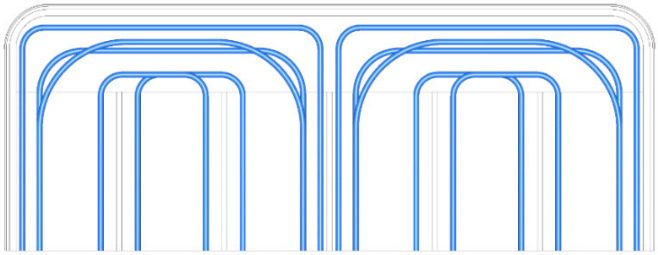

Figure 4.4.2 - WCLL BZ DWT arrangement [48]

4.4.3 Back Supporting Structure and attachments

The back supporting structure is a continuous steel plate in poloidal direction, with a radial thickness of 100 mm. It provides mechanical attachments to blanket units and to the manifold distribution system that feeds the modules. It represents the backbone of the blanket segment, providing three distinct functions:

- Supporting the structural loads of the BZ and providing stiffness to the whole structure;
- Housing FW water coolant manifolds, as well as water and LiPb spinal collectors;
- Neutron shielding for the vacuum vessel.

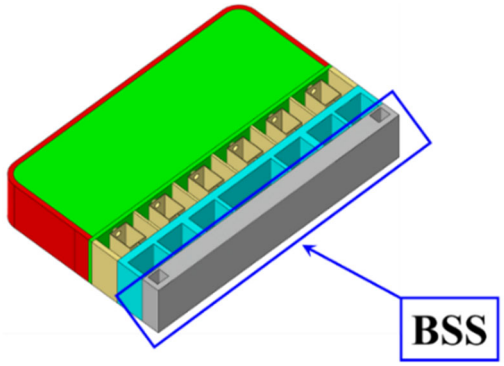

Figure 4.4.3 - WCLL2018.v0: detail of the BSS [48]

Inlet and outlet manifolds, located between the module back plate and the BSS, are foreseen for each segment and for each system (FW, BZ and Lead-Lithium). The design of manifolds is driven by the

position of the feeding pipes, that for the outboard module is roughly at 1/3 of the poloidal height of the segments (from the top), while for inboard modules is at the top of the segments (Figure 4.4.4).

The proposed solution for the DEMO 2017 design is to direct the flow of both water and LiPb to the bottom of the segments using different spinal collectors. From that point, different manifolds will distribute the coolant and the breeder to the blanket units. Once the top of the segments is reached, fluids are collected in outlet spinal collectors developing from the top to the outlet pipes.

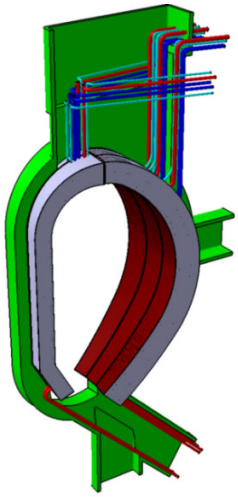

Figure 4.4.4 – EU DEMO sector piping system [32]

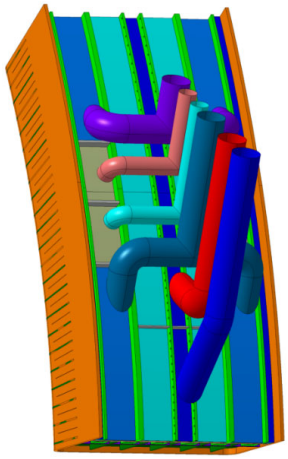

Figure 4.4.5 – Detail on OBC pipes connection. BSS removed for clarity [48]

The water cooling system is connected to the Primary Heat Transfer System (PHTS) through feeding pipes hosted in VV the upper port compartment, whereas the PbLi is conveyed to and from the breeding zone through pipes routed at the upper and lower port, linked to the ex-vessel PbLi loop. In particular, the following piping lines of BB sector are routed in the upper port:

- FW water inlet and outlet pipes
- BZ water inlet and outlet pipes
- PbLi Outlet pipes

In Table 4.4-1 the characteristics of water feeding, and outlet pipes are reported.

Table 4.4-1 - WCLL BB water cooling system integration and sizing [48]

	D_{ext}	D_{int}	Section	L	Vol
	m	m	m^2	m	m^3
IB FW feeding pipe (1 segment)	0.1143	0.10372	0.00845	40	0.3380
IB BZ feeding pipe (1 segment)	0.1683	0.15272	0.01832	40	0.7327
OB FW feeding pipe (1 segment)	0.1413	0.12822	0.01291	40	0.5165
OB BZ feeding pipe (1 segment)	0.2191	0.19882	0.03105	40	1.2419

4.5 Primary Heat Transfer System

The WCLL PHTS is constituted by two independent primary systems the BZ primary system and the FW primary system (FW PHTS). The BZ primary system delivers the power to the PCS, by means of two Once Through Steam Generators (OTSG), and the FW primary system is connected to the Intermediate Heat Storage System (IHTS), which is in charge of accumulating the energy during the

power pulse and delivers the heat during the dwell time to the PCS. A 3D CAD model of the PHTS is shown in Figure 4.5.1.

The Primary Heat Transfer Systems (PHTSs) are designed to remove heat from IVCs (breeding blanket, divertor) and from the VV itself during the plasma operation. Each cooling loop includes components such as pumps/blowers, heat exchangers (HXs), pressurizers (PRZs) for water, inlet/outlet headers for coolant distribution or collection, and various valves (isolation, control, etc.). The HX transfers heat to the secondary BoP side. PHTSs designs 2018 are based on DEMO base line 2015 (which are available for the HCPB, WCLL BB concept, VV and divertor) scaled in 16 sectors as in the baseline 2017. The designs update for DEMO baseline 2017 is still in progress. The designs have been developed based on the selection of coolants. Water is the coolant for the WCLL blanket, the VV and the divertor, while helium is the coolant for the HCPB and HCLL blankets, and LiPb and helium are adopted as dual coolants for the DCLL blanket. For the latter, two potential types of primary HXs (with primary coolant LiPB and He) and the integration of these two coolants in a single component will need to be investigated. The pulsed nature of tokamak devices poses a significant engineering challenge in the development of the balance of plant, since this regime of operation is quite undesirable for the turbomachinery. To address this issue, an IHTS coupling the PHTS and the power conversion system (PCS) and an Energy Storage System (ESS) are proposed. Alternative PHTS options e.g. for WCLL BB PHTS would consist of one PHTS directly connected with the PCS, which is a straightforward solution comparable with proven PWR NPP technology. This solution would have the lowest total coolant inventory but would require the availability of a turbine compatible with the pulsed operation of DEMO and then is not actually applicable. This concept has been investigated with the addition of a small ESS or an auxiliary boiler.

The preliminary sizing of the main components was defined considering velocity and pressure drops constraints, and it was carried out considering the parameters reported in [48]. The main parameters defined in the preliminary sizing have been used to select the reference configuration and develop a 3D CAD model. The final parameters (i.e. pipes diameters lengths and volumes) are extrapolated from the CAD model and are reported in [49]. The pipes diameters and thickness have been defined on the basis of European Standard EN-10220.

The main components of PHTSs (BZ and FW) are:

- sector collectors and distributors;
- loop collectors and distributors;
- Steam Generators (SGs);
- Heat Exchangers (HEXs);
- hot and cold legs and pumps

One loop per system is foreseen, which are symmetrical with respect the radial-poloidal direction of the tokamak, located at about 71 m from each other.

4.5.1 Sector collectors

The sector collectors and distributors are connected to the BZ and FW feeding pipes. In particular, the sector collector is in charge to collect the hot water from the outlet BZ and FW pipes. The sector distributor is in charge to distribute the cold water to inlet pipes. One collector and one distributor per system and per sector is foreseen, and each of them is connected to 2 inboard segments and 3 outboard segments. The pipes diameters have been defined considering a maximum velocity of 12 m/s [50].

4.5.2 Ring

The loop collectors and distributors, hereinafter called “rings”, collects and distributes water from (to) the sector collectors to the hot and cold legs. The pipes diameters have been sized assuming that a quarter of the total mass flow rate flows in each quarter of ring, and considering a maximum velocity of 12 m/s, in order to limit pressure drop due to friction factor. The BZ PHTS foresees one hot leg and two cold legs per loop. Instead, the FW PHTS foresees two hot legs and two cold legs per loop. The pipes diameters have been sized considering as reference velocity 15 m/s.

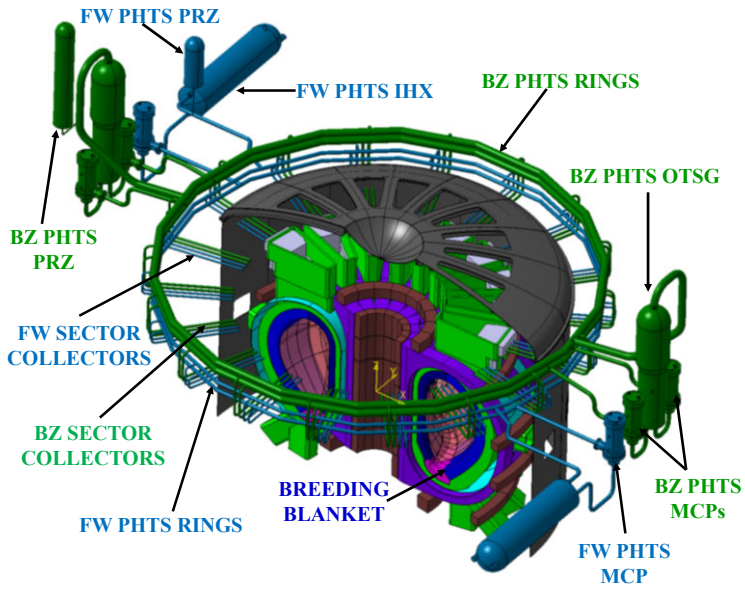

Figure 4.5.1 - WCLL PHTS CAD model integrated with tokamak building

4.5.3 BZ Once Through Steam Generator

The BZ PHTS transfers energy from the BZ of the BB to the PCS during the pulse mode (2 h). for a total power of 1483 MW_{th}. Two OTSGs are heated by the primary water coolant coming from the breeding zone of the breeding blanket. The primary coolant inlet and outlet temperature are 295 °C and 328 °C, respectively, at 15.5 MPa. Thus, the total mass flow rate is 7661 kg/s [49].

In the WCLL BZ PHTS, the thermal power removed by one OTSG is 742 MW_{th}, the corresponding mass flow rate of the primary system is 3830.5 kg/s. The OTSG secondary side (water) pressure is assumed 6.41 MPa and the feedwater coolant inlet temperature is 238 °C. The objective is to produce super-heated steam at 299 °C. Therefore, the feedwater mass flow rate is 404 kg/s. The main thermal-hydraulic parameters of primary and secondary side are summarized in Table 4.5-1.

The selected OTSG is characterized by 7569 tubes, with a length of 12.987 m. A square lattice is considered with a p/D of 1.28. Main geometrical features are reported in Table 4.5-1. Main geometrical parameters of SGs are reported in Table 4.5-2.

Table 4.5-1 - Primary and secondary systems OTSG TH parameters [50]

Parameter	Units	DEMO SG
Primary system		
N° SG	--	2
SG Power	MW_{th}	742
Coolant Mass flow/SG	*kg/s*	3830.5

Pressure	*MPa*	15.5
Temperature		
Inlet	*°C*	328
Outlet		299
Secondary system		
Pressure	*MPa*	6.41
Temperature		
Inlet	*°C*	238
Outlet		299
Feedwater flow/SG	*kg/s*	404
Internal Tubes Do	*mm*	15.88
Tubes Thickness	*mm*	0.864

Table 4.5-2 - BZ PHTS OTSG parameters [50]

Parameter	**Units**	**Value**
SG Power	MW_{th}	742
Primary side water T_{in}	*°C*	328
Primary side water T_{out}	*°C*	295
Secondary side water T_{in}	*°C*	238
Secondary side water T_{out}	*°C*	299
No. of tubes	--	7569
Tube D_o	*mm*	15.88
Thickness	*mm*	0.864
Heat transfer area	m^2	4903

4.5.4 FW PHTS IHX

In the reference design, during the power pulse (2 h [50]) the FW system delivers the power to the IHTS through two water/HITEC heat exchangers, and the corresponding energy is accumulated in the ESS. The overall power transferred through each intermediate heat exchanger is 219.9 MWth. The main thermal-hydraulics parameters are reported in Table 4.5-3. The reference configuration assumes the temperature cycle 295-328 °C for the primary water coolant system. The secondary fluid considered is the HITEC molten salt. The thermodynamic cycle of the intermediate system is 280-320 °C. The horizontal IHX is typical liquid-liquid heat exchanger tube and shell with two passes. Pressurized water coolant flows inside U-shaped tubes, in counter current direction with respect the HITEC, which flows shell side. Considering the reference thermodynamic cycle, the primary side water mass flow rate per IHX is 1136 kg/s, and the secondary side molten salt mass flow rate is 3524 kg/s. The main parameters of the IHX are reported in Table 4.5-3. The reference pipe dimensions of the primary to intermediate heat exchanger are reported in Table 4.5-4. The main geometrical data of the selected IHX are reported in Table 4.5-5. An alternative design is based on a direct cycle (without the ESS) and an OTSG is installed in the FW PHTS instead of the IHX. This solution is not analyzed in this work.

Table 4.5-3 - WCLL BB and FW PHTS main data [50]

Main parameters	**Unit**	**MS Ref. Cycle**
DEMO FW-PS power	MW_{th}	439.8
N° IHX	-	2
IHX Power	MW_{th}	219.9
Primary side operating temperature range	*°C*	295-328
Secondary side operating temperature range	*°C*	280-320

Water Mass flow total	*kg/s*	2272
Molten salt mass flow total	*kg/s*	7048

Table 4.5-4 - Water-molten salt HEX tube dimensions [50]

Water side - tube side	Unit	Value
Tube Do	*m*	0.015876
t	*m*	8.640E-04
Tube Ai	m^2	1.572E-04

Table 4.5-5 - FW PHTS intermediate heat exchanger parameters [50]

Parameter	Units	Value
IHX Power	MW_{th}	219.9
Primary side water T_{in}	*°C*	328
Primary side water T_{out}	*°C*	295
Secondary side HITEC T_{in}	*°C*	280
Secondary side HITEC T_{out}	*°C*	320
No. of tubes	--	5211
Tube D_o	*mm*	15.88
Thickness	*mm*	0.864
Length of tubes	*m*	28.9
Heat transfer area	m^2	7513
V water tubes	m^3	23.7
D_{ext} vessel	*m*	3.5

4.5.5 Pumps

Six pumps are installed in current preliminary PHTS design of DEMO. 4 MCP, 2 per loop, are installed in the cold legs of the BZ PHTS. The other two MCP are installed in in the FW PHTS. According with the main data of the PHTS, the pressure drops calculated in the systems and a postulated efficiency of 78%, it results that the power of these pumps is 2.294 MW and 1.419 MW, respectively for those installed in the BZ PHTS and in the BZ PHTS. It implies that they can be medium and small PWR pumps.

Table 4.5-6 - PHTS MCP power [50]

	Density	Mass flow	Pressure drop	Volumetric flow	Head	epsilon	Total pumping power	MCP
	kg/m^3	*kg/s*	*MPa*	m^3/s	*m*		*MW*	*MW*
FW PHTS	737.1	2272	0.974	3.082	99.32	0.78	2.838	1.419
BZ PHTS	737.1	7661	0.934	10.39	95.25	0.78	9.178	2.294

4.5.6 Pressurizers design

For each PHTS (BZ and FW) is foreseen a pressurizer (PRZ). This component has been sized on the base of the PWR experience. The result of the design is a FW PRZ total volume of 24.5 m^3. The BZ pressurizer has a water volume of 53 m^3.

4.6 Tokamak Building

The tokamak building represents the secondary and ultimate nuclear confinement barrier for the radioactive material contained inside the building towards the environment and the public. Its is mainly

driven from the tokamak structures which are enveloped inside the bioshield [52]. The building requires large space because of the number and the size of the components to be housed such as: the cryostat which encloses the tokamak machine and its auxiliary systems, the Primary Heat Transfer Systems (PHTS), the vacuum vessel pressure suppression system (VVPSS), the heating, ventilation and air conditioning system the cryo-distribution system, and the electrical power supplies. In addition, safety classified protection and mitigation systems are located in the tokamak building such the decay heat removal system, the detritiation systems, and the toroidal field (TF) coil quench detection system [51]. The presence of these and other systems in the Tokamak might generate challenging environmental conditions in particular because of the huge magnetic energy of magnets housed in the buildings and of the significant enthalpy of coolant fluids at high temperature, which can cause the mobilization of radioactive inventories such as tritium, activated corrosion products and activated dust, challenging the confinement safety function. The definition of radioactive inventories inside the tokamak building is important, since the early stage of the design, in order to maintain them, through design solutions, below certain values.

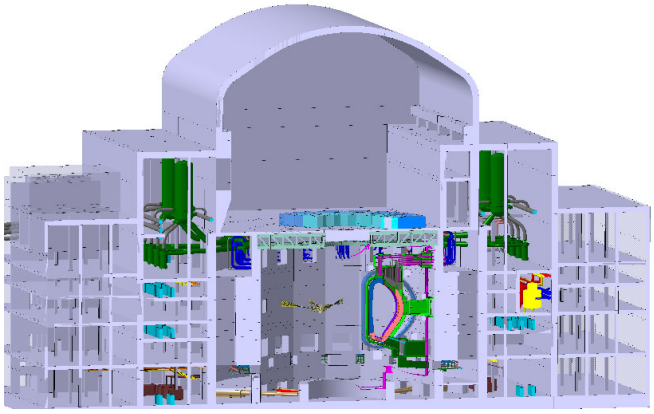

Figure 4.6.1 – EU DEMO tokamak building

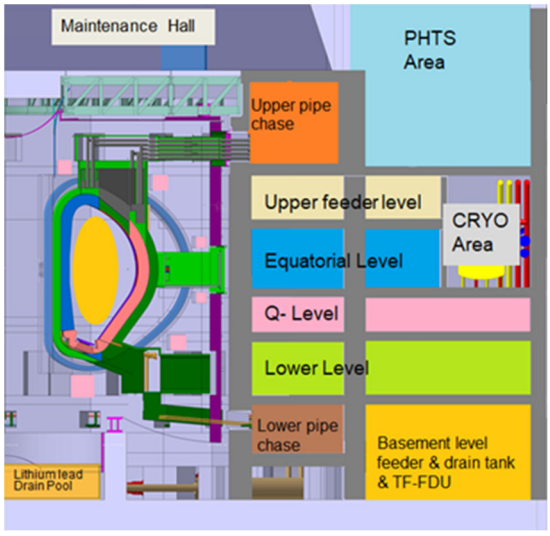

Figure 4.6.2 – Tokamak building levels

The tokamak building has several levels corresponding to the cryostat penetrations and additional levels above and below the machine used for auxiliary equipment. Some rooms of the tokamak building are also assigned as expansion volumes to limit the pressure in leak accident cases [51].

- Basement Level: dedicate to the drain tanks of the VVPSS, particularly important for the WCLL model as well as the lower pipe chase and the LiPb tanks. The galleries are dedicated also to the supply of the magnet systems via the cryo-lines coming down.
- Lower Port Level: which consists of 8 Port Cells located around the bio-shield and connected to the galleries to provide service via the door lintel of the Port Cells such as power, instrumentation and pneumatic. Vacuum services, local air cooler and detritiation system are available in each Port Cells
- Q Level: created following the ITER experience to provide a zone with milder environmental conditions in terms of radiation dose, temperature, pressure and humidity, being not connected to any VV port.
- Equatorial Port Level and Feeder Level: hosting NBI Port Cells and cryo-lines.
- Upper Level: housing the upper pipe chase and the PHTS area

The radioactive confinement safety function could be challenged by an over pressurization of the building beyond 2 bar absolute. To avoid this over pressurization, enough volume inside the building

must be made available for accidental scenarios. However, as reported in paragraph 5.3, some modification to the connection between compartments should be made to kept the pressurization of TCR compartments under the limit of 2 bar during an ex-vessel LOCA [54].

The tokamak building must be located in the central position of the site. A preliminary solution of DEMO plant site and tokamak building layout is reported in Figure 4.6.3.

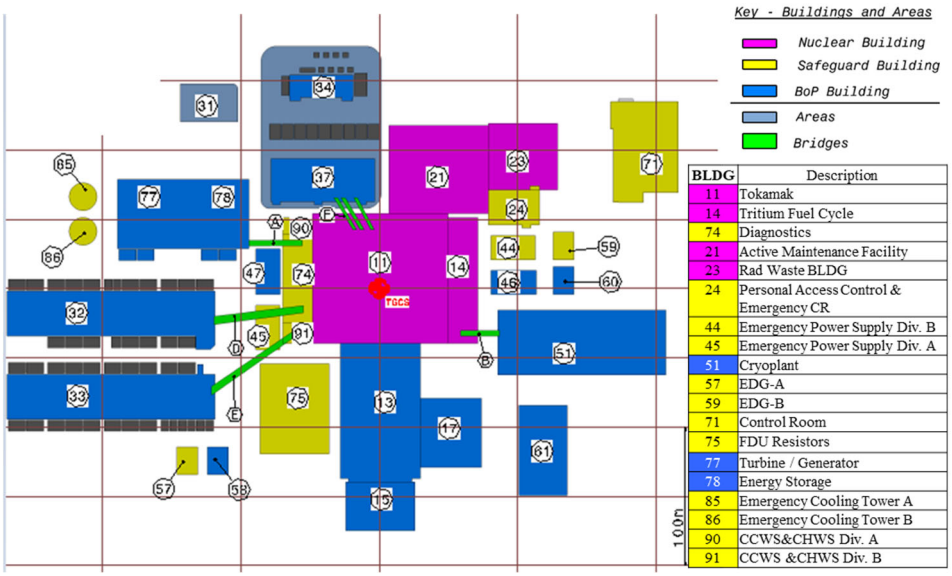

BLDG	Description
11	Tokamak
14	Tritium Fuel Cycle
74	Diagnostics
21	Active Maintenance Facility
23	Rad Waste BLDG
24	Personal Access Control & Emergency CR
44	Emergency Power Supply Div. B
45	Emergency Power Supply Div. A
51	Cryoplant
57	EDG-A
59	EDG-B
71	Control Room
75	FDU Resistors
77	Turbine / Generator
78	Energy Storage
85	Emergency Cooling Tower A
86	Emergency Cooling Tower B
90	CCWS&CHWS Div. A
91	CCWS &CHWS Div. B

Figure 4.6.3 – DEMO preliminary plant site layout [53]

4.7 Vacuum vessel pressure suppression system

The vacuum Vessel Pressure Suppression system (VVPSS) aims at protecting the VV and its internal structures from overpressure events [55]. Moreover, it has to provide the scrubbing of radioactive aerosols and tritium migrating from the VV as well as mitigate hydrogen explosion risk by mean of passive autocatalytic recombiners (PARs) directly installed in the atmosphere of the suppression tanks. However, this last solution is currently under study in the framework of WPSAE activities.

The EU DEMO VVPSS concept is currently under design. For the helium cooled blanket concepts (HCPB, HCLL and DCLL), a combined VVPSS and Expansion Volume (EV) concept is being explored to accommodate the expansion of helium in the event of a LOCA. To minimize the amount of water and volumes to be decontaminated from tritium, dust and ACP after an accident scenario, one of the main last design changes for the VVPSS consisted in splitting in several tanks the suppression pool for steam condensation. The large steam mass flow rate transport large amounts of dust and tritium and ACP into the VVPSS tanks. At the end of an accident scenario the VVPSS-ST trapped the majority of the radioactive DEMO inventory and they have to be managed and decontaminated before the restarting of the tokamak machine. To avoid steam and radioactive flows inside neutral beam ports, pipework connecting the VV to the VVPSS has been attached to the upper port (Figure 4.7.1).

The VVPSS for the EU DEMO WCLL includes:

- One vapor suppression tank for small leakages (Tank A);
- Five suppression tanks for DBA events (tank B to F);
- Relief Lines to allow gas transfer from the vacuum vessel to VVPSS tanks;
- Rupture Disks (RD) connecting the in-VV volume to the Expansion Volumes;
- Bleed Lines (BL) to avoid burst of the RD in case of small leakage.

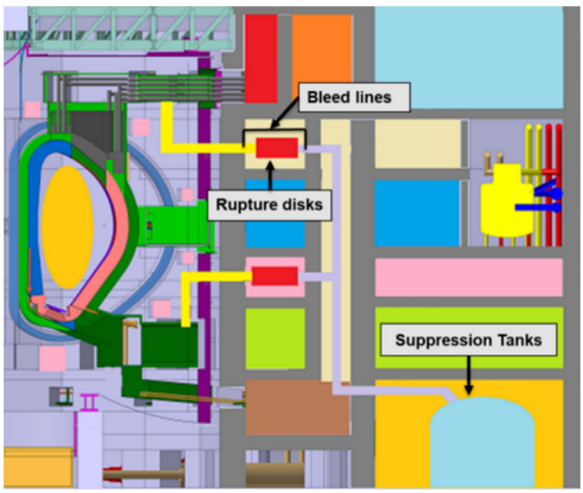

Figure 4.7.1 –VVPSS connection to VV upper port

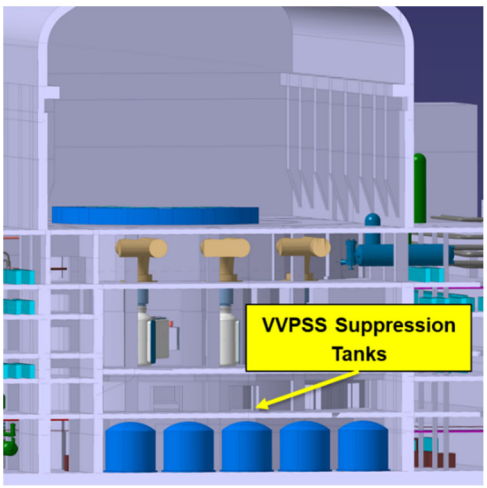

Figure 4.7.2 - VVPSS suppression tanks inside the tokamak building

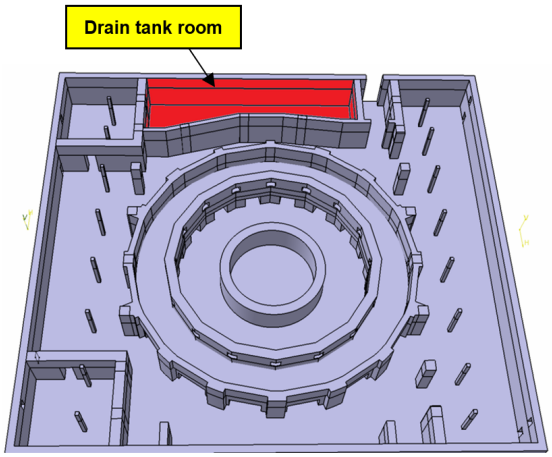

Figure 4.7.3 - Tokamak building basement level with drain tank room available volume in red

The pressurization of the VV leads to the bleed valves opening when VV pressures reaches 90 kPa absolute. If the pressure reaches 1.5 bar absolute, the rupture discs open in order to stop the pressure increase [20].

The suppression tanks are filled with water at room temperature. Water in the tank could also be cooled down during an accident, however, up to now the DEMO safety approach is to avoid the use of active systems, for such a reason any active cooling system is foreseen for the VVPSS.

In the basement level of the tokamak building a “Drain tank room” with a floor surface of 581 m^2 and a height 8.2 m (total volume 4764 m^3) has been provided to allocate VVPSS suppression tanks and relief lines (Figure 4.7.2, Figure 4.7.3). Actually, because of the limited available floor surface, the maximum number of tanks to be placed in the drain tank room was fixed to be at least six.

5 EU DEMO MELCOR model

MELCOR [56][57] is a fully integrated severe accident code able to simulate the thermal-hydraulic phenomena in steady and transient condition and the main severe accident phenomena characterizing the RPV, the reactor cavity, the containment, and the confinement buildings typical of LWR. The estimation of the source term is obtained by the MELCOR code as well. It has been developed at Sandia Laboratories for the U.S. Nuclear Regulatory Commission as a tool for the evaluation of second-generation plants PRA (probabilistic risk assessment). MELCOR has a modular structure based on the "control volume" approach. Each MELCOR package simulates a different part of the transient phenomenology. In particular the CVH and FL packages simulate the mass and energy transfer between control volumes, the HS package simulates the thermal response of the heat structure and the COR evaluates the behavior of the fuel and structures contained in the core and lower plenum and their degradation phenomena. It is to underline the role of the CVH/FP packages that provide the boundary condition for other packages. MELCOR is being developed at Sandia National Laboratories (SNL) for the US Nuclear Regulatory Commission (U.S.NRC).

The Idaho National Laboratory (INL) Fusion Safety Program (FSP) made fusion specific modifications to the MELCOR code, including models for water freezing, carbon, beryllium and tungsten oxidation in steam and air environments, beryllium, flow boiling in coolant loops, air condensation, and radiative heat transfer in enclosures [58], that allowed MELCOR to assess the thermal hydraulic response of DEMO fusion reactors cooling systems and the transport of radionuclides as aerosols during accident conditions. Recent updates to the MELCOR code involve a model for transporting HTO, the material oxidation correlations for Safety Analysis Data List (SADL), aerosol transport and density [59].

The MELCOR code is composed of a number of major modules. Main packages involved in MELCOR are:

- Core (COR) package: it models the relocation of core and lower plenum structures during melting and debris formation and ejection into the reactor cavity consequently the reactor vessel failure. This package also calculates the thermal-hydraulic response of core internal structures, considering energy transfer to and from Control Volume (CV) and Heat Structure (HS) packages.
- Control Volume Hydrodynamics (CVH) and FLow path (FL) packages: they model the thermal-hydraulic behavior of liquid water, water vapor and gases. The CVH input defines the initial state of each volume, requiring geometry and composition. FL package is instead concerned with connections between control volumes, through which control volume masses may flow. It is also important to underline that control functions (CF) or tabular functions (TF) can be associated with CVH and FL packages, in order to simulate for example sources and sinks of mass or energy, valves, pumps, etc.
- Control Function (CF) package: in this package user can define functions of variables that can be used by other packages in the code. There is a series of available types of control functions that can have a several number of uses, some of which contains a difficult control logic; it is for example used to control the opening of a valve, or the pump head associated with a flow path.
- RadioNuclide (RN) package: it models the release of fission products from fuel and debris, and aerosol dynamics with transport through flow paths and deposition on structure surfaces. Boundary conditions, like fluid parameters, structures surface temperatures and source terms are provided by other MELCOR packages. It is also possible to consider the wash-off of radionuclides deposited on heat structures from the drainage of water films and the aerosol removal by safety features.

5.1 In-vessel and ex-vessel PHTS nodalization

A description of the MELCOR nodalization is summarized below. Mass and enthalpy of pressurized water and other non-condensable gases in the VV, VVPSS and BZ and FW primary cooling loop have been nodalized with 275 different control volumes using the MELCOR CVH package. These volumes have been connected with 375 mass and heat flow paths using the MELCOR FL package.

The whole DEMO reactor has been modelled in three different regions simulating:

- 1 sector, which modules usually are the subject of the accident analysis;
- a group of 7 sectors (from sector 2 to sector 8);
- a group of 8 sectors (from sector 9 to sector 16).

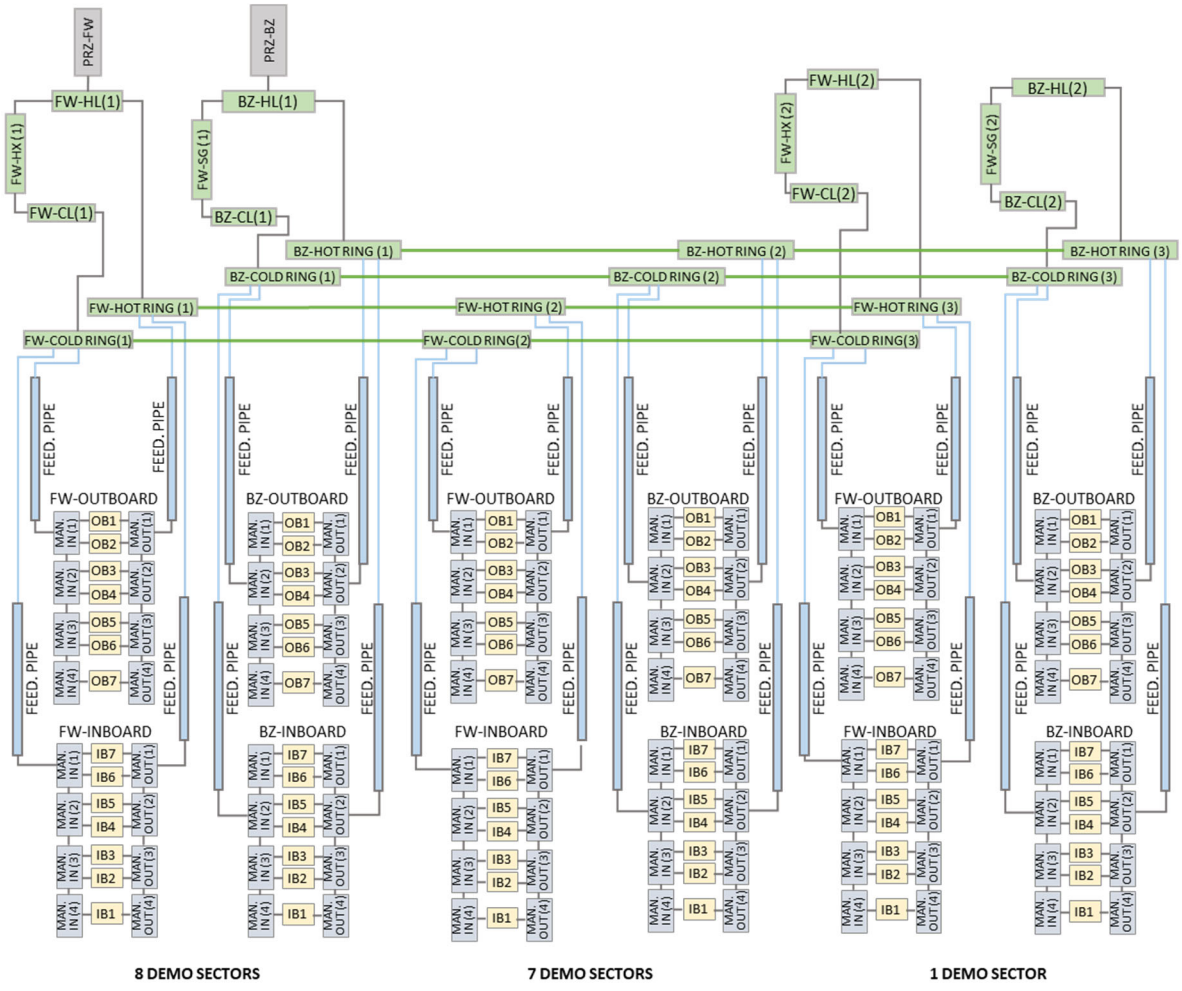

Figure 5.1.1 - Thermal hydraulic MELCOR nodalization scheme of the DEMO reactor

These three main regions are connected to ex-vessel components contained in the TCR (Figure 5 1) through control volume simulating EU DEMO feeding pipes. Each sector has been modeled in order to investigate both inboard and outboard segment behaviour during the accident sequence. Volumes from OB1 to OB7 (IB1 to IB7), connected to the manifold volumes, have been modelled separately. Water enters and exits each sector through inlet and outlet feeding pipes (Figure 5.1.3) connecting BM manifolds (Figure 5.1.2) with ring distributors. These are connected to the steam generators through hot and cold legs. Isolation valves in the OB loop (and in the IB loop also) have been foreseen to limit the amount of water entering in the TCR in case of LOCA. These valves are installed on the hot and the

cold legs of FW PHTS (upstream valves), and on the pipes connecting the loop collectors to the BB (hot/cold) manifolds (downstream valves). Furthermore, safety relief valves (SRVs), discharging in a suitable drain tank, similar to VVPSS, should be installed before each downstream trip valve to avoid overpressure in the loop after isolation valve closure.

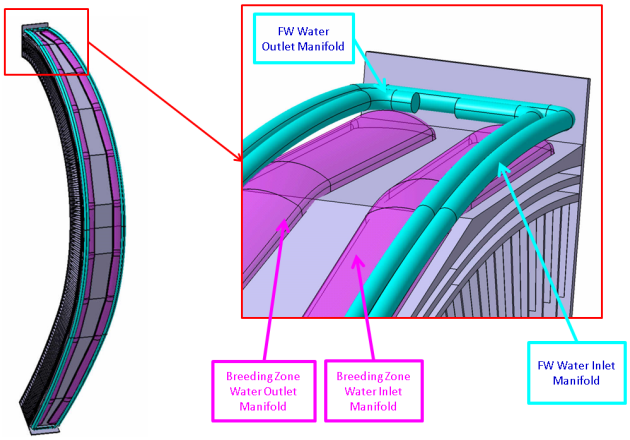

Figure 5.1.2 - BZ and FW cooling water manifolds [32]

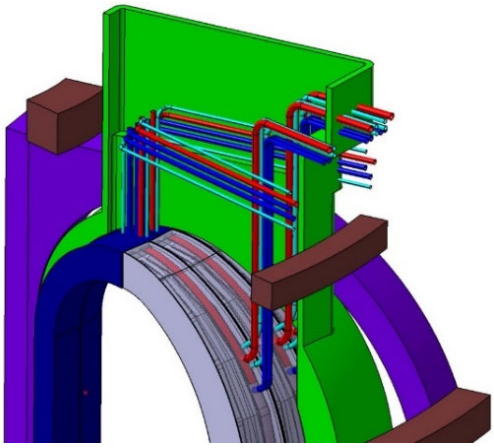

Figure 5.1.3 – DEMO sector piping system [32]

Inlet and outlet pipes are placed at centre of the manifolds and at the top of the manifolds, respectively for outboard segment and inboard segment.
In the Table 5.1-1 the main characteristics of the feeding pipe system nodalization for the first region simulating only 1 sector are reported. The different lengths of the feeding pipes tubes are related to the fact that the cold and hot collector rings are placed at different quote, as well as inboard modules are fed at the top of the segments while outboard modules are fed at about 1/3 of the poloidal height of the segments (from the top) [48].

Table 5.1-1 - Hydraulic parameters for feeding water pipes

Feeded manifold	**Hydraulic Diameter [m]**	**Flow Area [m^2]**	**Length [m]**	**Volume [m^3]**
OB-BZ (Inlet)	0.159	0.0199	19.5	0.7994
OB-BZ (Outlet)	0.159	0.0199	23.16	0.7994
OB-FW (Inlet)	0.092	0.00665	14.99	0.2660
OB-FW (Outlet)	0.092	0.00665	16.75	0.2600
IB-BZ (Inlet)	0.104	0.00861	15.8	0.3445
IB-BZ (Outlet)	0.104	0.00861	18.5	0.3445
IB-FW (Inlet)	0.064	0.00324	10.5	0.1297
IB-FW(Outlet)	0.064	0.00324	12.5	0.1297

As specified in the WCLL design description document [48], water manifolds have a length of 14.0 m ad 12.0 m, respectively for BZ and FW systems. For such a reason, to take into account hydrostatic pressure gradients, the manifolds volume has been nodalized by splitting them in different volumes linked by flow path. In Table 5.1-2 the main characteristics of the manifold nodalization are reported.

Table 5.1-2 - Hydraulic parameters for water manifolds

Feeded manifold	Hydraulic Diameter [m]	Flow Area [m^2]	Length [m]	Volume [m^3]
OB-BZ (1)	0.177	0.09	3.5	0.4032
OB-BZ (2)	0.177	0.09	3.0	0.3456
OB-BZ (3)	0.177	0.09	3.0	0.3456
OB-BZ (4)	0.177	0.09	4.5	0.5184
OB-FW (1)	0.0963	0.01768	3.5	0.1503
OB-FW (2)	0.0963	0.01768	3.0	0.1289
OB-FW (3)	0.0682	0.0065	3.0	0.1289
OB-FW (4)	0.0682	0.0065	2.5	0.1074
IB-BZ (1)	0.109	0.02892	4.5	0.1302
IB-BZ (2)	0.109	0.02892	3.0	0.0868
IB-BZ (3)	0.109	0.02892	3.0	0.0868
IB-BZ (4)	0.109	0.02892	3.5	0.1013
IB-FW (1)	0.066	0.005479	2.5	0.0393
IB-FW (2)	0.066	0.005479	3.0	0.0471
IB-FW (3)	0.066	0.005479	1.5	0.0236
IB-FW (4)	0.066	0.005479	1.5	0.0236
IB-FW (5)	0.066	0.005479	3.5	0.055

FW and BZ manifolds distribute water to the overall modules; even if since 2016 design the BB segment is designed as single segment concept, the overall segment has been divided in seven different volumes to correctly evaluate hydrostatic pressure gradient and also to take into account the poloidal distribution of the decay heat distribution (Figure 5.1.4).

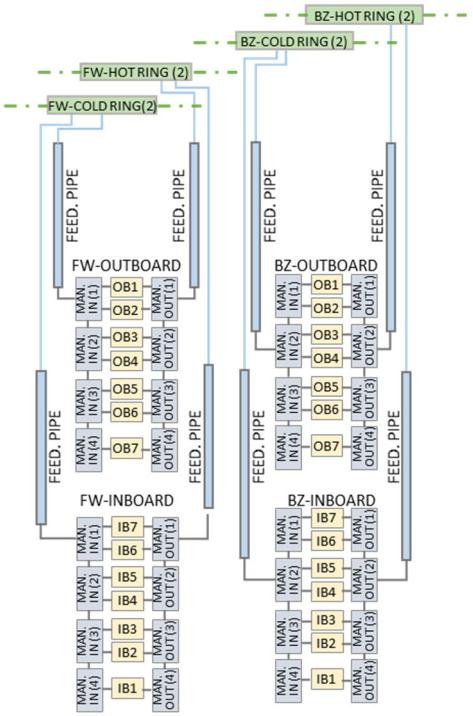

Figure 5.1.4 - Thermal hydraulic nodalization scheme of one segment

To correctly size each inboard and outboard module, data from WCLL DDD 2017 have been used. Data in Table 5.1-3 have been obtained considering that each breeding unit has a total height of 135 mm, a

radial thickness of about 440.0 mm in the inboard and 530.0 mm in the outboard segment. The total number of tubes of one breeding unit is 24 for the BZ and 10 for the FW. The total lengths of the tube have been calculated from data in [50].

Table 5.1-3 - Breeding modules nodalization and water inventory (1 sector)

Volume	Number of breeding unit	Volume BZ channels [m^3]	Volume FW channels [m^3]
OB-1	8	0.0519	0.0306
OB-2	17	0.1104	0.065
OB-3	17	0.1104	0.065
OB-4	16	0.1039	0.0612
OB-5	16	0.1039	0.0612
OB-6	16	0.1039	0.0612
OB-7	17	0.1104	0.0650
IB-1	14	0.0443	0.0178
IB-2	17	0.0538	0.0217
IB-3	18	0.057	0.0229
IB-4	18	0.057	0.0229
IB-5	9	0.0285	0.0115
IB-6	9	0.0285	0.0115
IB-7	8	0.0253	0.0102

The inventory of water for the in-vessel components is estimated by summing-up the water inventory of feeding pipes, manifolds and breeding modules.

Table 5.1-4 – Total in-VV water Inventory

Description	Sector 1 [m^3]	Sector 2 to 8 [m^3]	Sector 9 to 16 [m^3]	Total [m^3]
IB FW	0.1186	0.8302	0.9488	1.8976
IB BZ	0.2945	2.0615	2.356	4.712
IB FW manifold	0.371	2.597	2.968	5.936
IB BZ manifold	0.81	5.67	6.48	12.96
IB FW feeding pipe	0.2922	2.0454	2.3376	4.6752
IB BZ feeding pipe	0.5824	4.0768	4.6592	9.3184
OB FW	0.4090	2.863	3.272	6.544
OB BZ	0.6947	4.8629	5.5576	11.1152
OB FW manifold	1.0308	7.2156	8.2464	16.4928
OB BZ manifold	3.2256	22.5792	25.8048	51.6096
OB FW feeding pipe	1.1876	8.3132	9.5008	19.0016
OB BZ feeding pipe	1.782	12.474	14.256	28.512
Total				137.0

Coolant inventory data are in good agreement with those reported in [50]. The total DEMO in VV BZ cooling system inventory of water (without considering feeding pipes) is 80.4 m^3, and the total DEMO in VV FW cooling system inventory (without considering feeding pipes) is 30.87 m^3. The nodalization scheme of ex-vessel PHTS components is shown in Figure 5.1.5 and includes:

- Loop distributor outlet to distribute the outlet hot water from the BB;
- Loop distributor inlet to distribute the inlet cold water from steam generators;

- Steam generators;
- Hot and cold legs;
- Pumps;
- Pressurizers.

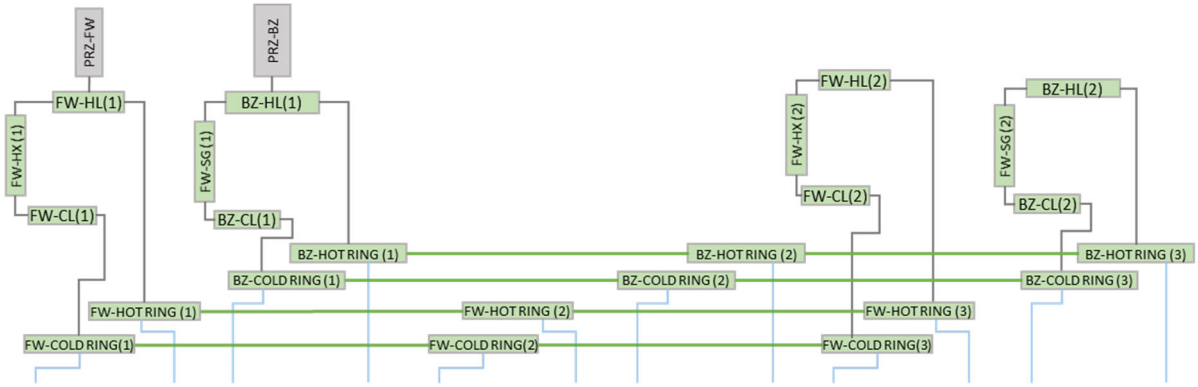

Figure 5.1.5 - Thermal hydraulic nodalization scheme of the DEMO PHTS

Both cold and hot ring distributors have been modeled, resulting in 4 control volume for each of the three regions. In the Table 5.1-5 the details of the nodalization are shown.

Table 5.1-5 - Hydraulic parameters for ring distributors pipes

Description	**Hydraulic Diameter [m]**	**Flow Area [m^2]**	**Length [m]**	**Volume [m^3]**
FW Inlet (1 sect.)	0.3	0.1164	9.875	0.633
FW Outlet (1 sect.)	0.3	0.1164	9.875	0.633
BZ Inlet (1 sect.)	0.56	0.2463	9.875	2.21
BZ Outlet (1 sect.)	0.56	0.2463	9.875	2.21
FW Inlet (7 sect.)	0.3	0.1164	69.125	4.431
FW Outlet (7 sect.)	0.3	0.1164	69.125	4.431
BZ Inlet (7 sect.)	0.56	0.2463	69.125	15.47
BZ Outlet (7 sect.)	0.56	0.2463	69.125	15.47
FW Inlet (8 sect.)	0.3	0.1164	79.0	5.064
FW Outlet (8 sect.)	0.3	0.1164	79.0	5.064
BZ Inlet (8 sect.)	0.56	0.2463	79.0	17.68
BZ Outlet (8 sect.)	0.56	0.2463	79.0	17.68

The total length of each ring distributor is 158.0 m. In the Table 5.1-6 the nodalization of steam generator and hot and cold legs is detailed.

Table 5.1-6 - Hydraulic parameters for ring distributors pipes

Description	**Hydraulic Diameter [m]**	**Flow Area [m^2]**	**Length [m]**	**Volume [m^3]**
FW Steam Generator (1)	-	-	-	23.7
FW hot leg (1)	0.36	0.101	11.0	1.28
FW cold leg (1)	0.34	0.090	6.42	0.745
BZ Steam Generator (1)	-	-	-	19.7
BZ hot leg (1)	0.66	0.341	25.25	10.68
BZ cold leg (1)	0.44	0.151	7.56	3.085

The BZ loop is connected to a pressurizer, operating at a nominal pressure of 15.5 MPa, with a total volume of 106 m^3, half filled with liquid water. The FW-PHTS pressurizer has a total volume of 50 m^3 and contains 25 m^3 of liquid water [50]. The pressurizers have been equipped with safety relief valves discharging in a suitable suppression tank to avoid overpressure in the BZ channels. The ex-vessel water total inventory is:

- 103 m^3 for the FW-PHTS
- 190.6 m^3 for the BZ-PHTS

The heat flow between a control volume and a component structure as well as that between two component structures have been taken into account by using the MELCOR HS package.

Lithium-lead in modules, divertor loops and first wall have been simulated through one dimensional heat structures following the scheme reported in Figure 5.1.6. The FW is modeled into two heat structures. The first heat structure models the heat transfer between the plasma volume and the coolant in the FW. The second heat structure models the heat transfer between the FW coolant and the BZ, which is simulated with a multiple layer HS of EUROFER and LiPb. The total FW surface is equal to about 1445 m^2, 507.18 m^2 for the IB sectors and 937.79 m^2 for the OB sectors.

During a LOCA, the lack of coolant can cause a temperature increase from decay heat. To investigate the capability of decay heat removal, a radiative structure-to-structure model is included in the analysis simulating thermal radiation from the BSS (last layer of BZ-HS) towards VV. The left surface of VV is maintained at 200°C to simulate the VV-PHTS and the presence of the decay heat removal system. However, the described VV nodalization allows also for convective heat exchange between the BSS and the steam flowing at high velocity in the interspace volume between the BSS and VV structure (CV853).

Decay heat of BB modules has been simulated as a volumetric heat generation into the heat structure. It is calculated, according to [60], as sum of contribution of BM caps and lateral walls, BM material mixture, BM back wall and BM back support and manifold.

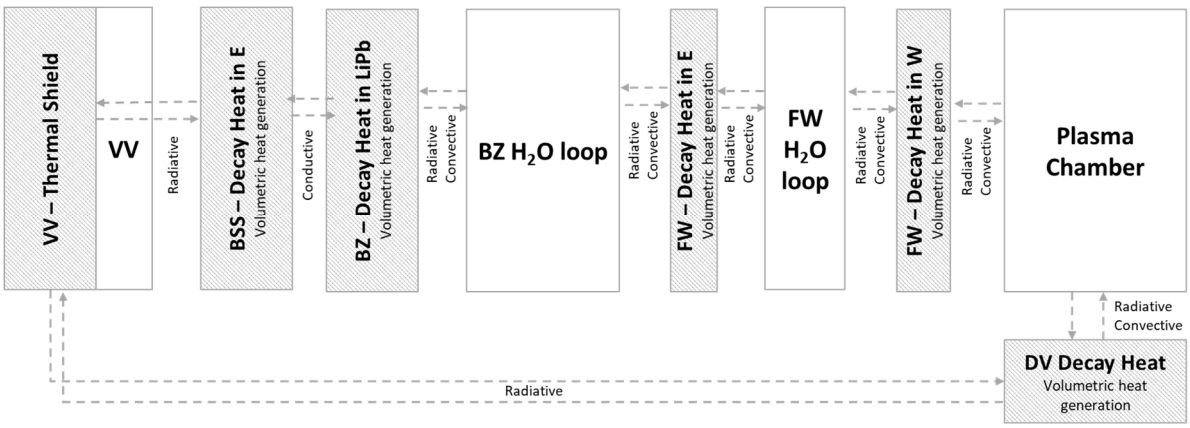

Figure 5.1.6 – MELCOR HS-CVH coupling

Vacuum vessel and external environment have been simulated with equivalent control volume. The left surface of VV is maintained at 200°C.

5.2 Vacuum vessel and VVPSS nodalization

The total in-VV volume available for steam expansion is about 6400 m^3: 1500 m^3 for the upper port volume, 2000 m^3 for the lower port volume and 2900 m^3 for the plasma chamber volume.

VV and VVPSS nodalization scheme is shown in Figure 5.2.1. The VV has been modeled with five different control volumes to consider the right position of all the connections simulating the plasma chamber, the upper port, the lower port, the interspace volume between the divertor and the VV structure (CV852) and the interspace volume between the back-supporting structure (BSS) of BB modules and VV structure (CV853). The preliminary dimensions and free volumes of these zones have been evaluated from EU DEMO baseline CAD model [31], which represents the components at "room temperature". Hence, the flow areas from the CAD are not real at the operating conditions, during which the thermal expansion of the structures may lead to a different configuration of the steam path toward the VVPSS. A very conservative hypothesis has been selected for this MELCOR model, by scaling some flow area with a factor 10 assuming segments and divertor cassettes dilatation. Flow area data are provided in Table 5.2-1.

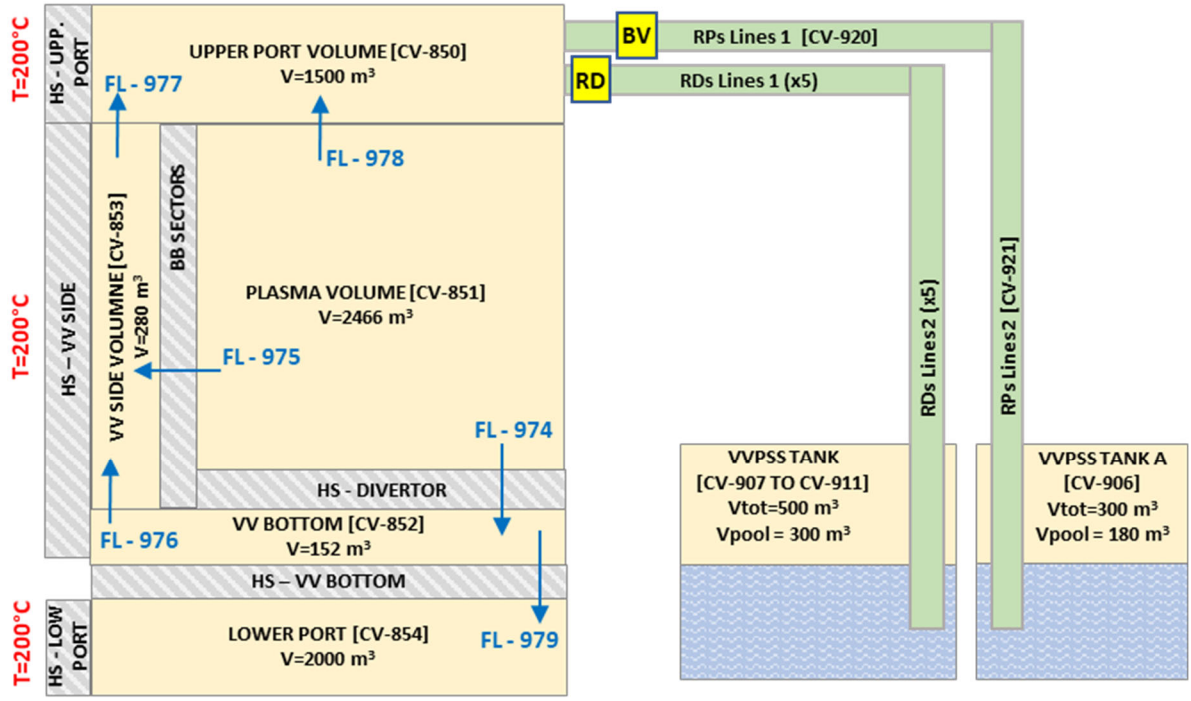

Figure 5.2.1 – VV and VVPSS nodalization scheme

Table 5.2-1 – VV flow phat

ID	Baseline model FLARA [m²]	Conservative FLARA [m²]
FL974	5.770	0.577
FL975	23.52	2.352
FL976	1.790	1.790
FL977	6.300	6.300
FL978	1.070	0.107
FL979	6.330	6.330

The developed model for the VVPSS consists of 17 control volumes and 18 flow paths. Each tank has been modeled separately (CV906 - CV911) with the associated rupture disks (RD) and bleed lines (BL). VVPSS components have been initialized at 40°C and 9.5 kPa.

Results of DBA described in 6.1.1 suggested to use the following flow area for bleed lines and rupture disk lines:

- Each bleed line has a flow area of 0.1 m^2, for a total flow area available for discharging steam in TANK A of 0.6 m^2.
- Each rupture disk line has a flow area of 1.6 m^2, for a total flow area available for discharging steam in TANK B to F of 8.6 m^2.

Tank A has a volume of 300 m^3 and contains 180.0 m^3 of subcooled water (40°C at 9.5 kPa). Each RD tank has a volume of 500 m^3 filled with 300 m^3 of subcooled water.

Basing on the ITER experience on VVPSS, each tank of the suppression system has to provide a suppression function, also the one connected to the bleed lines.

5.3 TCR nodalization

In this preliminary phase of the EU DEMO tokamak building design, connections are provided only between three compartments of the entire building:

- the Upper Pipe Chase (UPC) volume (Figure 5.3.2) where are located hot and cold PHTS distributor rings;
- Vertical Shaft (VS) volumes (Figure 5.3.3) which host divertor and limiters PHTS pipework;
- Lower Pipe Chase (LPC) volumes (Figure 5.3.4) where are routed all the pipework incoming and outgoing from the lower port, including the LiPb equipment.

Other compartments such as the PHTS area, housing cooling pipes and heat exchangers of the power conversion system, and the top maintenance hall, hosting remote handling equipment, are not connected to the previous compartments.

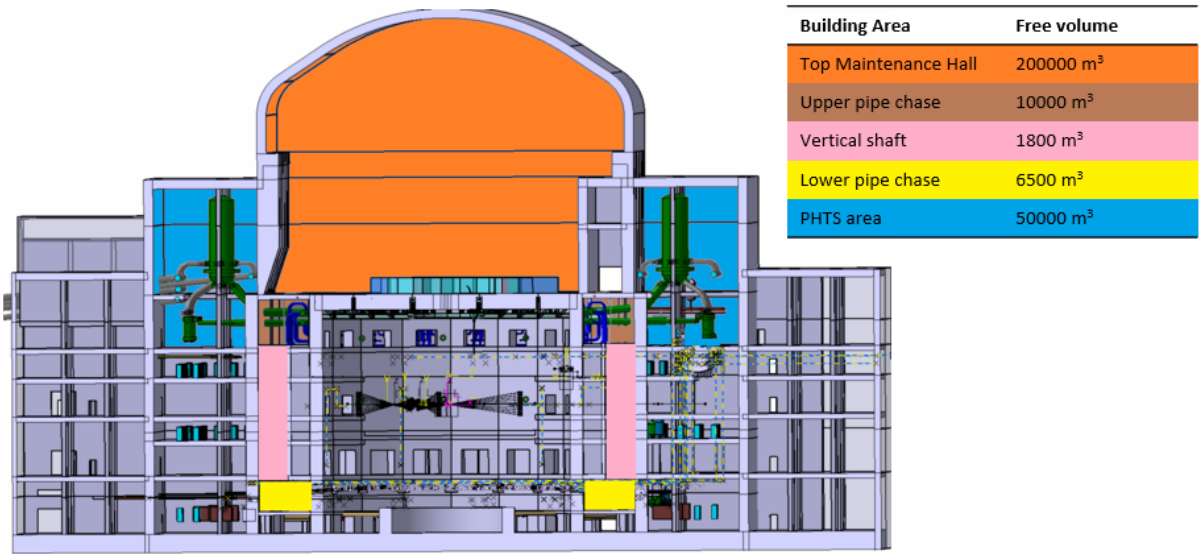

Figure 5.3.1 – Tokamak building compartment and free volumes available for steam expansion

Thus, in case of ex-vessel LOCA in the PHTS equipment area, around 50000 m^3 are available for steam expansion, however, if a break will occurs in the Upper pipe chase compartment the available volume is reduced to 18300 m^3 and probably is not enough to stay below the pressure limit imposed by design criteria.

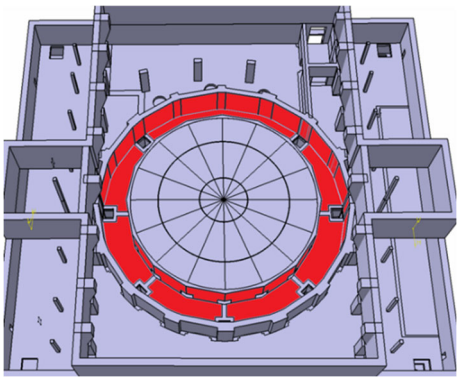

Figure 5.3.2 – Upper pipe chase volume (in red)

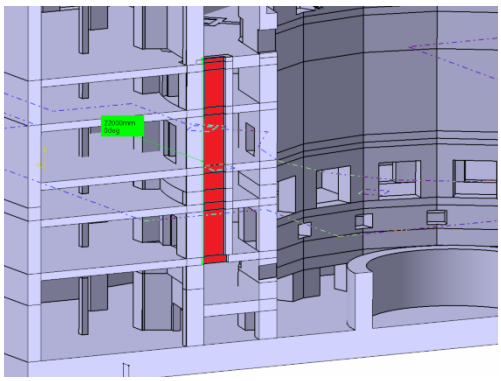

Figure 5.3.3 – Vertical shaft (in red)

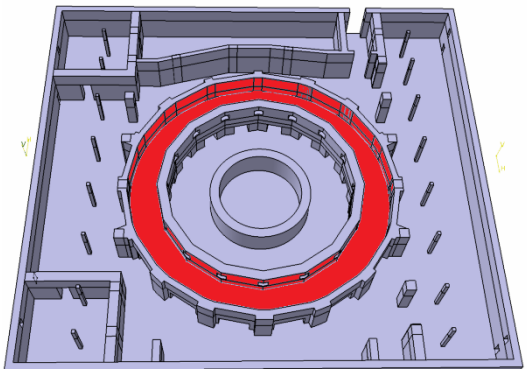

Figure 5.3.4 - Lower pipe chase (in red)

A simplified model scheme of the EU DEMO WCLL tokamak building has been made with the MELCOR code (Figure 5.3.5) in order to evaluate the thermal hydraulic behavior of main tokamak compartments during ex-vessel LOCA scenarios. The containment has been modeled with five control volumes (CV830 – CV834) and four flow path (FL980 – FL983) to simulate the expansion volumes and the connection of the EU DEMO containment which CAD model is reported in Figure 5.3.1.

The containment passive heat structures have been modeled, in particular for the evaluation of the aerosol deposition and for heat transfer with the external environment simulated with a time independent control volume (CV860) at the temperature of 30 °C and atmospheric pressure.

Table 5.3-1 – Containment flow path

ID	Description	State	FLARA [m^2]
FL980	7 VSs openings connecting UPC and VS	-	81.9
FL981	7 VSs openings connecting VS and LPC	-	81.9
FL982	Connection between UPC and PHTS area	Closed: actually any connection is foreseen	Not available
FL983	Connection between PHTS area and dome vault	Closed: actually any connection is foreseen	Not available

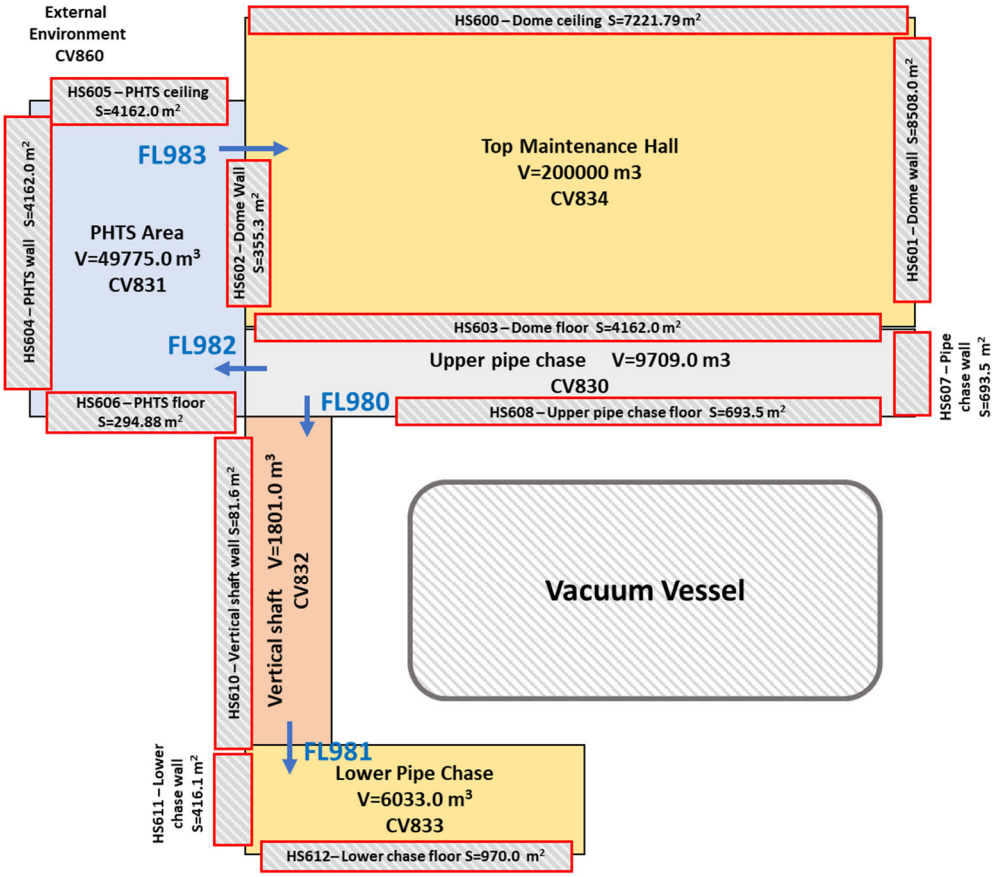

Figure 5.3.5 – MELCOR tokamak containment building nodalization

5.4 Divertor model

The divertor has been simulated with a two-layer rectangular heat structure having a total surface of 130.20 m^2 (equal to PFCs divertor surface). The upper layer simulating the PFCs is made of Tungsten. The second layer simulating the CB is made of EUROFER. The layer thickness has been modeled in order to obtain the correct divertor volume [42]. Volumes of water are not considered for the geometry definition of the HS.

Table 5.4-1 – Divertor model data

	Surface [m^2]	Thickness [m]
Tungsten Layer	130.2	0.0122
EUROFER Layer	130.2	0.2787

5.5 Source term modeling

In the safety analyses performed, the mobilized radioactive materials are activated dust and tritium (as tritiated water, HTO) from the VV, and HTO and activated corrosion products (ACP) from the failed FW/BL PHTS cooling loop [20].

The total W-dust inventory in the VV is 694 kg (5 kg of dust are due to the plasma disruption). This mass has been input to the problem as 2.11 µm mass median diameter particle into the atmosphere phase of plasma volume (CV851) at the beginning of the problem.

The mobilizable in-vessel tritium is 671.0 g. Tritium is assumed to be in the form of HTO; as a result of the coolant ingress within the VV, 4.454 kg of HTO are considered. The tritium concentration in primary

cooling system is 0.015 g-T/m^3 water, the total amount of tritiated water is 18.1 g in the FW-PHTS and 32.0 g in the BZ-PHTSS. The quantity of ACP in a FW/BL PHTS loop is 10 kg. A mobilization fraction of 7% has been used for ACP.

Source term data have been taken from DEMO safety data list [20].

6 Design basis accident analyses

Design basis accidents (DBAs) are those accident to be considered in the design phase of a power plant. In particular, DBAs must be analyzed using conservative assumptions to put specific requirements and limits on the design to ensure that they do not propagate to the stage that a release occurs. These limits must be set such that no key plant parameters exceed these limits in these design basis accident situations, it could be a pressure limit, or set-points for some safety operation such as closure of trip valves, triggering of rupture disks or opening of relief valves. Results of these analyses also define maximum loading conditions for the systems, structures and components involved in the accident scenario [62].

Design basis accidents are categorized according to their expected frequency, evaluated as the sum of the failure rate of the single failures occurring as a consequence of the initiating event. Because of the lack of operating experience for fusion power plant, data sources coming from nuclear, chemical and industrial fields have been used to quantify the probability of failure fore single component.

Table 6.1 - Frequency categories for design basis events [62]

Category	Description	Frequency/year
I	Normal operational events	> 1
II	Likely events (incidents)	10^{-2}–1
III	Unlikely events (accidents)	10^{-4} – 10^{-2}
IV	Extremely unlikely events (accidents)	10^{-6} – 10^{-4}

- Category I events are operational events and plant conditions planned and required for DEMO normal operation, including some fault events which can occur as a result of the DEMO intrinsic nature;
- Category II events includes likely event sequences not planned but likely to occur one or more times during the life of the plant but not included in Category I;
- Category III events are unlikely event sequences that are postulated but not likely to occur during the life of the plant;
- Category IV bounds extremely unlikely event sequences that are postulated but are not likely to occur during the life of the plant with a very large margin.

The identification and selection of DBA is the result of a Failure Mode and Effect Analysis (FMEA), based on a top-down approach, performed by means of the following steps:

- A full list of the possible failure modes is identified for each component;
- The possible actions that could prevent the failure of each failure mode are identified for each component;
- The possible consequences, and the actions that could prevent or mitigate each accident scenario are identified.

The outcome of the FMEA analysis is a list of elementary failures. However, because of the wide range of possible failures, the grouping of the postulated initiating events (PIEs) leading to the same consequences for the plant is usually done.

In the current pre-conceptual design stage of the European DEMO reactor, a FFMEA has been completed for all EU DEMO key systems and led to the selection of 21 Postulated Initiating Events

(PIEs) that envelope all identified failures [63]. In particular, in-vessel LOCA has been classified among the most representative events in terms of challenging conditions for plant safety, because it could cause substantial damage to components in the VV.

The preliminary thermohydraulic analyses of loss of coolant accidents for the WCLL EU DEMO concept are reported below. In particular, different accident scenarios have been studied:

- Two different accident scenarios related to the design of VVPSS;
- Two ex-vessel loss of coolant accident, involving the failure of FW and BZ, respectively;
- An in-vessel loss of coolant accident;
- A preliminary study of an in-box LOCA.

6.1 Multiple First Wall/Blanket PHTS pipe break inside the vacuum vessel

Parametric accident analyses of an in-vacuum vessel LOCA have been performed to determine the minimum flow area of VVPSS rupture disk pipes needed to maintain VV pressure below 2 bar. Two different studies have been performed:

- A “worst case” accident scenario involving the simultaneous failure of both FW and BZ PHTS;
- A “baseline case” scenario in which Inner Wall protection Limiters (IWLs) are foreseen to adsorb the plasma energy deposited by an unmitigated plasma shutdown, preventing the failure of plasma facing components and associated cooling system

Limiters could be foreseen in different areas of the DEMO first wall to prevent the plasma to touch the breeding blankets PFCs during all plasma transients such as ramp-up (which happens at every single pulse), Vertical Displacement Event (VDE) and loss of confinement. DEMO limiters must withstand very high heat fluxes for such a reason their design follows the monobloc approach, similarly to the divertor. However, unlike the divertor, which has to withstand a high steady-state heat flux, the heat flux for the limiters can be extremely high, but at the same time the duration of these loads are short [64]. Thermal loads can be so large that the plasma facing tungsten monoblocs can be damaged (i.e.: melted, evaporated, cracked), therefore the limiters may require more frequent replacement than the BB system [64].

In both the accident scenarios the postulated initiating event is a double-ended guillotine break of the BZ feeding pipe located inside the upper port, for a total break area of 0.0523 m^2. The primary cooling system involves a large amount of energy due to the pressurized water coolant (15.5 MPa), therefore the pressurized steam spilled into the vacuum vessel may damage the VV structures causing a loss of confinement function.

An unmitigated plasma disruption occurs because of the presence of steam and other impurities at the plasma edges. If the disruption is faced by the limiters, no additional leaks occur. While, if limiters fail and the temperature of the plasma facing structures affected by the plasma disruption increases up to the limit temperature for the EUROFER wall further steam and water are discharged inside the plasma volume. The unmitigated disruption affects 2 different outboard segments one of which will be completely broken and the other partially broken, causing the break of 262 FW channels, for a total break area of 0.02568 m^2.

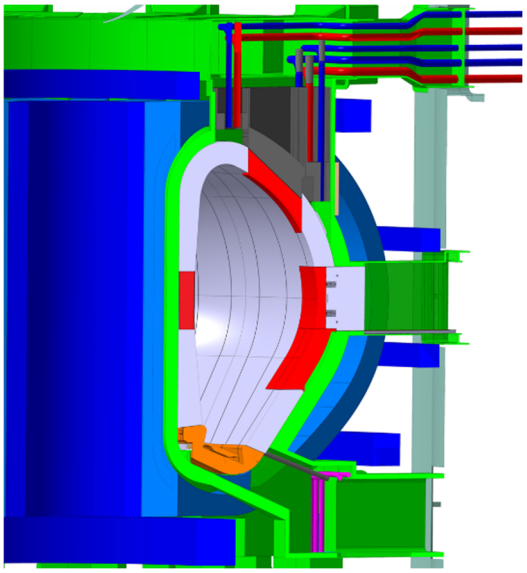

Figure 6.1.1. DEMO poloidal cross-section with inboard-midplane, upper, outboard midplane, and outboard lower limiters (in red)

The parametric study includes 11 simulations performed by varying the rupture discs flow area for both "worst case" and "base line case" accident scenarios.

6.1.1 Worst case scenario: Results and discussion

The postulated initiating event is a break in BZ-PHTS feeding pipe during plasma activity. Coolant is discharged inside the VV upper port volume. The fusion power is terminated through an unmitigated disruption with the possibility of further breaks in the FW cooling channels because of quick temperature transient due to high heat flux.

6.1.1.1 Event Sequence

Analysis requirements and main input data have been obtained from DEMO safety data list [20].

Table 6.1-1 – Possible transient sequence for a DBA with the failure of limiters function

Parameter	Specification
Definition of initiating event	Failure (guillotine break) of the BZ feeding pipe located inside the VV in the upper port region.
Possible transient sequence	▪ A double break size in the FW-PHTS distributor ring occurs, for a total break area of 0.2328 m^2; ▪ Fusion power is terminated by an unmitigated disruption affecting a plasma facing structure area of 1 m^2; ▪ Limiters fail to protect the BZ plasma facing structure; ▪ If melting temperature of the EUROFER is reached in the affected area the FW pipes breaks causing water injection inside the plasma volume. The failure of the FW structure affects only few millimetres of EUROFER, in such a way only water and steam contained in the FW-PS enters in the plasma chamber, while the LiPb mass remains inside the BZ modules not affected by any rupture; ▪ The FW of the failed loop is first cooled down with residual water present before complete emptying; ▪ After the coolant inventory is lost the FW will be cooled by radiation to the surrounding cooled in-vessel components;

- If an in-vessel LOCA occurs the bleed lines and rupture disks open at reaching the pressure set point;
- Isolation valves close when the set-point is reached;
- Coolant and radioactive inventories (tritium, dust and suspended sputtering/ACPs products) will be mobilized towards the TCR or toward the VV
- Feedwater pump stops immediately after the LOCA in the PHTS
- DHR system in operation for all the entire transient

6.1.1.2 Results and discussion

The postulated initiating event is supposed to occur at time t=0.0 s after a steady-state of 2000 s. Water mass flow rate transient from the feeding pipe rupture in the upper port in-vessel region (Figure 6.1.2) is characterized by an initial rapid increase where the maximum of about 2975.6 kg/s is achieved, 0.6 s after the guillotine break. The total amount of water discharged in the VV from the BZ-PHTS is 116802.0 kg (Figure 6.1.3). The connection between the upper port and the plasma volume allow for the injection of steam inside the plasma volume. The presence of steam impurities at the plasma edges causes an unplanned plasma termination with consequent deposition of plasma thermal and magnetic energy and on plasma facing components. As a result, FW temperature increases until the limit of 1000°C, causing the failure of 262 FW channels. About 51 tons of additional water are discharged in the plasma volume (Figure 6.1.3).

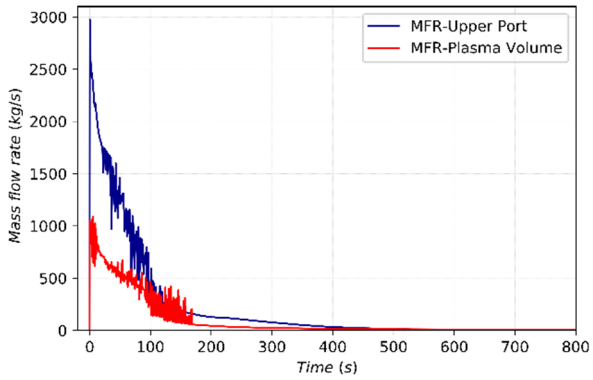

Figure 6.1.2 - MFR into upper port and plasma volume (Case_RD_1.6)

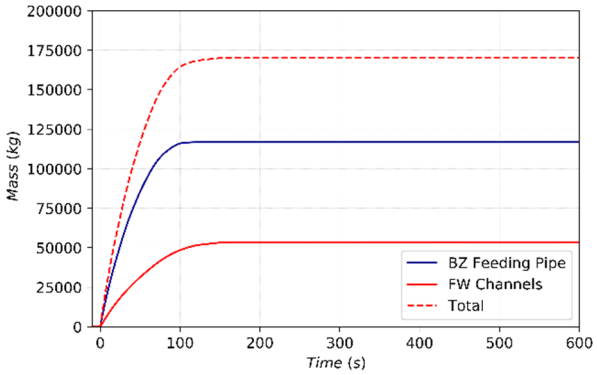

Figure 6.1.3 – Total mass discharged inside the VV (Case_RD_1.6)

The pressure response in the FW and BZ pressurizer is reported in Figure 6.1.4, while the pressure transient in-vessel OB4 volume cooling system is reported in Figure 6.1.5. Hot and cold leg of both PHTS are equipped with isolation valves, which begin to close when the pressure in the pressurizer is below 13.0 MPa. The signal for the detection of the abnormal event has a delay of 3 s and 7 additional seconds closure time of the valve is assumed. This set-point is reached 7.403 s and 8.34 s after the PIE for BZ and FW primary cooling system, respectively. The fully closed state is reached 10 s after the signal activation, when the pressure in the FW pressurizer is about 11.0 MPa and the pressure in the BZ pressurizer is 10.91 MPa. Because of the position of the breaks, upstream trip valves don't completely mitigate the depressurization of the PHTSs. In-vessel volumes, as well as distributor ring and feeding pipes, reach the equilibrium with the VV volumes 890 s after the PIE.

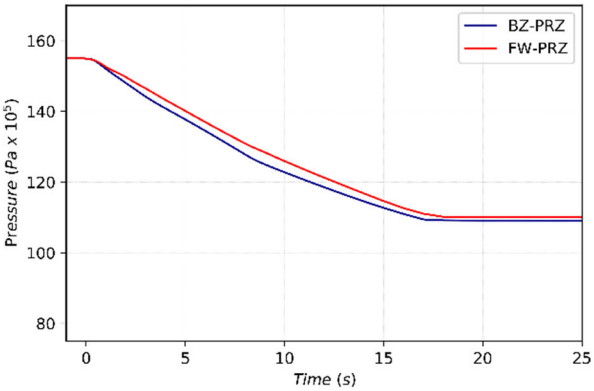

Figure 6.1.4 - Pressure in FW and BZ PHT pressurizer for a selected case (case RD_1.6)

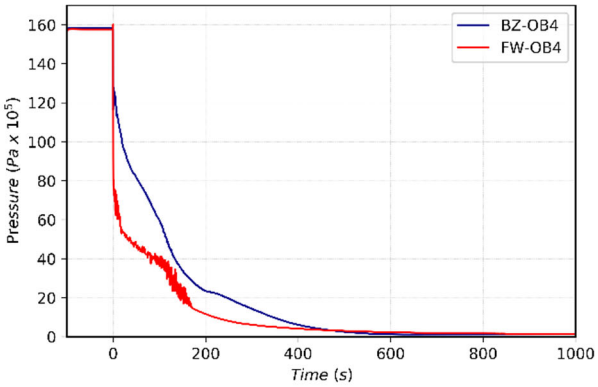

Figure 6.1.5 - Pressure in FW and BZ OB4 volumes (case RD_1.6)

These very large releases of water and steam lead to a rapid pressurization of the upper port and the plasma volumes. The maximum pressure reached in the VV volumes depends on the total flow area available for the discharge of steam in the VVPSS suppression tanks.

Pressure increases very quickly and reaches the first pressure peak of 1.5 bar at about 1.958 s, when the rupture discs open a path between the upper port and the suppression tanks. The timing of this peak is slightly influenced by the discharge area. Once the disks have ruptured pressure inside the VV continue to increase, because the total mass entering the VVPSS is lower than the mass entering the VV (Figure 6.1.11). A second pressure peak is reached at around 9.0 s, which value and timing are reported in Table 6.1-2 for different cases.

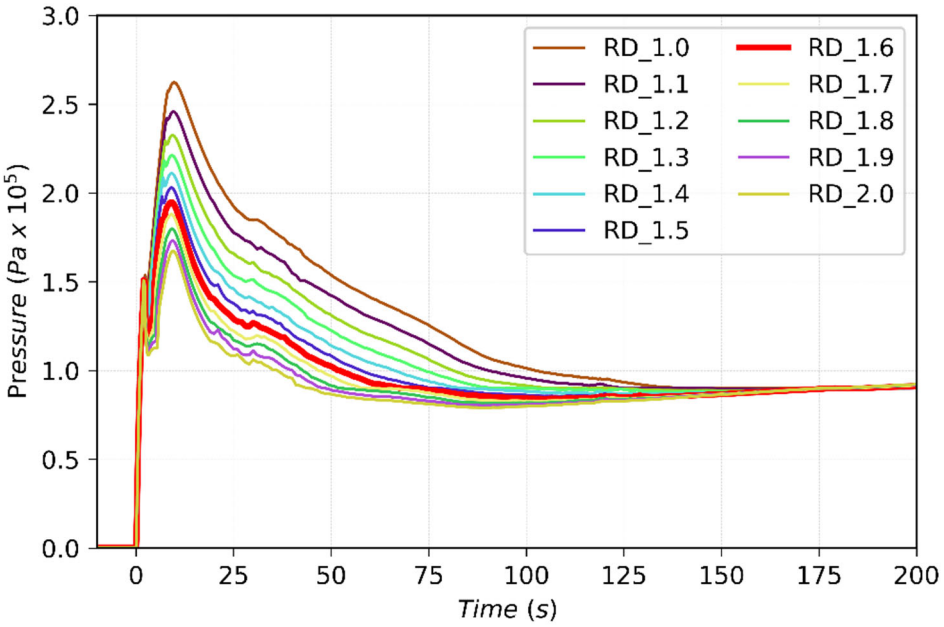

Figure 6.1.6 - Upper port pressure for different rupture disks flow area

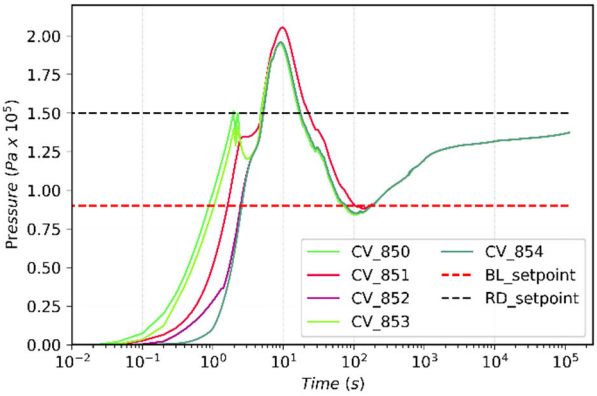

Figure 6.1.7- Pressure in VV volumes and triggering setpoint of RDs and BVs (Case_RD_1.6)

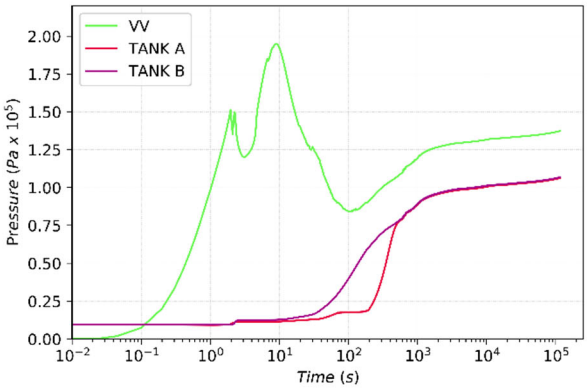

Figure 6.1.8- VV and VVPSS tank pressure (Case RD_1.6)

Table 6.1-2 – Pressure peak inside the upper port for different cases

Scenario	Total dischare flow area [m^2]	Peak pressure [bar]	Time [s]
RD_1.0	6×0.1 (BLs) + 5×1.0 (RDs) = 5.6	2.5967	9.7028
RD_1.1	6×0.1 (BLs) + 5×1.1 (RDs) = 6.1	2.4335	9.5054
RD_1.2	6×0.1 (BLs) + 5×1.2 (RDs) = 6.6	2.3022	9.3008
RD_1.3	6×0.1 (BLs) + 5×1.3 (RDs) = 7.1	2.1898	9.2028
RD_1.4	6×0.1 (BLs) + 5×1.4 (RDs) = 7.6	2.0896	9.1030
RD_1.5	6×0.1 (BLs) + 5×1.5 (RDs) = 8.1	2.0095	9.0003
RD_1.6	**6×0.1 (BLs) + 5×1.6 (RDs) = 8.6**	**1.9291**	**9.0058**
RD_1.7	6×0.1 (BLs) + 5×1.7 (RDs) = 9.1	1.8611	9.0089
RD_1.8	6×0.1 (BLs) + 5×1.8 (RDs) = 9.6	1.78066	9.2080
RD_1.9	6×0.1 (BLs) + 5×1.9 (RDs) = 10.1	1.7139	9.3073
RD_2.0	6×0.1 (BLs) + 5×2.0 (RDs) = 10.6	1.6558	9.5079

"Worst case" transient results shown that in order to maintain vacuum vessel pressure below 200 kPa a total relief flow area of 8.6 m^2 is required. In the design, this flow area will be provided by 5 RDs relief pipes (draining steam in related suppression tanks) and by 6 bleed lines. Flow rates toward the VVPSS are shown in Figure 6.1.9 and Figure 6.1.11, for bleed lines and rupture discs lines respectively.

Bleed lines valves are fully open if pressure in the VV volumes is higher than 90.0 kPa. If pressure drops below this set-point bleed valves are fully closed. As reported in Figure 6.1.9 the higher is the total flow toward the VVPSS the shorter is the time required by the VV pressure to drop below 90.0 kPa. As an example, if RDs lines have a flow area of 2.0 m^2 pressure in VV drops below 90 kPa after 45.0 s, while id RDs lines have a flow area of 1.0 m^2 the pressure of the VV decreases slowly and is below 90 kPa after about 140.0 s.

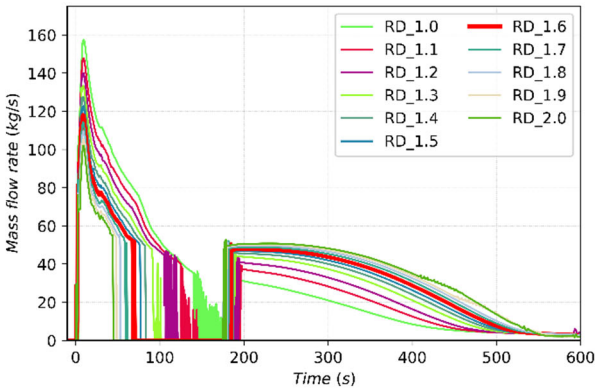

Figure 6.1.9- Mass of steam flowing toward the bleed lines tank (tank A)

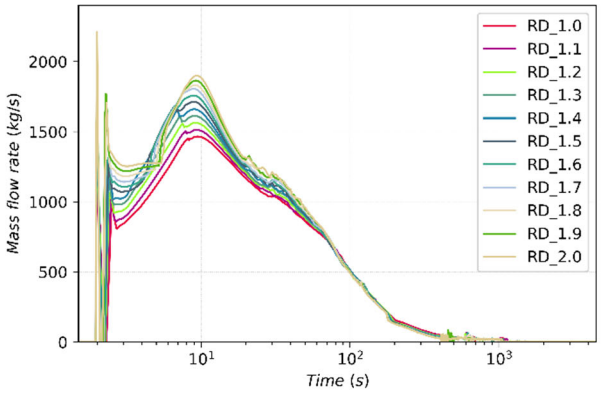

Figure 6.1.10 - Mass of steam flowing toward one rupture disk lines (tank B)

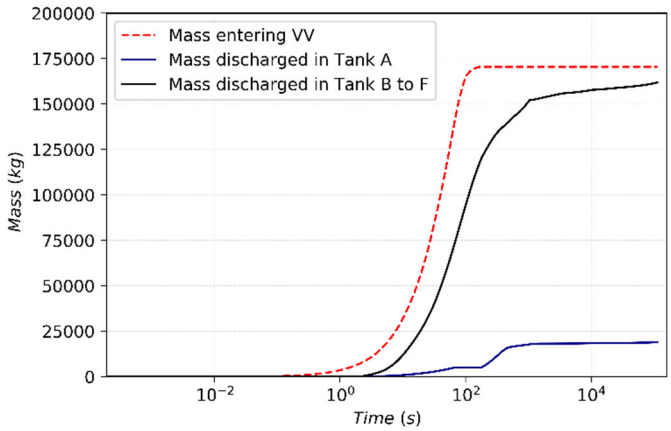

Figure 6.1.11 – Mass entering the VV vs total mass of steam discharged in the VVPSS tanks (Case RD_1.6)

In addition to the substantial VV pressurization, steam injection into the plasma chamber causes the formation of hydrogen by the exothermic reaction between the steam and hot tungsten walls, releasing 156 kJ/mol [65]:

$$W+3H_2O \rightarrow 3H_2 +WO_3$$

Mass of hydrogen in VV and VVPSS volumes are reported in Figure 6.1.12 and Figure 6.1.13, respectively. The total mass of hydrogen inside the VVPSS ranges between 471.0 g (case RD_1.0) and 520.3 g (case RD_2.0) while the one remaining in the VV ranges between 101 g and 150 g. Considering that the initial mass of hydrogen was set to 607.0 g (to take into account the initial mass of tritium inside the VV) the total mass of hydrogen produced ranges between 14.05 g and 14.19 g.

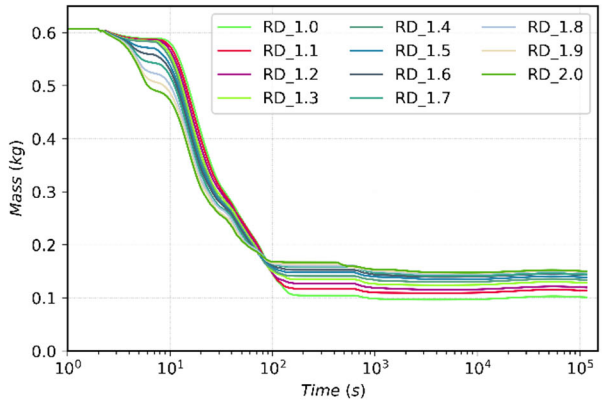

Figure 6.1.12 - Mass of hydrogen in VV volumes

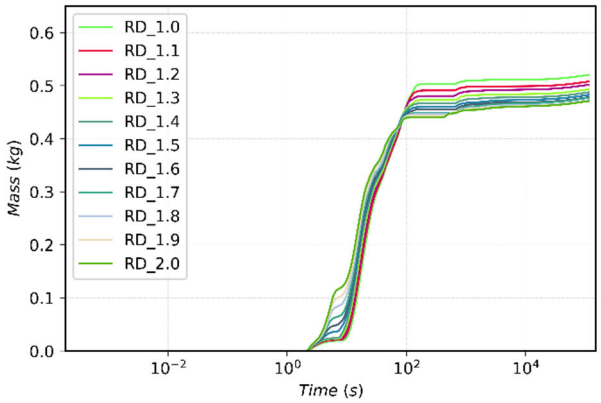

Figure 6.1.13 - Mass of hydrogen in VVPSS volumes

6.1.1.3 Source term mobilization

A benefit of the water ingress in the plasma chamber volume is that tritium, ACPs, and tungsten dust are transported into the VVPSS and will be trapped in the suppression tanks of the VVPSS. Amounts of radioactive material not transported will deposit on vacuum vessel surfaces. Therefore, while this kind of DBA could have a substantial amount of in-vessel damage, there are practically no environmental releases.

Figure 6.1.14, Figure 6.1.15 and Figure 6.1.16 show the total mass of tungsten dust, ACP and HTO in VVPSS volumes for different rupture disc line flow area. Transport of tungsten dust in VVPSS is strongly dependent on steam flow toward VVPPS pipework. Of the 694 kg of mobilizable tungsten dust, about 223.52 kg and 182.015 kg are confined in VVPSS suppression tanks, for case RD_2.0 and RD_1.0 respectively. After 32 h large part of the tungsten dust is suspended in the atmosphere and in the pool of VV volumes being the deposited mass around 3.0 kg for all the cases.

HTO mass follow a very similar behavior. In case of larger RD pipes 1.544 kg of HTO are moved into VVPSS-STs while 2.961 kg remains in the VV volumes. In the opposite case (RD_2.0), 1.727 kg of HTO are transported into the suppression tanks, and 2.733 kg are still in the VV after 32 h from the PIE.

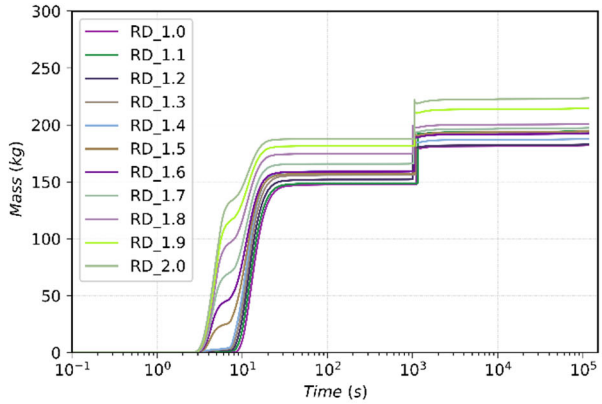

Figure 6.1.14 – Mass of W dust in VVPSS for different RDs flow area

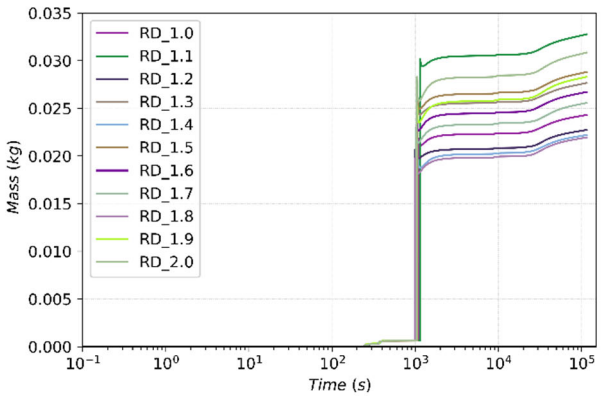

Figure 6.1.15 – Mass of ACP aerosol in VVPSS for different RDs flow area

The mobilization of ACPs inside the VVPSS tanks occurs together with the dry-up of the liquid phase inside the upper port volume. ACP are transferred from the liquid phase into the atmosphere of the volume and then mobilized toward the VVPSS-STs. 32 h after the PIE, of the initial 1.4 kg of ACP in

DEMO, around 800 g remain confined in the PHTS, 575 g are suspended in the VV atmosphere and around 25 g are transferred into the suppression system tanks.

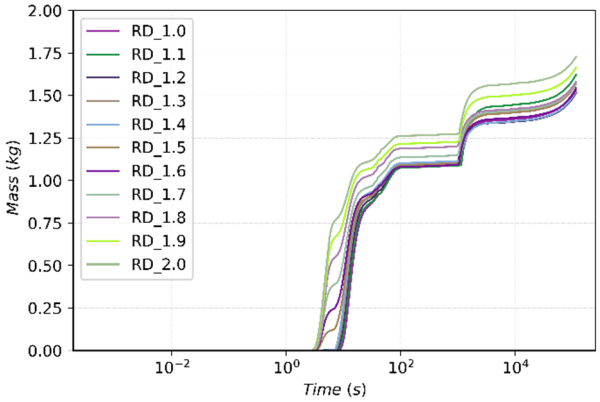

Figure 6.1.16 – Mass of tritiated water in VVPSS for different RDs flow area

6.1.2 Baseline scenario results

The postulated initiating event is a break in BZ-PHTS feeding pipe during plasma pulses. Coolant is discharged inside the VV upper port volume. The fusion power is terminated through a fast plasma disruption which damaging effects are mitigated by inner wall protection limiters.

6.1.2.1 Event Sequence

Analysis requirements and main input data have been obtained from DEMO BB Safety Data List.

Parameter	Specification
Definition of initiating event	Failure (guillotine break) of the BZ feeding pipe located inside the VV in the upper port region.
Possible transient sequence	▪ A double break size in the FW-PHTS distributor ring occurs, for a total break area of 0.2328 m^2; ▪ Fusion power is terminated by an unmitigated disruption affecting a plasma facing structure area of 1 m^2; ▪ Limiters protect the BZ plasma facing structure; ▪ If melting temperature of the EUROFER is reached in the affected area the FW pipes breaks causing water injection inside the plasma volune; ▪ The FW of the failed loop is first cooled down with residual water present before complete emptying; ▪ After the coolant inventory is lost the FW will be cooled by radiation to the surrounding cooled in-vessel components; ▪ If an in-vessel LOCA occurs the bleed lines and rupture disks open at reaching the pressure set point; ▪ Isolation valves close when the set-point is reached; ▪ Coolant and radioactive inventories (tritium, dust and suspended sputtering/ACPs products) will be mobilized towards the TCR or toward the VV ▪ Feedwater pump stops immediately after the LOCA in the PHTS ▪ DHR system in operation for all the entire transient

6.1.2.2 Results and discussion

The postulated initiating event is supposed to occur at time t=0.0 s. The unmitigated plasma disruption is effectively stopped by limiters. During the disruption a small portion of all the limiters will undergo a heat flux of 10 GW/m^2. In this analysis 8 limiters have been considered. The temperature of the tungsten layer of each limiter has been imposed as boundary condition through tabular function. It has been assumed equal to 3400°C for 100 ms (from plasma disruption), after that the W temperature is reduced to 150°C (cooling water temperature) in 3s.

The pressure response in the FW and BZ pressurizer is reported in Figure 6.1.17 for a specific case, while the pressure transient in-vessel OB4 volume cooling system is reported in Figure 6.1.18. The decay heat in the BB modules led to the activation of FW-PHTS safety relief valve which set-point has been chosen to be 1.88 MPa. The first opening of SRV occurs 1749 s after the PIE.

The 13 MPa pressure set-point for the closure of BZ-PHTS upstream trip valves is reached 7.4. The fully closed state is reached 10 s after the signal activation, when the pressure in the BZ pressurizer is about 10.9 MPa. In-vessel volumes, as well as distributor ring and feeding pipes, reach the mechanical equilibrium with the plasma volume 600 s after the PIE.

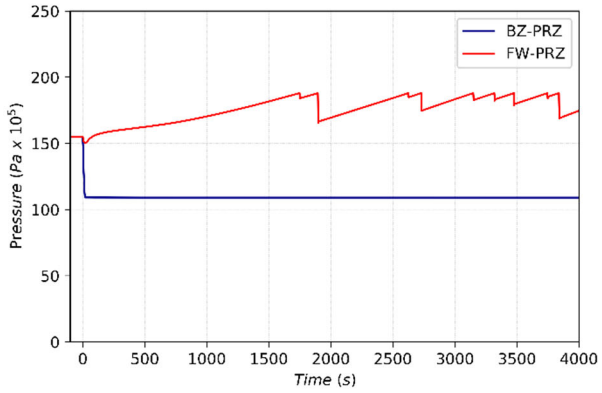

Figure 6.1.17 – VVPSS pressure (case RD_1.3)

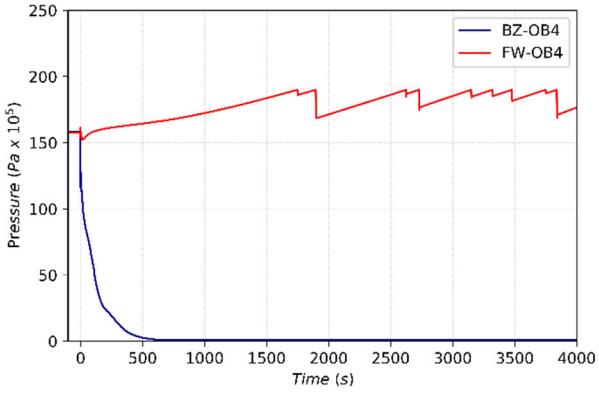

Figure 6.1.18 - VVPPS atmosphere temperature (case RD_1.3)

As in the previous case water mass flow rate transient from the feeding pipe rupture in the upper port (Figure 6.1.19) is characterized by an initial rapid increase where the maximum of about 2975.0 kg/s is achieved after around 0.7 s.

In Figure 6.1.20 the total mass of water and steam entering the upper port is shown. The total amount of water released from the BZ-PS into the VV is 117038 kg. Results of the pressurization in the VV caused by these huge amount of water entering the upper port is shown in Figure 6.1.21. The pressure trend is very similar to the “worst case” scenario, with a two different pressure peaks. However, in this case, because of the limiters the rupture discs line flow area required to withstand safety-imposed pressure limit is 1.3 m^2, resulting in a total area of 7.1 m^2 (Table 6.1-3).

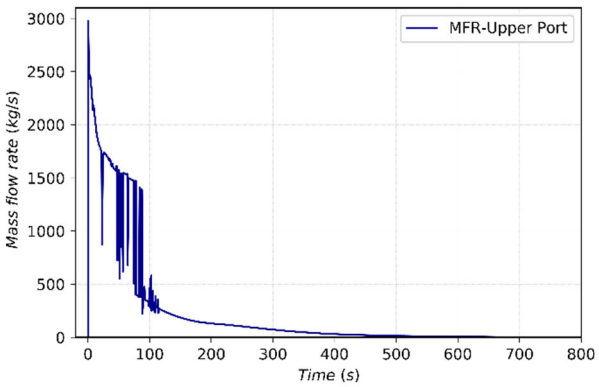

Figure 6.1.19 – Mass flow rate toward the upper port (case RD_1.3)

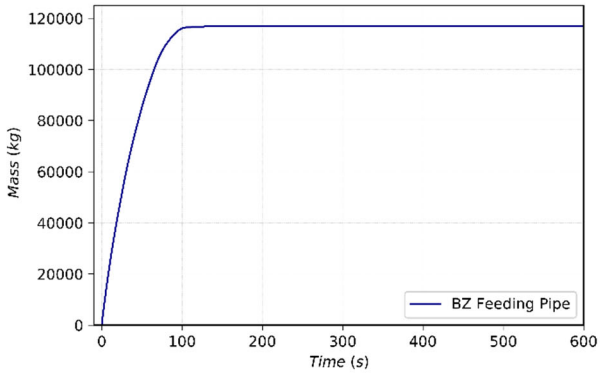

Figure 6.1.20 - Mass of water flowing toward the upper port (RD_1.3)

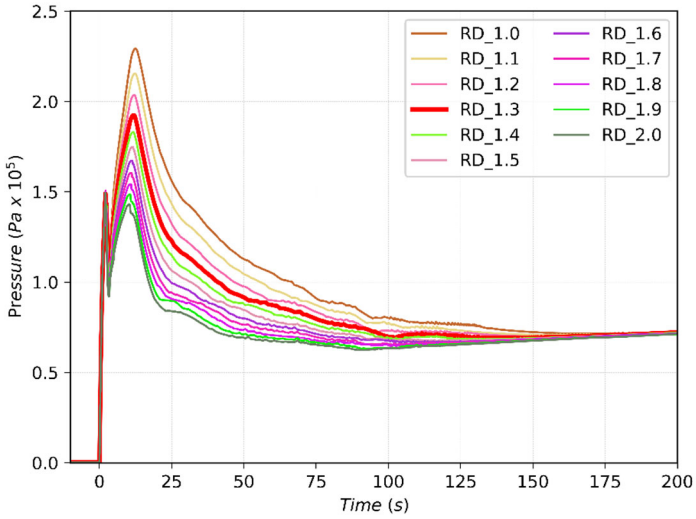

Figure 6.1.21 - Upper port pressure for different rupture disks flow area

Table 6.1-3 – Pressure inside the upper port for different cases

Scenario	Total discharge flow area [m^2]	Peak pressure [bar]	Time [s]
RD_1.0	6×0.1 (BLs) + 5×1.0 (RDs) = 5.6	2.2703	12.500
RD_1.1	6×0.1 (BLs) + 5×1.1 (RDs) = 6.1	2.1337	12.307
RD_1.2	6×0.1 (BLs) + 5×1.2 (RDs) = 6.6	2.0155	12.108
RD_1.3	**6×0.1 (BLs) + 5×1.3 (RDs) = 7.1**	**1.9051**	**11.900**
RD_1.4	6×0.1 (BLs) + 5×1.4 (RDs) = 7.6	1.8120	11.703
RD_1.5	6×0.1 (BLs) + 5×1.5 (RDs) = 8.1	1.7312	11.404
RD_1.6	6×0.1 (BLs) + 5×1.6 (RDs) = 8.6	1.6563	11.209
RD_1.7	6×0.1 (BLs) + 5×1.7 (RDs) = 9.1	1.5892	10.904
RD_1.8	6×0.1 (BLs) + 5×1.8 (RDs) = 9.6	1.5269	10.700
RD_1.9	6×0.1 (BLs) + 5×1.9 (RDs) = 10.1	1.4798	2.1197
RD_2.0	6×0.1 (BLs) + 5×2.0 (RDs) = 10.6	1.4789	2.1095

Flow rates toward the VVPSS are shown in Figure 6.1.22 and Figure 6.1.23, for bleed lines and rupture discs lines respectively. The higher is the total flow are available toward the VVPSS the shorter is the time required by the VV pressure to drop below 90.0 kPa. After about 907 s from the PIE pressure in the VV increases above 0.9 bar, from this point bleed valves are characterized by a long period of opening/close transitions until around 8000 s. To better simulate the behavior of bleed lines more specifications are required, in particular a pressure set-point for their closure is needed.

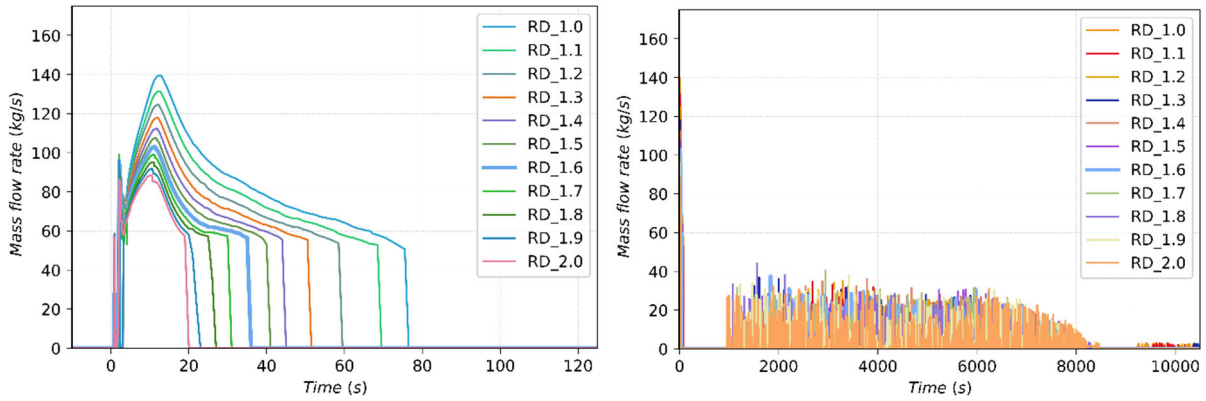

Figure 6.1.22 – Steam mass flow rate flowing toward the bleed lines tank (tank A)

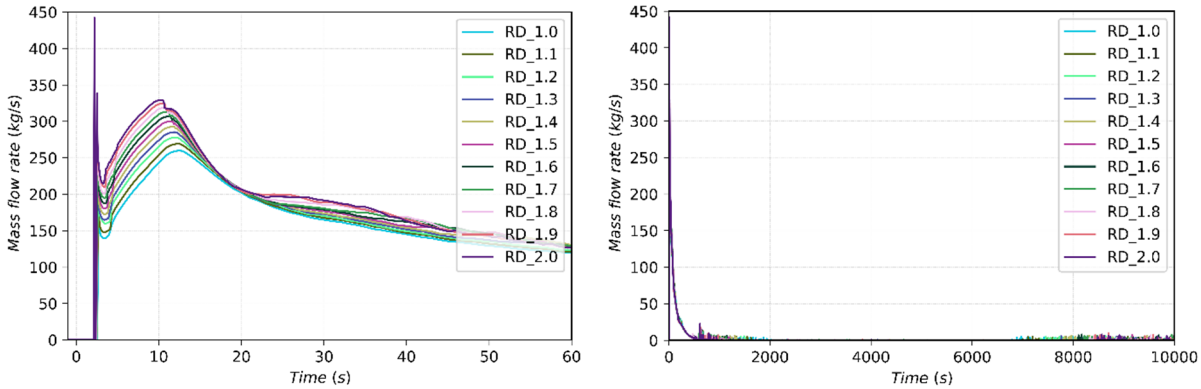

Figure 6.1.23 -Mass of steam flowing toward the rupture disk lines (tank B)

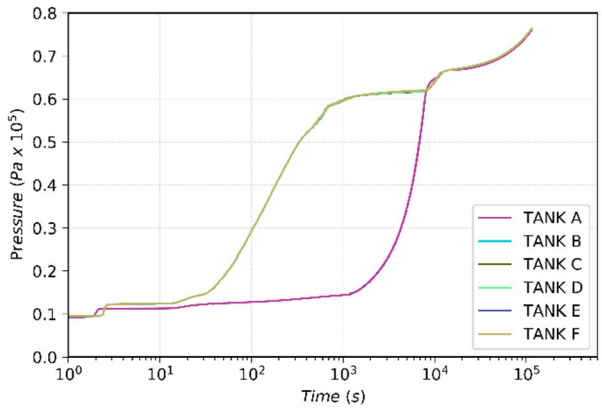

Figure 6.1.24 -Pressure in VVPPS suppression tanks (Case RD_1.3)

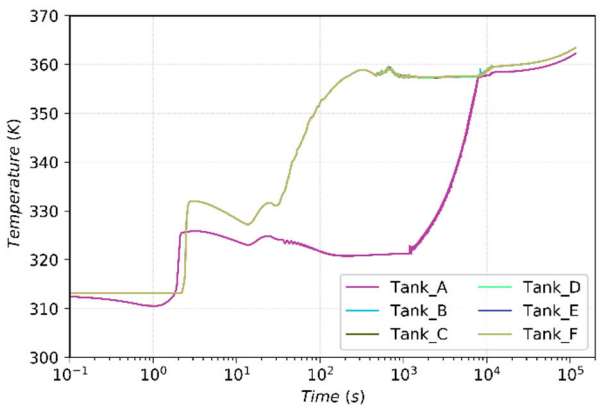

Figure 6.1.25 -Temperature in VVPPS suppression tanks (Case RD_1.3)

Pressure and temperature transient of VVPSS suppression tanks are shown in Figure 6.1.24 and Figure 6.1.25 respectively, for the RD_1.3 case. These physical parameters are important not only to evaluate efficiency of suppression tanks, but also because at the current stage of the EU DEMO VVPSS design tanks should be equipped with passive autocatalytic hydrogen recombiner in their atmosphere and their recombination efficiency strictly depends on pressure and temperature conditions.

Pressure in the VVPSS remains below the containment pressure of 98.0 kPa ensuring the confinement of ACP, tungsten dust and HTO.

The total mass of hydrogen in the VV and VVPSS volumes is shown in Figure 6.1.26, while a detail of hydrogen mass distribution in suppression tanks is shown in Figure 6.1.27. The total mass of hydrogen produced at the end of the simulation is 34.1 g. This mass adds to the 607.0 g of initial tritium. After 32 h from the PIE, 19.3 g of hydrogen remain inside the VV; 626.3 g are collected in the VVPSS atmosphere. In particular, 221.8 g are collected in Tank A connected with the bleed lines and the remaining 404.5 g are equally distributed in the 5 suppression tanks (Tank B to F).

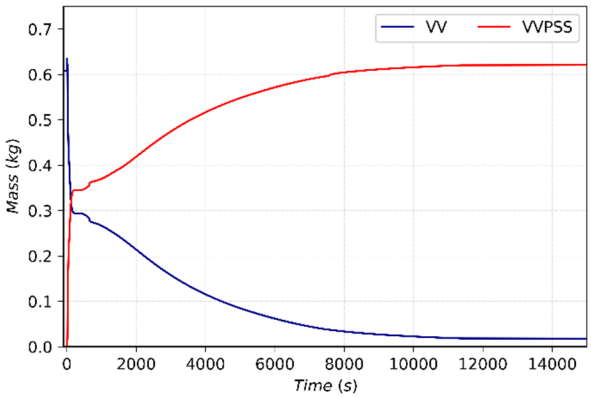

Figure 6.1.26 -Total mass of hydrogen in VV and VVPSS volumes (Case RD_1.3)

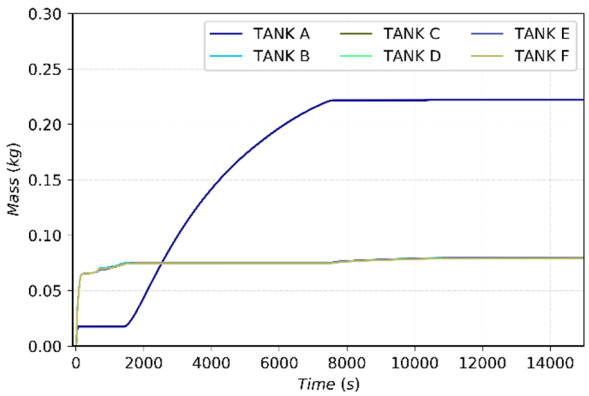

Figure 6.1.27 -Total mass of hydrogen in VVPSS suppression tanks (Case RD_1.3)

6.1.2.3 Source term mobilization

Trends related to tungsten dust, HTO and ACP mobilization, shown in Figure 6.1.28, Figure 6.1.29 and Figure 6.1.30, are very similar to those shown in par. 6.1.1.3 for the “worst case” scenario.

In this accident scenario the rupture occurs in the upper port, where the VVPSS pipework is connected. The mass of steam ejected from the BZ-PHTS is directly discharged into the VVPSS tanks. The lower amount of steam flowing toward the plasma chamber volume, cause lower transport phenomena in that volume. As a result, maximum mass of tungsten dust transferred to the VVPPS is 198 kg for case RD_2.0 against the 223.52 kg obtained for the “worst case”. After 32 h of simulation around 200 kg of tungsten dust are deposited on VV structure. Two orders of magnitude bigger than the previous case, to emphasize how particles gravitational settling is the dominant mechanism of aerosol mobilization in case of lack of high fluid flows.

Because of the lower mass of water released in the VV, after about 300 s there is no more liquid water in the upper port volume and ACP are moved to the gas phase and transferred to the VVPSS tanks. Of the 700 g of ACP in the BZ-PHTS at the steady-state only 4 g reach the suppression systems.

The faster evaporation of liquid water causes also a higher mobilization of HTO that passes from the liquid to the gaseous form and is moved under the action of a pressure cascade toward the VVPSS.

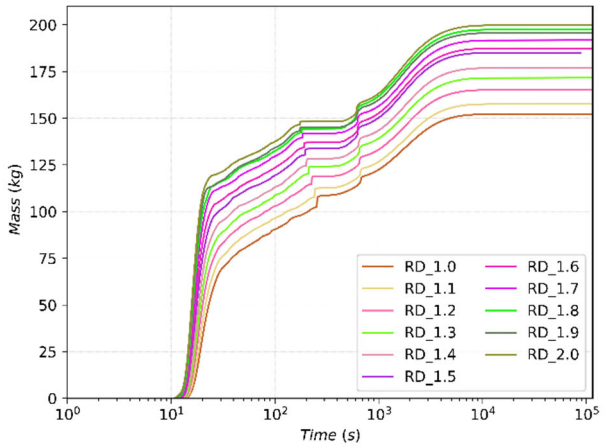

Figure 6.1.28 – Mass of W dust in VVPSS for different RDs flow area

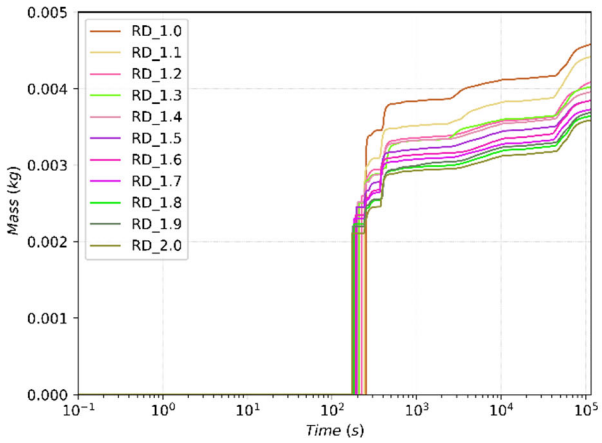

Figure 6.1.29 – Mass of ACP aerosol in VVPSS for different RDs flow area

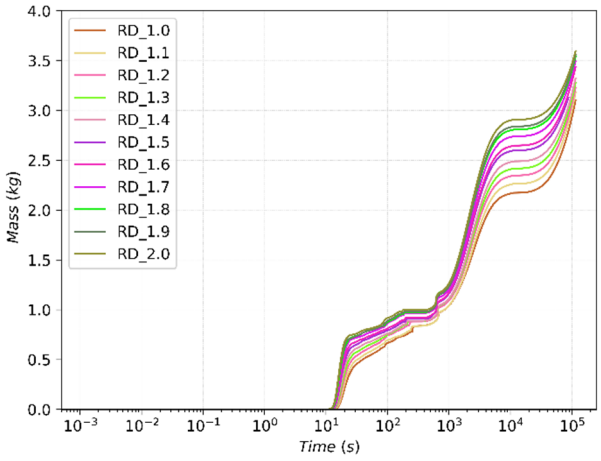

Figure 6.1.30 – Mass of tritiated water in VVPSS for different RDs flow area

6.1.3 Conclusions

The aim of these two simulations, which events have been classified as DBA, was to define the needed flow area of VVPSS suppression pipework to limit the VV pressure below the limit imposed by safety requirements. In both cases, a pipe rupture was initiated by opening a connection between the BZ feeding pipe and the upper port volume. Water injection inside the plasma volume in turn causes an unmitigated plasma shutdown transient. In the case in which limiters can mitigate the effects of a plasma disruption no further leaks are considered ("baseline" scenario). In the case in which limiters are not installed ("worst" scenario), the unmitigated plasma disruption causes an additional break of 262 FW channels. For each scenario a parametric study considering different sections for the 5 RDs lines connecting the upper port to the VVPSS has been performed. Due to the difference in the operating pressure (0.1 kPa in the VV vs. 15.5 MPa in the BZ-PHTS and in the FW-PHTS), after the tube rupture, water and steam enters the VV volume causing a rapid pressurization. The results indicate that the pressure dynamics inside the VV and its peak value strongly depend on the capability of the relief pipes to discharge an adequate flow of steam into the ST. In order to stay below the limit of 0.2 MPa, for the "worst case" scenario, a total discharge area of 8.6 m^2 is required, while in the "baseline" case scenario at least 7.1 m^2.

6.2 In-Vessel LOCA

The Design Basis Accident analysis of an in-vessel LOCA for WCLL blanket concept is described below. The postulated initiating event is a failure of FW facing plasma structure. Two different simulations were performed with the presence and absence of the downstream isolation valves, respectively:

- CASE 1: both upstream and downstream valves in operation;
- CASE 2: upstream valves only

6.2.1 Event Sequence

Analysis requirements and main input data have been obtained from DEMO BB Safety Data List and DEMO Accident Selection and Description.

Table 6.2-1 – Possible transient sequence for an in-vessel LOCA

Parameter	Specification
Definition of initiating event	Loss of coolant in the FW primary cooling circuit inside the VV because large rupture of the FW structure during the normal operation.
Possible transient sequence	▪ A double break size in the FW cooling pipes occurs. The number of failed pipes is 10 for a total break area of 0.00098 m^2 ▪ Fusion power is terminated by an unmitigated disruption affecting a plasma facing structure area of 1 m^2; ▪ The unmitigated disruption hits not the same zone of the PIE ▪ If melting temperature of the EUROFER is reached in the affected area the FW pipes breaks causing water injection inside the plasma volume. The failure of the FW structure affects only few millimetres of EUROFER, in such a way only water and steam contained in the FW-PS enters in the plasma chamber, while the LiPb mass remains inside the BZ modules not affected by any rupture; ▪ The FW of the failed loop is first cooled down with residual water present before complete emptying; ▪ After the coolant inventory is lost the FW will be cooled by radiation to the surrounding cooled in-vessel components; ▪ If an in-vessel LOCA occurs the bleed lines and rupture disks open at reaching the pressure set point; ▪ Isolation valves close when the set-point is reached; ▪ Coolant and radioactive inventories (tritium, dust and suspended sputtering/ACPs products) will be mobilized towards the TCR or toward the VV ▪ Feedwater pump stops immediately after the LOCA in the PHTS ▪ DHR system in operation for all the entire transient

6.2.2 Results and discussion

A 32 hours transient after the postulated initiating event is simulated. The PIE is supposed to occur at time t=0.0 s.

The pressure response in the FW and BZ pressurizer is reported in Figure 6.2.2, while the pressure transient in-vessel OB4 volume cooling system is reported in Figure 6.2.1. The BZ-PS is not affected by any rupture, so pressure remains high for all the transients. The decay heat in the BZ leads to an increase in the pressure. After about 100 s the SRV set point is reached and the hot steam produced inside the loop is discharged into a suppression tank, which is assumed to have which is assumed to have the same dimension of a RD tank of the VVPSS.

Hot and cold leg of both PHTS are equipped with isolation valves, which begin to close when the pressure in the pressurizer is below 13.0 MPa. This set-point is reached in the FW-PHTS 8.25 s after the PIE. When the fully closed state is reached the pressure in the FW pressurizer is about 11.0 MPa. Because of the position of the breaks, upstream trip valves don't completely mitigate the depressurization of the PHTSs. In-vessel volumes, as well as distributor ring and feeding pipes, reach the equilibrium with the VV volumes 25 s after the pipe in the case with downstream isolation valves in operation, and after about 800 s in the case in which only upstream trip valves are closed.

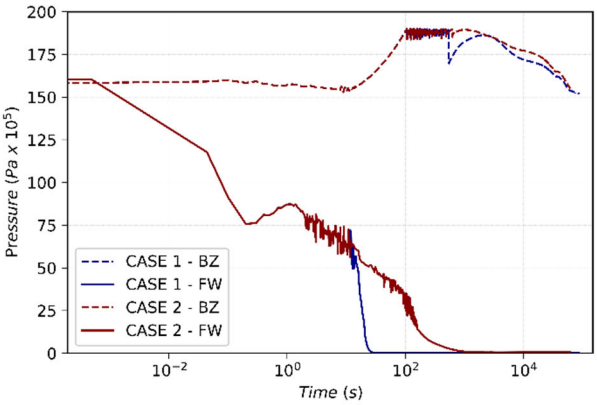

Figure 6.2.1 – Pressure transient in FW and BZ in-vessel volumes

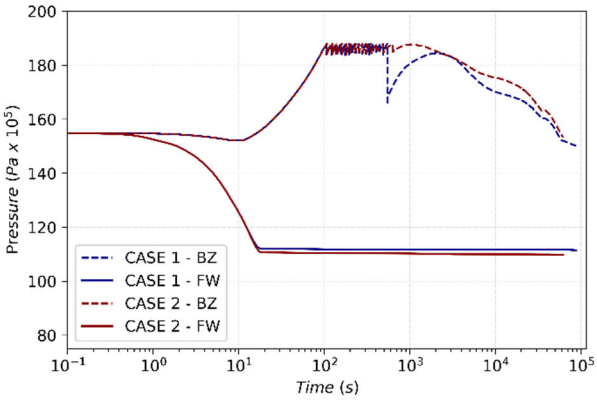

Figure 6.2.2 - Pressure transient in FW and BZ pressurizers

Fusion power is terminated by an unmitigated disruption damaging an area of 1m^2. The unmitigated plasma disruption causes the break of 262 FW channels involving 2 outboard segments, one of which is completely broken and the other partially broken, for a total break area of 0.02568 m^2. In this simulation it is supposed that only the first layer of the FW structure is affected by the rupture, in such a way only water and steam contained in the FW-PS enters in the plasma chamber, while the LiPb mass remains inside the BZ modules not affected by any rupture.

As a result, FW temperature (Figure 6.2.3) increases until the limit of 1000°C is reached.

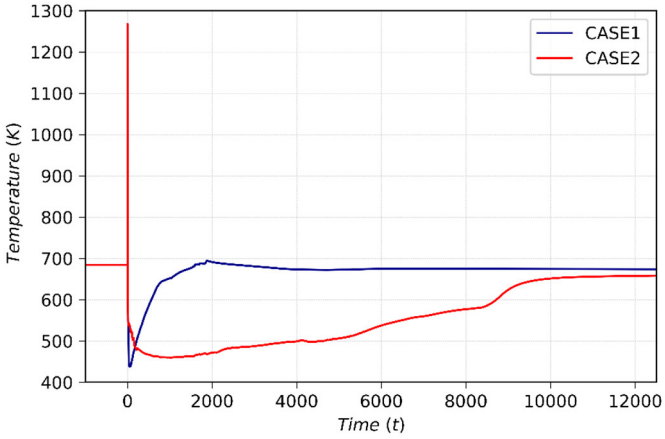

Figure 6.2.3 - Temperature FW-OB4 module affected by PD

The closure of isolation valves in front of a low pressure in the FW-PHTS affects not only the amount of water released toward the VV, but also the pressure transient inside the FW-PS channels and therefore the physical state of water and heat transfer coefficients.

Water mass flow rate transient from the ruptures in the FW channels is shown in Figure 6.2.4. The maximum flow rate toward the VV is 1161 kg/s and is not affected by valve operations, which intervention is del

In Case1 the mass flow rate quickly decreases until 30 s and then remains below 0.1 kg/s for the entire transient. In Case 2 (only upstream valves installed), mass flow remains higher than 1 kg/s for more than 2680 s, and a greater amount of water is released into the VV volume. In Figure 6.2.5 the effect of downstream trip valve is visible, thus the block of steam inlet into the VV. The total amount of water released in the VV is 15.6 tons with downstream isolation valves installed and 85.0 tons in Case 2.

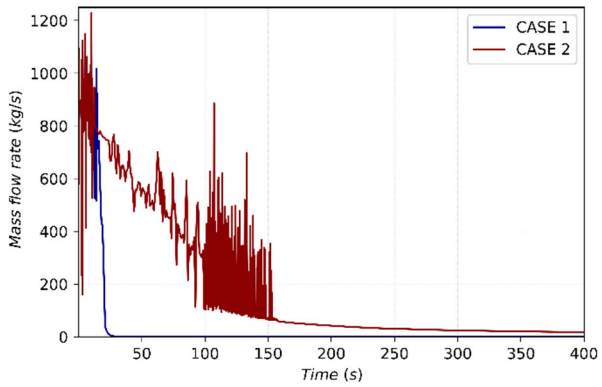

Figure 6.2.4 – Mass flow rate entering the VV

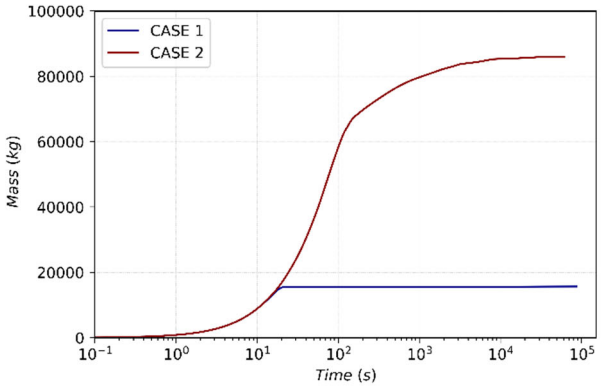

Figure 6.2.5 – Mass of water and steam entering the VV

The release of this amount of water within the VV leads to a rapid pressurization of the VV volumes (Figure 6.2.6 and Figure 6.2.7). Pressure increases very quickly and reaches the maximum pressure of 150 kPa which is limited by the pressure suppression system below the design pressure of 200 kPa. After that pressure start to decrease due to the triggering of 6 bleed lines and 5 rupture disk lines connecting the VV to the VVPSS, where suppression water, initially at 40°C, is available for the condensation of the steam arising from the FW-PS. The maximum pressure in the vacuum vessel is below the maximum pressure which the VV is designed to withstand in case of extremely unlikely events.

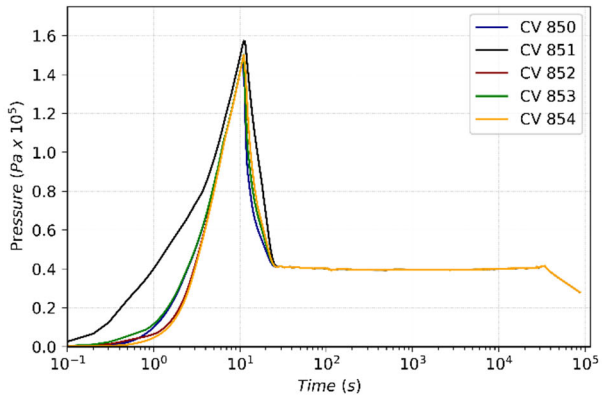

Figure 6.2.6 – Pressure in VV volumes (Case 1)

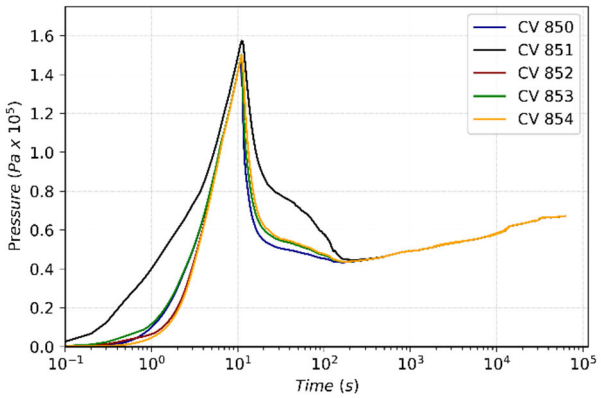

Figure 6.2.7 – Pressure in VV volumes (Case 2)

In Figure 6.2.8 and Figure 6.2.9 the pressure in VVPSS tank A and tank B are reported together with the pressure in VVPSS. In both cases the VVPSS pressure remains under atmospheric pressure ensuring

confinement of radioactive material. The detail of pressure inside each VVPSS suppression tanks is reported in Figure 6.2.10 and Figure 6.2.11.

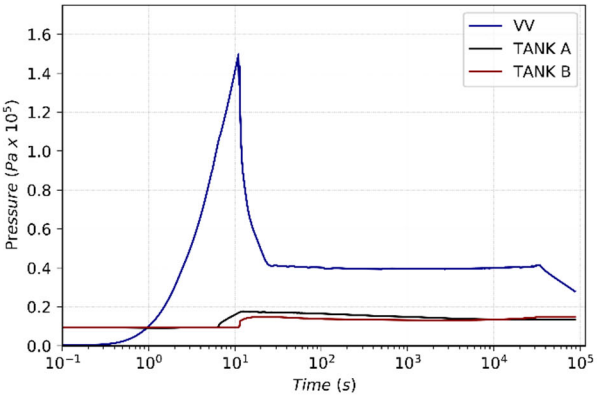

Figure 6.2.8 – VV, VVPSS Tank A and Tank B pressure transient (Case 1)

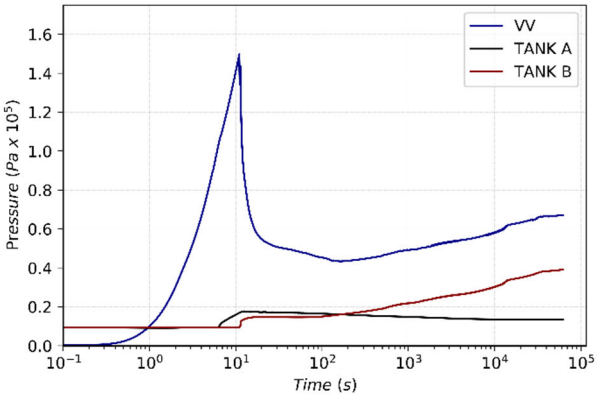

Figure 6.2.9 – VV, VVPSS Tank A and Tank B pressure transient (Case 2)

Summary of pressure values in different volumes are given below in Table 6.2-2. Time of intervention of BLs and RDs is reported in Table 6.2-3.

Table 6.2-2 – Pressure Values

Volume	**Maximum pressure [MPa]**		**Pressure at the end of the transient [MPa]**	
--	**CASE 1**	**CASE 2**	**CASE 1**	**CASE 2**
VV (CV851)	0.1573	0.1573	0.0279	0.0671
Tank A	0.01768	0.01768	0.01349	0.01349
Tanks B to F	0.01494	0.03909	0.0148	0.0390

Table 6.2-3 – VVPSS components intervention time

	Component	**Time [s]**
Case 1	Rupture discs	11.1
	Bleed Lines Valves	5.50
Case 2	Rupture discs	11.1
	Bleed Lines Valves	5.50

g

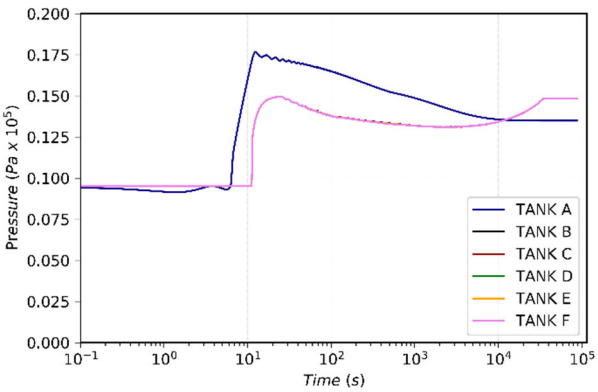

Figure 6.2.10 – VVPSS tanks pressure transient (Case 1)

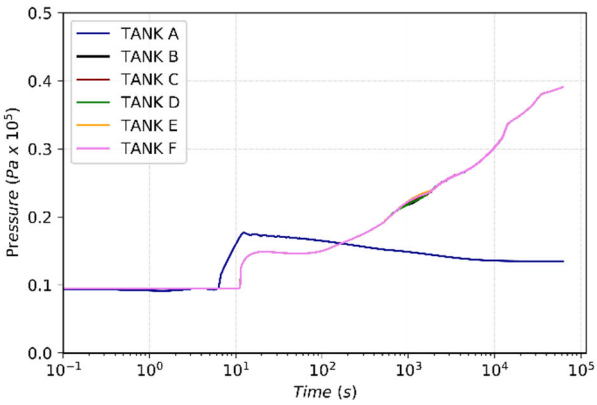

Figure 6.2.11 – VVPSS tanks pressure transient (Case 2)

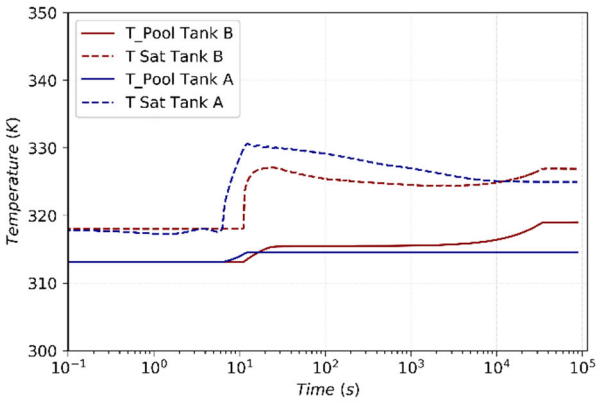

Figure 6.2.12 - Tank A and Tank B pool temperature (Case 1)

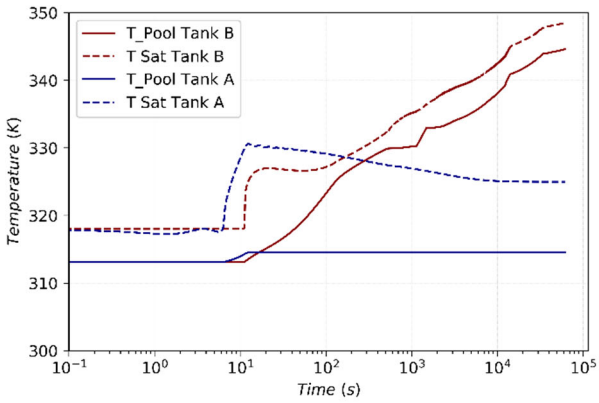

Figure 6.2.13 – Tank A and Tank B pool temperature (Case 2)

VVPSS pool temperature is shown in Figure 6.2.12 and Figure 6.2.13 together with the saturation temperature at pressure of the pool. In both the cases the water inside the suppression tanks remains subcooled for all the 32 h of the simulation.

Steam inside the VV react with FW and DV monoblocs tungsten layers leading to hydrogen generation. In Figure 6.2.14 and Figure 6.2.15 the mass of hydrogen distribution of hydrogen mass inside VV and VVPSS tanks is shown. The reaction between steam and tungsten dust deposited on the FW surface and on the divertor surface has not been considered in this simulation.

Chemical reactions between steam and tungsten hot surfaces within the vacuum vessel can produce about 622.40 g of hydrogen in CASE 1 and about 634.33 in CASE 2. Large part of this hydrogen moves into the VVPSS. The detail of hydrogen mass distribution inside the 6 VVPSS tanks is and inside the VV is reported in Figure 6.2.14 and Figure 6.2.15.

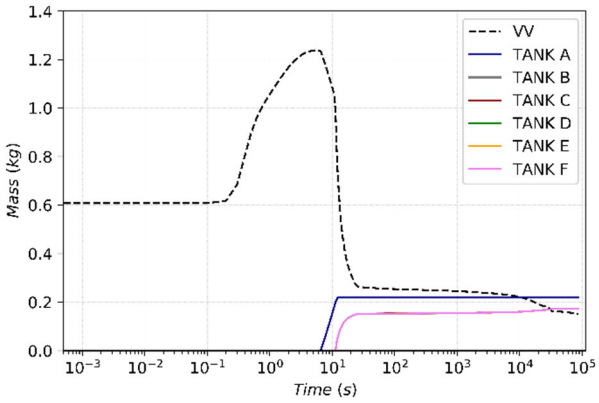

Figure 6.2.14 - Mass of hydrogen in VV and VVPSS tanks (Case 1)

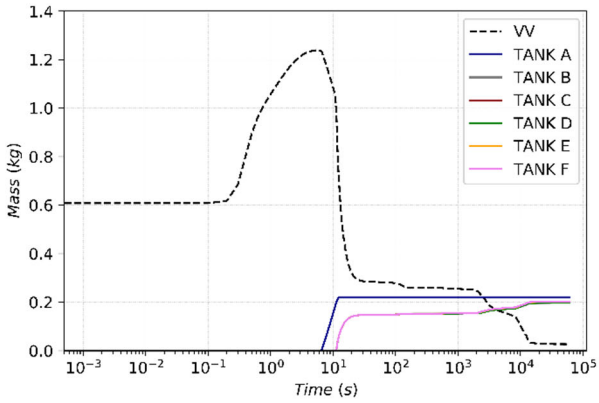

Figure 6.2.15 - Mass of hydrogen in VV and VVPSS tanks (Case 2)

In Figure 6.2.16 and Figure 6.2.17 the temperature transient for the FW structure is shown for outboard modules and inboard modules respectively, in the case in which downstream trip valves are installed (CASE 1). When the latter begins to close, temperature rapidly increases until the FW fails because the limit of 1000°C is reached in the OB1 module. After that, temperature decreases until about 1000 s because of cooling from steam and water flowing toward the plasma chamber. Then temperature increases again as a result of the incoming decay heat power and heat produced by the exothermic

reaction between tungsten and steam. The maximum value reached by the tungsten layer in this phase is 725 K.

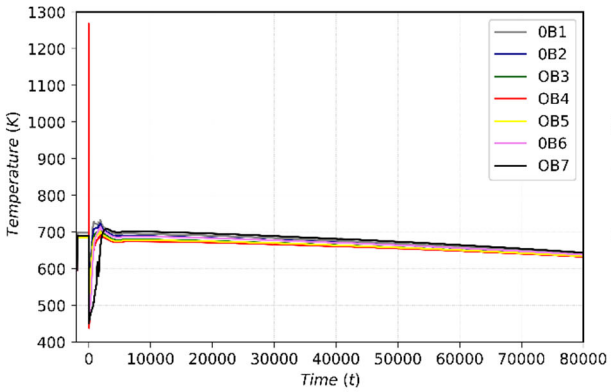

Figure 6.2.16 - Temperature FW outboard volumes (Case 1)

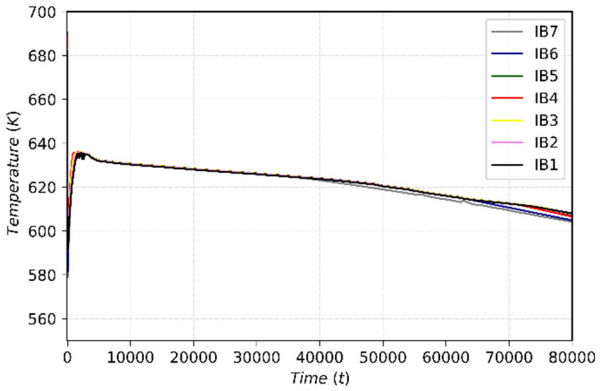

Figure 6.2.17 - Temperature FW Inboard volumes (Case 1)

In Figure 6.2.18 and Figure 6.2.19 the temperature transient for the FW structure is shown for outboard modules and inboard modules respectively, in the case in which downstream trip valves are not installed (CASE 2). In this case, after the failure of FW structure, temperature reaches lower values because of the long-term flow of steam toward the plasma chamber. However, the absence of isolation valves causes a depressurization of inboard modules resulting in their HS temperature.

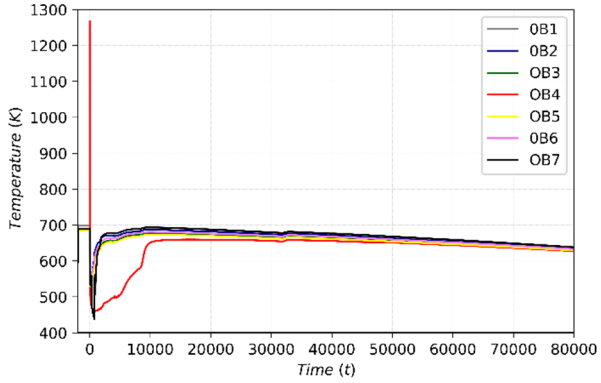

Figure 6.2.18 - Temperature FW outboard volumes (Case 2)

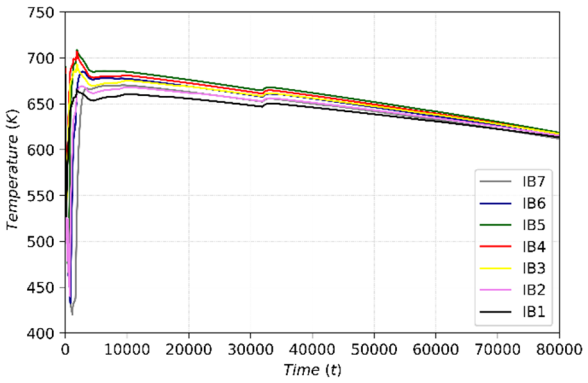

Figure 6.2.19 - Temperature FW inboard volumes (Case 2)

6.2.3 Source term mobilization

Due to the opening of the VVPSS valves and rupture disks a large amount of the mobilized inventories inside the VV are discharged to the VVPSS and to the drain tank. However, the presence of downstream isolation valves can affect the mobilization radioactive inventories, increasing gravitational particle settling phenomena. Trends related to tungsten dust, HTO and ACP mobilization, shown in Figure 6.2.20 to Figure 6.2.24.

The first two wave forms (Figure 6.2.20 and Figure 6.2.21) present the portion of tungsten dust inventories that reside within the VV and VVPPS for both Case 1 and Case 2. The mobilization of the tungsten dust from the VV toward the VVPSS tanks coincides with the VV pressurization event and

occurs mainly into the first 20 s. In fact, after 20 s the pressure in the VV is decreased to around 0.4 bar and the mass flow rate of steam toward the VV is decreased. Of the 694.0 kg of tungsten dust mobilized, around 564.0 kg is confined within suppression tanks. After 32 h of simulation, the remain 130.0 kg are still suspended in the VV volumes or has been deposited within various regions of the VV and its extensions. Figure 6.2.21 shows the mass of tungsten dust deposited on VV surfaces. The intervention of downstream isolation valves inhibits transport phenomena allowing for a faster and higher deposition.

As shown in Figure 6.2.22 the release and mobilization of ACP is a slower process, giving the possibility to the downstream isolation valves to effectively reduce the amount of ACP released. For Case1 of the 1.4 kg of ACP mobilized inside of the VV, only 0.1 kg is released in the VV, the remaining 1.3 kg remains confined in PHTS. For Case2 the total amount of ACP mobilized in the VV is 0.233 kg, and 1.167 kg remains in the PHTS. However, being the FW-PHTS the only system affected by the rupture the quantity of mobilizable ACP is 0.7 kg. In case 1, after 32 h of simulation the mass of ACP released has been entirely deposited on VV surfaces, while in case 2 a fraction is still suspended in the volume atmosphere.

The transport of HTO is shown in Figure 6.2.24. The first 20 s of the accident are governed by mass transport phenomena, and the waveform are identical for both the cases. However, in the long term scenario, in case 1 a large amount of HTO is transferred to the VVPSS because of evaporation phenomena. However, there is no significant difference between the two cases.

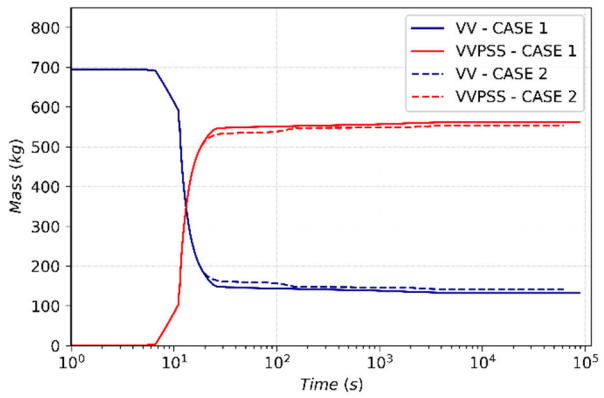

Figure 6.2.20 – Mass of W dust in VV and VVPSS volumes

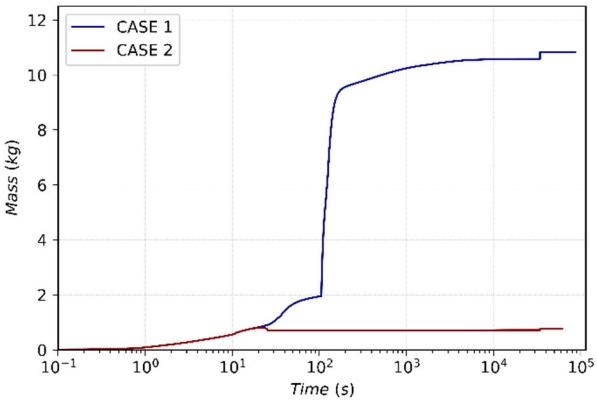

Figure 6.2.21 – Mass of W dust deposited on VV surfaces

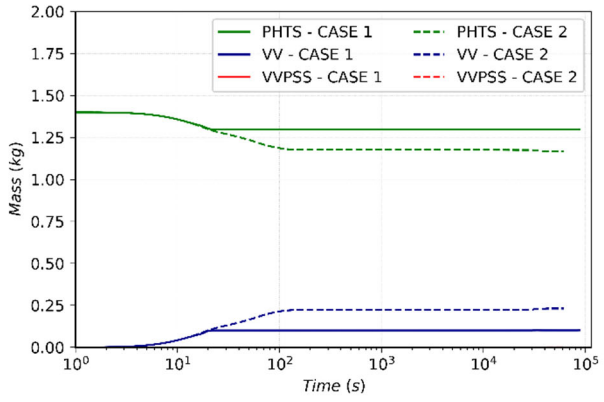

Figure 6.2.22 – Mass of ACP in PHTS, VV and VVPSS volumes

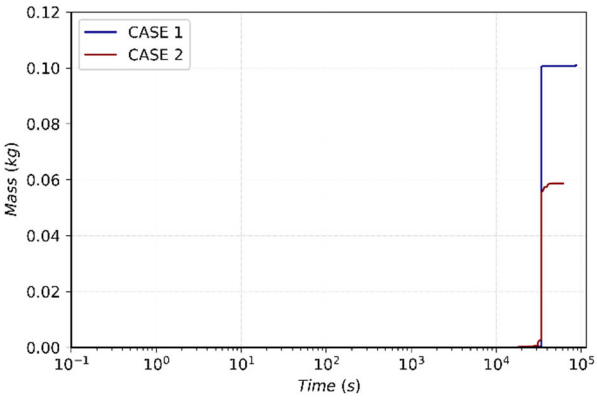

Figure 6.2.23 – Mass of ACP deposited on VV surfaces

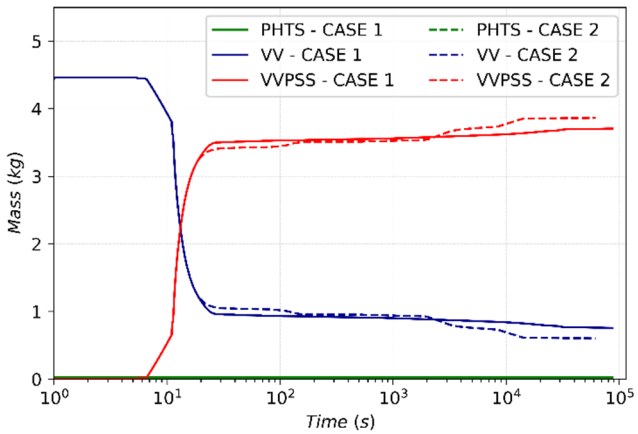

Figure 6.2.24 – Mass of HTO in PHTS, VV and VVPSS volumes

The lower amount of steam flowing toward the plasma chamber volume, cause lower transport phenomena in that volume. As a result, maximum mass of tungsten dust transferred to the VVPPS is 198 kg for case RD_2.0 against the 223.52 kg obtained for the "worst case". After 32 h of simulation around 200 kg of tungsten dust are deposited on VV structure. Two orders of magnitude bigger than the previous case, to emphasize how particles gravitational settling is the dominant mechanism of aerosol mobilization in case of lack of high fluid flows.

Because of the lower mass of water released in the VV, after about 300 s there is no more liquid water in the upper port volume and ACP are moved to the gas phase and transferred to the VVPSS tanks. Of the 700 g of ACP in the BZ-PHTS at the steady-state only 4 g reach the suppression systems. The faster evaporation of liquid water causes also a higher mobilization of HTO that passes from the liquid to the gaseous form and is moved under the action of a pressure cascade toward the VVPSS.

6.2.4 Conclusions

The aim of this simulation was to analyze the effects of an in-vessel loss of coolant accident (classified as DBA). Moreover, to evaluate downstream isolation valves effects in terms of radioactive releases and thermal hydraulic behavior of main DEMO components two different simulations have been performed. In fact, the large number of downstream valves (isolation and SRVs) to be installed, will give rise to safety and reliability constraints. For such a reason it is important to properly evaluate if they are indeed necessary from a safety perspective.

A pipe rupture was initiated by opening a connection between the VV and the FW channels. Water injection inside the plasma volume in turn causes an unmitigated plasma shutdown transient.

Due to the difference in the operating pressure (0.1 kPa in the VV vs. 15.5 MPa in the FW-PHTS), after the tube rupture, water and steam enters the VV volume causing a rapid pressurization. The results indicate the pressure increase in VV is very fast and the maximum pressure peak is 157 kPa. However, in both cases the intervention of VVPSS is enough to mitigate the transient and to keep the pressure well below the limit for the VV of 0.2 MPa.

In both the simulations small amounts of hydrogen are produced if compared with the tritium mass inside the VV, around 600 g. Results of source term mobilization shown that isolation valves can affect the releases of activated corrosion products inside the VV. In particular, the closure of downstream isolation valves reduces the total amount of ACP entering the VV of about 30%. This value can be increased by reducing the time required by trip valves to be in a fully closed state.

6.3 Ex vessel LOCA

The fundamental difference between in-vessel and ex-vessel loss of coolant is that during ex-vessel LOCA scenarios, the mobilized radioactive inventory does not include the large in-vessel tritium and dust source terms as long as the in-vessel components stay intact. However, during an ex-vessel event, the plasma burn is not inherently terminated at the state of the event. For such a reason a shutdown system is required to trigger plasma shutdown, while at the same time avoiding further failures of plasma facing components.

Basing on the last EU DEMO design concept, the DEMO PHTS systems are located outside the bioshield wall and are therefore in direct contact with the TCR environment. In the case of an ex-vessel LOCA in the TCR equipment area, more than 50000 m^3 (WCLL plant concept) are available for steam expansion. To demonstrate that this is acceptable from a safety standpoint, the pressure peak after ex-vessel pipe breaks should be kept under the limit of 2 bar.

Design Basis Accident simulations of ex-vessel LOCAs have been performed using the MELCOR code for the WCLL concept of EU DEMO reactor. The main goal was to estimate the ultimate pressurization of the tokamak building compartments and to quantify the potential radioactive releases from the plant.

The VV-DHRS was assumed to be in operation for all the accidental transient to ensure the integrity of VV internal structures. As result there is no tritium and tungsten dust releases inside the TCR volumes, however, HTO and ACP inside the PHTS are released in the TCR after the initiating event, and if the volume overpressure is significative, some leakages could occur toward the external environment. Should be considered that at this stage of the EU DEMO design phase, no overpressure mitigation systems (e.i. containment spray system, ice condenser, etc.) are foreseen for the containment.

As specified in par. 5.3 in the current design phase of the TCR only UPC, VS and LPC are connected forming a total free volume available for expansion of 17543 m^3; the PHTS area and the Top Maintenance Hall are designed as stand-alone compartments. Before starting with the accident analysis, being the PIE of this DBA a double guillotine break of a PHTS distributor ring, should be necessary to evaluate if the available volume (UPC + VS + LPC) is enough to stay below the pressure limit of 2 bar imposed by design criteria.

Four different cases have been studied by connecting different TCR compartments:

- CASE 1: UPC, VS and LPC are the only volumes available for steam expansion
- CASE 2: PHTS volume is made available by opening a connection with the UPC (FL982 in Figure 5.3.5). The PHTS volume used is 49975 m^3, design value of the WCLL TCR configuration.
- CASE 3: PHTS volume is made available by opening a connection with the UPC (FL982 in Figure 5.3.5). The HCPB TCR design is used with PHTS area that is extended along the length of the entire tokamak building (about 96.0 m), for a total volume of 120000 m^3.
- CASE 4: Top maintenance hall is made available (together with PHTS area) by opening a connection with the PHTS area (FL983 in Figure 5.3.5)

Table 6.3-1 – Containment flow path

	FLOW PATH	State	FLARA [m^2]
CASE 1	FL982	Closed	--
	FL983	Closed	--
CASE 2	FL982	Open	139.2 m^2
	FL983	Closed	--
CASE 3	FL982	Open	788.0 m^2
	FL983	Closed	--
CASE 4	FL982	Open	139.2 m^2
	FL983	Open	299.2 m^2

In Figure 6.3.1 and Figure 6.3.2 the pressure in the UPC is reported for a LOCA in the FW-PHTS and BZ-PHTS distributor ring, respectively. The pressure limit imposed for the TCR structure is exceeded with a wide margin in Case 1 and Case 2. These values cannot be accepted from a safety point of view because of damages to structures and components which can aggravate the accident scenario, and because of the high losses of radioactivity toward the external environment. In order to stay below the 2 bar openings towards the PHTS or the Maintenance Hall must be foreseen.

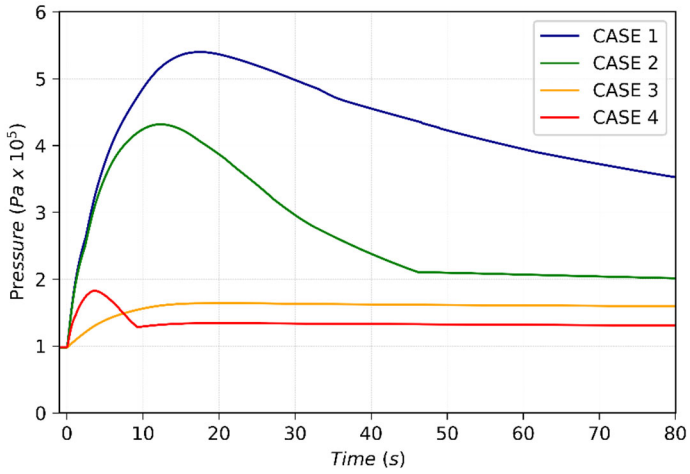

Figure 6.3.1 – Pressure in the UPC after a LOCA from the FW-PHTS distributor ring

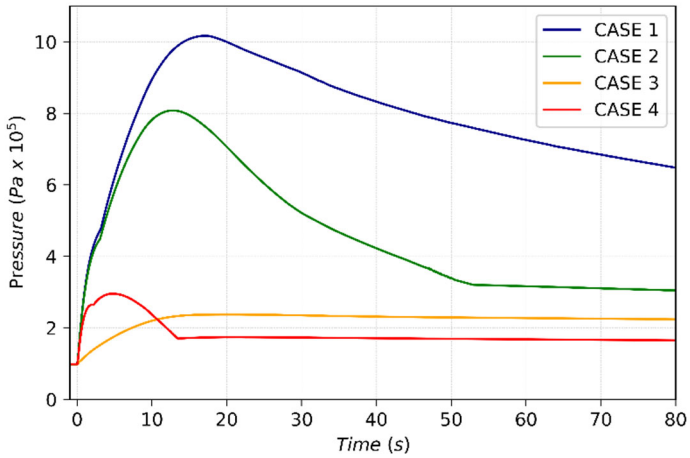

Figure 6.3.2 - Pressure in the UPC after a LOCA from the BZ-PHTS distributor ring

6.3.1 Ex-vessel LOCA from FW-PHTS

The postulated initiating event is a break in FW-PHTS distributor ring which occurs during the plasma burn. Coolant is discharged at a huge rate into the tokamak building upper pipe chase.

The fusion power termination system will actuate on a signal from a pressure sensor in the vault or primary cooling system and terminate plasma burn in three seconds. The plasma is terminated through a mitigated disruption with a possibility that the in-vessel cooling channels will undergo damage because of quick temperature transient due to high heat flux before plasma termination.

6.3.1.1 Event sequence

Analysis requirements and main input data have been obtained from DEMO BB Safety Data List and DEMO Accident Selection and Description.

Table 6.3-2 - Possible transient sequence for an ex-vessel LOCA from FW-PHTS

Parameter	Specification
Definition of initiating event	Loss of coolant in the FW primary cooling circuit inside the TCR because large rupture of the FW-PHTS distributor ring during the normal operation.
Possible transient sequence	▪ A double break size in the FW-PHTS distributor ring occurs, for a total break area of 0.2328 m^2; ▪ Over pressure signal inside the TCR actuate for plasma burn termination ▪ Fusion power is terminated 3 s after the signal activation by a mitigated disruption affecting a plasma facing structure area of 1 m^2; ▪ If melting temperature of the EUROFER is reached in the affected area the FW pipes breaks causing water injection inside the plasma volume. The failure of the FW structure affects only few millimetres of EUROFER, in such a way only water and steam contained in the FW-PS enters in the plasma chamber, while the LiPb mass remains inside the BZ modules not affected by any rupture; ▪ The FW of the failed loop is first cooled down with residual water present before complete emptying; ▪ After the coolant inventory is lost the FW will be cooled by radiation to the surrounding cooled in-vessel components; ▪ If an in-vessel LOCA occurs the bleed lines and rupture disks open at reaching the pressure set point; ▪ Isolation valves close when the set-point is reached; ▪ Coolant and radioactive inventories (tritium, dust and suspended sputtering/ACPs products) will be mobilized towards the TCR or toward the VV ▪ Feedwater pump stops immediately after the LOCA in the PHTS ▪ DHR system in operation for all the entire transient

6.3.1.2 Results and discussion

At the onset of the accident (t=0.0 s) a double-ended guillotine break with break area of 0.2328 m^2 is assumed to occur on the cold distributor ring of the FW primary heat transfer system. The two loops are allowed to equilibrate under steady normal operating conditions for 2000 s prior to the double guillotine break. Figure 6.3.3 and Figure 6.3.4 shows the pressure response in the FW and BZ pressurizer and in-vessel OB4 volume, for the first 250 seconds of this calculation, respectively. Hot and cold leg of both PHTS are equipped with trip valves, to limit the amount of water entering the TCR. The signal for the detection of the abnormal event has a delay of 3 s and 7 additional seconds closure time of the valve is assumed. It has been assumed that trip valves begin to close when the pressure in the pressurizer is below 13.0 MPa. This set-point is reached 1.95 s after the PIE and the fully closed state is reached after

11.95 s, when the pressure in the BZ pressurizer is 4.65 MPa. Because of the position of the break, upstream isolation valves have no effect on the depressurization of the FW in-vessel volumes which reach the equilibrium with the TCR pipe chase volume about 97.2 s after the PIE. The decay heat in the BZ loop, not affected by any rupture, led to the activation of safety relief valve which set point has been chosen to be 1.88 MPa. The first opening of SRV occurs at 88.0 s.

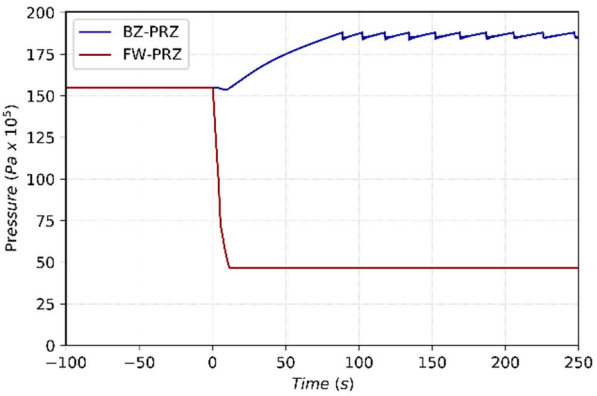

Figure 6.3.3 – Pressure transient in FW and BZ pressurizers

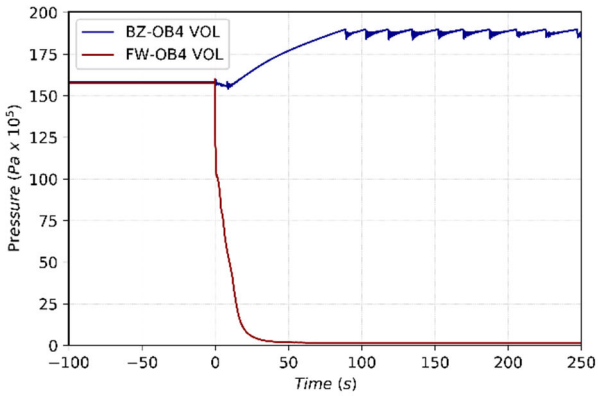

Figure 6.3.4 - Pressure transient in FW and BZ in-vessel volumes

The pressure difference between the PHTS and the TCR volume was so large that substantial amount of coolant was ejected into the TCR, causing an excursion of pressure and temperature to containment. The TCR pressure rapidly increases to a maximum of about 156.1 kPa. Then, both pressure and temperature decrease because of the presence of concrete heat structures, having a large surface and facing with the external environment simulated as a large control volume containing air and maintained at 30°C. However, any active or passive system is provided for the cooling of TCR volumes, pressure remain higher than the atmospheric pressure.

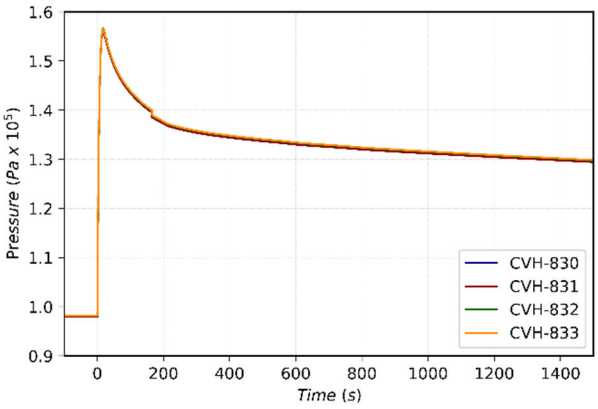

Figure 6.3.5 – Pressure transient in TCR volumes

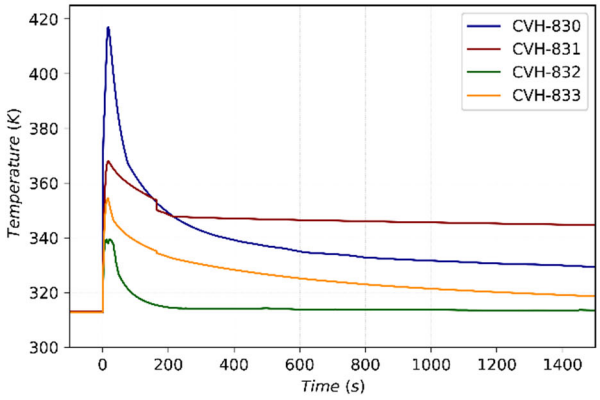

Figure 6.3.6 – Atmosphere temperature of TCR volumes

The initial mass flow rate of coolant at the break was extremely large (maximum flow rate of 17430.0 kg/s) and then followed by gradually decrease due to the progressively depleted primary system coolant inventory and to the intervention of trip valves. Figure 6.3.7 shows the mass flow rate variations at break as a function of accident time. As showed in Figure 6.3.8 more than 100 tons of water are released inside the TCR.

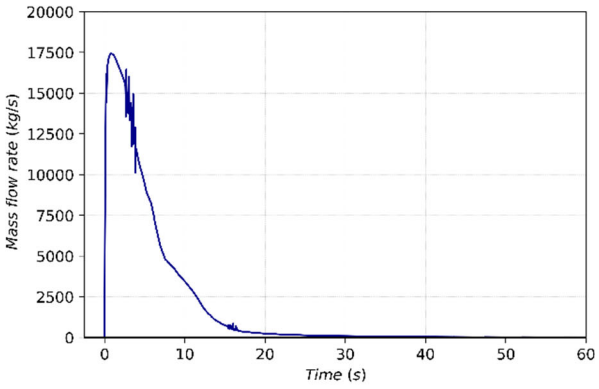

Figure 6.3.7 – Mass flow rate from ring distributor guillotine break

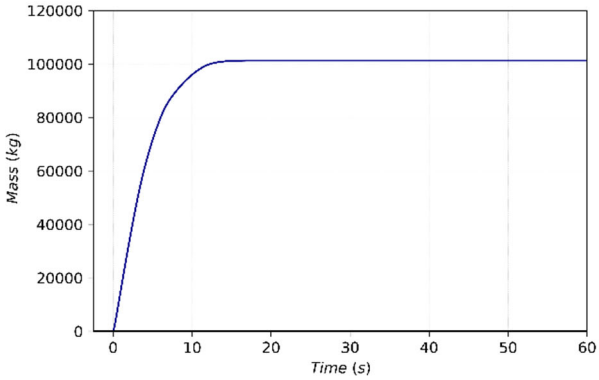

Figure 6.3.8 – Mass of water discharged into the Upper chase area

Overpressure detection in the TCR occurs in 0.6 s. The plasma control system triggers for a plasma shutdown 3 s after the signal. Thus 3.6 s after the PIE plasma facing surfaces are affected by an higher heat flux due to a mitigated plasma disruption. The FW temperature initially drops following the LOCA due to accelerated velocities in the FW coolant channels. The FW surface then begins to heat up as the coolant that remains in the cooling system stagnates following loop depressurization. The FW temperature rise reaches a momentary plateau when some cooling results from the venting of the HTS vault to the suppression pool and the remaining FW coolant vaporizes. A second temperature excursion subsequently occurs that is limited by conduction of the FW heating into the shield, which is still being cooled by a separate cooling system.

In this scenario, the FW temperature does not reach a temperature that would result in failure by melting.

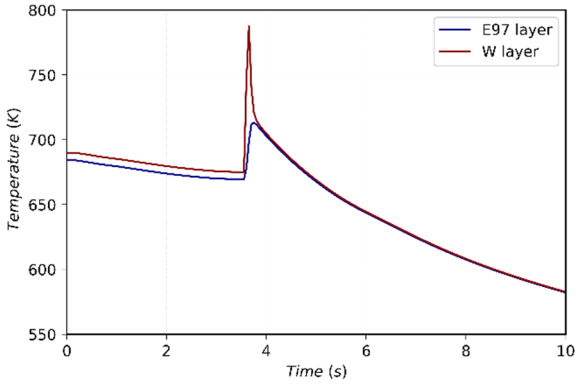

Figure 6.3.9 – Temperature peak on OB4 volume FW HS after a mitigated PD

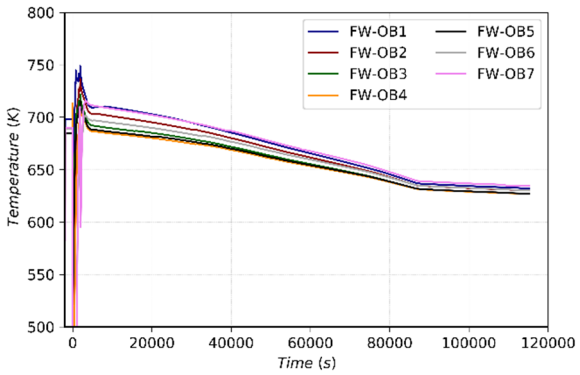

Figure 6.3.10 – FW temperature of outboard volumes (poloidal distribution)

After detection, the isolation valves in the secondary loop will isolate the failed heat exchanger. No environmental releases are expected.

6.3.1.3 Radiological releases

Because the integrity of in-vessel structure in maintained, there is no tritium and tungsten dust releases inside the TCR volumes. Only the HTO diluted in the FW-PHTS and loop related activated corrosion products are mobilized toward the TCR after the initiating event. Because the pressure inside the TCR remains higher than the atmospheric pressure, all the coolant spilled onto the TCR presents a direct environmental release. However, due to the small radioactive inventory in the FW loop, the environmental releases would be limited causing no serious radiological consequences. Only

atmosphere purification systems or overpressure systems can mitigate these releases, however they have not been considered in this simulation.

In Figure 6.3.11 the mass of ACP is shown for both TCR and PHTS volumes. A total ACP mass of 0.692 kg is released into the TCR, which correspond to the 98.85% of the total FW-PHTS ACP inventory.

Same results are obtained for the tritiated water (Figure 6.3.12). Of a mobile fraction of 17.74 g of HTO, 17.52 g are moved toward the TCR compartments.

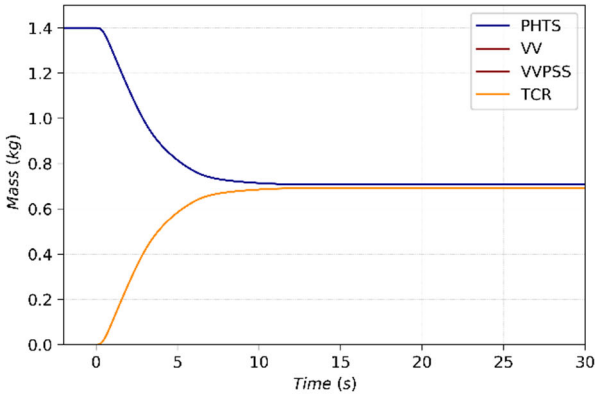

Figure 6.3.11 – ACP distribution in PHTS and TCR volumes

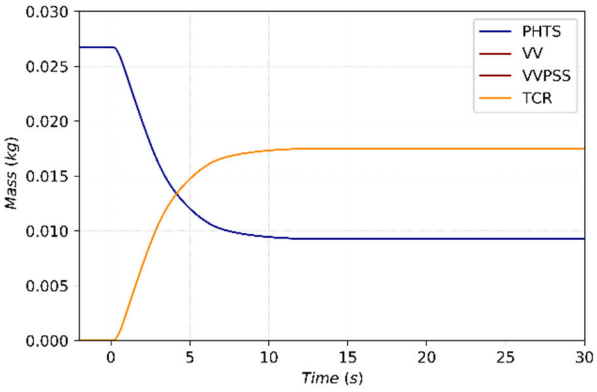

Figure 6.3.12 – HTO distribution in PHTS and TCR volumes

6.3.1.4 Conclusions

The aim of this simulation was to analyze the effects of an ex-vessel loss of coolant accident (classified as DBA). The PIE has assumed to be a double-ended guillotine break of the cold distributor ring of the FW primary heat transfer system, for a total break area of 0.2328 m^2. Analyses demonstrated that some further efforts are still needed in the design of a suitable TCR for the EU DEMO WCLL concept. Connections between different tokamak compartments should be foreseen to avoid overpressure of TCR. Moreover, if the connection between different TCR compartments will not be possible, overpressure mitigation systems (e.i. containment spray system, ice condenser etc.) shall be foreseen in the containment to avoid long term releases of tritiated water and activated products toward the environment.

6.4 In-box LOCA: preliminary study and methodology

To complete the wide range of DBA performed for the EU DEMO WCLL concept, a preliminary analysis of an in-box LOCA has been carried out.

This kind of accident has not been yet deeply investigated for the WCLL concept because of the lack of multi-phase safety-related system codes able to deal with water and liquid metals. In this context, a preliminary analysis of an in-box LOCA for the WCLL blanket concept has been performed employing custom models. The aim is to evaluate pressure and temperature transients following to the leakage of water from DWTs within one breeder module and the subsequent mass of hydrogen generated during the oxidation reaction between lithium-lead and water. In the case of a LOCA multiple rupture of these tubes is postulated, with consequent leakage of pressurized water in the LiPb side of the module.

For this study, the ENEA WCLL 2015 configuration has been considered [66]. The blanket is divided in 18 Sectors in toroidal direction. Each sector comprises 3 segments in the outboard blanket (OB) and 2 segments in the inboard blanket (IB). Each segment is divided in 7 modules for a total of 378 outboard modules and 252 inboard modules. The equatorial outboard module (Figure 6.4.1) has been selected as the affected reference module for the LOCA analysis. It consists of a EUROFER steel box, reinforced by an internal grid of radial-poloidal and poloidal-toroidal plates (stiffeners) to withstand water pressure in case of leakage. The module box is divided in 16 elementary cells in poloidal direction and 6 channels in toroidal direction. Each elementary cell is divided in the middle by a baffle plate. The PbLi enters from the bottom of the cell, flows in radial-poloidal direction and exits from the top of the elementary cell. First Wall is integrated in the module and cooled by an independent system made of square channels with dimension of 7x7 mm and pitch of 13.5 mm. BZ cooling tubes are placed along a toroidal-radial direction. The tubes are double walled and have external diameter of 13.5 mm, internal diameter of 8 mm and thickness of 1.25 mm. Each elementary cell contains 21 tubes. The tubes are grouped and joined to the manifolds of the BZ cooling water. The design data for OB4 are: mass flow rate of 7.38 kg/s, temperature of 285 °C and pressure of 15.5 MPa at the blanket inlet, 325 °C at the blanket outlet. The LiPb in the breeding modules is at 0.588 MPa and 599 K.

Water flows in Double-Wall Tubes (DWTs) in order to reduce the probability of water/LiPb chemical interaction. However, this probability is not negligible and the rupture of DWTs is included in the list of initiating events for DBA to be studied for the DEMO reactor [62].

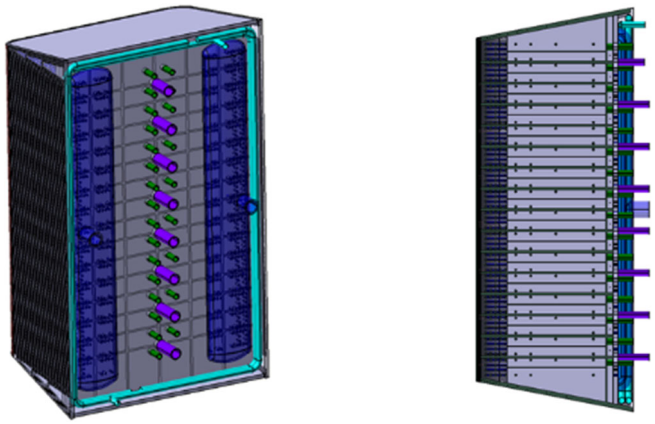

Figure 6.4.1 - DEMO Equatorial outboard module [66]

The rupture mass flow rate calculated in water simulation is transformed in its equivalent in terms of hydrogen and unreacted water steam. Both have been treated as non-condensable gas. Two different input decks, one for each fluid considered, have been coupled through an external interface to account for their reciprocal interaction.

6.4.1 Accident description

For this in-box LOCA analysis, the complete failure of all tubes in the inversion zone of the central elementary cell of the equatorial module has been considered (Figure 6.4.2). The resulting flow area, postulating a double-ended pipes break, is $2.12 \cdot 10^{-3}$ m^2.

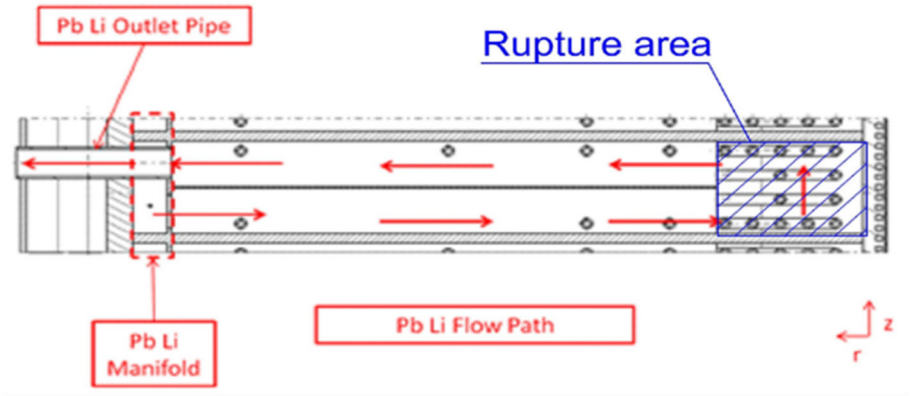

Figure 6.4.2 - Flow path of LiPb and rupture area considered for the analysis [66]

The rupture is supposed to take place in 5 s during which the flow area ranges from 0% to 100% of the total double break area. As conservative assumption, the affected module is supposed to be in adiabatic conditions respect to other modules and structures. Even if fusion power is terminated by overpressure signal in the breeding blanket module, if the module itself fails, coolant and radioactive inventories could be mobilized towards the vacuum vessel. liquid metal dust/water interaction and radioactivity transport are the main concerns in this scenario.

6.4.2 Methodology and assumptions

The MELCOR code, as other thermal hydraulics system codes, is not able to perform simulations with mixing of two or more different fluids, but only non-condensable gases can be added to the working fluid. The presence of both water and lithium-lead within the breeding blanket therefore cannot be simulated.

To overcome such constraint, two input decks have been detailed with two different working fluids: water and lithium-lead. The two input decks have been coupled through an external Phyton script to account for their reciprocal interaction.

The script performs the following operations:

- An External Data File (EDF-2 in Figure 6.4.3) is created to initialize the MELCOR run for the H2O case;
- The MELCOR H2O case runs for a timestep; at the end of the run mass flow rate, pressure and other common parameters are written in a new EDF (EDF-1 in Figure 6.4.3);
- Such data are used by the Python script to evaluate the amount of hydrogen and heat produced by the chemical reaction between LiPb and water;
- Such data are added to EDF-1 which is read by MELCOR input for LiPb case;

- The MELCOR LiPb case runs for a timestep; at the end of the run OB4 module pressure and other common parameters are added to the EDF-2 which is used to run the H2O case for the next time step;
- Iterations are repeated for the other timesteps until the final time is reached.

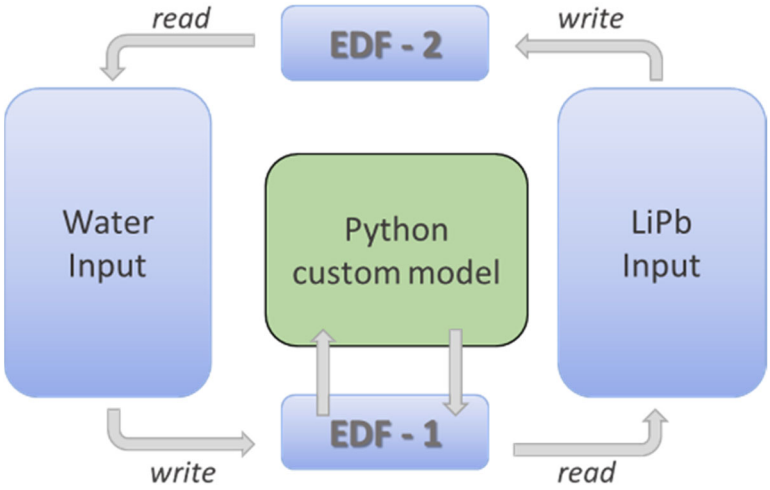

Figure 6.4.3 - Calculation methodology scheme

Even adopting this procedure for the analysis, limitations for MELCOR multicomponent capabilities remain. Several simplifications have been made to perform the simulation. To simulate steam injection into the breeding blanket volumes, a user defined non-condensable gas has been used. Pressure and temperature of steam and hydrogen injected are controlled through EDF, assuming an ideal gas isentropic expansion to the pressure of LiPb side for the evaluation of the steam inlet temperature. The temperature of produced hydrogen is the same of the previous timestep. Then, the energy balance is performed by the code, taking into account the reaction heat, added through an independent heat structure, which heat flux is controlled by the EDF. The hydrogen and heat generated by the LiPb-Water reaction are given by:

$$Li_{17}Pb_{83} + 8.5\ H_2O \rightarrow 8.5\ Li_2O + 8.5H_2 + 83Pb + 19.0\ kJ/mol\text{-}LiPb \qquad (A)$$

$$Li_{17}Pb_{83} + 17\ H_2O \rightarrow 17\ LiOH + 8.5H_2 + 83Pb + 25.8\ kJ/(mol\text{-}LiPb) \qquad (B)$$

The first one (A) occurs in excess of LiPb, while the second in excess of water. From the thermal and hydrogen generation points of view, the reaction (A) is very conservative.

Preliminary experimental campaigns [67] to estimate the water flow rate in the accident suggested to consider a jet of water penetrating into the LiPb volume and, as the reaction will occur mainly at the interface between the liquid metal and water, a condition of excess of water has been assumed as more realistic. Therefore, the reaction (B) has been assumed in the present analyses. The reaction of all the water injected into the LiPb circuit is assumed instantaneous. The reacting water is instantaneously substituted with the correspondent hydrogen generated by the selected chemical reaction. This hypothesis could be very conservative, and in absence of a correct reaction kinetic model implemented, several calculations at different fraction of water participating to the reaction were performed. At this purpose, the C_{react} parameter has been used to represent the fraction of water that entering the breeding zone reacts with the breeder material.

6.4.3 MELCOR model

Water circuit has been nodalized using 34 control volumes (CVHs) connected with flow path to model all reactor components. The 17 undamaged sectors have been modeled using one CVH. The damaged sector has been modeled in detail as reported in Figure 6.4.4. Water circuit is supposed to break in the central part of the OB4 module and the break involves all the 21 DWTs. The broken module (OB4 in Figure 6.4.4) is connected to a time dependent volume (LiPb TDV volume in Figure 6.4.4) to simulate the LiPb side. This volume receives information during the MELCOR LiPb run to set the right pressure and temperature for each time step.

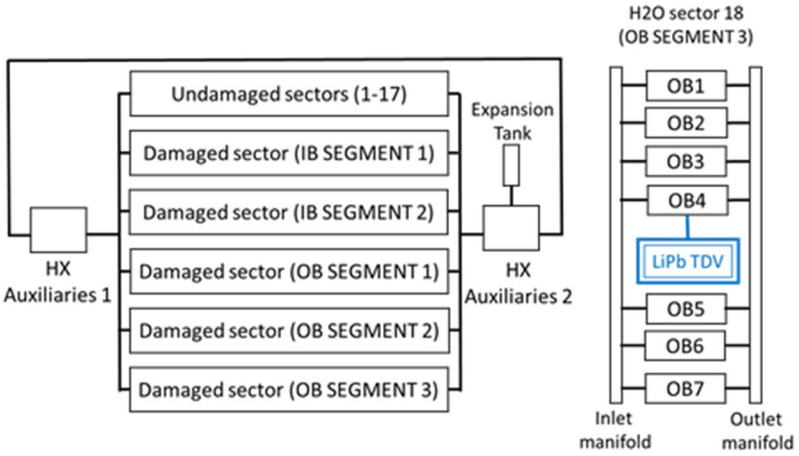

Figure 6.4.4 - Water circuit scheme

The lithium lead circuit has been nodalized with 23 control volumes (CVHs). Two different time dependent control volumes (the blue in Figure 6.4.5) have been used to simulate the effects of LiPb-water reaction within the OB4 module. Their function is to inject steam and hydrogen in the breeding zone depending on the fraction of reacting water.

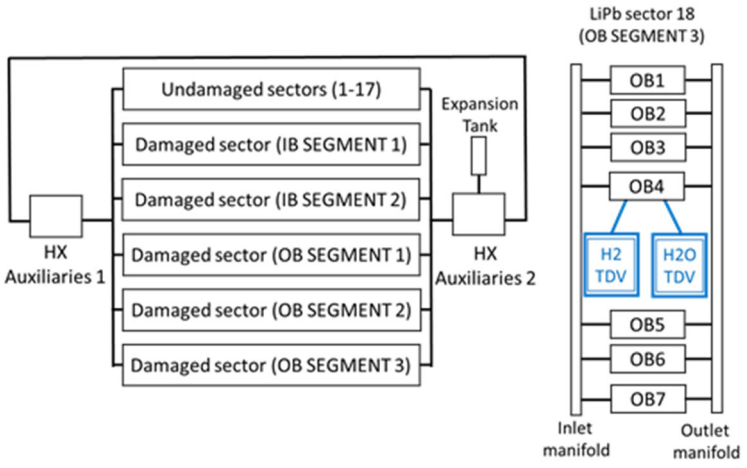

Figure 6.4.5 - Lithium lead circuit scheme

For both circuits, ex-vessel components including loop distributor, steam generator, pumps and pressurizer have been modeled using 2 CVHs. BZ cooling loops, manifolds, caps and back supporting structure (BSS) have been modeled through Heat structures (HSs). The decay heat has been assumed as 1.2% of the full power.

Both LiPb and water runs exchange information on parameters thanks to the custom interface, which made possible to perform coupled analyses. Simulations time has been selected to reach thermal and mechanical equilibrium between the two loops.

Water mass flow rate from the rupture transient (Figure 6.4.6) is characterized by an initial rapid increase from 0 to 5 s when the maximum of about 136 kg/s is achieved. After that, the mass flow rate decreases slowly until 25 s and then declines until the end of the transient. The intermediate and final phases are characterized by instabilities due to reduced pressure difference and vaporization effects within water circuit.

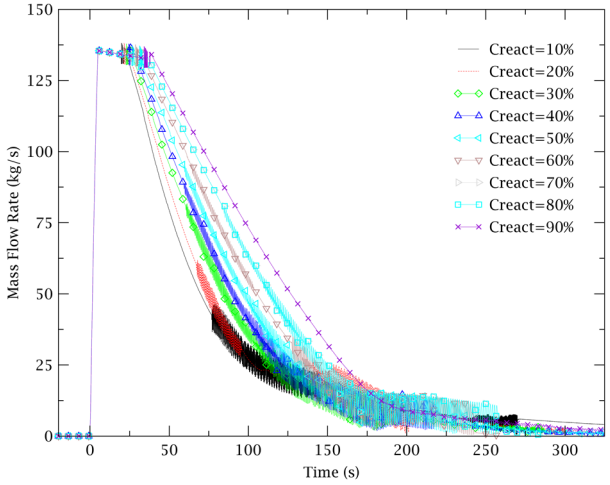

Figure 6.4.6 – Water mass flow rate from rupture

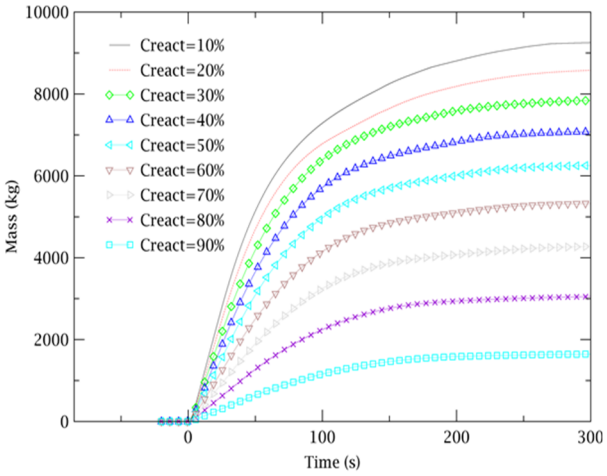

Figure 6.4.7 - Non-reacting water entering in the breeding module

Non-reacting water mass flow rate entering the breeding zone for different values of C_{react} is reported in Figure 6.4.7. The larger is the reaction rate, the lower is the non-reacting water flowing from the water side to the breeding zone. At the end of the transient, with a of 10%, about 9.5 ton of water flowed from the DWTs to the breeding zone.

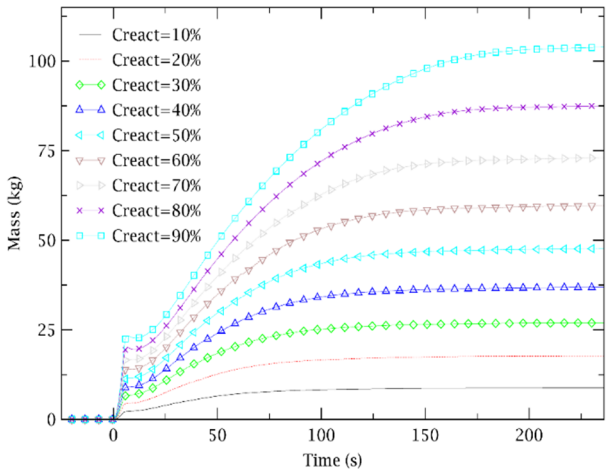

Figure 6.4.8 – Hydrogen generation rate for different reaction coefficients

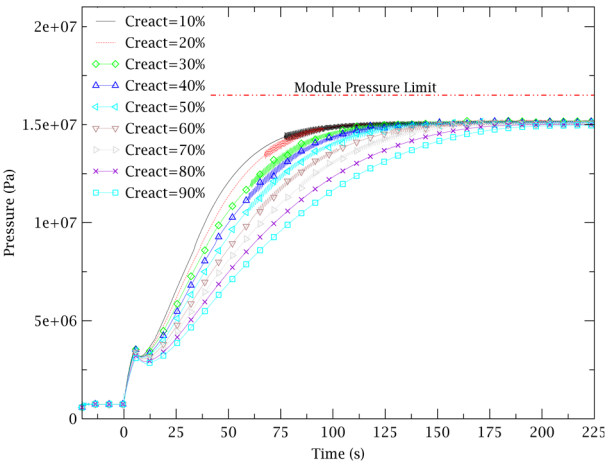

Figure 6.4.9 - Breeding module pressure for different reaction coefficients

Hydrogen production rate (Figure 6.4.8) was obtained using the reaction with excess of water. For each kilogram of reacted water 0.056 kg of hydrogen are produced. The total amount of hydrogen in the broken module reaches a maximum of about 103 kg after 225 s for a of 90%.The fast release of these

amounts of water and hydrogen within the module, along with the reaction energy release, lead to a rapid pressurization of the LiPb loop. Pressure in the module (Figure 6.4.9) is 3.6 MPa at 5 s after the break. After the initial peak, pressure in the damaged module drops to a value of 2.9 MPa and then it starts to increase again due to the combined effect of mass release and reaction. The maximum value of pressure is 14.99 MPa and could be reached between 125 s and 220 s depending on the parameter.

The temperature in the damaged breeder module increases because of heat released by the reaction and decay heat produced after reactor shutdown (Figure 6.4.10). The maximum temperature of 627 K is reached by the module for a C_{react} of 90%. This temperature is below the limit temperature value of EUROFER (823K).

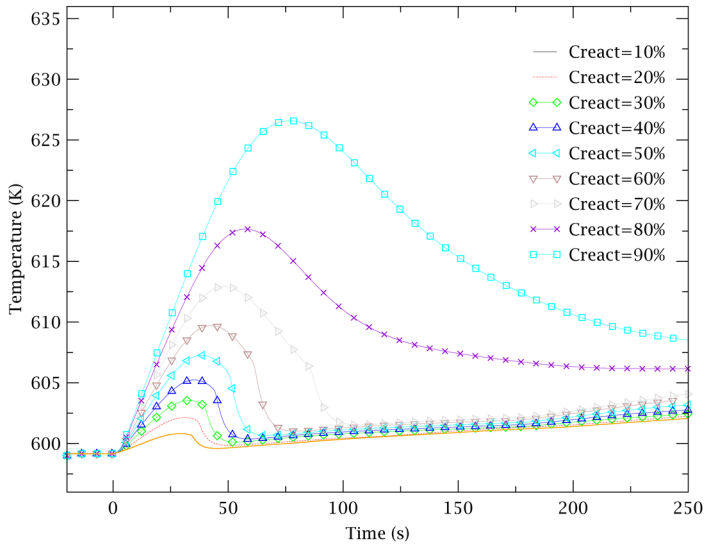

Figure 6.4.10 - Breeding module temperature for different reaction coefficients

6.4.4 Conclusions

This paragraph describes an application of a custom methodology developed to analyze the effects of an in-box LOCA for the WCLL blanket concept of the EU DEMO reactor. Due to the difference in the operating pressure, after the tubes rupture, water enters the breeding module and reacts with lithium lead generating hydrogen and thermal power. To better simulate the mutual influence of the two circuits during the transient, a python script has been developed and used to couple the two sides, which uses two working fluids and requires different inputs. The results obtained for LiPb loop show first a fast pressurization of breeding blanket in which pressure reaches the maximum value of 14.9 MPa which is below the design pressure limit of breeding blanket box which are verified to withstand a pressure of 15.5 MPa + 10% [66]. The parametric analysis, carried out using the fraction of reacting water as parameter, shows faster pressurization for smaller reaction coefficients. This result is related to the methodology used for simulations. The rupture mass flow rate calculated in water simulation is transformed in its equivalent in terms of hydrogen and unreacted water vapor. Both the reaction products are treated as non-condensable gas in LiPb simulation. The higher amount of steam for lower reaction coefficient leads to faster pressurization, as it does not condense.

In the future, the developed model will be improved to consider all these effects, in order to better analyze and understand the reliability of the results.

7 Beyond design basis accidents analyses

Beyond design basis accidents (BDBAs) correspond to hypothetical event sequences that are studied in order to demonstrate the ultimate safety margin of the DEMO design.

They may be defined by starting with a design basis accident and postulating additional independent failures that may aggravate an event sequence. Because they are considered highly improbable may also be defined as an event that has an assessed frequency below that for Cat. IV events in Table 6.1.

Analysis of selected beyond design basis events is performed using best estimate assumptions and may take into account the functions of systems, structures and components that are not necessarily classified as Safety Important [68].

Like DBAs analyses, the focus is on radiological consequences to the public from internally initiated events and, therefore, on demonstrating that DEMO meets the "no evacuation" objective, by providing strong confidence that the design (and operation) of the facility assure the protects the public protection such that there is no technical justification for public evacuation in these hypothetical events, remaining the application of the no-evacuation criterion to hypothetical events to government and regulatory bodies. The dose limit to avoid the need of evacuation for beyond design basis accidents is specified in the PSRD [19]: 50 mSv total predicted early dose from exposure over a 7-day period.

7.1 Ex-VESSEL LOCA without plasma shutdown

The Design postulated accident is a loss of coolant in the FW primary cooling loop due to large rupture in the cold ring of the coolant loop distributor (0.04921 m^2 area). Fusion power is not terminated because the failure of the plasma shutdown and monitoring system has been postulated as an additional safety challenge. Two different simulations were performed with the presence and absence of the downstream isolation valves, respectively:

- CASE 1: both upstream and downstream valves in operation;
- CASE 2: upstream valves only

VVDHRS (VV decay heat removal system) was assumed to be functioning during the accident and providing cooling for the VV and BMs.

7.1.1 Event Sequence

Analysis requirements and main input data have been obtained from DEMO BB Safety Data List.

Table 7.1-1 – Possible transient sequence for an ex-vessel LOCA without plasma shutdown

Parameter	Specification
Definition of initiating event	Loss of coolant in the FW primary cooling circuit inside the TCR because large rupture of the FW-PHTS distributor ring during the normal operation.
Definition of aggravating event	Fusion power is not terminated because of a failure in the plasma shutdown system.
Possible transient sequence	▪ A double break size in the FW-PHTS distributor ring occurs, for a total break area of 0.2328 m^2; ▪ Fusion power is not because the failure of the plasma shutdown system; ▪ If a temperature higher than 1325 °C is reached in the FW, it fails causing water injection inside the plasma volume. ▪ An unmitigated plasma disruption occurs because of steam impurities at the edges of the plasma. The disruption affect a FW surface of 1 m^2

- The failure of the FW structure affects only few millimetres of EUROFER, in such a way only water and steam contained in the FW-PS enters in the plasma chamber, while the LiPb mass remains inside the BZ modules not affected by any rupture;
- The FW of the failed loop is first cooled down with residual water present before complete emptying;
- After the coolant inventory is lost the FW will be cooled by radiation to the surrounding cooled in-vessel components;
- If an in-vessel LOCA occurs the bleed lines and rupture disks open at reaching the pressure set point;
- Isolation valves close when the set-point is reached;
- Coolant and radioactive inventories (tritium, dust and suspended sputtering/ACPs products) will be mobilized towards the TCR or toward the VV
- Feedwater pump stops immediately after the LOCA in the PHTS
- DHR system in operation for all the entire transient

7.1.2 Results and discussion

The 32 h accident simulation starts after a steady state calculation of 2000 s.

Figure 7.1.1 shows the pressure response in the FW and BZ pressurizer. It has been assumed that trip valves begin to close when the pressure in the pressurizer is below 13.0 MPa. This set-point is reached 1.95 s after the PIE and the fully closed state is reached after 11.95 s, when the pressure in the FW pressurizer is 4.83 MPa. Pressure trends in pressurizers are equal for both Case 1 and Case 2. The plasma energy, led to the activation of BZ safety relief valve which set point has been chosen to be 1.88 MPa, after around 18.0 s, against the 88.0 s obtained for the DBA with plasma shutdown.

In Figure 7.1.2 the pressure transient for in-vessel OB4 volume is shown. In the Case 1 scenario, characterized by closure of downstream trip valves, inside in-vessel volumes the pressure decreases until the isolation valves are fully closed (11.95 s). Then, because of plasma burns pressure quickly re-increases and reaches 18.8 MPa at 59.23 s, when SRV discharge steam to prevent an overpressure accident.

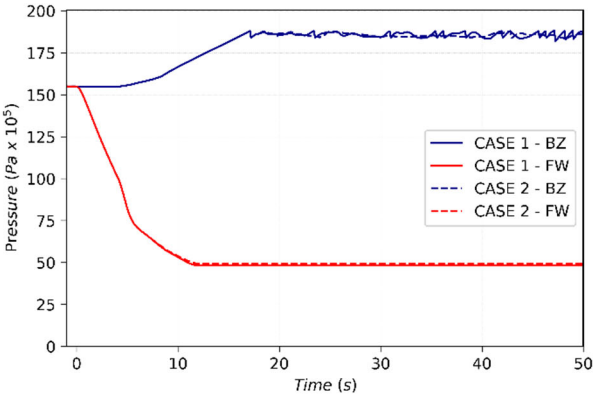

Figure 7.1.1 – Pressure transient in FW and BZ pressurizers

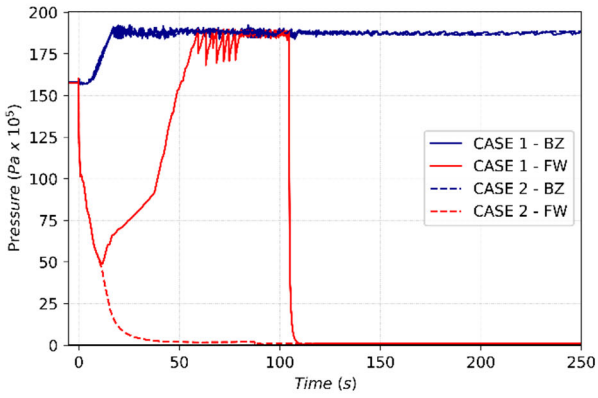

Figure 7.1.2 - Pressure transient in FW and BZ in-vessel volumes

The initial mass flow rate toward the TCR was extremely large (maximum flow rate of 17430.0 kg/s) and then followed by gradually decrease due to the progressively depleted primary system coolant inventory. Figure 7.1.3 shows the mass flow rate variations at break as a function of accident time. As showed in Figure 7.1.4 around 100 tons and 118 ton of water are released inside the TCR in Case 1 and Case 2, respectively. In the case with downstream isolation valves in operation (CASE 1) the mass flow

rate decreases until and remains very low for the whole transient. In CASE 2 (only upstream valves installed), mass flow rate decreases slowly, and a greater amount of water is released in the TCR vault.

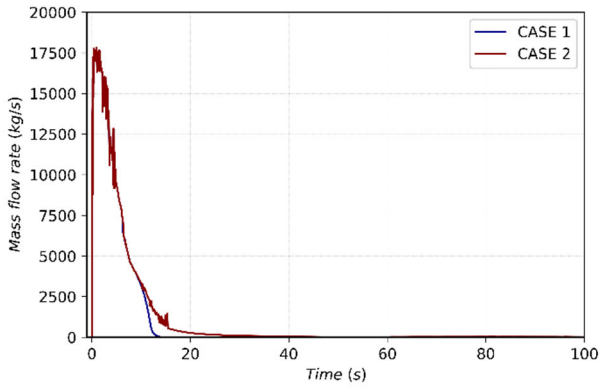

Figure 7.1.3 – Mass flow rate from ring distributor guillotine break

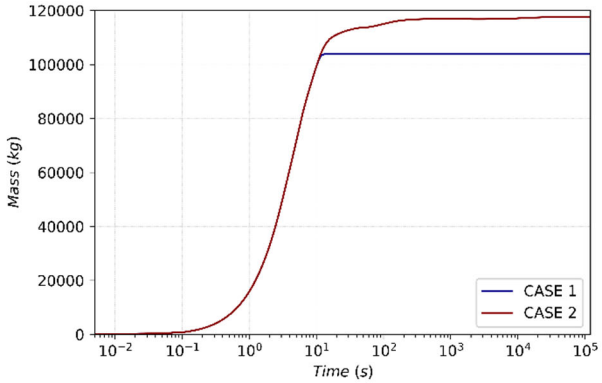

Figure 7.1.4 – Mass of liquid water and steam discharged into the Upper Chase area

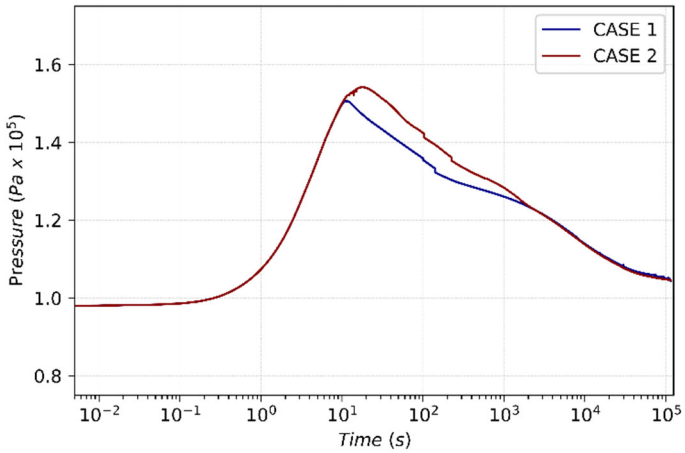

Figure 7.1.5 – TCR pressure

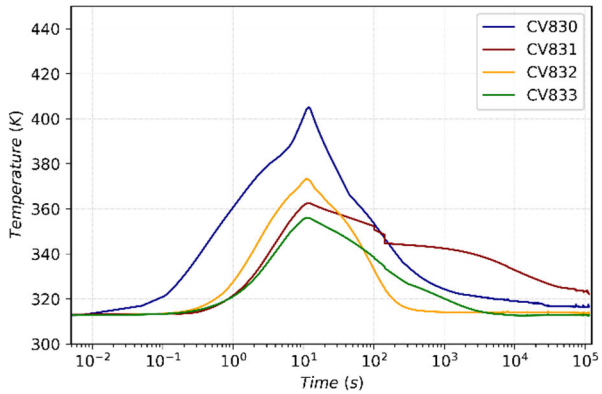

Figure 7.1.6 - Atmosphere temperature of TCR volumes (Case 1)

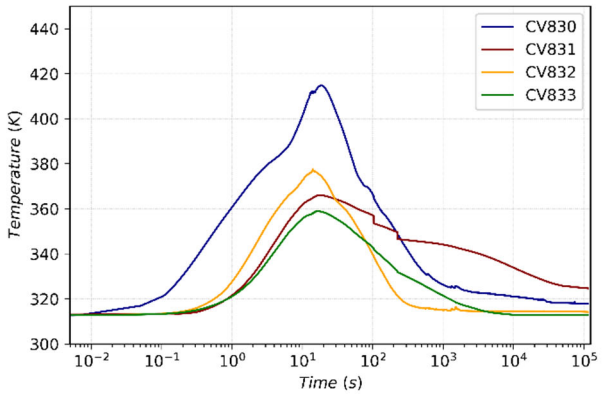

Figure 7.1.7 - Atmosphere temperature of TCR volumes (Case 2)

The release of this amount of water within the TCR leads to a rapid pressurization of the containment (Figure 7.1.5). Pressure increases very quickly and reaches 150 kPa in around 10 s if downstream valve are installed, otherwise pressure in TCR vault reaches a maximum of 154 kPa after 20 s from the beginning of the transient (CASE 2). After that, pressure decreases because of the only effect of the

steam condensation on TCR wall surfaces which are initialized at 30°C. Despite the very large surface available for steam condensation, pressure in the TCR remains above the atmospheric pressure for all the 32 h of the simulation. In Figure 7.1.6 and Figure 7.1.7 the TCR vault atmosphere temperature is shown for different TCR compartments. The maximum atmosphere temperature is reached in the upper pipe chase volume (CV 830) where more than 400 K are reached.

The closure of isolation valves in front of a low pressure in the FW-PHTS affects not only the amount of water released toward the TCR, but also the pressure transient inside the FW-PS channels and therefore the physical state of water and heat transfer coefficients. As an example, in Figure 7.1.8 the temperature of FW structure is shown. In Case 1 the failure is occurs later because of the closure of downstream trip valves. This could be seen as a positive effect because more time for the recovery of the plasma shutdown system is available. However, if that is not the case, the FW volume are pressurized at 18.8 MPa when the breach toward the VV is opened.

The failure point of the FW structure is located in the upper part of the segment module (OB1 volumes) and is reached after 87.55 s and 104.4 s, for Case 2 and Case 1, respectively.

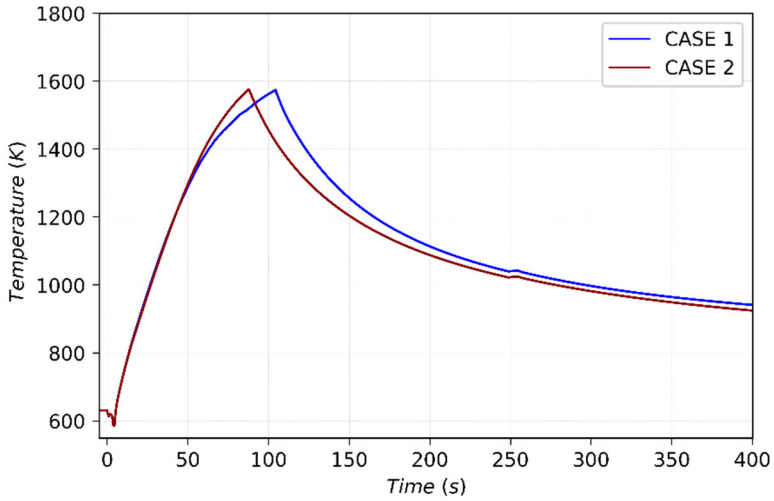

Figure 7.1.8 - OB1-FW temperature

The temperature limit is reached in all the OB1 volumes, causing a failure of the entire toroidal ring. The failure of a single FW channel has been assumed for each OB1 volumes. The resulting flow area is 0.004704 m^2.

The break of the OB1-FW structure causes the release of steam and water inside the plasma chamber, which in turn causes an unmitigated plasma shutdown transient. As specified in Table 7.1-1 the unmitigated disruption affects a FW area of 1 m^2 causing the failure of the break of 262 FW channels. An equivalent opening of 0.02568 m^2 is opened between a OB4 volume and the plasma volume. The total masses of steam and water flowing toward the plasma chamber are reported in the figures below. In the case in which downstream isolation valves are not installed (Case 2), a large part of the FW-PHTS inventory is discharged into the tokamak building volumes, thus when the in-vessel breach occurs there's not enough inventory to cause a VV pressurization. This fact is highlighted in Figure 7.1.9 and Figure 7.1.11. In contrast, in Case 1, downstream isolation valves mitigate the total mass discharged in the TCR, and when the in-vessel breach occurs more than 6000 kg of pressurized steam (Figure 7.1.10) are injected in the VV.

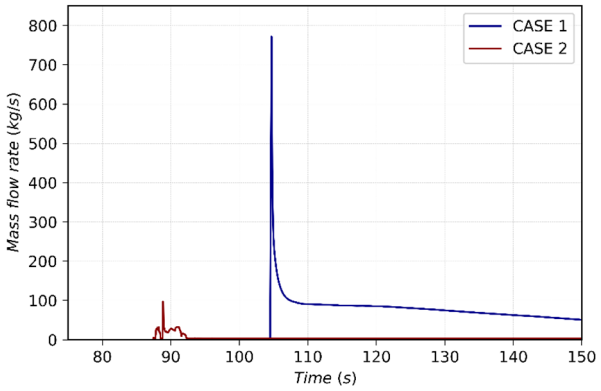

Figure 7.1.9 – Mass flow rate entering VV

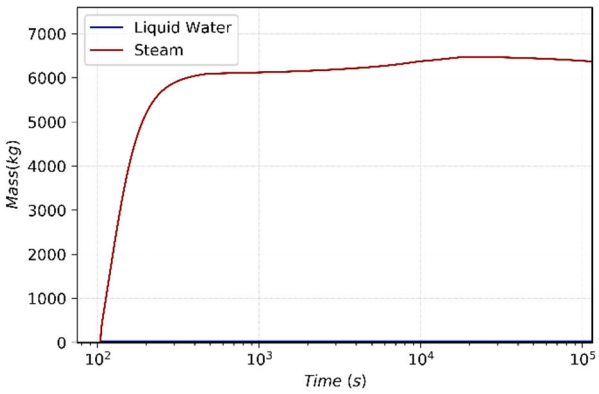

Figure 7.1.10 - Mass of steam and water entering the VV (Case 1)

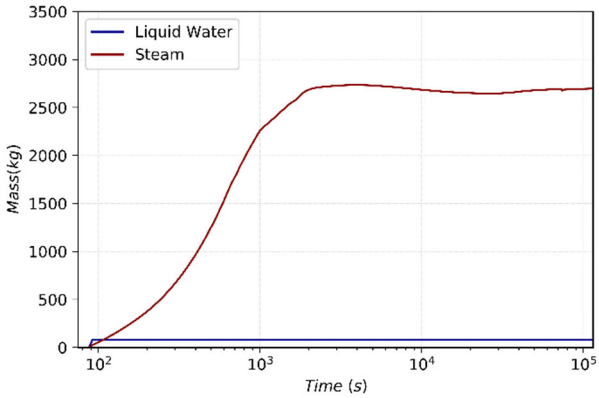

Figure 7.1.11 - Mass of steam and water entering the VV (Case 2)

As shown in Figure 7.1.12, pressure transient in the VV is characterized by a relatively fast pressurization in Case 1, and by a very low pressurization in Case 2 which increases until the mechanical equilibrium with the TCR volumes is reached. The maximum pressure peak is 1.231 bar after 135.9 s for Case 1 and 1.227 bar after 2305 s for case 1. Thus, the setpoint of 0.9 bar for the opening of VVPSS Tank A is reached in both the accident scenarios.

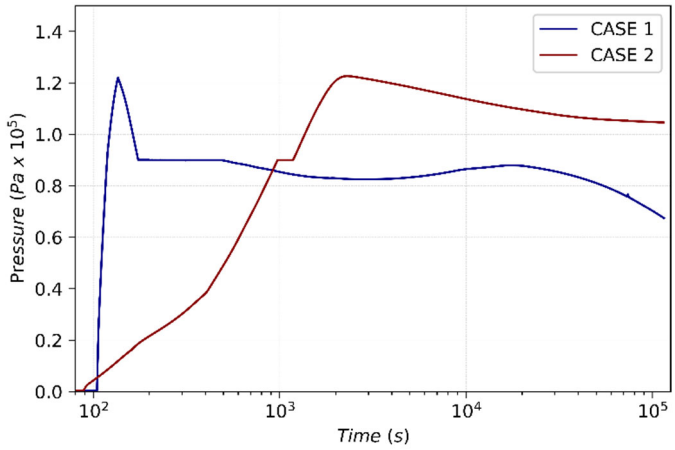

Figure 7.1.12 – Pressure in the plasma volume

Summary of pressure values in different volumes are given below in Table 7.1-2. Time of intervention of BLs Table 7.1-3.

As reported in Figure 7.1.13 and Figure 7.1.14 the presence of downstream valves ensures the isolation between the VV and the external environment.

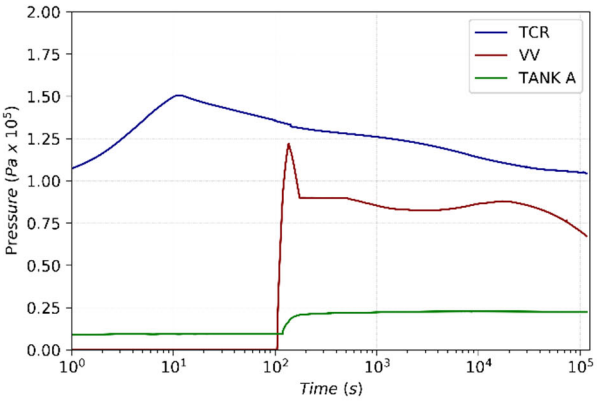

Figure 7.1.13 – Pressure in TCR, VV, VVPSS volumes (Case 1)

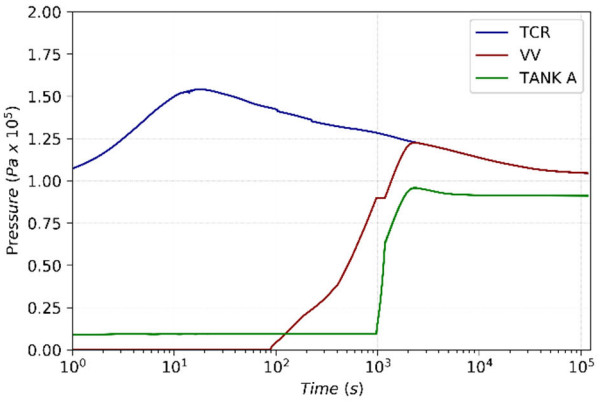

Figure 7.1.14 – Pressure in TCR, VV, VVPSS volumes (Case 2)

Table 7.1-2 – Pressure Values

Volume	**Maximum pressure [MPa]**		**Pressure at the end of the transient [MPa]**	
--	**CASE 1**	**CASE 2**	**CASE 1**	**CASE 2**
TCR	0.150	0.1541	0.1043	0.1040
VV	0.122	0.1226	0.0674	0.1046
VVPSS – Tank A	0.022	0.0958	0.0223	0.0911

Table 7.1-3 – VVPSS components intervention time

	Component	**Time [s]**
Case 1	Rupture discs	--
	Bleed Lines Valves	106.2
Case 2	Rupture discs	--
	Bleed Lines Valves	989.5

Steam inside the VV could react with FW and DV tungsten layers leading to hydrogen generation. The total mass of hydrogen produced in Case 1 is 139.8 g. The mass produced in Case 2 is 31.6 g. In Figure 7.1.15 and Figure 7.1.16 the mass of hydrogen in VV, VVPSS and TCR volumes is shown. The reaction between steam and tungsten dust deposited on the FW surface and on the divertor surface has not been considered in this simulation. If VV is isolated from the TCR by isolation valves, 360.5 g of hydrogen builds up inside the plasma chamber and about 386.9 reaches the tank A of VVPSS. Instead, in the case in which downstream isolation valves are not closed, the hydrogen produced inside the plasma chamber can reach TCR compartments. Results are summarized in the table below.

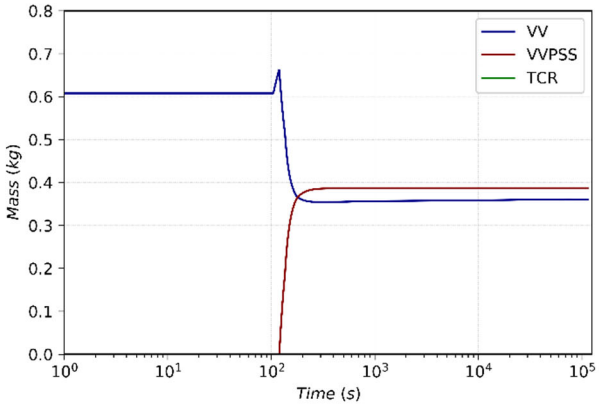

Figure 7.1.15 – Mass of hydrogen in VV, VVPSS and TCR volumes (Case 1)

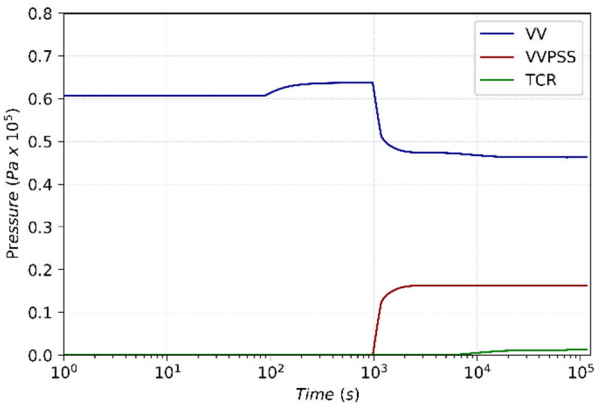

Figure 7.1.16 – Mass of hydrogen in VV, VVPSS and TCR volumes (Case 2)

Table 7.1-4 – Mass of Hydrogen

(32 h from the beginning of the accident sequence)

Volume	Mass of hydrogen [kg]	
--	CASE 1	CASE 2
TCR	-	0.0130
VV	0.3605	0.4631
VVPSS	0.3869	0.163

7.1.3 Radiological Releases

Figure 7.1.17 present the portion of tungsten dust inventories that reside within the VV and VVPPS for both Case 1 and Case 2. After a simulation time of 32 h, of the 694.0 kg of mobile tungsten dust:

- in Case 1 around 639 kg remain in the VV volumes and 58.98 kg are moved in the tank A of the VVPSS;
- in Case 2 around 669.653 kg remain confined in the VV and around 25 kg of dust is transported into the VVPSS.

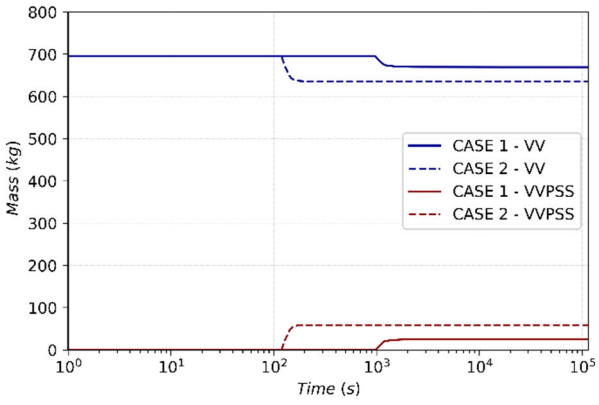

Figure 7.1.17 – Mass of W dust in VV and VVPSS volumes

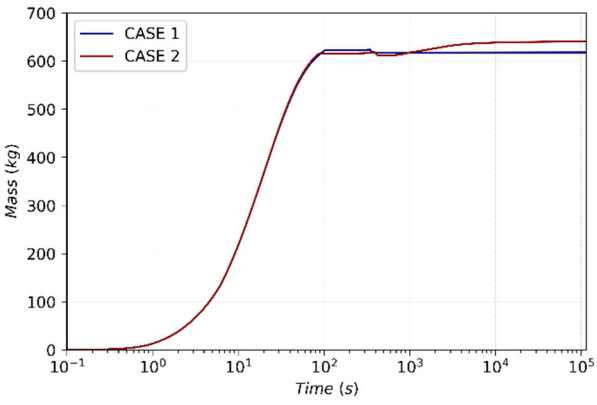

Figure 7.1.18 – Mass of W dust deposited on VV surfaces

In both cases large part of the tungsten dust in VV is deposited internal structures (Figure 7.1.18).

In Case 1 the intervention of downstream isolation valves inhibits transport phenomena toward the TCR. However, in Case 2 there is a connection between the VV and the TCR and at the end of the simulation around 162 g of tungsten dust into the TCR compartments can be found

As shown in Figure 7.1.19 and Figure 7.1.20 ACP release occurs mainly in the TCR. Only few grams are mobilized in the VV and the amounts in the VVPSS could be neglected cause of its low valueS. The mobilization of ACP in the TCR is very similar in both cases, in fact the release occurs immediately after the ex-vessel break, after 10 s of the 0.7 kg of ACP initially in the FW-PHTS, 0.6911 kg are discharged in the TCR. At the end of the simulation the only activated corrosion products confined in the PHTS barriers are those in the BZ-PHTS that maintains its structural integrity.

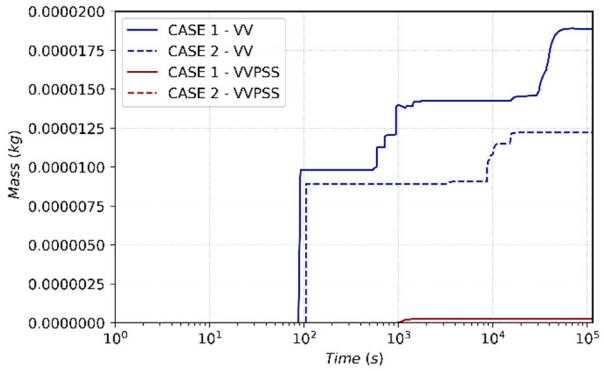

Figure 7.1.19 – Mass of ACP VV and VVPSS volumes

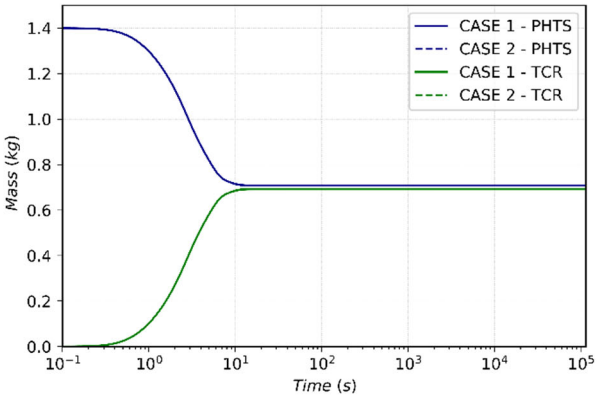

Figure 7.1.20 – Mass of ACP in PHTS and TCR volumes

In conclusion, concerning the mobilization of tritiated water, results are shown in Figure 7.1.21 and Figure 7.1.22. Should be noted that 2.5 kg and 1.4 kg of HTO reaches the TCR in Case 2 and Case 1, respectively. These amount of HTO can be entirely released in the external environment because of the higher pressure in the TCR. To reduce the radiological hazard, detritiation system be foreseen together with suppression or containment cooling systems.

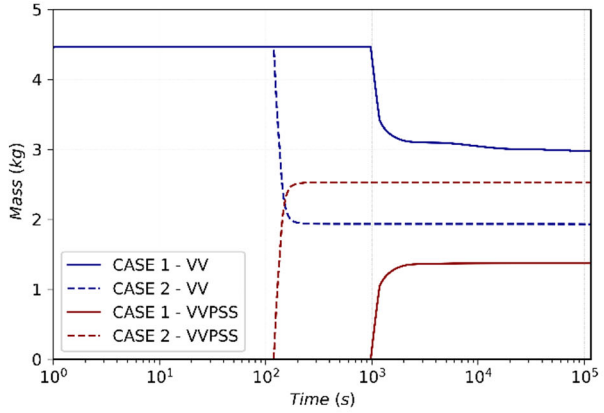

Figure 7.1.21 – Mass of HTO in VV and VVPSS volumes

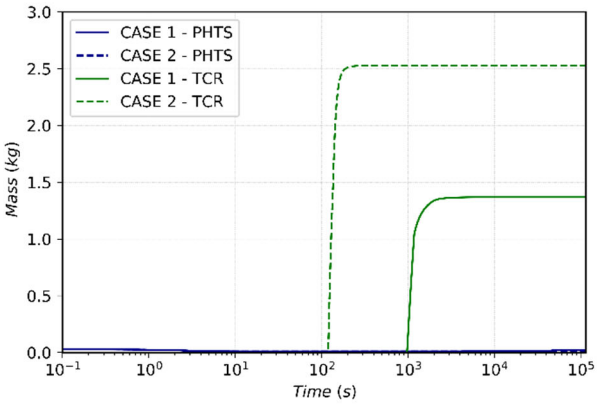

Figure 7.1.22 – Mass of HTO in PHTS and TCR volumes

7.1.4 Conclusions

A pipe rupture was initiated by opening a connection between the TCR vault and the FW cold loop distributor. Due to the difference in the operating pressure (98.0 kPa in the TCR Vs. 15.5 MPa in the FW-PHTS), after the tube rupture, water and steam enters the TCR vault causing a rapid pressurization. The results indicate the pressure increase in the building is very fast and the maximum pressure peak is 154 kPa in the case in which downstream trip valves are not installed. In the other case, the trip valve closure allows less steam to be injected in the TCR causing a pressure peak of 150 kPa.

Because of a non-execution of the plasma shutdown signal all the OB1-FW structures melts causing the release of steam and water inside the plasma chamber, which in turn causes an unmitigated plasma shutdown transient. If downstream trip valves are closed, larger inventories of water and steam are injected inside the plasma chamber. However, the pressurization of the VV is quite slow, because of the large amount of water previously discharged into the TCR, and not enough to cause the opening of VVPSS rupture discs.

Results related to the mobilization of the radioactive source term, demonstrated the possibility of a serious radiological hazard because of the large amounts of tritiated water released in the TCR.

7.2 LOFA without plasma shutdown

Another Beyond Design Basis Accident (BDBA) involving the failure of the plasma shutdown system has been performed. In this case the pustulated initiating event has been assumed to be a pump trip in the FW primary cooling circuit.

Because there is no direct inherent feedback between transients in the cooling systems and the plasma, an active system is required to terminate the plasma burn to limit the heat up of in-vessel components and to prevent these LOFA event from propagating into an in-vessel LOCA event with the potential for significant hydrogen generation. The aggravating event considered in this analysis is the failure of the plasma shutdown system. For such a reason the plasma burns continuously until the FW is overheated and fails.

All the OB1 modules (16 sectors and 3 segments per sector, i.e. 48 modules) of the DEMO reactor are supposed to fail simultaneously when the temperature limit for the EUROFER wall (1325°C) is reached. However, the number of FW channels in which the melting conditions are reached is unknow, for such a reason three different accident scenario have been simulated:

- Rupture of 10 FW channels/module (total double break area 0.04704 m^2)
- Rupture of 5 FW channels/module (0.02352 m^2)
- Rupture of 1 FW channel/module (0.004704 m^2)

An unmitigated plasma disruption occurs because of the injection of steam and impurities inside the VV volume. Further steam and water masses may be discharged inside the plasma volume. Hot water and steam inside the plasma chamber allow for the possibility of hydrogen generation by tungsten-steam chemical reactions.

The decay heat removal system is considered in operation for the duration of the accident transient (72 h).

In the table below information about safety relief valves and isolation valves involved in the simulation are summarized. Enthalpy of water increases because of plasma heating, therefore SRV setpoint is an important parameter in this simulation because the pressurized steam spilled into the vacuum vessel may damage the VV internal structures causing a loss of confinement function.

Both downstream and upstream isolation valves have been used in this simulation.

Table 7.2-1 - SRVs and trip valves setpoint

Valve Type	Position	Load [MPa]	Unload [MPa]
		Set point for opening	*Set point for closure*
SRV	BZ - Pressurizer	16.5	16.0
SRV	FW - Pressurizer	16.5	16.0
Isolation Valve	Upstream (cold/hot leg)	14.0	
Isolation Valve	Downstream (Feeding pipe)	14.0	
SRV	Before each downstream isolation valve	16.5	16.0

7.2.1 Event Sequence

Analysis requirements and main input data have been obtained from DEMO BB Safety Data List and DEMO Accident Selection and Description

Table 7.2-2 - Possible transient sequence for a LOFA without plasma shutdown

Parameter	Specification
Definition of initiating event	Pump trip in FW primary cooling circuit is postulated
Definition of aggravating event	Fusion power is not terminated because of a failure in the plasma shutdown system.
Possible transient sequence	▪ If a temperature higher than 1325 °C is reached in the FW, it fails causing water injection inside the plasma volume. ▪ An unmitigated plasma disruption occurs because of steam impurities at the edges of the plasma. The disruption affects a FW surface of 1 m^2 ▪ The failure of the FW structure affects only few millimetres of EUROFER, in such a way only water and steam contained in the FW-PS enters in the plasma chamber, while the LiPb mass remains inside the BZ modules not affected by any rupture; ▪ The FW of the failed loop is first cooled down with residual water present before complete emptying; ▪ If an in-vessel LOCA occurs the bleed lines and rupture disks open at reaching the pressure set point; ▪ Isolation valves close when the set-point is reached; ▪ Coolant and radioactive inventories (tritium, dust and suspended sputtering/ACPs products) will be mobilized towards the TCR or toward the VV ▪ Feedwater pump stops immediately after the LOCA in the PHTS ▪ DHR system in operation for all the entire transient

7.2.2 Results and discussion

The postulated initiating event is supposed to occur at time t=0.0 s. As shown in Figure 7.2.1 a pump shutdown transient has been assumed [69]. Pump mass flow rate decreases quickly and reaches the 10% of the nominal value in about 6.5 s. The mass flow rate in the OB1-FW module is shown in Figure 7.2.2. Mass flow rate decreases from 7 kg/s to 1 kg/s in 6.85 s and then fluctuates between 0.0 and 0.2 kg/s until the temperature limit of EUROFER is reached. The MFR peak at 73.0 s is due to the melt of FW channels.

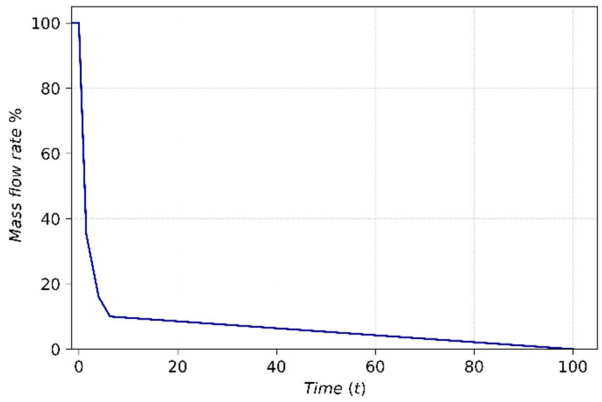

Figure 7.2.1 – FW pump shutdown transient

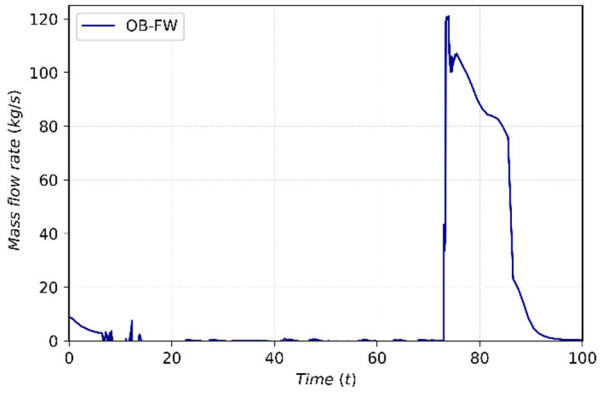

Figure 7.2.2 – Mass flow rate in OB1-FW module

As specified in Table 7.2.2 fusion power is not terminated because of a failure in the plasma shutdown system. As a result, FW temperature increases until the limit of 1598 K is reached. The temperature transient of OB1-FW structure is shown in the figure below.

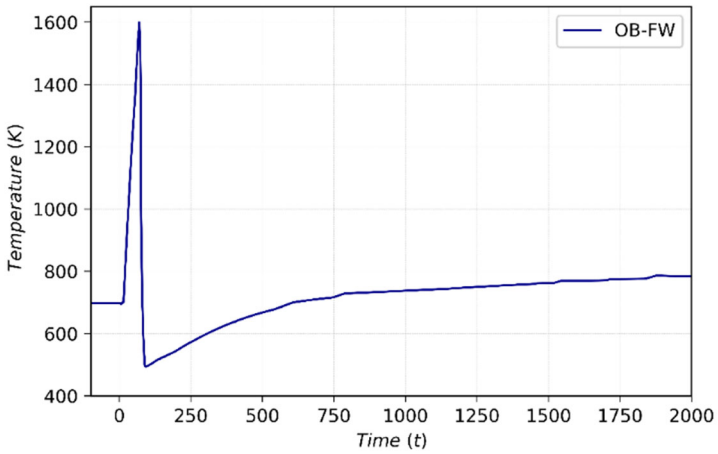

Figure 7.2.3 – OB1-FW module temperature

The break of the OB1-FW structure causes the release of steam and water inside the plasma chamber, which in turn causes an unmitigated plasma shutdown transient. According to the nodalization scheme three different flow-path have been used to simulate 16x3 simultaneous ruptures. However, the number of FW melted channels is unknow, for such a reason three different scenarios have been simulated:

- Rupture of 10 FW Channels/module: total double break flow area equal to 0.04704 m^2
- Rupture of 5 FW Channels/module: total double break flow area equal to 0.02352 m^2
- Rupture of 1 FW Channel/module: total double break flow area equal to 0.004704 m^2

The unmitigated plasma disruption causes the break of 262 FW channels involving 2 outboard segments, one of which is completely broken and the other partially broken, for a total break area of 0.02568 m^2. In this simulation it is supposed that only the first layer of the FW structure is affected by the rupture, in such a way only water and steam contained in the FW-PS enters in the plasma chamber, while the LiPb mass remains inside the BZ modules not affected by any rupture.

Water mass flow rate transients from the FW-PHTS to the VV and the mass of water and steam entering the VV are reported in Figure 7.2.4 and Figure 7.2.5. Results are summarized in Table 7.2-3.

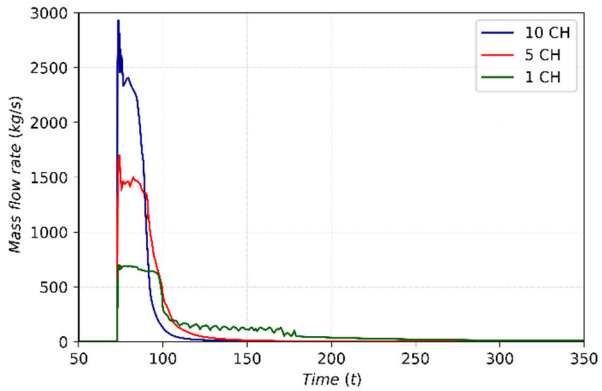

Figure 7.2.4 - Mass flow rate toward VV

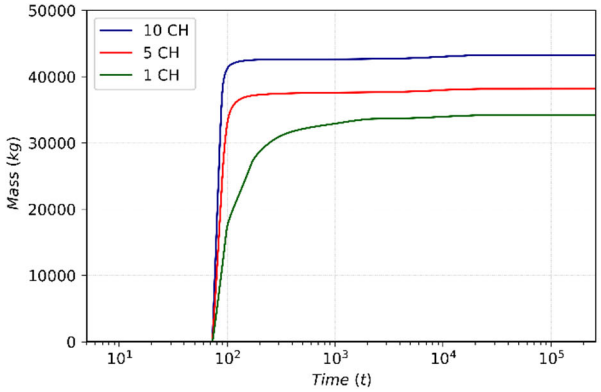

Figure 7.2.5 - Integral MFR toward VV

Table 7.2-3 – Mass discharged toward VV

CASE	Maximum MFR [kg/s]	Integral MFR [kg]
10 channels	2930.57	43,261
5 channels	1698.55	38,162
1 channel	698.85	34,224

The amount of steam and water released into the VV is affected by the trip valve closure. In Table 7.2-4 the intervention time of isolation valves is reported.

Table 7.2-4 – Trip valves intervention time

CASE	Component	Signal [s]	Complete closure [s]
10 Channels	Upstream FW – ISLV Downstream FW – ISLV	81.5	91.5
5 Channels	Upstream FW – ISLV Downstream FW – ISLV	84.5	94.5
1 Channel	Upstream FW – ISLV Downstream FW – ISLV	92.5	102.5

The release of this amount of water within the VV leads to a rapid pressurization of the VV volumes.

Pressure increases very quickly and in the case in which 10 channels melt for each DEMO sector the pressure inside the plasma chamber is higher than the design pressure limit of 200 kPa. In both the other cases pressure peak is limited by the intervention of VVPSS passive components.

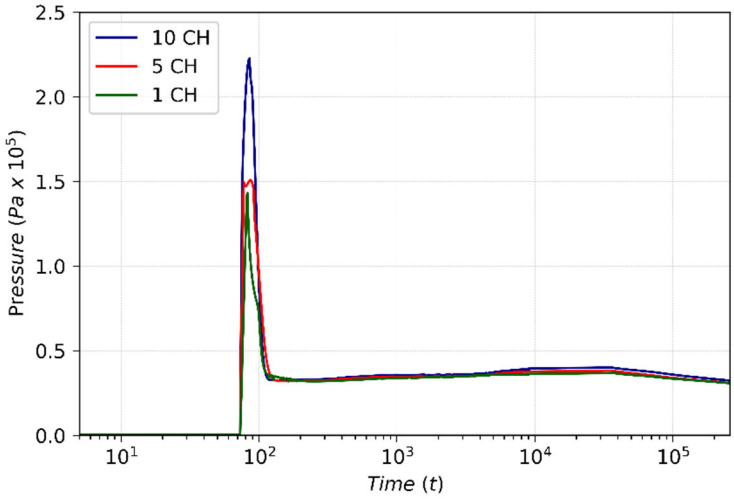

Figure 7.2.6 – Pressure inside the Plasma Chamber (CV851)

Pressure values inside the plasma chamber are summarized in Table 7.2-5.

Table 7.2-5 – Pressure inside the plasma chamber

	10 Channels	5 Channels	1 Channel
Maximum pressure [MPa]	0.2226	0.1509	0.150
Pressure at the end of the transient [MPa]	0.03241	0.03093	0.03088

Differently from the analyses previously before, for this accident scenario the tank A of the VVPSS has a volume of 300 m^2 filled with 30 m^3 of subcooled water and no suppression function has foreseen, gases coming from the VV are discharged in the tank atmosphere.

In Figure 7.2.7 the pressure in VVPSS are reported together with the pressure in VV. Should be noted that, apart from the initial pressure peak, in all the three cases the VV and VVPSS pressure values remain under atmospheric pressure ensuring confinement of radioactive material. A detail of pressure transient in all VVPSS tanks is reported below in Figure 7.2.8.

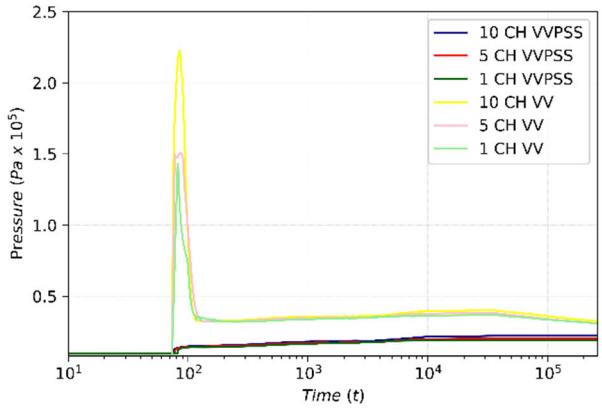

Figure 7.2.7 - Pressure in VV and VVPSS (tank B to F)

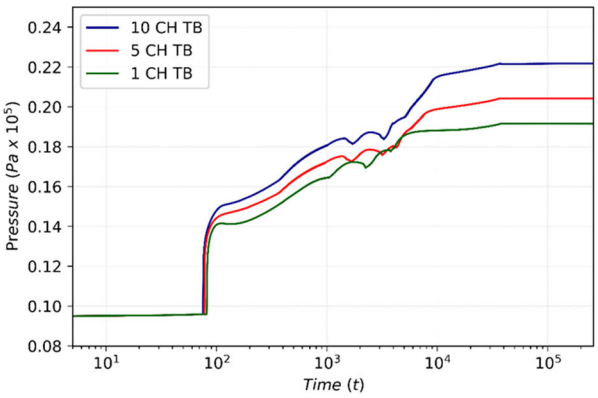

Figure 7.2.8 - Pressure in VVPSS (tank B to F)

Table 7.2-6 - VVPSS components intervention time

CASE	Component	Signal [s]
10 Channels	Rupture discs	76.5
	Bleed Lines Valves	74.54
5 Channels	Rupture discs	77.5
	Bleed Lines Valves	76.5
1 Channel	Rupture discs	82.5
	Bleed Lines Valves	78.5

gg

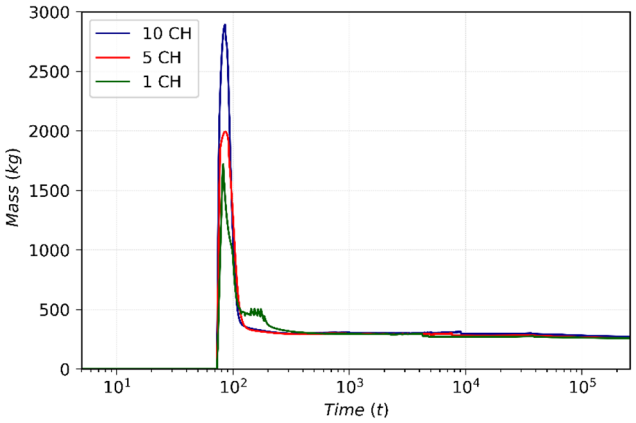

Figure 7.2.9 – Mass of steam in VV

In Figure 7.2.10 the mass of hydrogen produced is shown. About 300 g of hydrogen are produced in all the three cases. However, should be noted that the reaction between steam and tungsten dust deposited on the FW surface and on the divertor surface has not been considered in this simulation.

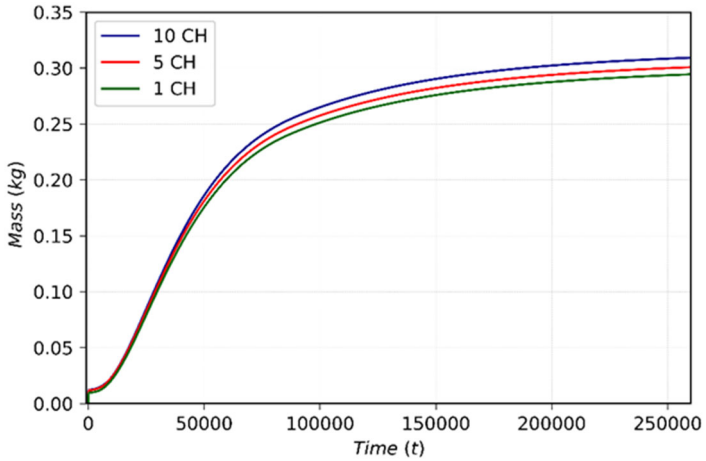

Figure 7.2.10 - Mass of Hydrogen produced by W-H2O reaction

In Figure 7.2.11 and Figure 7.2.12 the temperature transient for the FW structure is shown for outboard modules and inboard modules respectively, in the case in which 10 FW channels melt. In this case, after the failure of FW structure, temperature reaches lower values because of the long-term flow of steam toward the plasma chamber.

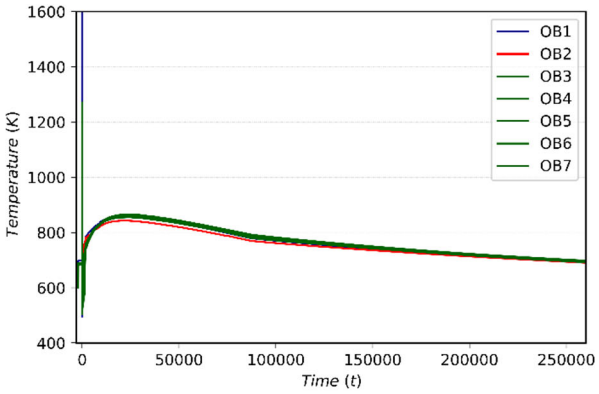

Figure 7.2.11 - Temperature FW outboard modules

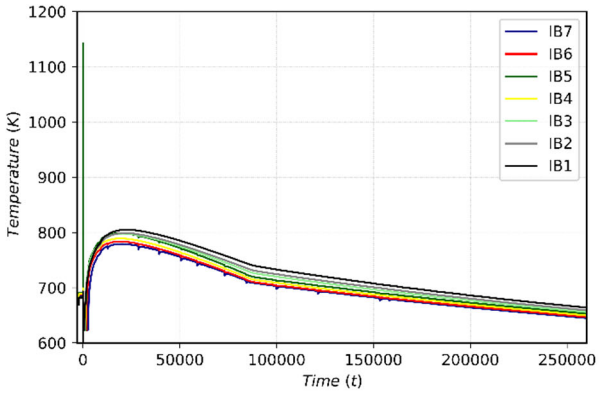

Figure 7.2.12 - Temperature FW inboard modules

7.2.3 Source term mobilization

In this analysis, the mobilized radioactive materials are activated dust and tritium (as tritiated water - HTO) from the VV, and HTO and activated corrosion products (ACP) from the failed FW/BL PHTS cooling loop. According to DEMO safety data list [20], the quantity of tungsten dust mobilized in the VV as a result of the coolant ingress is 694 kg (5 kg of dust are produced following to the plasma disruption), and the quantity of mobilizable in-vessel tritium is 671.0 g. Tritium within primary cooling system is assumed to be in the form of HTO; as a result of the coolant ingress within the VV, 4.454 kg of HTO are considered. The tritium concentration in primary cooling system is 0.015 g-T/m^3 water, so the total amount of tritiated water is 18.1 g in the FW-PS and 32.0 g in the BZ-PS. The quantity of ACP in a FW/BL PHTS loop is 10 kg, a mobilization fraction of 7% has been used for ACP. A preliminary analysis to quantify the leak of tritiated water from the system has been performed by activating the

HTO Transport Model included in the MELCOR code for fusion applications. The total mass of ACP, tungsten dust and tritiated water released in VV and VVPSS are reported in Figure 7.2.3 to Figure 7.2.18, for the case in which 10 FW channel fail. Source term masses at 72 h of simulation are summarized in Table 7.2-7,Table 7.2-8,Table 7.2-9.g

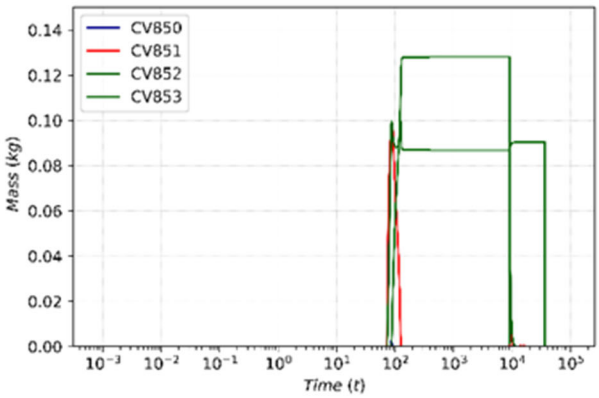

Figure 7.2.13 - Mass of ACP in VV volumes(10 channels melt)

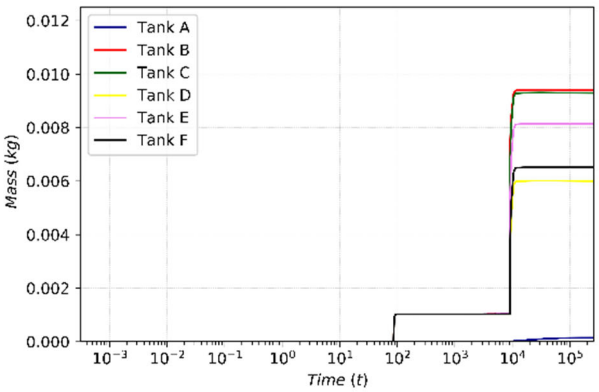

Figure 7.2.14 - Mass of ACP in VVPSS tanks (10 channels melt)

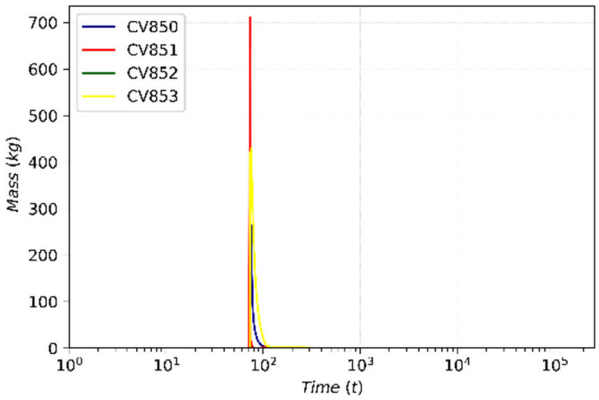

Figure 7.2.15 - Mass of tungsten dust in VV volumes (10 channels melt)

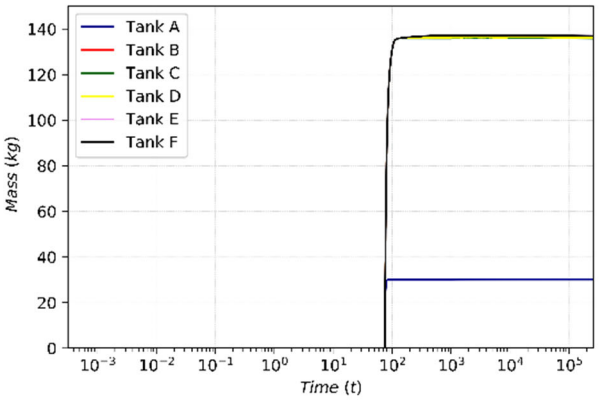

Figure 7.2.16 - Mass of tungsten dust in VVPSS tanks (10 channels melt)

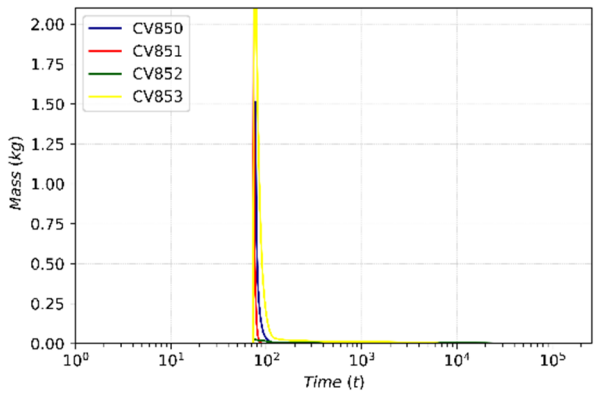

Figure 7.2.17 - Mass of HTO in VV volumes (10 channels melt)

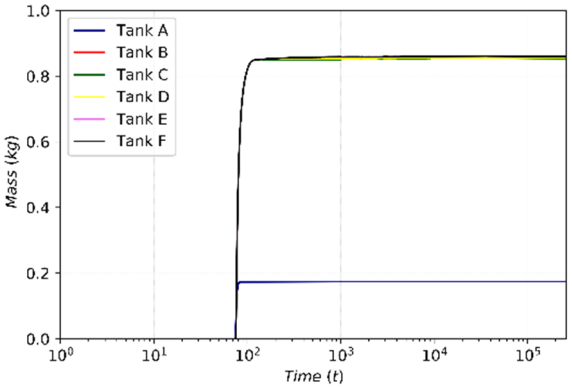

Figure 7.2.18 - Mass of HTO in VVPSS tanks (10 channels melt)

Table 7.2-7 – Mass of ACP [g]

Volume	10 channels	5 channels	1 channel
VV	--	--	
VVPSS	39.49	36.9	53.3

Table 7.2-8 – Mass of tungsten dust [kg]

Volume	10 channels	5 channels	1 channel
VV	--	--	
VVPSS	672.76	672.57	672.39

Table 7.2-9 –Mass of tritiated water [g]

Volume	10 channels	5 channels	1 channel
VV	2.285	2.844	3.4
VVPSS	4.458 E+3	4.455 E+3	4.458 E+3

To quantify leakage of radioactive aerosols from confinement barriers and from the containment, data from [20] have been used. The nominal leak rate is assumed to be 100% TCR air volume per day when the pressure in the TCR volume exceeds the atmospheric pressure. Concerning VV and VVPSS the nominal leak rate is assumed to be 1% of volume per day when the volume pressure exceeds the atmospheric pressure.

These quantities have been evaluated during the post-processing phase considering volume pressure and aerosol concentrations in the volume atmosphere.

Results are reported in the Table 7.2-10 for the worst case in which 10 channels melt. Pressure inside VVPSS tanks never exceeds the atmospheric pressure, while in the VV pressure leak of radioactive material can occur in the short period following the FW break (pressure in VV remains above the atmospheric pressure for 22.76 s).

Table 7.2-10 –Releases from DEMO first confinement barrier

Volume	10 Channels		
--	W dust [g]	ACP [g]	HTO [g]
VV	0.7602E-3	2.297E-07	3.307E-05
VVPSS	--	--	--

7.2.4 Conclusions

The aim of this simulation was to analyze the effects of a loss of flow accident (classified as BDBA. Moreover, to evaluate the effects in terms of radioactive releases and thermal hydraulic behavior of main DEMO components three different simulations have been performed. In fact, the number of FW channels in which the temperature limit is reached cannot still be correctly estimated.

Once the FW structure is overheated and fails, a pipe rupture for each DEMO segment was initiated by opening a connection between the VV and the FW channels. Water injection inside the plasma volume in turn causes an unmitigated plasma shutdown transient.

Due to the difference in the operating pressure, after the tube rupture, water and steam enters the VV volume causing a rapid pressurization. The results indicate the pressure increase in VV is very fast and

the maximum pressure peak is function of the number of melted channels. In particular, if 10 FW channels are supposed to melt for each DEMO segment, the intervention of VVPSS is not enough to mitigate the transient and to keep the pressure below the limit for the VV of 0.2 MPa. In all the simulations about 300 g of hydrogen are produced, however the interaction between steam and tungsten dust has not been taken into account in these simulations.

8 Hydrogen explosion mitigation

Several quantities of dust can be produced in fusion power devices by the energetic interaction between plasma particles and wall structures, either during normal operation or under postulated accident conditions. A dust explosion can be initiated by the rapid combustion of flammable particulates suspended in air. The condition necessary for a dust explosion is a simultaneous presence of dust cloud of appropriate concentration in air that will support combustion throughout the process and a suitable ignition source [28]. Dust can be involved also in oxidation reaction producing high quantities of hydrogen. In order to avoid that flammable concentrations could be achieved, the production of hydrogen must be limited and properly monitored. In particular, the simultaneous presence of H_2 and dust in the VV volume enhances the risk of explosion. For such reasons, technical solutions to avoid the risk of explosion in tokamak reactors must be investigated.

8.1 Hydrogen production in fusion reactors

The hydrogen produced during normal operation is treated by the plasma fueling systems and discharge cleaning systems, therefore it doesn't constitute a serious risk to safety. The potentially dangerous sources of hydrogen, however, are related to the oxidation reactions between water steam and PFCs or hot dust or liquid metal [70].

In tokamak devices the PFCs and dust particles are mainly tungsten and beryllium. A major concern is the reactivity of these materials with steam during an accident, such as loss of coolant or a wet bypass. During such events hot dust of W and Be, mobilized and mixed with steam, or the hot PFCs surfaces can be hit by steam leading to hydrogen generation in a very short time, according to the following reactions:

$$Be + H_2O \rightarrow BeO + H_2 + 370\ kJ/mol\text{-}Be$$

$$W + 3H_2O \rightarrow 3H_2 + WO_3 + 156\ kJ/mol\text{-}W$$

These reactions are significant above 500°C [71]. Inside the vessel these temperatures are reached mainly on the divertor surface, where the production of hydrogen is related to the large amount of free dust available. The combination of these high temperatures and the presence of air (for example due to a loss vacuum accident), could lead to a hydrogen-steam–air mixture, that could be ignited. In these cases, hydrogen combustion would lead to hydrogen explosion, damaging the integrity of the structures. This loss of containment represents a danger to the public because of the not mitigated release of radioactivity towards the external environment.

In some fusion plants, beryllium is used as main component of first wall and divertor, this due to its low atomic number, its ability to remove oxygen from the plasma, and its ability to pump hydrogen continuously during short discharges. The beryllium reaction rate with steam strongly depends from temperature, physical form and microstructure of the beryllium [72]. Experimental results [73], demonstrated that for porous beryllium reaction rates with steam are 200 times higher than those for solid material at comparable temperatures. Furthermore, the porous beryllium reaches temperatures over 1300°C due to the exothermic heat of reaction developing self-sustaining reactions. This high chemical reactivity of porous beryllium in steam suggested that designers should consider more stable compounds or different beryllium forms with lower effective reaction areas.

In this context tungsten has been identified as an ideal candidate for the coating of plasma facing structures because of its refractory and a low erosion property. A disadvantage is represented by the fact that alloys of tungsten will become highly activated when exposed to high neutron fluences and will

form volatile oxide species in the presence of water. This could lead to a production of hydrogen, which quantities could change with temperature, steam pressure and gas velocity [65]

Concerning, lithium-water reactions, two exothermic chemical reactions appear to be significant [74]:

$$Li + ½\ H_2O \rightarrow ½\ Li_2O + ½\ H_2 + 157\ kJ/g\text{-}mole\text{-}Li$$

$$½\ Li_2O + ½\ H_2O \rightarrow LiOH + 69\ kJ/g\text{-}mole\text{-}Li$$

Steam injected into liquid metal reacts with the lithium in the alloy to produce one mole of hydrogen per mole of steam reacted. This causes no change in the number of gas moles and only slight change in gas temperature since most of the heat is transferred to the liquid metal.

In tokamaks destinated to energy production, a widely used compound containing lithium is the eutectic lithium-lead alloy, proposed as tritium breeder for the WCLL concept of the EU DEMO. As for all liquid metals, problems arise because of its chemical reactivity with commonly present materials, like air, water, and concrete. The energy released from the interaction with water could lead to increased temperatures and pressures, which could cause an accident. Liquid metal-water reaction severity will be a strong function of the contact mode and location and the degree of separation of liquid metal and water, the phase of water, and the order of events in a transient are all possible significant factors in determining the frequency and consequences of liquid metal-water reactions. Both the frequency and consequence will likely decrease with increasing separation between liquid metal and water, since the pouring contact mode may entail more mixing between liquid metal and water, hence more reaction.

The consequence of the contact between $Li_{17}Pb_{83}$ and steam is an exothermic reaction that could lead to significant hydrogen gas production. It is only limited by the amounts of reactants present.

The H_2 and heat generated by the LiPb-Water reaction are:

$$Li_{17}Pb_{83} + 8.5\ H_2O \rightarrow 8.5\ Li_2O + 8.5H_2 + 83Pb + 19.0\ kJ/mol\text{-}LiPb$$

$$Li_{17}Pb_{83} + 17\ H_2O \rightarrow 17\ LiOH + 8.5H_2 + 83Pb + 25.8\ kJ/(mol\text{-}LiPb)$$

the first one occurs in excess of LiPb and the second in excess of water. From the thermal and hydrogen generation points of view, the first reaction is very conservative. Preliminary calculations performed for the WCLL concept of the EU DEMO reactor to estimate the water flow rate in the accident, suggested to consider a jet of water penetrating into the LiPb volume and, as the reaction will occur mainly at the interface between the liquid metal and water, a condition of excess of water has been assumed as more realistic.

At typical fusion power plant operating temperatures, the reaction of $Li_{17}Pb_{83}$ with liquid water leads to high pressures, attained due to the potential vaporization of water and potential hydrogen production. Then, pressures greater than the water supply pressure could be reached because one mole of gas will be produced for each mole of water introduced. Consequently, steam explosion may also be possible. In conclusion, the reaction between the $Li_{17}Pb_{83}$ and water steam could represent a serious hazard, Internals should be designed to withstand accidental pressurization following to a water leak into the liquid metal. Another important fact to consider is the higher radioactivity of the $Li_{17}Pb_{83}$, so the design should consider way to effectively and safely routinely remove mercury, thallium, bismuth, and polonium from the $Li_{17}Pb_{83}$ [74].

The H_2 inventory in EU DEMO reactor, as a consequence of an abnormal events, is in the preliminary phase of definition.

Currently only an analysis dealing with the $Li_{17}Pb_{83}$-steam reaction in WCLL concept after a LOCA for the evaluation of the H2 inventory is reported in [75]. The results are available for the evaluation, in terms of range and not in terms of absolute values, of the H2 production due to the reaction between Li17Pb83 and steam. The reaction of all the steam inserted into the LiPb circuit is firstly supposed and considered instantaneous. This hypothesis could be very conservative, and in absence of a correct reaction kinetic model implemented, sensitivity analyses at different fraction of water participating to the reaction were foreseen.

For each kg of reacted water, the hydrogen produced is

$$\frac{n_{H_2}}{n_{H_2O}} \cdot \frac{M_{M_{H_2}}}{M_{M_{H_2O}}} = \frac{8.5}{17} \cdot \frac{2.01588}{18.01528} = 0.056 \frac{kg_{H_2}}{kg_{H_2O}}$$

The reaction of all the steam inserted into the LiPb circuit is firstly supposed and considered instantaneous. This hypothesis could be very conservative, and in absence of a correct reaction kinetic model implemented, sensitivity analyses at different fraction of water participating to the reaction are foreseen. A parameter, C_{reaz}, has been used to control the fraction of water which reacts with eutectic LiPb. Results have been obtained varying C_{reaz} between 10% and 100% ($\Delta C_{reaz} = 10\%$).

At the end of the analysis the H_2 inventory calculated by means of the MELCOR code in the failed BZ is shown in Figure 8.1.1 considering the different reaction rates.

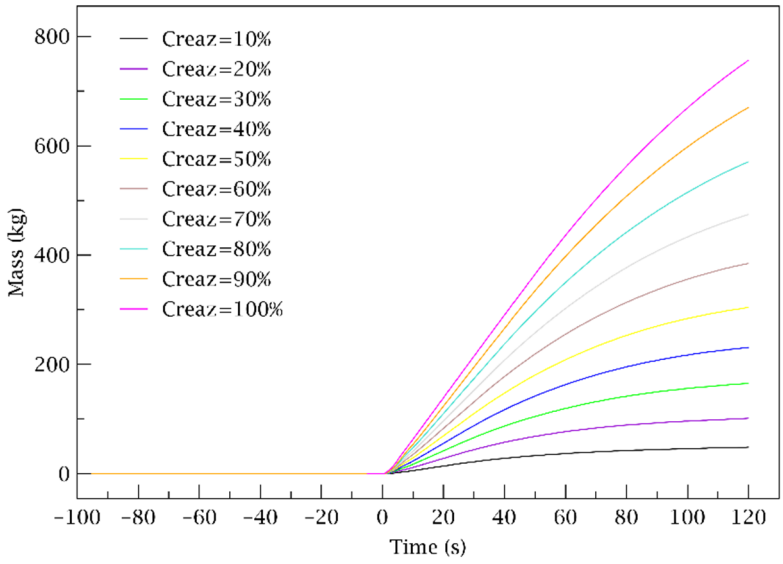

Figure 8.1.1 - Total amount of hydrogen in BZ [75]

Despite the large inventory of H_2 production in the case in which 100% of the amount of water reacts with Li17Pb83, if an expansion volume adequately dimensioned is connected with the BZ (400 m^3, half filled with $Li_{17}Pb_{83}$ at a pressure of 0.3 MPa) the maximum pressure in the BZ (15.1 MPa) does not overcome its design target (15.5 MPa).

A certain margin exists also in the very conservative conditions, but in any case, a loss of H_2 due to the failure of the BZ cannot be excluded and technical solutions are required to avoid the risk of explosion. A safety strategy could be to limit accumulation of dust inside the VV or VVPSS, in order to bind the amount of hydrogen and keep concentrations below flammability limit (for hydrogen-air mixtures the lower flammability limit is 4.0 vol% H_2 and the upper flammability limit is 75.0 vol% H_2) [71].

8.2 Hydrogen risk mitigation: technical solutions in fusion plants

As well as for fission power plants, for fusion power devices the main environmental and safety issue is the control of the radioactive substances, and their confinement into the reactor buildings during accidental conditions, preventing significant release of radioactivity to the environment [70][76]. In the framework of safety in future fusion power plants, hydrogen production and subsequent combustion must be avoided since the pressure and energy generated may threaten the integrity of the confinement structures causing the dispersion of radioactive and toxic products towards the public environment.

In particular, the vacuum vessel represents the first confinement barrier to this radioactive material. In the event of a postulated accident involving ingress of steam into the VV, hydrogen could in principle be produced by chemical reaction with hot metal and dust. If the ingress of air into the VV is also postulated, reaction of air with hydrogen and/or dust cannot be completely excluded and could lead to a possible explosion which could compromise the VV integrity.

The research of technical solutions to avoid the risk of H_2 explosion in large fusion power plants is still in progress. The first objective is to preclude the occurrence of flammable gas mixtures. The second objective, if flammability limits are exceeded anywhere, is to prevent continued penetration of the flammable range to more dangerous concentrations.

Solutions to preclude the occurrence of flammable gas mixtures could be:

- **Injection of an inert gas:** a system that inject inert gas such as nitrogen N_2 or carbon dioxide CO_2 in the VV. However, the disadvantage is that hydrogen is not removed from the system, but only diluted. So, to reach a full inertization huge quantities of inert gas must be injected, but this will pressurize the VV causing the activation of the ST. Moreover, this solution is complex to realize because large tanks available for the inert gas storage, ducts for the gas injection and active systems to trigger the intervention of the system are needed [77][78];
- **Hydrogen Recombination System**: consists of self-starting and self-feeding autocatalytic recombiners that trigger spontaneously as soon as the hydrogen concentration begins to increase in the atmosphere [79][80]. In fusion devices they could be installed inside the VVPSS-ST to deal with possible concentration of hydrogen in the free volume atmosphere, but it remains the risk that the explosion occurs in the VV before the opening of the path towards the ST. Moreover, the efficiency of the hydrogen recombination system depends on the local atmosphere composition in the recombiner box and on their location;

If flammability limits are exceeded, it is necessary to prevent continued penetration of the flammable range to more dangerous concentrations. In this case, hydrogen igniters can be used to avoid unacceptable combustion pressures and temperatures. The cloud of hydrogen and air, accumulated in the atmosphere of the STs, could be burned by ignitors. Slow deflagration can be obtained through combustion chambers in local volumes where flammable limits are exceeded, inert gas is not present and recombiners could be overwhelmed [70]. This internal ignition allows handling hydrogen risk at the source, burning in a controlled way any mixture of H_2 and air as soon as it crosses the flammability limits, which is the most effective mitigation measure. As for PARs their strength is the ability to operate without an external power source and to remain functional for the entire duration of the accident sequence.

For fusion devices hydrogen igniters and recombiners could represent the first line of defence for the hydrogen risk mitigation. If, during an accident sequence, a non-controlled detonation occurs in the ST,

it could be associated to the failure of recombiners and ignitors or to their inability to cover all possible ignition conditions.

8.3 MELCOR simulations for hydrogen mitigation

Some preliminary accident analyses to supply the range within the hydrogen mitigation systems have to run have been performed for the EU DEMO WCLL blanket concept.

The aim is to identify the potential for hydrogen production in the DEMO vessel in accident situations and look at possible solutions to prevent the risk of hydrogen and dust explosion. The hydrogen in the VV can lead combustion that involves in deflagration and detonation. In addition, the tungsten dust could enhance the effects of H_2 reaction as demonstrated by experiments [81].

8.3.1 MELCOR hydrogen mitigation model

The MELCOR ESF package have been used to model the thermal-hydraulic behavior of passive autocatalytic hydrogen recombiners.

The hydrogen mitigation system consists of passive autocatalytic recombiners (PARs) installed in each tank of the VVPSS. The aim is to prevent that hydrogen concentrations increase to levels that could produce large scale hydrogen deflagration or even detonations.

In Table 8.3-1 the main MELCOR parameters used by the code to calculate the total gas flow rate through a PAR unit are summarized. From the PAR gas flow rate together with user provided PAR efficiencies, and the internally calculated hydrogen mole fractions, the hydrogen reaction rate is calculated. This rate is then multiplied by the current timestep and the user provided number of active PAR units to determine the change in hydrogen, oxygen, and steam masses. These differential masses are treated as masses sources/sinks.

Table 8.3-1 – Main input parameters for PAR modelling with MELCOR

Parameter	Description	Value
IPROPT	Hydrogen Recombiner flow model	Fischer (default MELCOR model)
IETAPR	Hydrogen Recombiner efficiency model	Constant efficiency
EPAR	Hydrogen reaction efficiency	0.85
HPAR0	Minimum H_2 mole fraction for which the PAR unit start operating	0.02
HPARR	Minimum H_2 mole fraction for which the PAR unit stop operating	0.005
OPAR0	Minimum O_2 mole fraction for which the PAR unit start operating	0.03
OPARR	Minimum O_2 mole fraction for which the PAR unit stop operating	0.005

8.4 In-VV LOCA results

As shown in § 6.2 the hydrogen could be produced during the accident sequence is 634.33 g. Moreover, it is supposed that about 671.0 g of mobilizable tritium, forming part of the source term, can chemically react with the catalytic layer of the PARs. Before the triggering of rupture discs the maximum amount of hydrogen in the plasma volume is around 1.3 kg. However, it should be noted that the reaction between steam and tungsten dust deposited PFCs has not been considered in this simulation, as well as the reaction with LiPb supposing that only the first layer of the FW has been affected by the rupture.

Moreover, it is supposed that about 671.0 g of mobilizable tritium, forming part of the source term, can chemically react with the catalytic layer of the PARs.

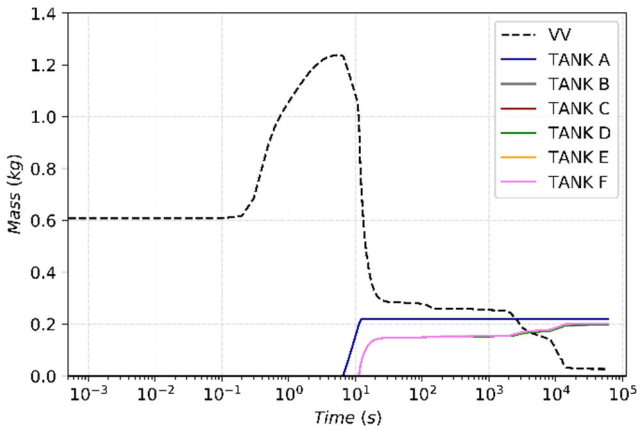

Figure 8.4.1 – Mass of hydrogen in VV and VVPSS volume without PAR (§ 6.2)

Preliminary simulations have been performed assuming 150 kPa as set point for trigger of VVPSS-RDs and 90 kPa for the opening of bleed lines. Being the maximum pressure reached in the VV equal to 157.4 kPa, the mass of hydrogen will be discharged in all the six tanks of the VVPSS. The injection of hot steam and hydrogen inside the VVPSS cause an increase in pressure and temperature of VVPSS tanks. It's important to take into account these values because they can affect recombiner efficiency. As shown in Figure 8.4.2 pressure is very low and probably outside the operational criteria of PAR (0.1 to 0.3 MPa) for large part of the accident sequence. Maximum temperature value in tank A is about 126.8°C and decreases below 317 K (maximum operational temperature for PARs) about 3000 s after the PIE.

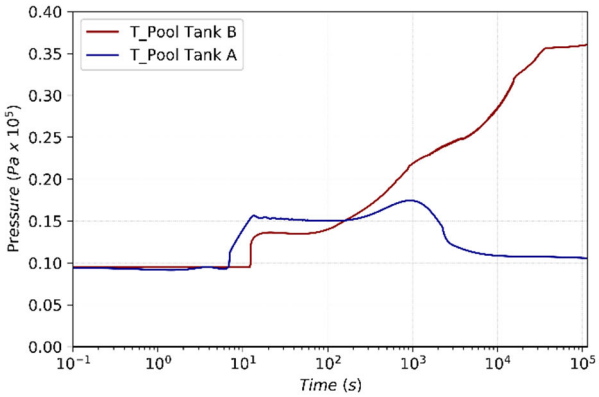

Figure 8.4.2 – VVPSS volumes pressure transient

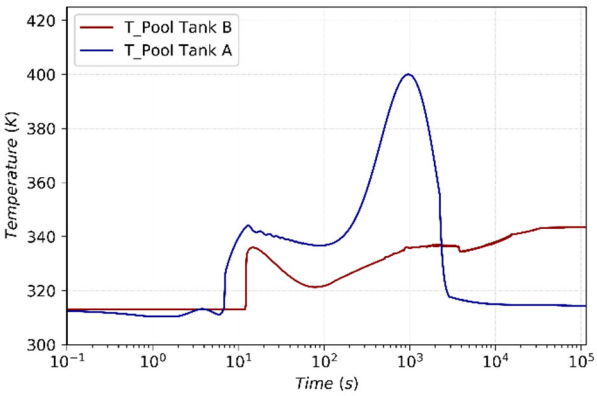

Figure 8.4.3 – VVPSS volumes temperature

The results in Figure 8.4.4 show hydrogen mass inside VVPSS tanks, while in Figure 8.4.5 the mass fraction of hydrogen in the atmosphere of VVPSS ST volumes is shown.

As reported in Table 8.3-1 the recombination process starts when hydrogen mole fraction reaches value of 0.02 and stops after oxygen mole fraction drops to 0.005.

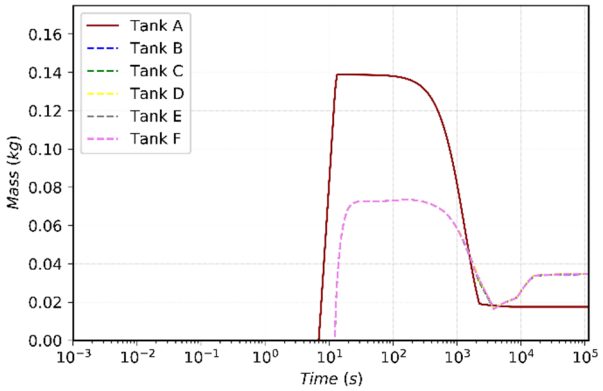

Figure 8.4.4 – Mass of hydrogen in VVPSS

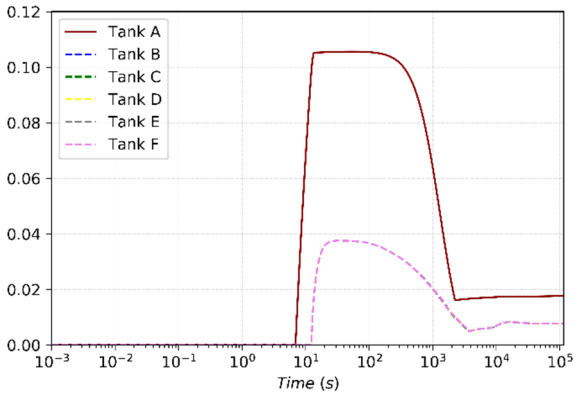

Figure 8.4.5 – Hydrogen mass fraction in VVPSS atmosphere

After 32 h of simulation, at the end of the recombination process 17.54 g, 173.17 g and 11.8 g are still confined in tank A, tanks B to F, and VV, respectively. So around 1.102 kg of hydrogen are removed by the PARs, which correspond to around the 84.48% of the initial mass of hydrogen.

The results in Figure 8.4.6 shows the hydrogen removal rate of a PAR unit, while in Figure 8.4.7 the total mass of hydrogen removed by PAR is shown. Figure 8.4.7 shows the mole fraction of oxygen inside the VVPSS tanks.

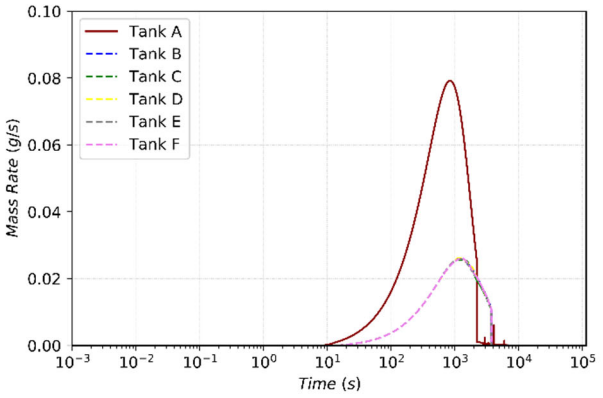

Figure 8.4.6 – Hydrogen removal rate

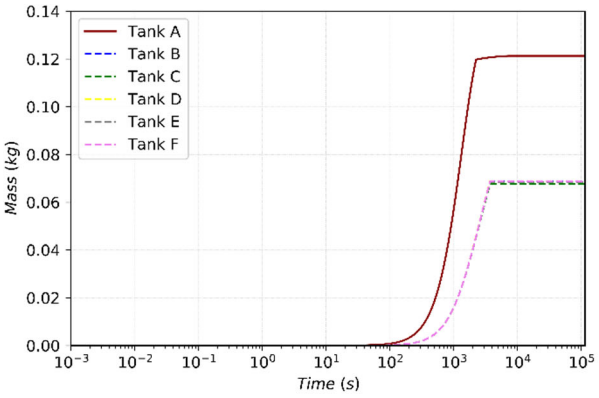

Figure 8.4.7 - Mass of H_2 removed by PAR

Table 8.4-1 – Data related to PAR operation

Parameter	**Tank A**	**Tank B to F**
Time at which PAR start operating [s]	7.9	24.8
Time at which PAR stop operating [s]	7173.0	1020
Total mass removed by the PAR [g]	121.27	68.741 (x5 ST)
Mass of hydrogen still inside the tank after 32 h [g]	17.54	34.63 (x5 ST)

8.5 LOFA without plasma shutdown results

The loss of flow accident analysis is classified as BDBA because of the failure of the plasma shutdown system. The plasma burns continuously until the FW is overheated and fails. The high temperatures reached by the plasma facing components cause a hydrogen production higher than that obtained during an in-VV LOCA (DBA). Because the mass of hydrogen inside the STs is enough to ensure PARs activation, it was not necessary to change the setpoint for trigger of VVPSS-RDs. All the five RDs connecting the VV to the VVPSS breaks when the pressure in the VV is 150 kPa, and hydrogen is equally distributed among the different tanks.

The behavior is the same in all the STs. For such a reason only the results for Tank B are shown in the figures below. However, they are representative for the other four suppression tanks.

As shown in Figure 8.5.1 chemical reactions between steam and tungsten hot surfaces within the vacuum vessel can produce about 300 g of hydrogen. The reaction between steam and tungsten dust deposited on the FW surface and on the divertor surface has not been considered in this simulation. Moreover, it is supposed that about 671.0 g of mobilizable tritium, forming part of the source term, can chemically react with the catalytic layer of the PARs.

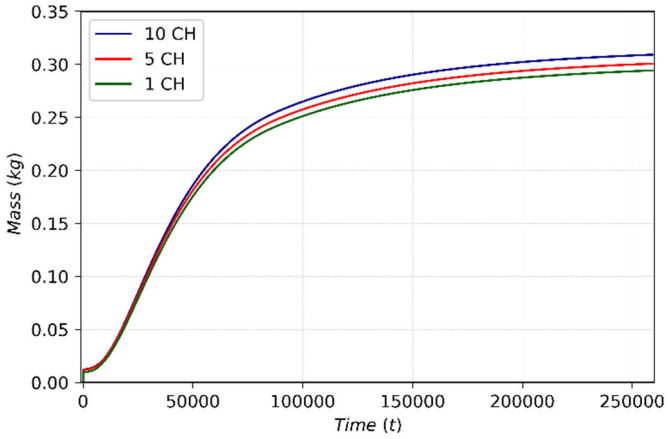

Figure 8.5.1 – Mass of H_2 produced because of W-steam interaction

The injection of steam inside the VVPSS cause an increase in pressure and temperature of VVPSS tanks. It's important to take into account these values because they can affect recombiner operation.

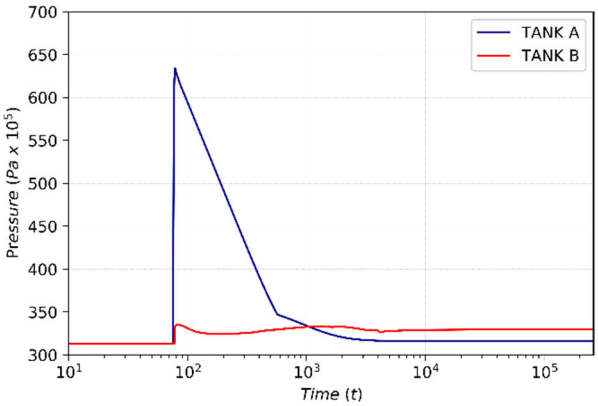

Figure 8.5.2 – VVPSS temperature

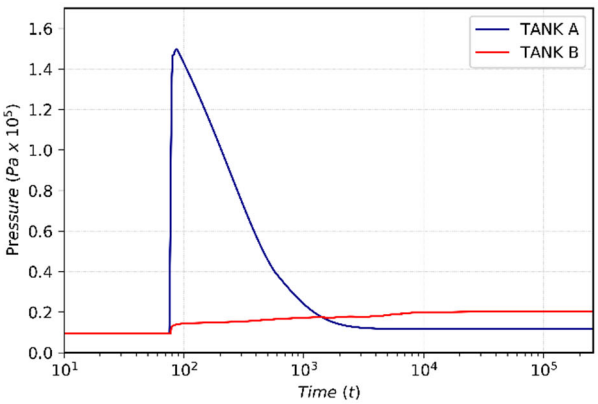

Figure 8.5.3 - VVPSS pressure

Because there is no suppression of steam inside tank A high values of temperature and pressure are reached (Figure 8.5.2 and Figure 8.5.3). However, pressure remains between the operational criteria of PAR (0.1 to 0.3 MPa) for the entire accident sequence. Maximum temperature value in tank A is 372.55°C and decreases below 144°C (maximum operational temperature for PARs) about 322.5 s after the PIE.

The results in Figure 8.5.4 show the mass of H_2 inside the VVPSS tanks. The maximum value of 128 g is reached.

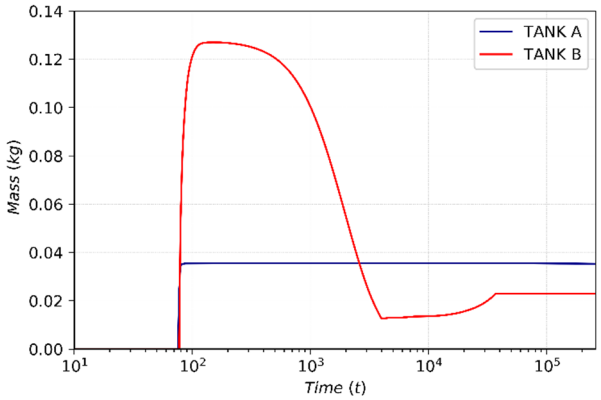

Figure 8.5.4 – Mass of hydrogen in VVPSS

The recombination process does not occur in Tank A, where the mole fraction of H_2 remains below 0.02 for the entire duration of the accident sequence. In other STs the recombination process starts when hydrogen mole fraction reaches value of 0.02 (about 98 s) and stops after H_2 mole fraction drops to 0.005 (3981 s).

Because all the VVPSS suppression tanks are involved in the hydrogen recombination process, the mass of oxygen available for the catalytic reaction is higher than that in the previous accident analysis (in-VV LOCA). The process of recombination is efficient; at the end of the accident sequence about 60% of hydrogen has been removed by the PARs.

The results in Figure 8.5.5 show the hydrogen removal rate of a PAR unit, while in Figure 8.5.6 the total mass of hydrogen removed by PAR is shown. Figure 8.5.7 shows the mole fraction of oxygen inside the VVPSS tanks.

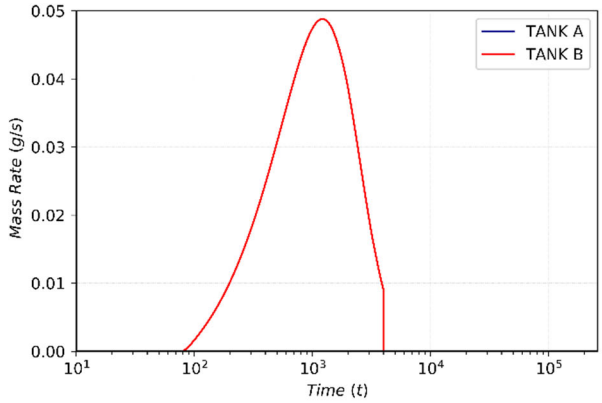

Figure 8.5.5 – Hydrogen removal rate

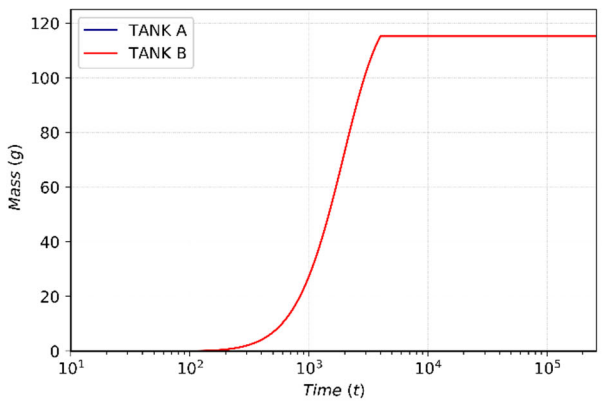

Figure 8.5.6 - Mass of H_2 removed by PAR

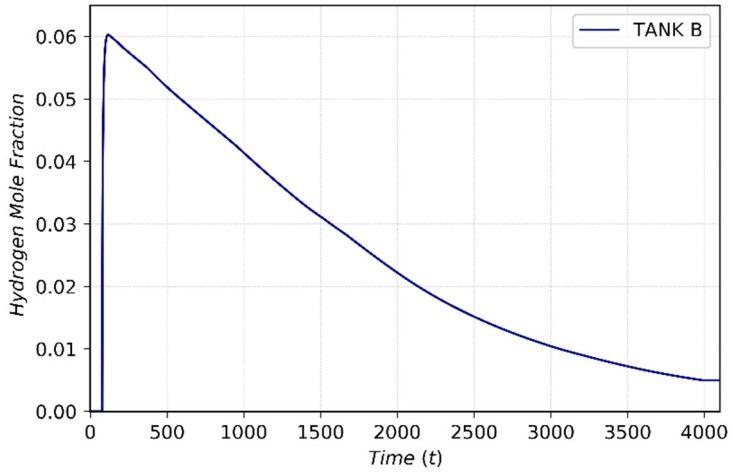

Figure 8.5.7 – Hydrogen mole fraction inside VVPSS

Table 8.5-1 – Data related to PAR operation

Parameter	Tank A	Tank B to Tank F
Time at which PAR start operating [s]	--	97.9
Time at which PAR stop operating [s]	--	3981.0
Total mass removed by the PAR [g]	--	576.15
Mass of hydrogen still inside the tank after 72 h [g]	--	115.006

8.6 Conclusions

A preliminary concept of hydrogen mitigation system (HMS) has been proposed with the aim to prevent that hydrogen concentration increases to levels that could produce large scale hydrogen deflagration or even detonations. The HMS consists of passive autocatalytic recombiners (PARs) installed in each tank of the VVPSS. Two different accident sequences have been performed to investigate hydrogen mitigation systems performance.

The first was an in-VV LOCA with steam suppression in tank A. In this case the HMS was able to remove about the 84.4% of the mass hydrogen inside the reactor.

The second accident sequence was a LOFA without suppression of steam in tank A. The catalytic reaction occurs in all the five STs, but it does not occur in Tank A, where the mole fraction of H_2 remains below 0.02 for the entire duration of the accident sequence. At the end of the accident sequence the HMS was able to remove about the 60% of the mass hydrogen inside the reactor.

9 Uncertainty and sensitivity analysis with the RAVEN code

As is well known, one of the main problems encountered in performing safety studies for fusion and fission reactors is related to the uncertainty of physical parameters and to the lack of information on the availability and reliability of components and their behavior under foreseen power plant operating conditions. This lack of information could affect the development of the accident sequence which could be studied with a probabilistic approach by means of sensitivity analysis and dynamic event tree tools. The tool that will be employed to deal with these uncertainties is RAVEN (Reactor Analysis and Virtual control ENviroment) [82], a software tool under development at the Idaho National Laboratory, that acts as the control logic driver and post-processing tool for different applications.

9.1 The RAVEN tool

RAVEN has been originally developed to perform parametric and probabilistic analysis based on the response of complex system codes, in order to quantify the safety margins related to safety-related events [83]. Nowadays RAVEN is a multi-purpose probabilistic and uncertainty quantification platform, which can be coupled with any system code. RAVEN is capable of investigating the system response as well as the input space using Monte Carlo, Grid, or Latin Hyper Cube sampling schemes, but its strength is focused toward system feature discovery, such as limit surfaces, separating regions of the input space leading to system failure, using dynamic supervised learning techniques.

It is expected that, as with any new technology, RISMC (Risk Informed Safety Margin Characterization) will face an initial period of resistance and a strong momentum will be needed to overcome the tipping point after which its tools and concepts will be broadly adopted in the nuclear community. A coherent strategy needs to be employed in order to mitigate the resistance as much as possible, and, thus, the friendliness of new tools and clearness of information should be part of this strategy. As for all PRA software, the capability to control the plant evolution during the simulation is a plus for uncertainty propagation. In system safety analysis codes, a similar need is expressed by the implementation of the control logic of the plant. As a consequence, the optimization of resources imposes the integration of this task under a common project that is RAVEN. Consequently, the plant control logic is simulated by RAVEN; this also offers the flexibility to easily implement proprietary control logic without changing RELAP or MELCOR source code.In summary, from a user prospective, RAVEN is a tool that [84]:

- Determines the calculation flow to achieve the most accurate evaluation of risk accounting for probabilistic behavior and uncertainty propagation;
- Visualizes simulations results (thousands and more) and provides the data mining capability to deeply understand the plant behavior;
- Provides the capability to investigate risk mitigation strategies by suggesting directions and quickly assessing impacts

RAVEN has been developed in a highly modular and pluggable way in order to enable easy integration of different programming languages (i.e., C++, Python) and, coupling with any system code [85]. RAVEN is composed by three main software systems that can operate either in coupled or stand-alone mode:

- Control Logic System
- Graphical User Interface
- Probabilistic and Parametric framework

The probabilistic and parametric framework represents the core of the RAVEN analysis capabilities. The main idea behind the design of the system is the creation of a multi-purpose framework characterized by high flexibility with respect to the possible performable analysis. The framework must be capable of constructing the analysis/calculation flow at run-time, interpreting the user-defined instructions and assembling the different analysis tasks following a user specified scheme. In order to achieve such flexibility, combined with reasonably fast development, a programming language naturally suitable for this kind of approach was needed: Python.

As can be inferred from above, RAVEN is coded in Python and is characterized by an object-oriented design. The core of the analysis performable through RAVEN is represented by a set of basic components (objects) the user can combine, in order to create a custom analysis flow. A list of these components and a summary of their most important functionalities are reported as follow [82]:

- *Distribution*: In order to explore the input/output space, RAVEN requires the capability to perturb the input space (initial conditions of a system code). The initial conditions, that represent the uncertain space, are generally characterized by probability distribution functions (PDFs), which need to be considered when a perturbation is applied. In this respect, a large library of PDFs is available to choose from.

- *Sampler*: A proper approach to sample the input space is fundamental for the optimization of the computational time. In RAVEN, a "sampler" employs a unique perturbation strategy that is applied to the input space of a system. The input space is defined through the connection of uncertain variables and their relative probability distributions.

- *Model*: A model is the representation of a physical system (e.g. Nuclear Power Plant, etc.); it is therefore capable of predicting the evolution of a system given a coordinate set in the input space.

- *Reduced Order Model (ROM)*: The evaluation of the system response, as a function of the coordinates in the input space, is very computationally expensive, especially when brute-force approaches (e.g. Monte Carlo methods) are chosen as the sampling strategy. Reduced Order Models are used to lower this cost, reducing the number of needed points and prioritizing the area of the input space that needs to be explored. They can be considered as an artificial representation of the link between the input and output space for a particular system.

9.2 Development of the RAVEN-MELCOR coupling

One of the objectives of this Ph.D. work was to develop an external code interface for the coupling between RAVEN and MELCOR.

The interface has three main functions [86]:

- interpret the information coming from RAVEN;
- translate such information in the input of the driven code;
- manipulate output data file to create a database.

To allow RAVEN storing output data coming from MELCOR, a Python output parser has been developed to convert the plot binary file generated by MELCOR into a CSV file. To overcome the handling of large datafiles the interface allows to create a CSV file with only variables required by the users. So, it is possible to obtain a database that comprises the required variables from all MELCOR packages. Figure 1 shows the procedural framework used for sensitivity and uncertainty analyses. A MELCOR input deck is used as template, the chosen parameters are specified as string with special

characters. RAVEN can identify such parameters and replaces the string with values sampled from a specified distribution. The sampled values are implemented into N number and consequently N-MELCOR input decks are generated. Data resulting from simulations are stored into a database that can be used to perform statistical analyses.

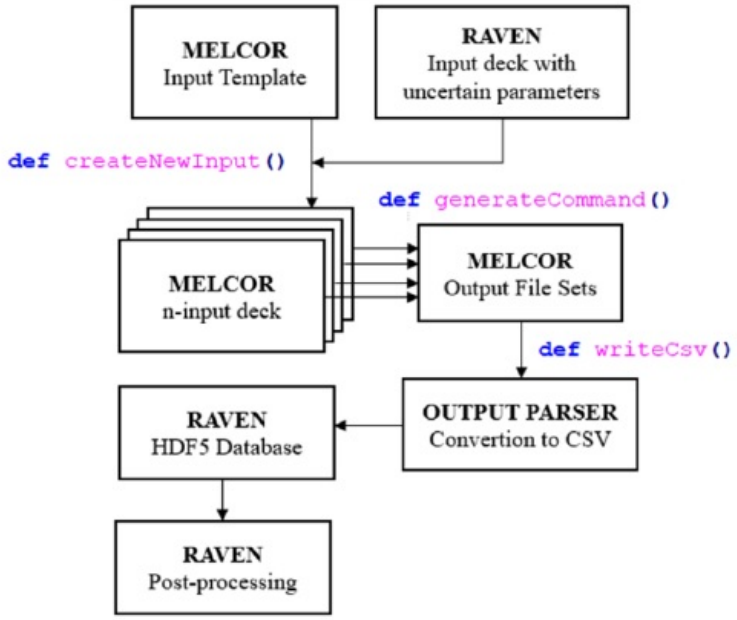

Figure 9.2.1 - RAVEN-MELCOR coupling

9.3 Sensitivity analysis for an ex-vessel LOCA without plasma shutdown

As described in par. 8, for the EU DEMO WCLL BB concept, the possibility of a tungsten-steam reaction during severe accidents is a safety concern because the hydrogen produced from the reaction could pose a flammability or detonation hazard. The potentially dangerous sources of hydrogen are related to the oxidation reactions of PFCs, such as first wall and divertor, and hot dust.

9.3.1 Accident description

The description of the accident is the same reported in par. 7.1.

9.3.2 Variables and sampling

A set of 10 parameters has been chosen to perform this sensitivity study. The parameters are listed in Table 9.3-1 together with the associated distribution. All the selected perturbations are based on a normal distribution. Upper and lower bound have been imposed in order to avoid non-physical cases and MELCOR spurious failures to occur. The sample size needed to obtain a significative output statistic was selected using the Wilks formula [87] The parameter to be perturbed have been selected as they may affect FW temperature transient and the steam partial pressure inside the VV.

Table 9.3-1 – Perturbed parameters

Variable	Description	Mean μ	Sigma σ
FLARA_PIE	Distributor ring break area	0.04921 m^2	0.004921 m^2
FLARA_PD	FW break area after plasma unmitigated disruption	0.02568 m^2	0.002568 m^2
DISR_POW	Power deposited on FW by the plasma disruption	10.0 GW	500.0 MW
MOD_DH	Modules decay heat multiplicative factor	1.0	0.05
DIV_DH	Divertor decay heat multiplicative factor	1.0	0.05
ISL_CLOSE_P	Trip valve closure setpoint	12.965E+6 Pa	12.965E+5 Pa
T_BREAK	FW break temperature	1450.15 K	145.0
DIL_974	FL974 flow area	0.577 m^2	0.0577 m^2
DIL_975	FL975 flow area	2.352 m^2	0.0235 m^2
DIL_978	FL978 flow area	0.107 m^2	0.0107 m^2

9.3.3 Main outcomes from the sensitivity analysis

The maximum pressure reached in the containment is $1.4589 \cdot 10^5$ Pa, with a standard deviation of 2.815 kPa. Figure 9.3.1 shows a scatter plot for the maximum pressure reached in the TCR and the flow area of the break in the FW distributor ring, with the related Pearson's coefficient. The general trend is so that as the distributor ring break area increases, the maximum pressure reached inside the TCR also increases. The time at which the maximum pressure peak inside the TCR is reached can ranges between 37.0 s and 106.5 s, after the FW-PHTS distributor ring failure.

Figure 9.3.2 shows the pressure evolution inside the VV for all the histories simulated. It is possible to notice how the perturbed variables can affect the pressure transient within the VV. Two main different trends can be distinguished. A high FW melt temperature causes a time delay in the in-vessel breach. Moreover, because of the long time required to close upstream trip valves (10 s after signal detection) large amounts of water are already released in the TCR. Therefore, when the in-vessel breach occurs the FW-PHTS pressure and inventory are such as to cause an overpressure in the VV lower than pressure setpoint for RDs intervention. The RDs, which allow for the discharging of steam and hydrogen in the VVPSS suppression tanks, are not triggered in the 70% of the simulated scenarios.

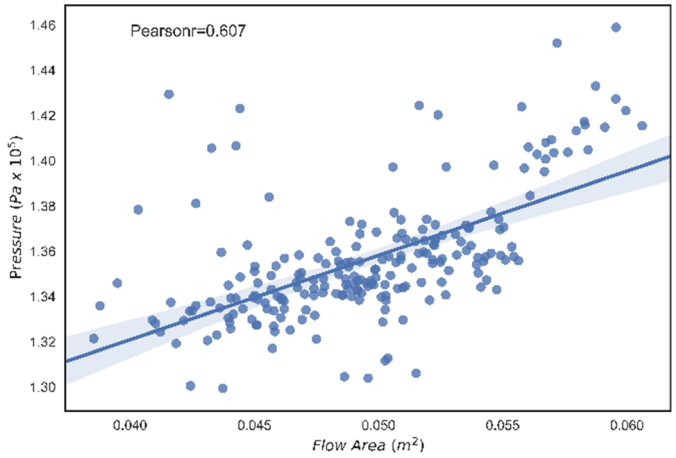

Figure 9.3.1 - Maximum pressure in the TCR vs break flow area

Results shown that for FW melt temperature higher than 1450 K the VVPSS RDs are never triggered. In all these cases, hydrogen and other source term masses are not discharged inside the VVPSS-STs and can accumulate inside the TCR volumes. To avoid these worst accident scenarios, the pressure setpoint for the RDs opening should be decreased, at least below the 5% quantile reported in Table 9.3-2. In such a way also these low-pressure in-vessel LOCA scenarios could be safely accommodated avoiding radioactive release inside the containment building.

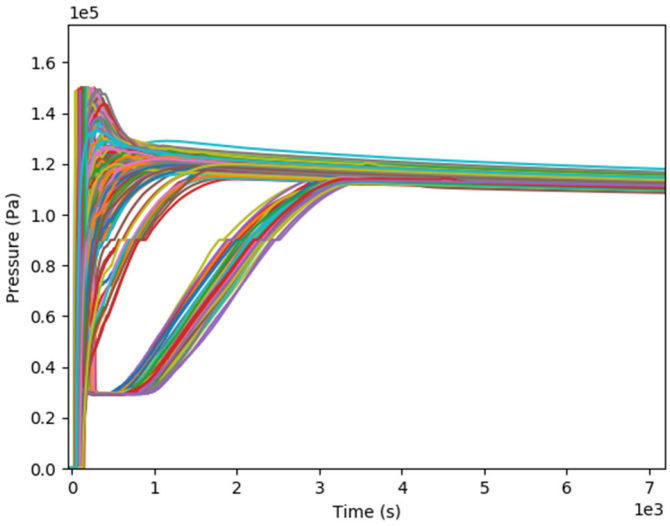

Figure 9.3.2 – VV pressure

Table 9.3-2 - VV maximum pressure, descriptive statistic

Mean μ	Sigma σ	0.05 quantile	0.95 quantile
134.0 kPa	12.9 kPa	118.59 kPa	150.02 kPa

In Figure 9.3.3 the correlation between the mass of hydrogen produced at the end of the simulation and the temperature characterizing the failure of the FW is shown, along with the univariate distribution of both variables on separate axes.

Hydrogen production is lower than 100 g when the FW temperature at which plasma in-vessel breach occurs is lower than 1590 K. For higher FW melt temperature, the total mass of hydrogen produced

increases very quickly. However, the total mass never exceeds 800 g. It should be noted that the reaction between steam and tungsten dust deposited on the FW surface and on the divertor surface has not been considered in this simulation, because of the lack of an accurate model.

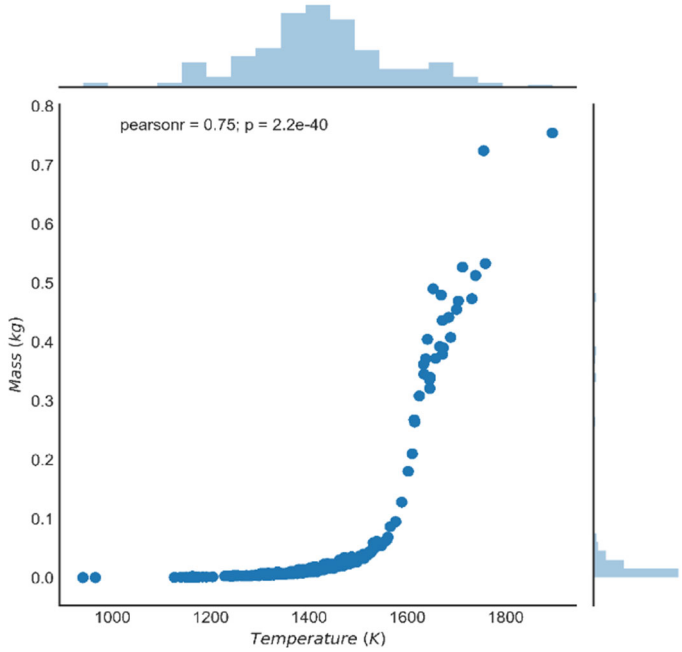

Figure 9.3.3 - Mass of hydrogen produced vs FW melt temperature

In Table 3.1-1 the results of the sensitivity analysis for the hydrogen mass generated during the in-vessel phase of the accident progression are reported.

Table 9.3-3 - Hydrogen mass production, descriptive statistic

Mean μ	**Sigma σ**	**0.05 quantile**	**0.95 quantile**
69.2 g	142.3 g	1.3 g	336.3 g

Hydrogen generation commences almost simultaneous with the failure of the FW armor and terminates and ends maximum 300 s after the PIE. The sudden injection of water steam inside the VV cools the plasma-facing structures (Figure 9.3.4) and ultimately reduces hydrogen production. Additional cooling to modules and VV is provided by the VV decay heat removal system which is considered in operation for the entire duration of the accident transient.

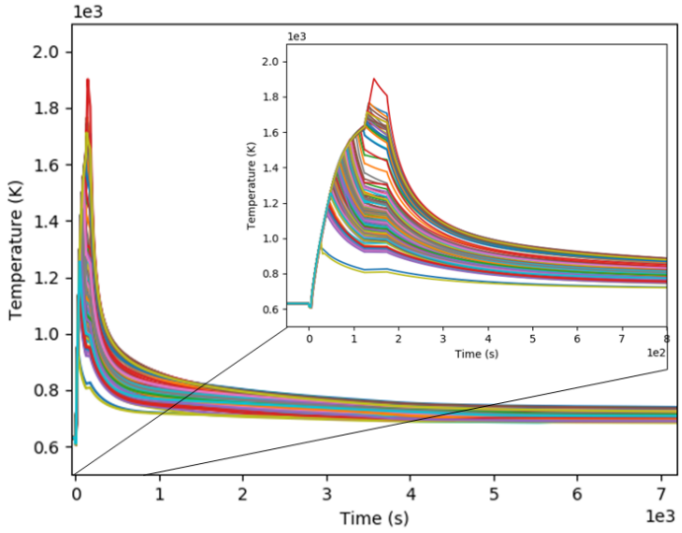

Figure 9.3.4 - FW temperature

9.3.4 Conclusions

Results showed that FW temperature at which plasma in-vessel breach occurs is a parameter that affects not only the mass of hydrogen produced, but also the overall VVPSS response. This study showed that if for FW melt temperature is higher than 1450 K the RDs are not triggered and the VVPSS function to retain the radioactive inventory is lost. Focusing the attention on hydrogen production, it is to underline that its uncertainty is mainly related to the temperature behavior of the FW, while the partial pressure of steam inside the VV has a low ranked influence for this accident scenario. Since the hydrogen production rate is a very strong function of temperature, the correct modelling of the FW cooling by thermal radiation and heat conduction between the FW and module back supporting structure is vital.

9.4 Fukushima Daiichi Unit 3

9.4.1 Introduction

The Great East Japan Earthquake hits at 14:46 on Friday 11 March 2011 on the east coast of Japan. The earthquake and consequent tsunami waves damaged residences and industrial establishments, including five NPPs.

The purpose of this work is to perform a sensitivity and uncertainty analysis of the severe accident transient occurred at Fukushima Daiichi nuclear power plan Unit 3 of Tokyo Electronic Power Company (TEPCO) with RAVEN coupled with severe accident code MELCOR 2.1, evaluating influence of input parameters on selected FoMs. MELCOR nodalization and models has been developed following the Best Practice Guidelines given in SOARCA [88] to better represent the plant response to the severe accident.

The Fukushima accident is the first world severe accident in a boiling water reactor (BWR), offering, despite of the tragic consequences, an unique opportunity for studying core degradation and thermal-hydraulic response of nuclear reactors in critical conditions and the possibility for severe accidents computer codes to be tested, improved and validated. Fukushima Daiichi Unit 3 (FU-3) is BWR/3 of 2381 MWt with a steam flow rate generation in nominal operation conditions of 4440 t/h. The operation pressure in reactor pressure vessel, that is the active core region pressure, is 7.03 MPa considering an average core temperature of 286 °C. Missing datas plant were scaled from Peach Bottom plant, similar to FU-3 but larger (3514 MWt).

9.4.2 MELCOR model

MELCOR nodalization include representation of RPV – Reactor Pressure Vessel components, PCV – Primary Containment Vessel components, Reactor Building. They are all build up in CVH - Control Volume Hydrodynamics package, responsible for modelling the thermal-hydraulic behavior of liquid water, water vapor, and gases in MELCOR, giving boundary conditions to all other packages. Core and lower plenum structures, including their thermal response and relocation during degradation, melting, slumping, and debris formation, are modelled in COR package. The bottom of RPV has been taken as the reference level (0 m).

9.4.2.1 RPV associated components

The in-vessel model includes downcomer, recirculation loops, jet pumps, steam separators, steam dryers, steam dome and four steam lines, as well as lower plenum and core region.

Lower plenum and core structures were represented in COR package model, using 19 axial levels (AL) and 6 rings. Active core region (3.71m, [89]) is represented by 4 concentric CVHs rings and core structures, based on [89]. Each ring is divided into 5 vertically stacked CVHs and ten core axial levels (9-18th AL), based on [89] which calculates power peaking factor with 10 nodes. The 19th AL, assumed 0.5 m above TAF – Top Active Fuel, includes the top guide and the upper tie plates. Each of 40 active core cells are coupled two by two with one CVH control volume, modelling the response and relative power of the included fuel assemblies, giving an accurate and continuous representation of the regional fuel collapses and subsequent degradation. The 5th and 6th ring, models the outer bypass region (annular region between the active core and the internal surface of the core shroud) and the downcomer region. There are in total 20 CVHs simulating core channels and 4 CVHs as bypass regions. The core channel volumes are connected to the relative bypass volumes with flow paths that open when the fuel channel boxes fail, allowing natural circulation in the open core after channel box failure. Lower plenum has been divided into 8 axial levels (AL), whose divisions are ruled by transitions from the control rod guide

pipes to control rod drive tubes (2th to 3th AL), from spherical to cylindrical vessel shape (4th to 5th AL) and by the presence of the core support plate (7th to 8th AL), whose thickness has been set 0.25 m [91]. Lower plenum core cells are coupled with one CVH control volume. Each flow path in the core and lower plenum nodalization simulates the effects of flow blockages and changes in resistance during core degradation [92].

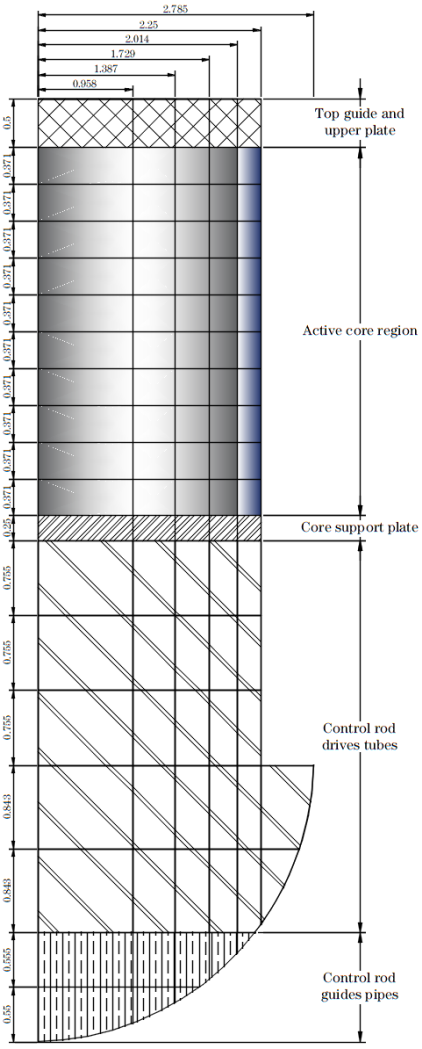

Figure 9.4.1 – COR nodalization

Table 9.4-1 - Axial and radial peaking factor

AL	**9**	**10**	**11**	**12**	**13**	**14**	**15**	**16**	**17**	**18**	**19**
Elevation (m)	5.3	5.671	6.042	6.413	6.784	7.155	7.526	7.897	8.268	8.639	9.01
Axial Peaking Factor	0.82	1.42	1.29	1.17	1.1	1.04	1.04	1.02	0.84	0.26	0.0

Ring	**1**	**2**	**3**	**4**	**5**	**6**
FAs Number	124	136	144	144	0	0
Peaking Factor	1.19	1.17	1.01	0.63	0.0	0.0

According to [89] there were 93 t of Uranium in the Unit 3, corresponding to 105 500 kg of UO_2, contained in 516 FAs of 9x9(A) type and 32 MOX FAs of 8x8 type.

	Num	Rods/FA	Partial length rods/FA	Pellet radius (mm)	Length (m)	Partial Length (m)
9x9 FA	516	74	8	4.8	3.71	2.16
8x8 FA	32	60	0	5.2	3.71	-

There are 137 control rods in the cross-shape configuration, each one containing 7 kg of B4C and 93 kg of stainless steel as reported in [93]. Masses calculated from geometrical data and introduced in the MELCOR model are reported in the following Table.

	Steel	Zircaloy	Boron Carbide
Supporting Structure	34559	598	-
Non-Supporting Structure	20790	15930	959
Channel boxes	-	16315	-

Water with a calculated steam quality of 14% enters in a common control volume from core CVs representing the shroud head region, and from here to steam separators, steam dryer and four steam lines, discharging steam exhaust from RPV to a time-independent control volume simulating main turbine. Two recirculation loops and 10 jet pumps per loop provide 9389 kg/s flow rate of coolant in the core [89].

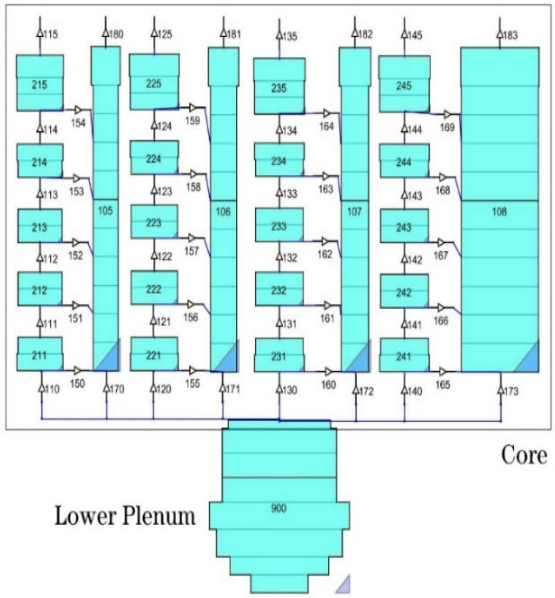

Figure 9.4.2 – CVH nodalization of core and bypass channesl

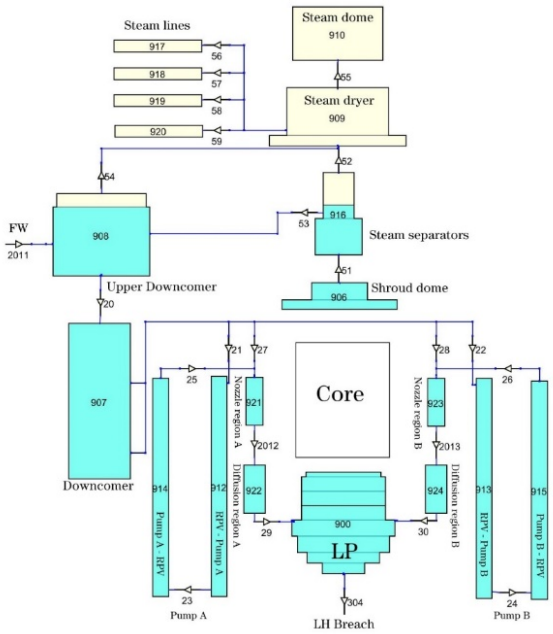

Figure 9.4.3 – Vessel CVH nodalization

9.4.2.2 PCV

The primary containment model includes Drywell (DW), pedestal, vent lines and Wetwell (WW). At time zero drywell did not contain pool. Its Pressure and Temperature have been set respectively 0.106 MPa and 50 °C due to stop of HVH (containment vessel cooling system) [90]. Free volume is of 3483 m^3, (92.4% of total, NUREG/CR-5942, table 4.2). The DW was connected to the WW with 8 vent lines. Each vent line had a volume of 58.75 m^3 [89] and was composed of a vent pipe and 12 downcomers immersed in the suppression pool (Figure 9.4.4).

Vent lines are also connected to the suppression chamber through vacuum breaker flow paths, one for each vent line CV, which are assumed to open when the wetwell pressure exceeds the drywell pressure by 3.4 kPa.

The wetwell has a toroid shape which could be divide in eight sections according to SRVs exhausts in the suppression pool, from A to H as shown in Figure 9.4.4.

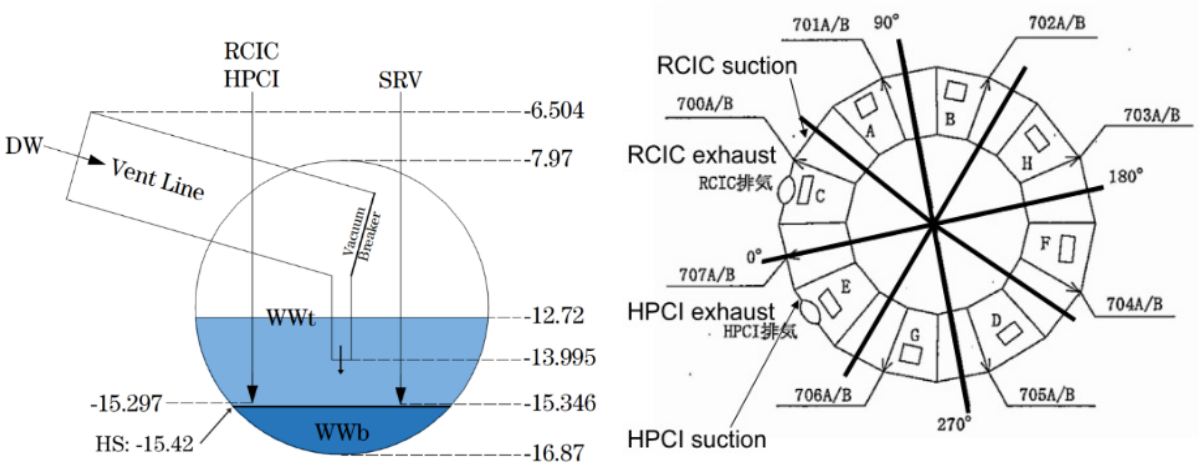

Figure 9.4.4 – Toroidal suppression chamber

The suppression chamber had a free non-pool volume of 3160 m^3 with a suppression water volume of 2980 m^3 [94]. Each wetwell section has been modeled with two CVs connected with flow path, one simulating the bottom of suppression pool (WWb – Wetwell bottom) and the other the upper water pool and the free chamber (WWt – Wetwell top). In order to avoid a complete suppression pool stratification when steam is discharged, an imaginary horizontal heat structure (1 mm thickness) is inserted between the two different CVs, to simulate also the natural circulation, since the code will calculate convection heat transfer from the WWt CV to HS and from the HS to WWb CV [95]. A 2D view of the primary containment model is shown in Figure 9.4.5.

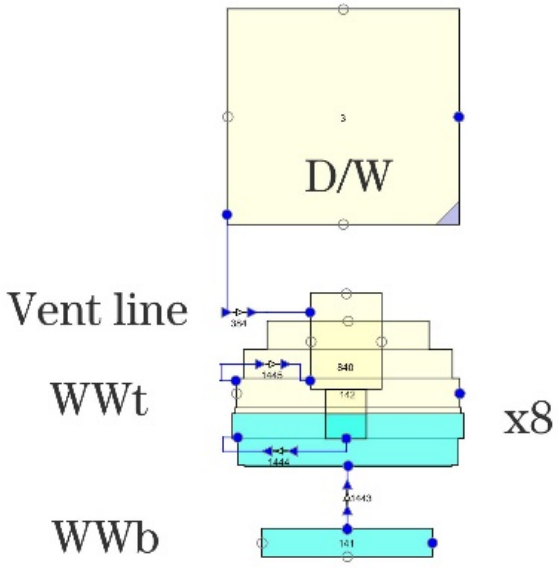

Figure 9.4.5 – Containment nodalization scheme

9.4.2.3 Reactor Building

The RB model follows the reference [96] and is shown in Figure 9.4.6. The torus room is modeled as a single control volume. The reactor building floors 1-4 are associated to the same one CV as the spent fuel pool and the fifth RB floor combined in the same CV. The decay heat power of the spent fuel pool, 540 kW [89] is added as an enthalpy source in the spent fuel water volume (1390 m^3 [89]). Environment and “shield volume”, space between the drywell head and the concrete shield plugs, are also modeled. All initial conditions of RB control volumes have been set as atmospheric ones, 0.1013 MPa and 25°C.

Leakage from DW to RB location was assumed to be at the drywell head, from the “shield volume” to the reactor hall. The leak area was increased linearly from at the atmospheric pressure to at 0.71 MPa, giving leak rate of approximately 0.5% of containment free volume per day at the design pressure 0.48 MPa [89]. When DW pressure exceeds 3.6 bar, leak area is assumed to be linearly proportional to DW pressure with higher area, in agreements with DW pressure decreases after about 24 hrs.

After corium ejection, molten-concrete interactions take place in cavities. Fukushima Daiichi Unit 3 had two different sump cavities, but there are missing information about their geometrical data. Therefore, the MELCOR model is based on public cavities information about Unit 1.

The Main cavity (Figure 9.4.7) is related to the pedestal CV. Sump 1 and Sump 2 cavities are related to Sump CV. The concrete type in the Fukushima plant is basaltic. MELCOR’s default concrete type CORCON basalt was used [88].

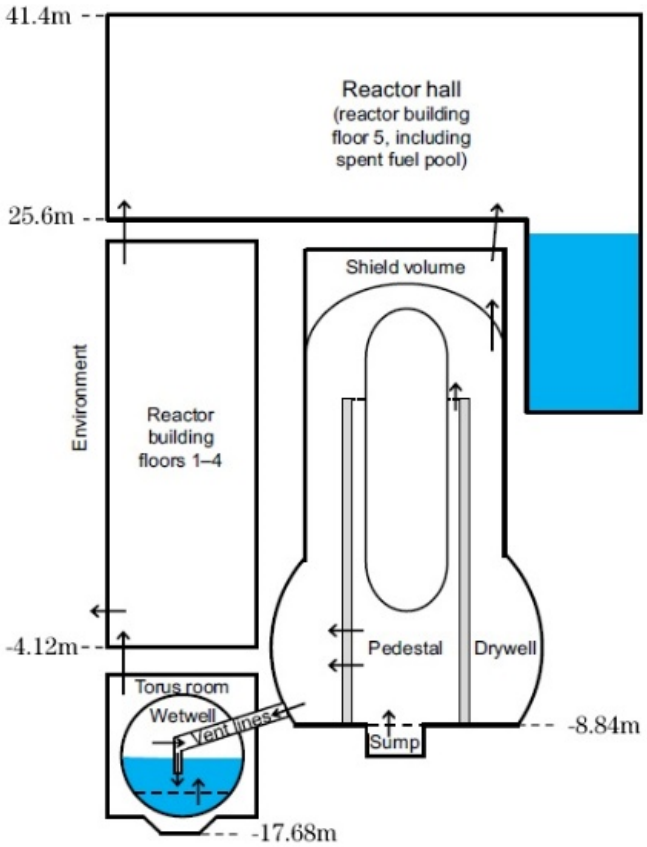

Figure 9.4.6 - External conventional containment nodalization

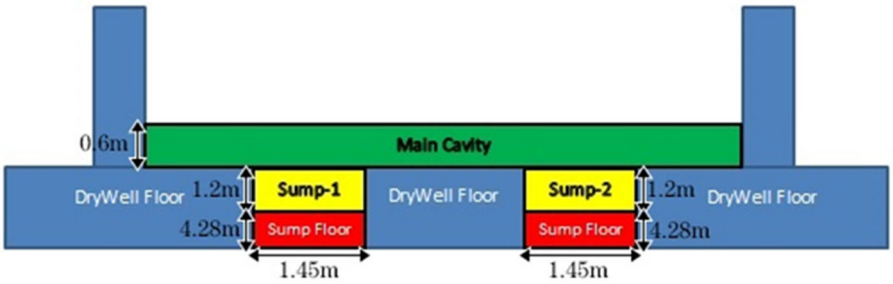

Figure 9.4.7 – Main cavity nodalization

9.4.2.4 MELCOR model

MELCOR core degradation modelling are mostly based on loss of global support or local temperature exceeding temperature-based failure criterion. Main input parameters relative to core degradation are:

- Urbanic–Heidrick correlation for Zircaloy oxidation, with cut-off temperature of 1100 K and enhanced oxidation rate at 1873 K;
- Fuel cladding failure at 1173 K with release of mobile gap FPs (Cs, Te, I) in RPV;
- Unoxidized Zircaloy melting temperature of 2100 K;
- Molten Zircaloy breakout oxide shell temperature of 2350 K, with its candling and refrozen at cooler axial levels downward;
- Maximum molten Zr breakout flow rate per unit width: 0.2 kg/m-s;
- Effective temperature at which the eutectic formed from UO2 and ZrO2 melts of 2479 K

If the fuel does not collapse due to reaching the liquefaction temperature or the supporting core plate structure beneath fuel has not failed, then a parametric life-time model for prolonged damage and weakening at sustained high temperatures becomes involved, acknowledging thermal-mechanical weakening of the oxide shell as a function of time and temperature [98]. B4C model is active, with B4C melting temperature set to 1700 K, taking account eutectic interaction with stainless-steel.

When core debris relocates from a position above the lower core support structures (slumping) there is direct interaction between over-heated or molten core debris and a pool of water. Heat transfer coefficient from in-vessel falling debris to lower plenum pool was set to 2000 W/m^{2}K, debris hydraulic diameter was defined to correspond to the average end-state conditions observed in the FARO tests [99], 1cm in core region and 2mm in lower plenum, and the average ‘fall velocity’ was set to 0.01 m/s. Once debris relocate to lower head, it increases its temperature based on debris-lower head heat transfer coefficient, set to 100 W/m^2-K. Metallic molten pool (MP1) as well as higher melting temperature mixed oxide molten pool (MP2) can exists, with heat transfer coefficient calculated from the internal model.

Vessel breach can occur by penetrations failure at temperature threshold of 950 K or by creep damage calculated using a one-dimensional temperature profile through the lower head and Larson-Miller parameter.

Masses available for ejection are those molten in lower head, imposed activating solid debris ejection switch. Constraints on the mass to be ejected at vessel failure are eliminated setting to 0 SC1610-2 and SC1610-2 [88]. However, in case of gross failure of vessel wall, it is assumed that all debris in the bottom axial level of the corresponding ring, regardless its state, is discharged linearly over 1s time step without taking into account failure opening diameter [56].

Molten core-concrete interaction is modelled in agreement with the MACE data: a 10x surface boiling heat flux multiplier and 5x debris conductivity multiplier for oxide and metallic debris were used to enhance the ex-vessel debris-to-water MELCOR heat transfer model [98], reducing the rate of concrete ablation, in case water is present.

The reactor hall explosion occurred on 14 March at 11:01 (68 h and 15 min after the earthquake) has been simulated through the Burn package. In Fukushima Daiichi Unit 3 the explosion took place in the reactor hall, simulated setting an igniter inside the reactor hall CV which appears at the explosion time. The dimension of the generated flow path from the reactor hall CV to the environment CV is set as -1, which gives a default dimension equal to the radius of a sphere of the same volume of the target CV (Sandia National Laboratories, 2008).

Following MELCOR best practice, fission products were divided into 17 radionuclide classes, lumped chemically except for uranium class, or combinations of other radionuclide classes (e.g. CsI and Cs_2MoO_4). The default CORSOR-Booth model was used for the releases from the core. Fission products are predominantly in the condensed phase carried as aerosol particles, with exception of noble gases. Caesium was divided into 3 different classes: 5% of caesium initial inventory as CsOH (i.e. representing the gap inventory), 6% as CsI and 89% as Cs2MoO4 for the duration of the calculation.

Table 9.4-2 – Initial core inventory

Class name	Representative	Initial inventory (kg)	DCH power at shutdown (MW)
1 – Noble gases	Xe, Kr	360.25	11.40
2 – Alkali metals	Cs, Rb	10.24	0.99
3 – Alkaline earths	Ba, Sr	159.64	15.41
4 – Halogens	I, Br	6.78E-21	7.93E-21
5 – Chalcogens	Te, Se	33.29	6.61
6 – Platinoids	Ru, Pd, Rh	232.24	2.65
7 – Early trans elements	Mo, Tc, Nb	200.97	18.77
8 – Tetravalent	Ce, Zr, Np	1053.99	11.80
9 – Trivalent	La, Pm, Y, Pr, Nd	1215.4	29.41
10 – Uranium	U	89977.95	2.92
11 – More volatile	As, Sb	4.47	5.52
12 – Less volatile	Sn, Ag	6.53	2.00
13 – Boron	B	4.04E-5	1.20E-5
14 - Water	H2O	-	-
15 – Concrete	-	-	-
16 – Cesium Iodide	CsI	27.66	17.17
17 - Cesium-molybdate	Cs2MoO4	264.69	25.34
		Total decay power at shutdown	150.0

9.4.3 Accidental sequence models

This chapter analyses the MELCOR model of safety systems operations and particular events occurred during the accident. The summary of events modelled in the MELCOR simulation is shown in Table 9.4-3.

Table 9.4-3 Accident Time history

Date and time	Time after earthquake		Event
11 March 14:46	0.0 s	0.0 s	Earthquake, scram, loss of offsite power, start of DDFPs and isolation of RPV
11 March 15:05	19 min	1140 s	RCIC start
11 March 15:25	39 min	2340 s	RCIC stop
11 March 15:38	52 min	3120 s	Tsunami and Station Blackout
11 March 16:03	1 h 17 min	4620 s	RCIC start
12 March 11:35	20 h 50 min	75 000 s	RCIC stop
12 March 12:06	21 h 20 min	76 800 s	Wetwell spray system start
12 March 12:35	21 h 49 min	78 540 s	HPCI start
13 Marc 2:42	35 h 56 min	129 360 s	HPCI manual stop
13 March 3:05	36 h 19 min	130 740 s	Wetwell spray system stop
13 March 5:08	38 h 22 min	138 120 s	Wetwell spray system start
13 March 7:39	40 h 53 min	147 180 s	Drywell spray system start
13 March 7:43	40 h 57 min	147 420 s	Wetwell spray system stop
13 March 8:41	41 h 55 min	150 900 s	Wetwell vent valve opened
13 March 8:50	42 h 4 min	151 440 s	Drywell spray system stop
13 March 8:55	42 h 9 min	151 740 s	Wetwell vent line rupture disk burst
13 March 9:25	42 h 39 min	153 540 s	Fresh water injection start
13 March 11:17	44 h 31 min	160 260 s	Wetwell vent valve closed
13 March 12:20	45 h 34 min	164 040 s	Fresh water injection stop
13 March 12:30	45 h 44 min	164 640 s	Wetwell vent valve opened
13 March 13:12	46 h 26 min	167 160 s	Seawater injection start
14 March 1:10	58 h 24 min	210 240 s	Seawater injection stop
14 March 3:20	60 h 34 min	218 040 s	Seawater injection start
14 March 5:16	62 h 30 min	225 000 s	Wetwell vent valve closing assumed
14 March 10:55	68 h 9 min	245 340 s	Wetwell vent valve opening assumed
14 March 11:01	68 h 15 min	245 700 s	Hydrogen explosion
14 March 11:01	68 h 15 min	245 700 s	Seawater injection stop
14 March 11:55	69 h 9 min	248 940 s	Wetwell vent valve closing assumed

9.4.4 Systems operation simulation

This section focuses on the MELCOR model of different safety systems whose operation occurred during the development of the accident.

9.4.4.1 RCIC and HPCI model

The RCIC - Reactor Core Isolation Cooling and HPCI – High Pressure Coolant Injection systems provide cooling and supplies make-up water to maintain adequate water level in RPV. RCIC is a non-safety system but provide important safety role in case of loss of ultimate heat sink and loss of AC power. RCIC and HPCI work in same way, differing on flow capacity. Steam is extracted from steam line, driving a small turbine which runs a pump. The turbine-driven pump supplies make-up water from the CST - Condensate Storage Tank to the RPV in the feedwater injection line at the normal reactor operating pressure, while the turbine exhaust is discharged in the suppression pool. A design flow functional test system may be performed by drawing suction from the CST and discharging through a full flow test return line to the CST. All the valves to control the amount of water injection are driven by DC power from the batteries. The required mission time for the RCIC in the Fukushima Daiichi NPP

units in an SBO situation was four hours, but it can operate longer depending on the manipulation of plant systems consuming DC power [100].

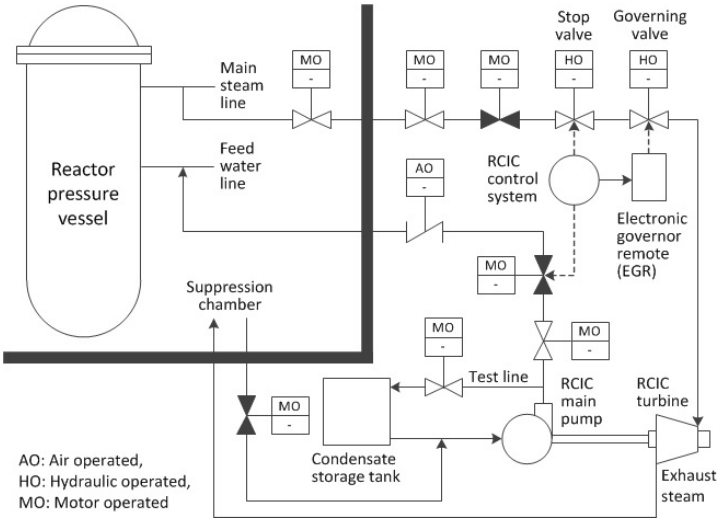

Figure 9.4.8 – RCIC scheme

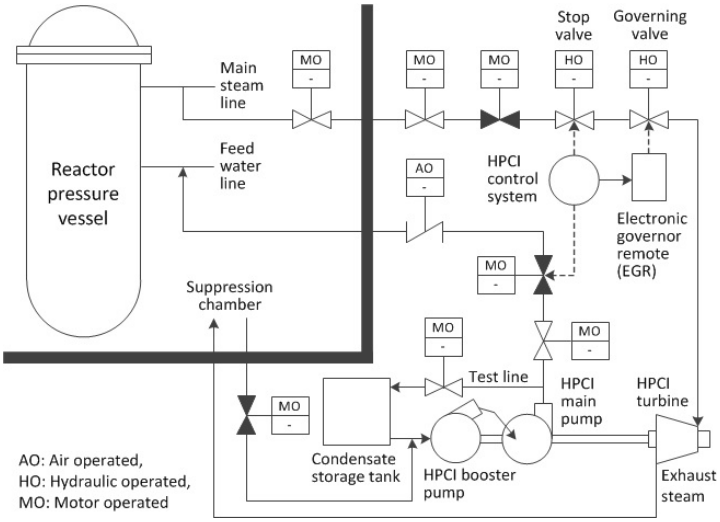

Figure 9.4.9 – HPCI scheme [100]

The mass flow rates of injected water and extracted steam during the accident are unknown but design values are public and presented in Table 9.4-4.

Table 9.4-4 - RCIC and HPCI systems Design Specifications [98]

	RCIC Design Specifications		**HPCI Design Specifications**	
	Upper Pressure	**Lower Pressure**	**Upper Pressure**	**Lower Pressure**
Pressure (MPa-abs)	7.83	1.14	7.83	1.14
Power (kW)	373	60	3132	522
Water injected (kg/s)	26	26	268	268
Steam extracted (kg/s)	2.51	2.51	14.60	8.72

Operation times of the RCIC and HPCI systems were taken from [90], and they are included in Table 9.4-3Table 9.4-3 Accident Time history. Turbine is simulated through introduction of a CV, characterized by the turbine exhaust properties (pressure greater than WW of 50kPa at saturated

temperature condition), acting as enthalpy sink that would be lost in the turbine. The mass flow rate of the steam through the turbine depends on the pressure difference between the RPV and WW and density of steam in the steam lines.

During the accident the operators manually controlling steam extraction and the water injection to the RPV, through a test loop line, to save battery power and control RPV water level without repeated start and stop of emergency system.

9.4.4.2 Safety relief valves operation model

The overpressure protection and automatic depressurization (ADS) of the reactor pressure vessel were provided by SRVs, which were connected to the four steam lines, discharging steam to wetwell. The overpressure protection was achieved by the continuous SRVs opening and closing at a pre-set high and low RPV pressure. The relief function, which operated at a lower pressure than the safety one, was guaranteed by nitrogen pressure provided through AC power or by 85 L accumulators (one for each SRV), while the safety function had spring force as drive source. The activation relief and safety valves pressures were different and summarized in the following table.

Table 9.4-5 - Relief and Safety mode opening pressure

	Relief Function		**Safety Function**	
	Opening P (MPa)	Closing P (MPa)	Opening P (MPa)	Closing P (MPa)
SRV C	7.54	7.25	7.74	7.45
SRV A, E, G	7.61	7.31	7.81	7.51
SRV B, D, F, H	7.68	7.38	7.88	7.58

There were 8 SRVs, so it has been supposed that there were 2 SRVs on each steam line, each one discharging steam in one of the 8 wetwell CVs.

According to [101], during the period from the earthquake until the tsunami hit, SRV C, which had the lowest relief function working pressure, repeatedly opened and closed through nitrogen pressure provided by AC power. However, at 15:38 on March 11th, AC power was loss since the tsunami hit, causing the nitrogen pressure supply piping closure. From this point, the required nitrogen pressure for opening started coming from accumulators, ensuring relief function only for eight movements per SRV, until nitrogen pressure inside 85 L accumulators was consumed.

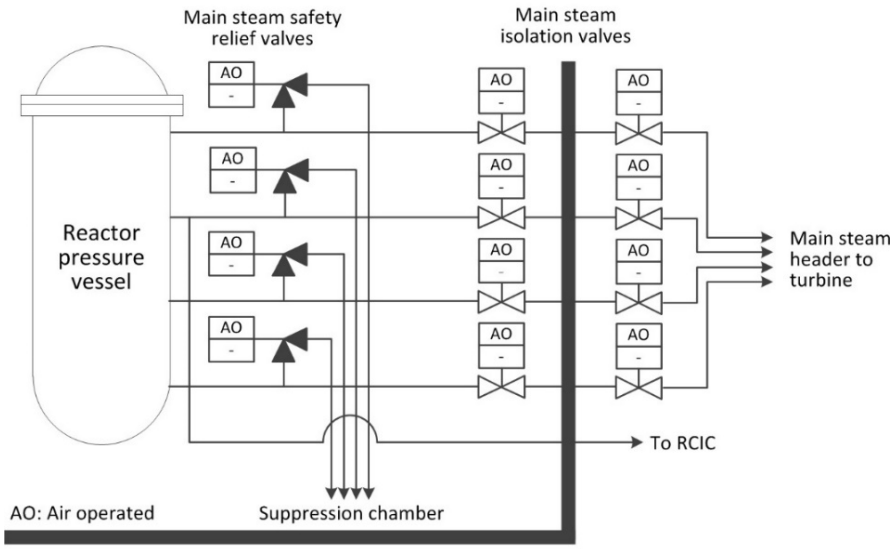

Figure 9.4.10 - SRV and MSIV scheme

After all, SRVs operated 8 times in relief function, the safety operation is simulated and allowed until the ADS occurred. According to [89] the total capacity of the eight SRVs discharging to the wetwell was 2 913 t/h, which results to 101 kg/s for one valve. After the HPCI stop (129 360 s), the ADS actuated by operators is modelled through the opening of SRV flow path when the RPV pressure exceeds 7.4 MPa.

9.4.4.3 Containment venting system model

The purpose of the containment venting system is consequently to avoid overpressure in the PCV in order to protect and maintain the integrity of the containment preventing the possibility of a direct and uncontrolled release of radioactivity to the environment. Vent paths include a train from drywell and a main one from the suppression chamber, in order to benefit of radionuclide scrubbing removal by pool.

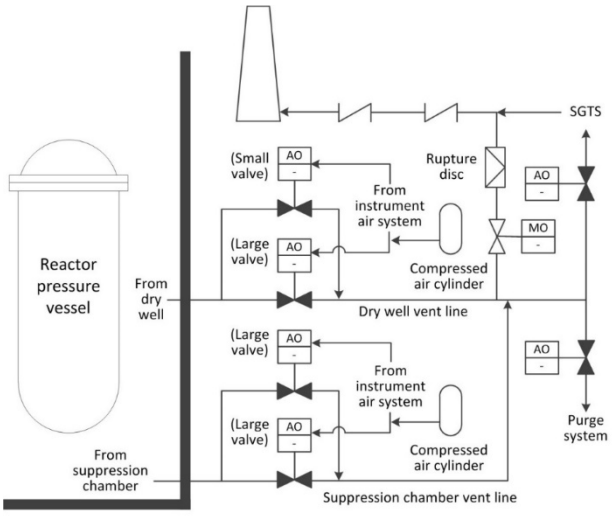

Figure 9.4.11 – Venting lines scheme

Referring to figure and accident events, the MO (motor operated) valve manually opened to 15% at 08:35 on March 13, while the AO (air operated) valve opened and closed several times, some of which are not even reported. The venting line can start its function when the rupture disk burst, at the activation

pressure of 528 kPa [101]. The MO valve operation is not modelled, while rupture disk and AO valve are simulated. Following the AO's time table.

Table 9.4-6 – AO time history [102]

Date	Notes
13 March 08:41	Venting Line Set, attend Disk Rupture
13 March 11:17	AO valve closed due to tank pressure loss
13 March 12:30	AO valve was confirmed to be opened. D/W pressure drop began later (480 kPa at 12:40 and 300 kPa at 13:00)
13 March 14:30	D/W pressure began rising, from 230 kPa at 14:30 to 260 kPa at 15:00
13 March 21:10	D/W pressure drop, supposing an AO opening at 20:30
14 March 00:50	D/W pressure increased; it is like venting terminated at this time
14 March 05:20	Solenoid began to open the S/C vent bypass valve. This was completed at 06:10. Even if S/C vented was maybe activated at 05:20
14 March 11:55	D/W pressure increased. It is like venting that started at 05:20 terminated at 12:00

There is a great uncertainty in the venting line operation, however the MELCOR model considers the previous table, with recorded and TEPCO assumed venting system interventions.

9.4.4.4 Containment spray system (CSS) model

Emergency spray systems include core spray systems, that provide make-up coolant from the suppression pool to the RPV, and primary containment spray systems, used to refrigerate and depressurize the suppression chamber and the drywell, driving water from the suppression pool or the CST to the dry containment or to the upper non-pool section of the suppression chamber. There are two different trains, each one containing both the core and the containment spray system. Containment spray system was operated using the DDFP – Diesel Driven Fire Pump: TEPCO analysis evaluated a mass flow rate of 13.8 kg/s as the maximum flow rate elaborated from the DDFP. Consequently, when the spray was simultaneously working in the wetwell and the drywell, the maximum flow rate was split between the two CVs (6.9 kg/s). The spray system has been modeled with 6 spray flow paths, three for each train, representing the spray line from the CST to the wetwell, the line from the wetwell to the drywell, and the line from the wetwell pool to the relative wetwell upper free volume. Maximum DDFP mass flow rates are assumed constant during spray system operation.

Operation times of the sprays were taken from [102], and they are included in Table 9.4-7.

Table 9.4-7 – Spray operations

Date	Time	Event	Notes
12 March 12:06	76800s	Alternative S/C spray by DDFP started	
13 March 3:05	130740s	The operators in the main control room received a report that the alternative water injection line by the DDFP into the RPV had been established. The change was made to use the alternative water injection line into the RPV instead of the alternative S/C spray line.	Exact time at which S/C spray by the DDFP stopped is unknown. This is the timing at which the operators in the main control room received the report. It is likely that water injected by DDFP did not reach the RPV at this timing because of the high RPV pressure.
13 March 5:08	138120s	Alternative S/C spray by DDFP started	
13 March 7:39	147180s	Alternative D/W spray by DDFP started. The change was made to use the D/W spray line into the RPV instead of the S/C	It is assumed that the total flow rate of S/C spray and D/W spray was equal to that of the S/C spray which had been

		spray line. At this timing, both the S/C and D/W spray lines were working.	activated on 13 March 03:05.
13 March 7:43	147420s	Alternative S/C spray by DDFP stopped.	
13 March 8:40 to 9:10	151740s (08:55)	Alternative D/W spray by DDFP stopped. The change was made to use the alternative water injection line instead of the D/W spray line.	It is likely that D/W spray stopped at 8:55 which was estimated by the rapid increase in PCV pressure. It is likely that the injected water did not flow into the RPV.

9.4.4.5 Fire engine injection model

Water were injected in the RPV also through fire engines. The entire volume of alternative water injected by fire engines seems unlikely that was discharged into the reactor. There is the possibility that part of the discharged water was instead sent to other systems and equipment. Therefore, TEPCO in a MAAP analysis of Fukushima Daiichi Unit 3 severe accident assumed a smaller amount of water injected into the RPV than the discharged one. The MELCOR model is based on the most recent assumption made by TEPCO MAAP analysis.

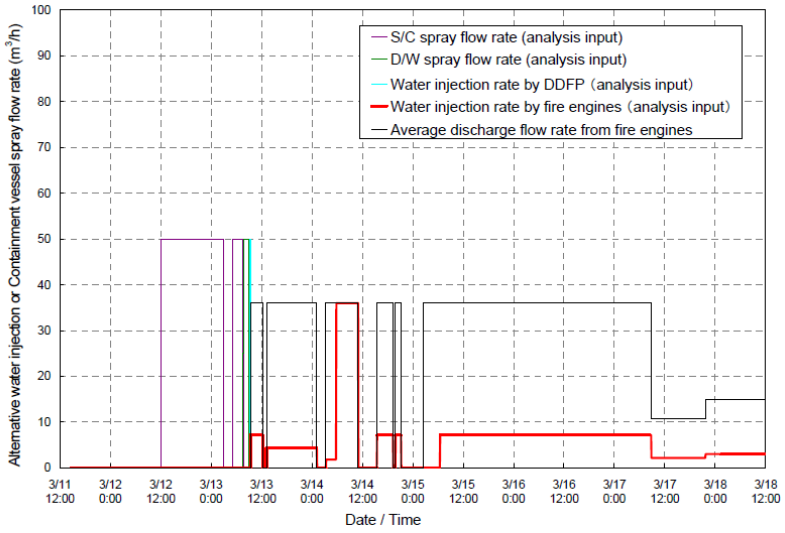

Figure 9.4.12 – Water injections postulated

Following the relative table about discharged water by fire engines and MAAP analysis assumption, based on Figure 9.4.12.

Table 9.4-8 – Water injection history

Time / Duration	Flow rate discharged by fire engines	Flow rate injected in RPV (MAAP)	Mass of water (ton)	
	t/h	t/h	Dischar.	MAAP
13 March 09:25 13 March 12:20 (10500 s)	36	7	105	20.416
13 March 13:12 14 March 01:10 (43080 s)	36	4.5	430.8	53.850
13 March 09:25 13 March 12:20 (10500 s)	36	1.5 (1/3 duration) 36 (2/3 duration)	276.6	188.242

Latest events are not considered, since they occurred in the latest part of the accident, not modelled in the MELCOR model. As shown in the previous table there is a significant difference between discharged and TEPCO RPV injected water by fire engines. The RPV injection through fire engines is simulated with a flow path from the CST CV to the upper downcomer CV, water assumed at 10°C.

9.4.5 Accident Analysis Results

Initial conditions of transient are given by a steady state MELCOR calculation, performed for 1000s. After a stabilization period, variation versus time of all parameters are negligible. Values are in general agreements with reference operational status. In following

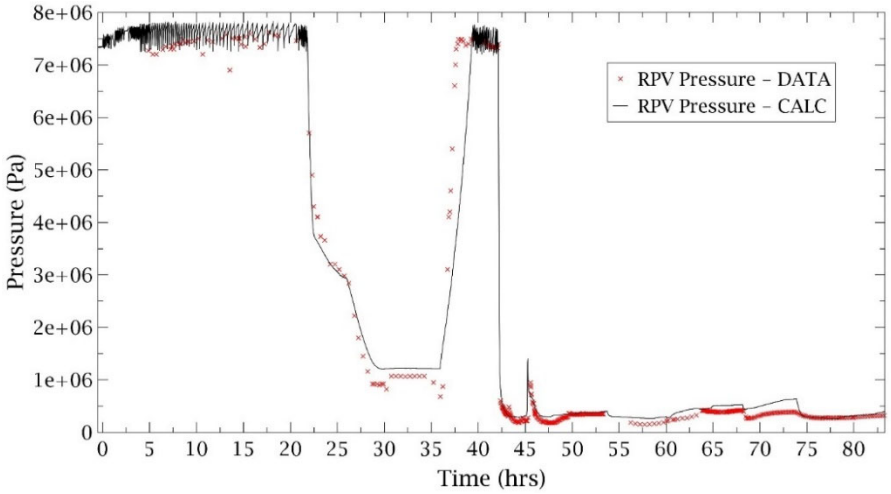

Figure 9.4.13 and Figure 9.4.14 presented RPV, WW, DW pressures and RPV liquid level, respectively.

The entire simulation will be analyzed in time ranges in following sections.

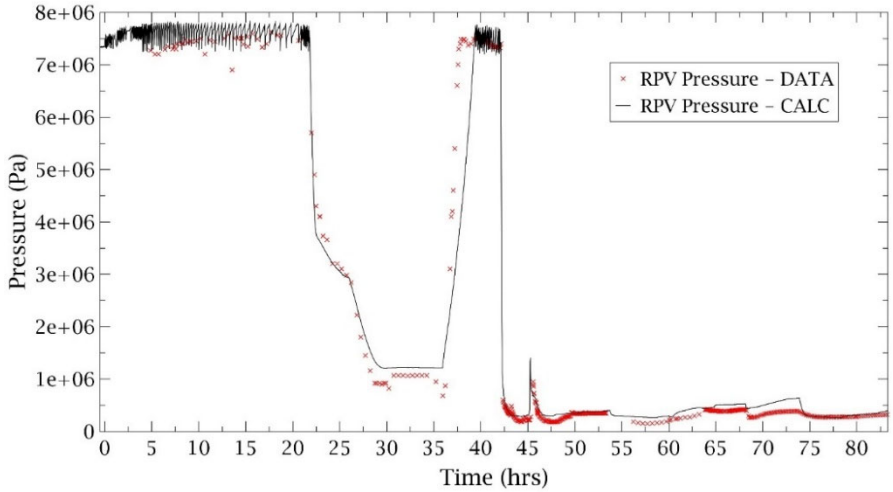

Figure 9.4.13 – RPV pressure calculation and data

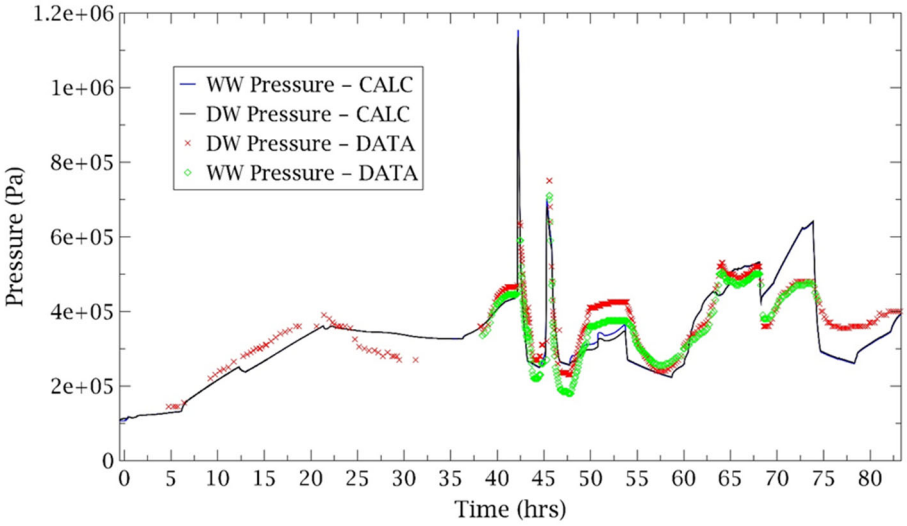

Figure 9.4.14 - WW/DW Pressure calculation and datas

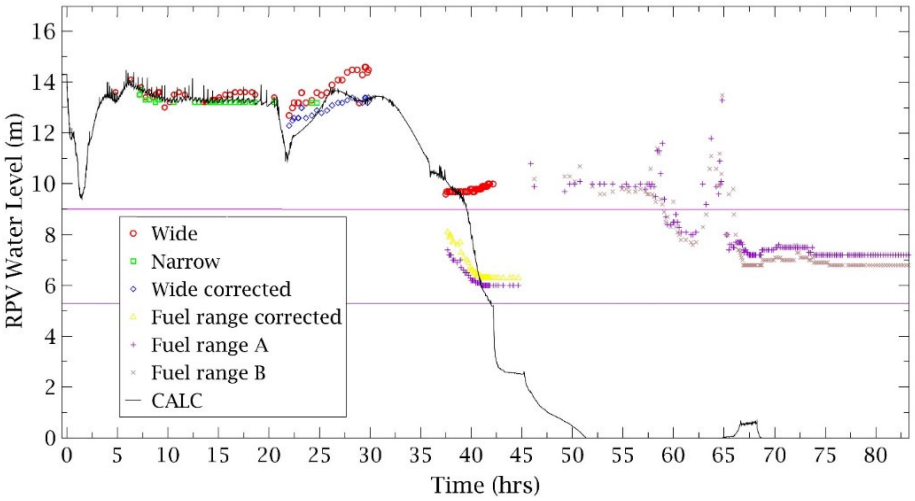

Figure 9.4.15 - RPV water level

9.4.5.1 11 March 2011 Accident results (short term)

After the earthquake, the automatic reactor protection system successfully SCRAM the reactor. SCRAM time was on March 11th 2011 at 14:47, considered as 0:00h in this analysis. However, the earthquake damaged the electricity transmission system between the NPP and external facilities, causing the total loss of off-site electricity (Station Black Out-SBO).

Emergency Diesel Generators (EDGs) started automatically at 0:01h in response of loss of all off-site power, restoring AC power. Meanwhile the RPV was isolated through the closing of Main Steam Line Isolation Valves (MSIVs). Consequently, the reactor pressure increased due to the continuous steam generation, until the safety relief valve "C" (SRV-C) opened at the pre-set opening pressure of 7.54 MPa in relief function at 14:52 and started to cycle maintaining the reactor pressure between accepted values discharging steam in the suppression chamber (SC). After all SRVs consumed nitrogen accumulators reserves, safety function SRVs operation is established, with RPV pressure ranging from 77.4 bar to

74.5 bar of SRV-C. RPV water level start to decrease till 0:19h, when RCIC starts to operate automatically due to RPV water low level signal.

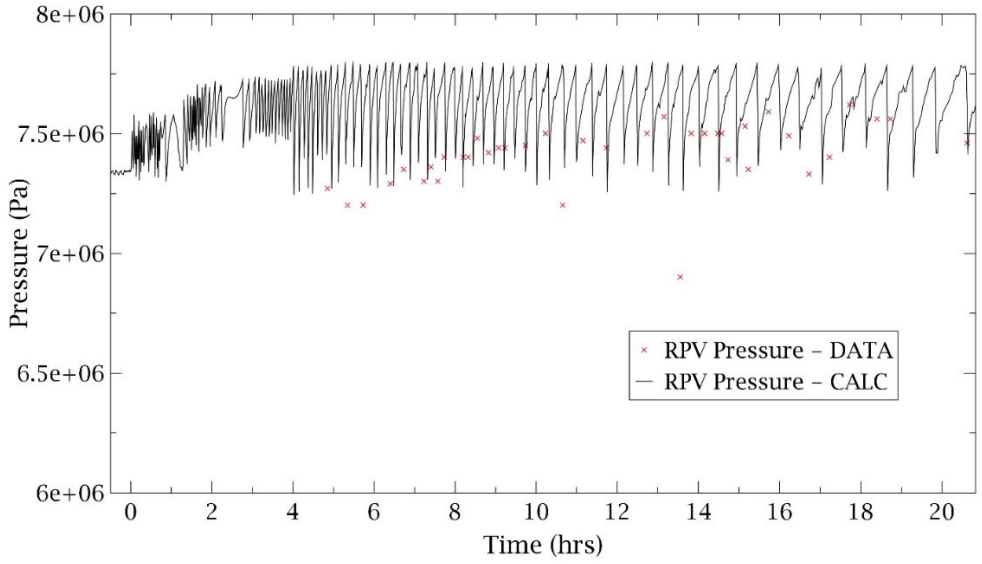

Figure 9.4.16 – RPV pressure during RCIC operation

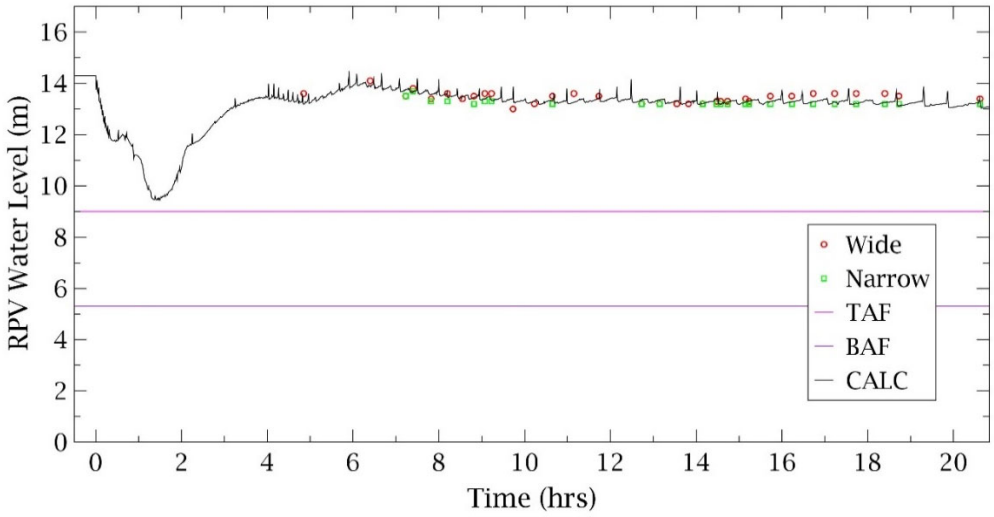

Figure 9.4.17 – RPV Water level during RCIC operation

At this stage, the steam extraction by RCIC turbine and water injected into RPV are nominal values of 2.51 kg/s and 26 kg/s respectively. So, RPV water level start to increase till 0:39h, when RCIC water injection stopped automatically due to RPV water high level signal.

At 0:52h, the tsunami generated by the earthquake flooded in the NPP's site, making totally unavailable the seawater pumps and diesel generators, with loss of AC power and SBO. The damages of the tsunami were not only to power supplies, but also to buildings, machineries and equipment installations, causing an extremely difficult access and movement within the plant, precluding the immediate and continuous injection of water through alternative systems.

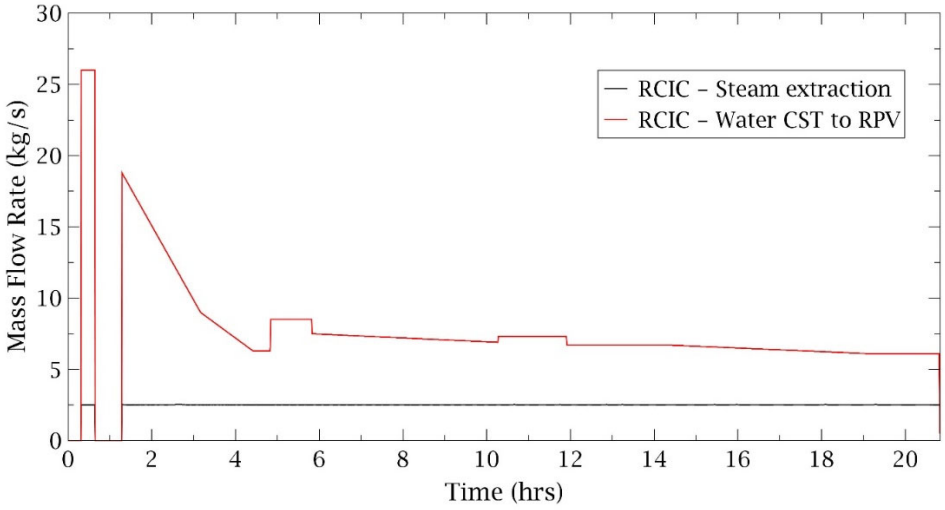

Figure 9.4.18 – RCIC injections and extractions mass flow rate (short term)

Without make-up water provided by RCIC and the continuous operation of SRVs, the RPV water level started to decrease again, consequently at 01:17h operators, from the Main Control Room (MCR), reactivated the RCIC system using DC power, remained available in the Unit 3. Operators tried then to avoid excessive power consuming by disconnecting lightning and non-safety instrumentation at the MCR and mainly distributing the RCIC injection pump flow into RPV and, through a test loop line, back into the Cooling Storage Tank (CST), in order to prevent the continuous automatic stop of the emergency system at high reactor water levels and automatic restart at low water level, avoiding excessive battery depletion due to repeated RCIC de-activation and re-activation, ensuring also stable reactor water levels. In order to reproduce operators adjusted RCIC flow rate to RPV, injected water from RCIC in calculation was tuned according to response of water level. Assumed steam extraction from RPV and water injection from CST to RPV is on Figure 9.4.18.

9.4.5.2 12 March 2011 results

RCIC stopped automatically at 20:50 h, likely due to electric trip caused by high turbine exhaust pressure [88].

Therefore, of the 20.5 hours of operation of RCIC, the WW pressure (around 40 bar) and temperature increased, forcing operators at 21:20h to active WW spray systems, through Diesel Driven Fire Pumps (DDFPs), to cool and stabilize WW pressure.

At 21:49h the High-Pressure Coolant Injection (HPCI) system automatically started after the water level reached the low set point, causing a great depressurization of RPV because of the large capacity of the emergency system.

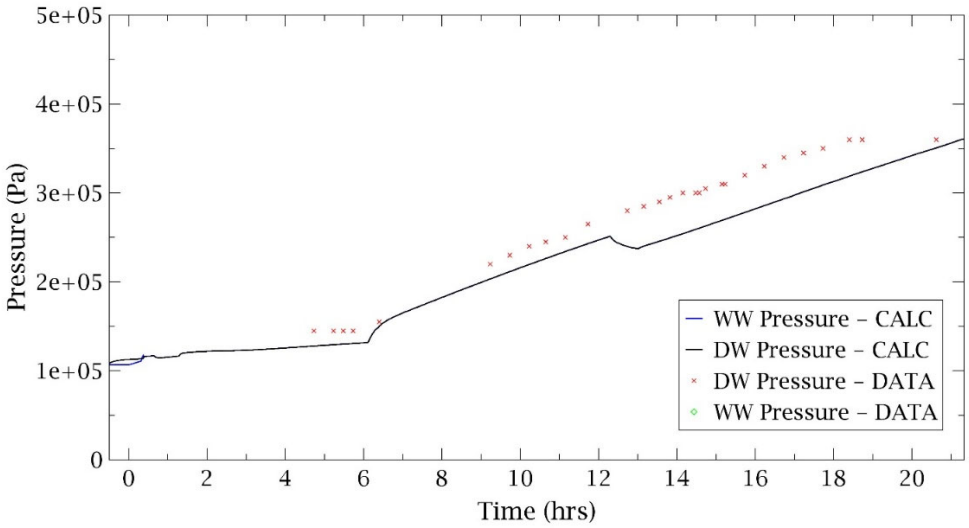

Figure 9.4.19 - DW/WW Pressure during RCIC operation

During the accident the operators manually controlling steam extraction and the water injection to the RPV, as in RCIC operation, through a test loop line, to save battery power and control RPV water level without repeated start and stop of emergency system. Water injection and steam extraction was adjusted in calculation as shown in Figure, in order to reproduce pressure and water level in RPV. The pressure response was dominated by the assumed steam extraction, the RPV water level was dominated by water injection to the RPV.

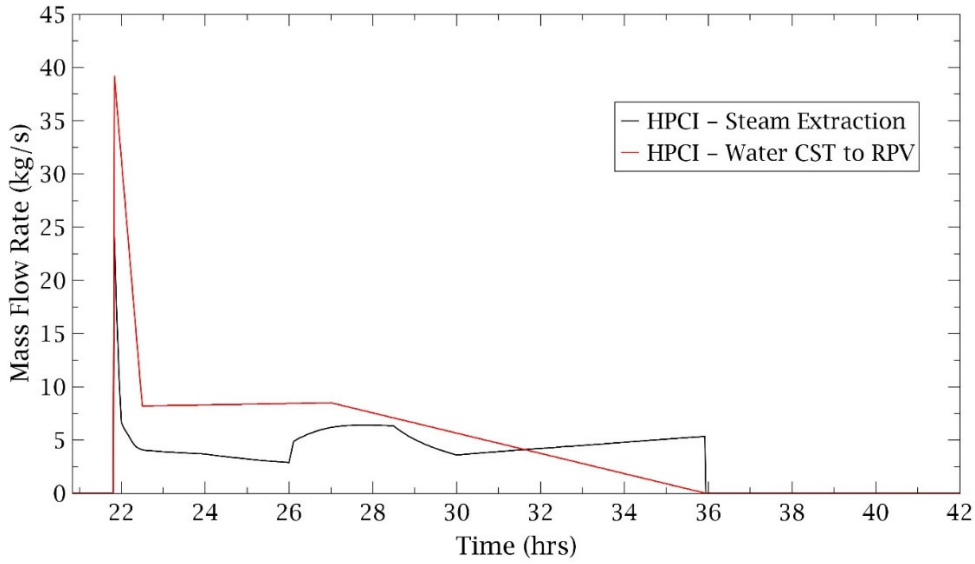

Figure 9.4.20 – HPCI injection and extraction assumed mass flow rate

At 20:36 sensors which monitored the reactor water level were unavailable due to the loss of DC batteries, which were restored at 03:51 on 13 March, at 37:05h following earthquake, using batteries from the Hirono Thermal Power Station.

9.4.5.3 13 March 2011

The continuous operation of HPCI caused a depressurization of RPV and a consequent decrease of the pressure at the HPCI turbine inlet under its design range. The possible turbine damages and the

consequent generation of a release flow from the RPV to the PCV forced operators to manually stop the HPCI at 35:56h, since the automatic shutdown for low RPV pressure (0.8 MPa) did not occurred.

The pressure started increasing and at 36:19 the operators decided to use DDFP to provide make-up water to the reactor, by switching them from the SC's spray line to the RPV injection line. However, the discharge pump pressure was not sufficient to exceed RPV pressure and no safety injection could occur. Without core cooling system, operators tried to restore the injection through HPCI system at 36:49h, but the restart attempts were unsuccessful, carrying to the continue increase of RPV pressure which exceeded 7 MPa at 04:30 (37:44h).

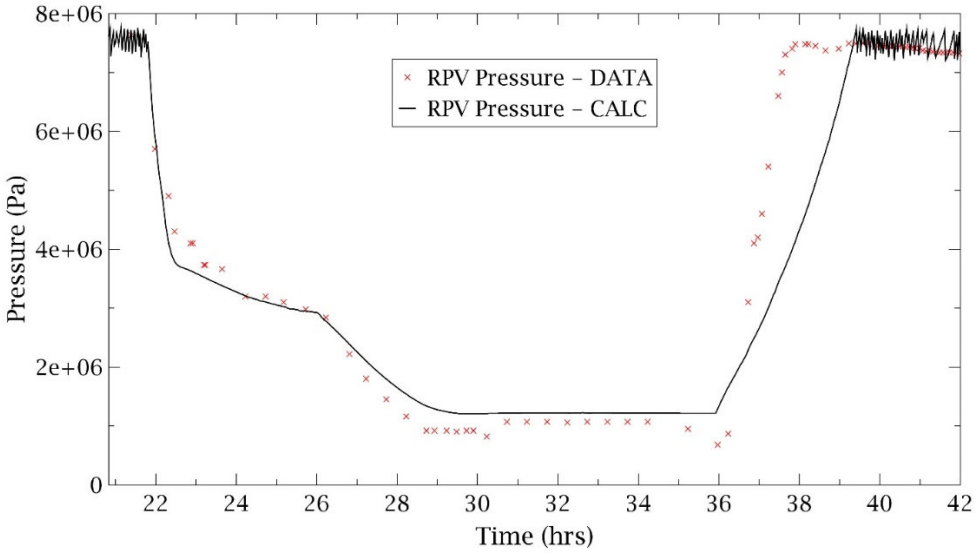

Figure 9.4.21 - RPV Pressure during HPCI operation and repressurization

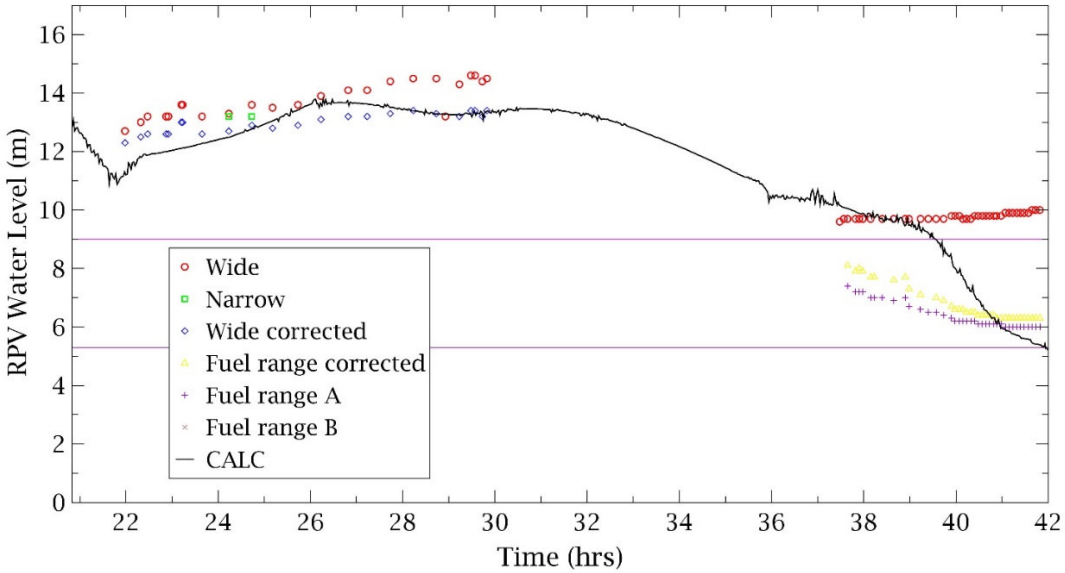

Figure 9.4.22 - RPV water level during HPCI operation and repressurization

The DDFPs that were previously connected to the RPV injection line were changed back to the WW spray injection at 05:08 (38:22h). At this point the only way to cool the core was through fire engines, and at 05:21 works started to establish a line for seawater injection into the Unit 3 RPV from backwash valve pit. At 06:30 there were two fire engines at the Unit 3 complex, one dispatched from Units 5-6

and one arrived from the Fukushima Daiini NPP. The seawater injection line was completed at 07:00, however its operation was delayed by the Site Superintendent as a result of a TEPCO headquarters communication which signaled to continue freshwater injection, if available, rather than sea water. The line was consequently changed to a borated fresh water source.

To guarantee the injection of water through fire engines, the RPV should be depressurized and operators, using batteries gathered from cars, opened a SRV causing a drop in the reactor pressure at 09:08 (42:22h). During the depressurization of the reactor a pressure surge was noticed in the PCV, causing a pressure increase in the WW carrying to the venting line rupture disc to burst (0.63 MPa) at 09:20 (42:34h) and the consequent PCV venting operation starting until 11:17 (44:31h) when a valve on the vent line prematurely closed.

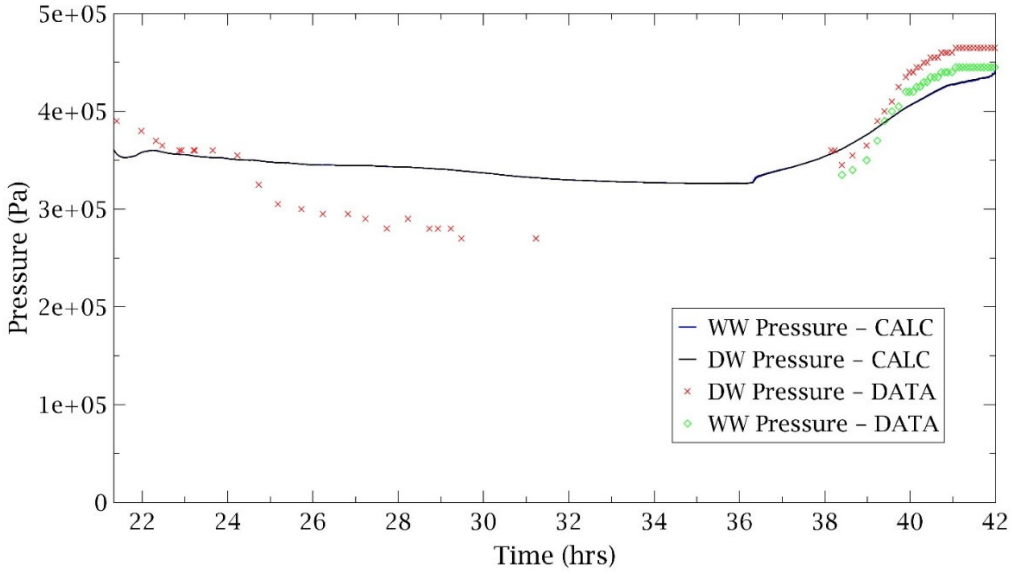

Figure 9.4.23 - DW/WW Pressure during HPCI operation and repressurization)

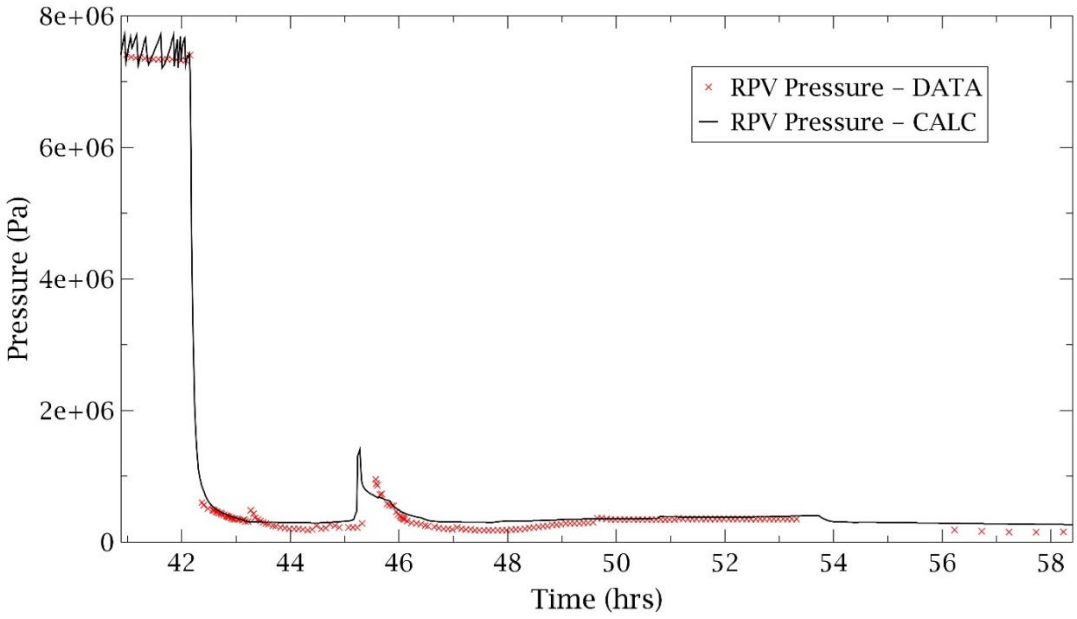

Figure 9.4.24 - RPV Pressure depressurization

After the depressurization, borated freshwater injection started at 09:25 (42:39h). The borated fresh water injection continued until the water tanks were empty at 12:20 (45:34h), consequently the Superintendent decided to start seawater injection through the line completed hours before. The fire engines were repositioned, the seawater injection line restored and at 13:12 (46:26h) the injection started.

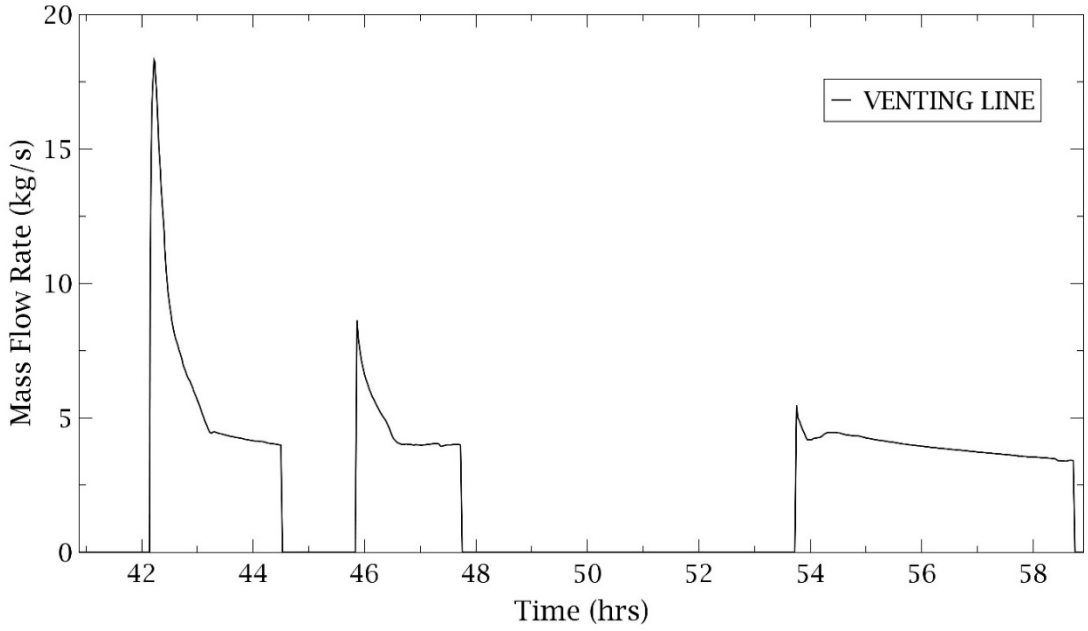

Figure 9.4.25 - Venting Line mass flow rate

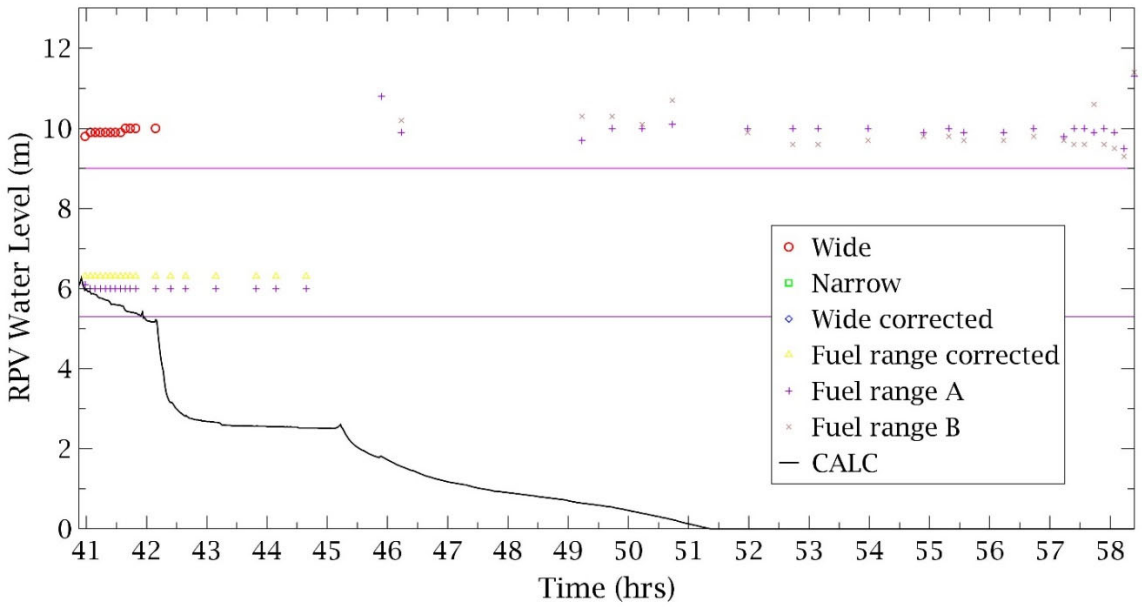

Figure 9.4.26 - RPV water level from depressurization time

Meanwhile these injection operations at 07:39 (40:53h) the Containment Spray System was switched from WW to DW, starting DW spraying at 07:43 (40:57h) until about 08:50 (42:04h). At this time spray line was changed to core injection line, but since the AC power had not been restored the high-pressure injection was impossible, forcing to use fire engines as the only reactor cooling system.

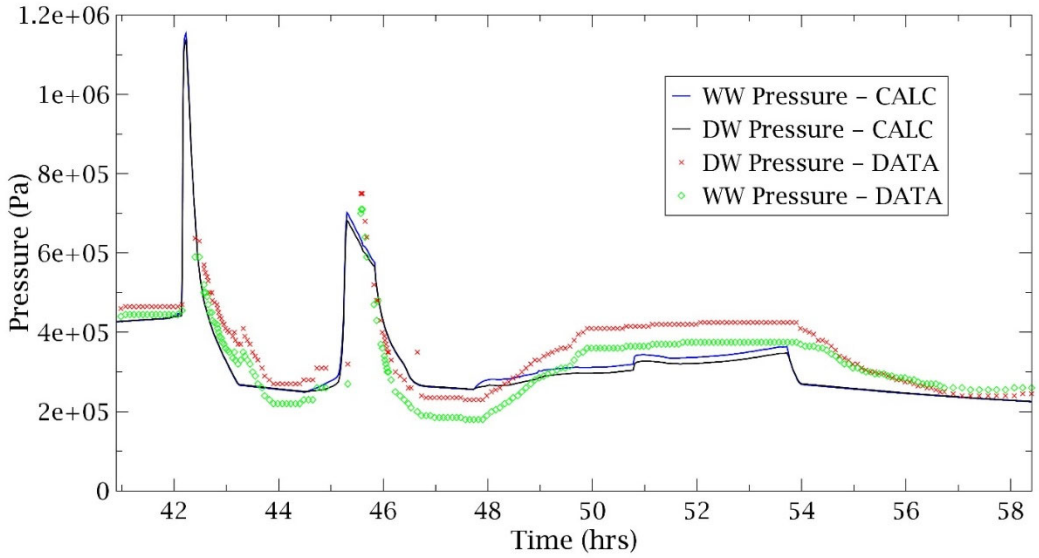

Figure 9.4.27 - DW/WW Pressure from depressurization

As said, the first pressure spike of WW/DW pressure is caused by depressurization of RPV, discharging steam in WW. This pressure peak, calculated as 115 bar in MELCOR, causes venting line rupture disk to burst, discharging about 50000 kg of water vapor to the stack for the first operation, as calculated in MELCOR. Meanwhile, core degradation started at 41hr 55min, at onset of hydrogen generated by cladding oxidation. The second pressure peak of WW/DW after RPV depressurization, is caused indeed by large relocation of corium. MELCOR predicts begin of core support plate fails at 45hrs 04mins, that caused about 50% fuel rods to fail and its slumping into lower plenum within few minutes. As seen in figure, MELCOR predicts eutectics temperature of 2479 K reached in clad hottest core cell at about same time.

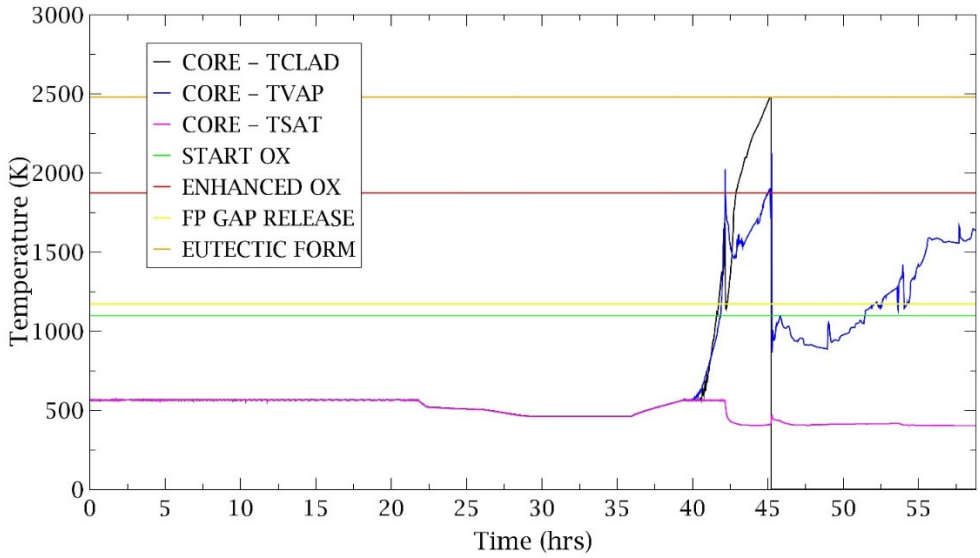

Figure 9.4.28 - COR Temperatures and degradation thresholds

At time when corium slumping into lower head, its water level is about 2.5m. After a small rising due to corium occupied volume, lower plenum water level begins to decrease due to high vaporization, till lower head dryout predicted at 51hrs 20 min. Pressure reaches 70.1 bar in calculation.

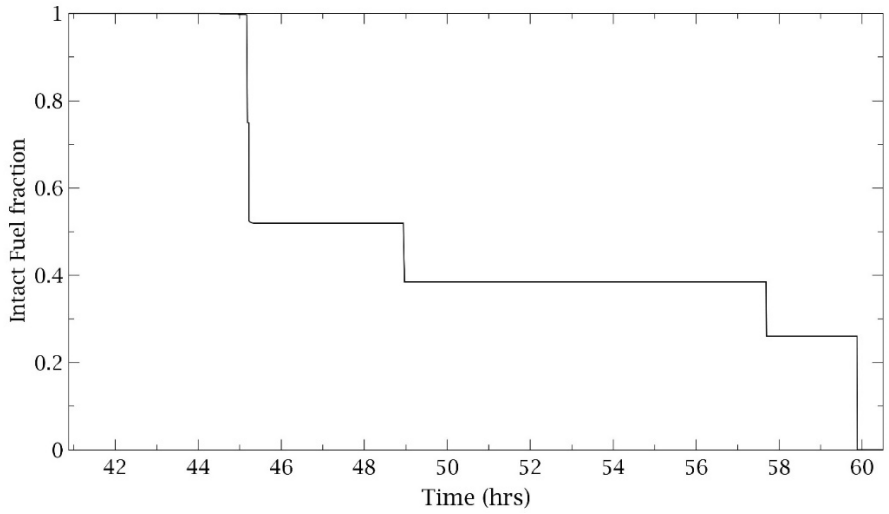

Figure 9.4.29 - COR degradation: Intact fuel fraction

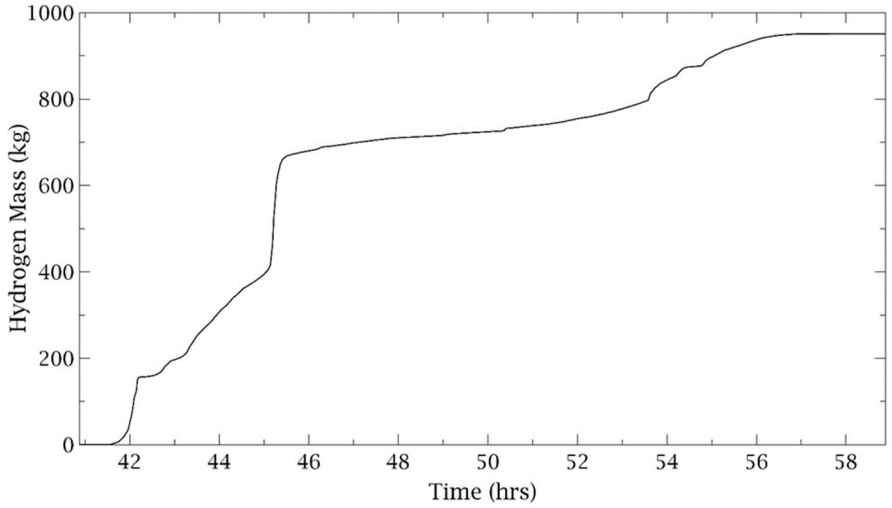

Figure 9.4.30 - Hydrogen generation due to core degradation

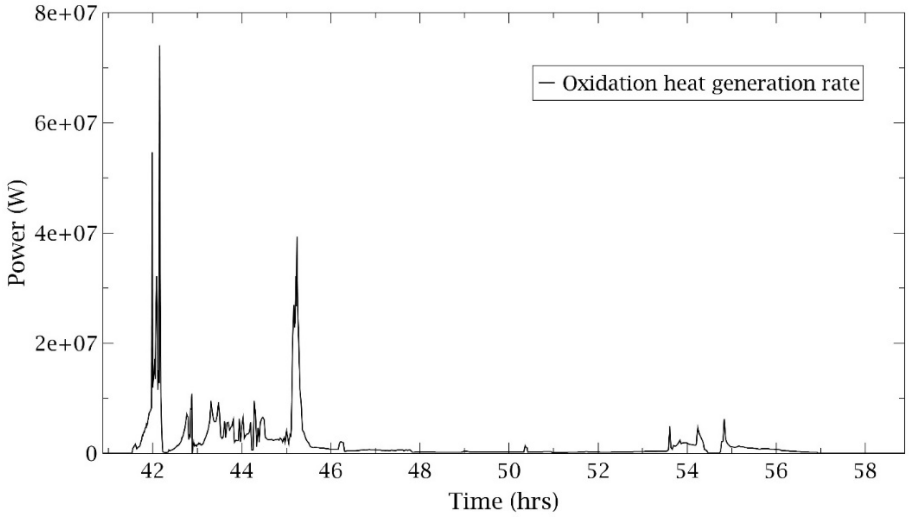

Figure 9.4.31 – Oxidation heat generated

9.4.5.4 14 March 2011

The seawater injection continued until 01:10 (58:24h) when it was halted since the pit water level decreased to an excessive low level. The injection restarted two hours later after the pit refill and the intake hose was lowered deeper inside the pit. At 06:20 the drywell pressure reached 0.47 MPa and the reactor water level sensors indicated that the fuel was uncovered. At 06:30 the evacuation order was given because of possible hydrogen explosion. The order was lifted at 06:45 and the activities of backwash valve pit refilling restarted. At 11:01 (68:15h) an explosion occurred in the Unit 3 Reactor hall, injuring workers and damaging hoses and fire engines, causing the interruption of seawater injection in Unit 2 and 3 and delaying operations in the Unit 1. At this time the RPV was 0.391 MPa, the DW pressure 0.48 MPa and the WW pressure was about 0.47 MPa.

At time of explosion, core degradation has produced about 950 kg of H2 in MELCOR calculation. H2 generation start at onset of core degradation, with first highest oxidation heat generation peak. Second peak of hydrogen production is at corium slumping into lower head, as shown in Figure.

Hydrogen were probably escaped from DW to Reactor Hall trough head flange, weakened due to high differential pressure. MELCOR calculates about 95 kg hydrogen leaked to reactor Hall at the time of explosion.

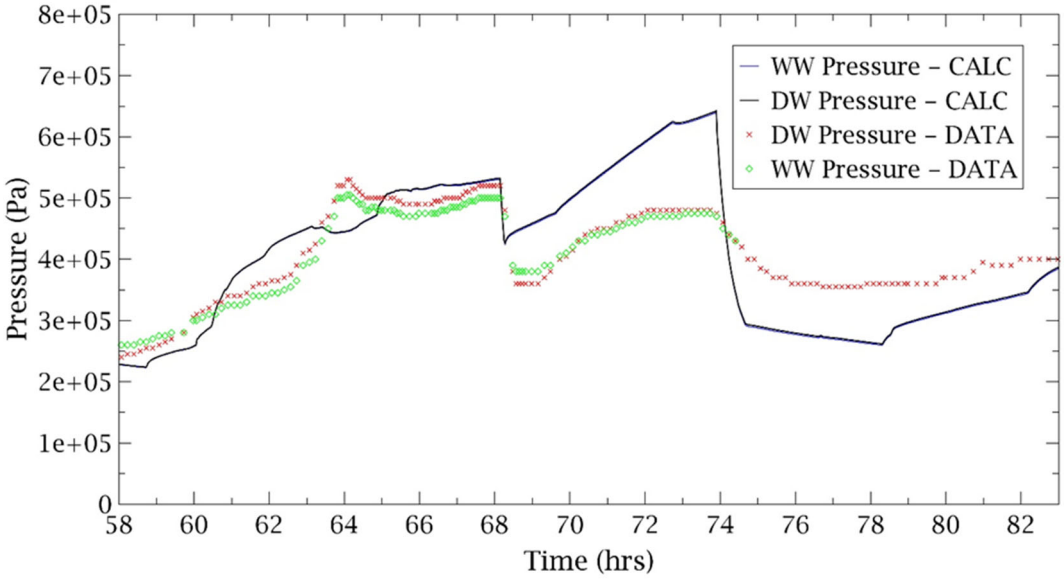

Figure 9.4.32 – WW/DW Pressure during Fire Injection operation

MELCOR predicts vessel breach at 60 hrs 5 min. The total mass ejected through the lower head breach is presented in the following figure. In the same table also MELCOR main materials masses retained inside the RPV at the end of the calculation are plotted. The calculation ends after the main accidental events, when the reactor was maintained in stable conditions through the continuous water injection by fire engines and the restoration of offsite AC power. At this point (83 hrs) the total mass ejected from the RPV predicted by MELCOR is 123893 kg, composed by 63.4% UO2, 17.4% SS, 3% SSOX, 4.4% Zr, 10.4% ZrO2, 1.4% BC4 and Inconel.

Main materials masses retained inside the RPV are summarized in the following table. MELCOR predicts a total of 80586 kg core mass retained, composed by 33.4% UO2, 31.8% SS, 8.7% SSOX, 16.6% Zr, 7.4% ZrO2, 2.2% BC4 and Inconel.

TEPCO has not yet been able to inspect the actual state of the core, so it is not possible to verify the calculation result.

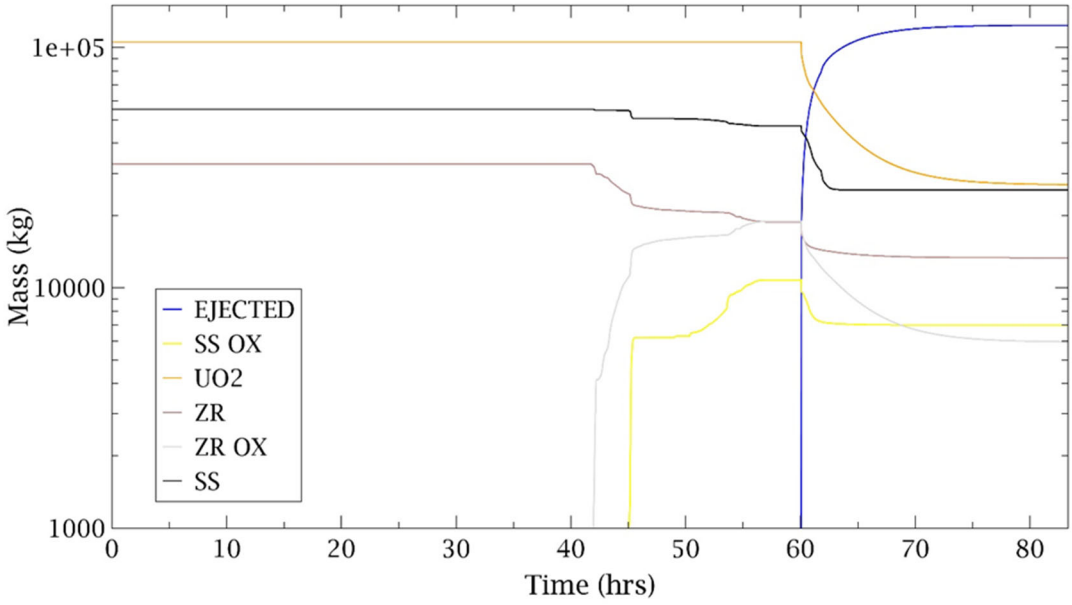

Figure 9.4.33 – Core masses and ejected mass

Material	Initial condition	Converted to OX at LH fail	Ejected	Retained
UO2	105500 kg	-	74.5% (78604 kg)	25.5% (26896 kg)
SS	55343 kg	14.8% (8194 kg)	45.7% (21562 kg SS)	54.3% (25587 kg SS)
		10790 kg SSOX	35.2% (3795 kg SSOX)	64.8% (6995 kg SSOX)
ZR	32843 kg	43% (14000 kg)	29.2% (5500 kg Zr)	70.8% (13343 kg Zr)
		18923 kg ZrO2	68.5% (12957 kg ZrO2)	31.5% (5966 kg ZrO2)

Calculated main states of reactor core degradation are illustrated in the following figure, from onset of degradation to final state, after vessel lower head fail and partial core ejection. Note that reactor liquid level is not showed.

Concrete ablation starts at RPV lower head fails. According to this calculation, the basemat concrete ablates 1.68m net radius and 0.74m in height in sumps at the end of calculation.

Under high radiation levels, seawater injection restarted at 15:30 and it was stopped at 02:30 on 15 March to provide water injection for Unit 2.

These are the main events occurred in the first days after the earthquake. On 15 March 2011, five days later the beginning of the accident, the electricity was restored and continuous attempts to refill the spent fuel pool (SFP) and to inject fresh water to the reactor were carried out.

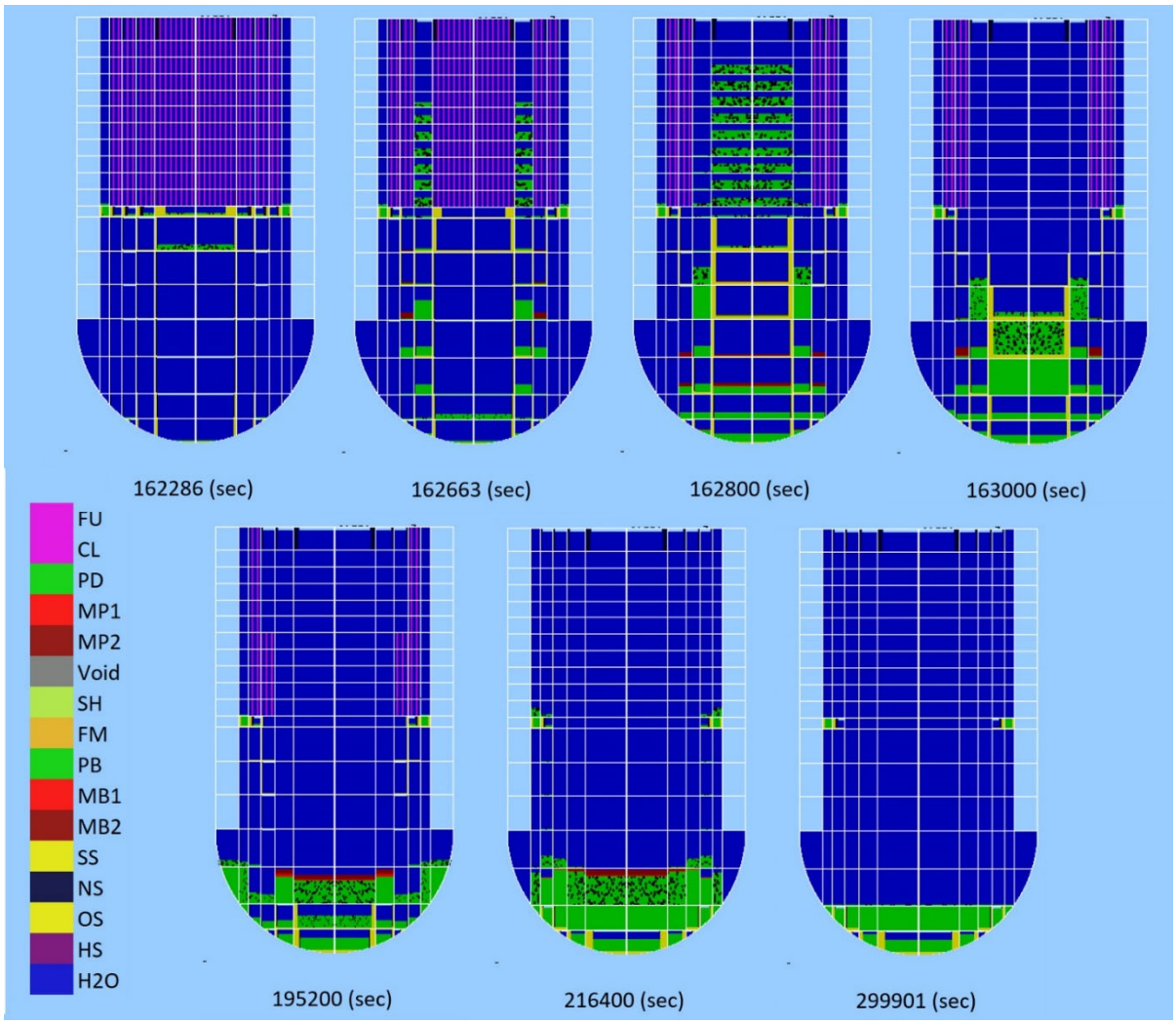

Figure 9.4.34 – Core degradation progression

Source term – Releases to environment

MELCOR modelled leak paths to environment comprises 3 ways:

- Venting line from WW
- Reactor Hall to environment caused by explosion
- Containment leakage

Release fraction are presented as sum of these leakage. However, almost all of the release comes through the venting line path, because the system is not filtered. Practically, all release begins after 42 h when the containment venting starts to operate and stops at its closure.

Mass flow rate released are presented in following Figure.

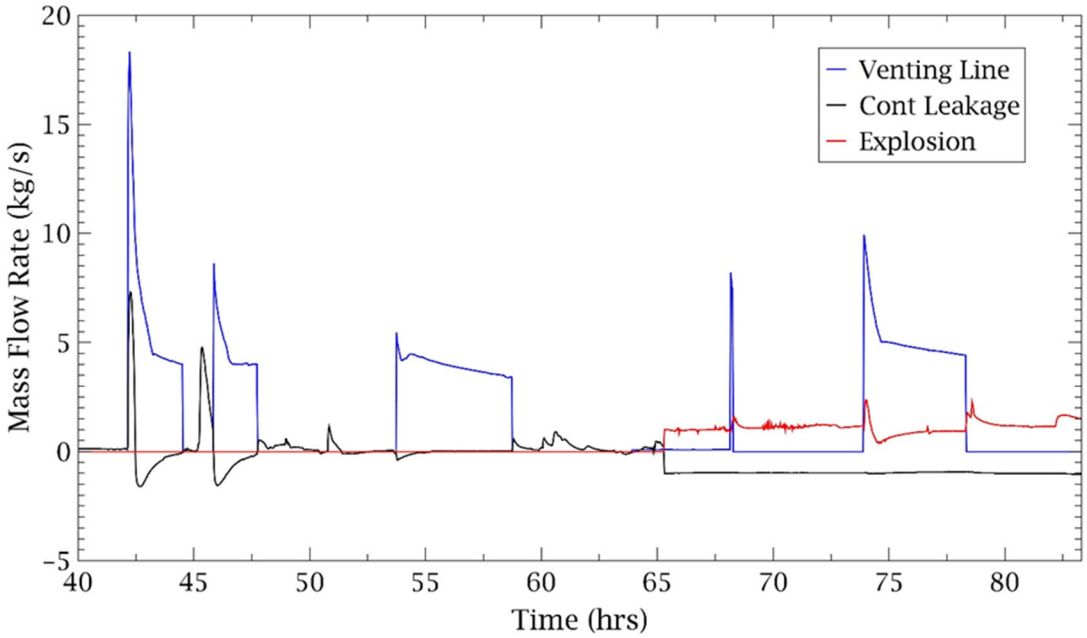

Figure 9.4.35 – Containment bypass mass flow rate

The principal radionuclides considered for the present analysis are caesium and iodine. With the exception of the noble gases, the fission products are predominantly in the condensed phase carried as aerosol particles.

Fission products released by containment venting path are previously scrubbed in the suppression pool. Noble gases were not retained in the suppression pool water, and therefore they were totally released to the atmosphere. So, releases were very small for all the fission products in the aerosol form. Nonetheless, practically all source term result from there. At the end of calculation, 3 gr of I2 and 6.62 gr of CsI are released. It's means that 3.386 gr of Cs and 6.234 gr of I are released as element.

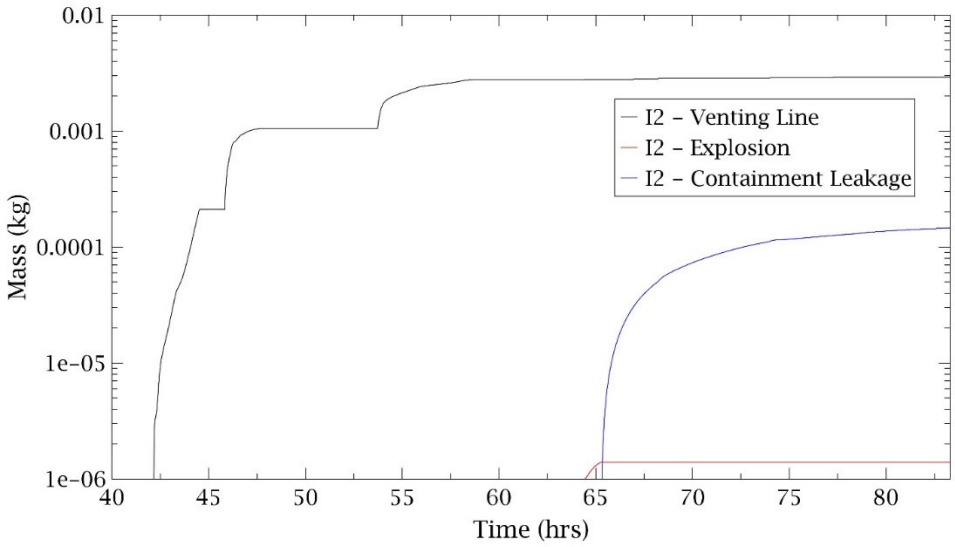

Figure 9.4.36 - I2 released to environment

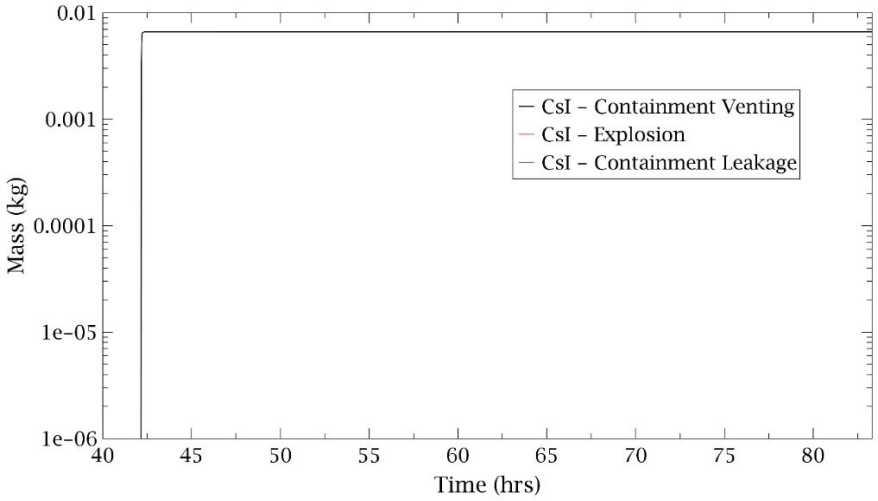

Figure 9.4.37 - CsI released to environment

9.4.6 Variables and sampling

A set of 14 uncertain parameters (see Table 9.4-9) were selected for use in this analysis, based on [103], plus recirculation pump seals leak flow area. The selected parameters are known to affect timing of cladding failure, fuel rod failure, hydrogen generation, melt relocation in core (radial and lateral spreading), refreezing behavior of draining molten core materials etc.

Table 9.4-9 – Fukushima 3 selected uncertainty parameters

Variable	Description	Distribution		LB	UB	Unit
SC1020 (2)	Time constant for the relocation of molten material	Uniform	-	10	100	s
SC1020 (1)	Time constant for the relocation of solid material	Uniform	-	100	1000	s
SC1131 (2)	Maximum ZrO2 temperature permitted to hold up molten Zr in clad (break-through temperature)	Normal	μ=2350 σ=235	2100	2540	K
SC1141 (2)	Maximum melt flow rate per unit width after breakthrough	Uniform	-	0.1	2	kg/m-s
SC1132 (1) TMLT	Effective temperature at which the eutectic formed from UO2 and ZrO2 melts	Normal	μ= 2479 σ= 83			K
HFRZZR	Candling heat transfer coefficient for Zr	Uniform	-	7500	20000	kg/m^2-s
DHYPD core	Particulate debris equivalent diameter in core region	Uniform	-	0.5	2	cm
DHYPD lp	Particulate debris equivalent diameter in lower plenum region	Uniform	-	2	5	mm
HDBH2O	HTC from in-vessel falling debris to pool	Uniform	-	1000	2000	W/m^2-K
VFALL	Velocity of falling debris	Uniform	-	0.01	1	m/s
HDBLH	Heat transfer coefficient from debris to lower head	Uniform	-	100	1000	W/m^2-K
PORDP	Porosity of particulate debris	Normal	μ= 0.4 σ= 0.04	0.3	0.5	
Area_seal	Recirculation pump seals leak flow area	Normal	μ = 3.0E-5 σ= 3.0E-6			m^2

Once all the variables have been selected a sampling strategy needs to be employed. The sampling strategy is used to perturb the input space in relation to variable distributions. In this analysis the Monte Carlo sampling strategy has been performed setting a limit of 197 calculations.

SC1020(1), SC1020(2): Radial relocation models of molten and solid debris simulate the gravitational levelling between adjacent core rings that tends to equalize the hydrostatic head, influencing corium large scale movement. The relocation rates have times constants, which default values, 60 s for molten debris and 360 s for solid debris, was chosen as an order-of-magnitude value based on engineering judgment and recommendations of code users [56]. Because the technical base for time constants values were insufficient, boundaries of these uncertainty parameters were selected based on order of magnitude. A uniform distribution was chosen since there is no reason to believe the default is the central tendency of a distribution, with lowers and uppers bound set to encompass an order of magnitude range, 10-100s for molten debris radial relocation time constant, 100-1000s for solid debris radial relocation time constant [104].

SC1131(2): The Zircaloy breakout temperature controls retention of molten zircaloy within outer ZrO2 shell till breakout temperature, when molten Zr breaches the oxide shell and candles down the outside of the fuel rod, terminating or decreasing oxidation reaction rates in the originating core cell. The relocation of the oxidizing melt has the effect of terminating the intense local fuel heating, since the chemical heating source has relocated to a cooler region of the vessel, affecting hydrogen generation and fission products release. The lower bound is set to Zr melting temperature (2100 K), the upper bound is set to 2540 K based on qualitative consideration of the alpha-Zr(O) phase diagram and observations/analyses of the Phebus experiments[104][105]. Normal distribution suggests a most probable value of 2350 K, as used in SOARCA uncertainty analysis [104], with decreasing likelihood for values away from the most probable.

SC1132(1): After Zr melting and candling by exceeding breakout temperature, there will be UO2/ZrO2 eutectic reactions forming complex U-Zr-O mixture having lower melting temperature than either ZrO2 or UO2. This temperature affects fuel failure and molten pools generation. Temperature at which eutectic will melt, is input in MELCOR as sensitivity coefficient SC1132(1) and ZrO2/UO2 melting temperatures in MP_PRC record.

SC1141(2): Molten clad drainage rate controls maximum flow rate per unit surface width (kg/m-s) of molten pool after breakthrough of flow blockage or molten material released after clad oxide shell breakout. This is an uncertain input that influences in-vessel accident progression [104], input in MELCOR as sensitivity coefficient SC1141(2). Mean value is set as SOARCA best-practice value of 0.2 kg/m-s, determined by CORA-13 experiment [92], with uniform distribution and exploratory bounds of 0.1 kg/m-s and 2 kg/m-s, since there is no basis to inform distribution bounds [104].

HFRZZR: Candling heat transfer coefficients influence freezing of relocating molten material as zircaloy and steel, and thus tendency to form blockage. SOARCA uses default values of MELCOR 2.1, that are order-of-magnitude, due to a large degree of phenomenological uncertainty. We can try to estimate heat transfer coefficient relying on conduction analogy [103]: $h_c \approx k/dx$

Where maximum conduction length dx can be estimated as: $dx \approx \frac{\sqrt{2}p-d}{2} \approx 0.005m$

Material	K (W/m-K)	h_c (W/m^2-K)	Default h (W/m^2-K)
Zr	58.4	12000	7500
ZrO2	2.49	500	7500
UO2	3.96	800	7500

Steel	34.5	7000	2500
Steel Ox	20	4000	2500
CRP	48	10000	2500

Table 9.4-10 - Candling heat transfer coefficient estimate

Focusing on Zircaloy, a value of 12000 W/m^2-K is estimate for candling heat transfer coefficient. Based on SOARCA value of 7500 W/m^2-K and [103], a uniform distribution is used with lower bound of 7500 W/m^2-K and upper bound of 20000 W/m^2-K. It should be noted that use of a high heat transfer coefficient does not result in the freezing of a large mass with resulting complete blockage, unless sufficient heat sink is available to absorb the latent heat (i.e. clad, pellets, influenced by thermal resistance of gap).

DHYPD: Particulate Debris characteristics, like hydraulic diameter, porosity and fall velocity influences heat transfer and oxidation surface areas during in-vessel phase of accident. PD diameter may be specified separately for core and lower plenum regions, where debris arrives melted, conglomerated or finely fragmented. Once core collapse due to loss of supporting structures or due to temperatures-threshold criteria, MELCOR convert fuel rods in PD, that relocates and fills available space, limited by debris porosity. In core region seems reasonable PD size on the order of fuel pellets diameter, that is about 1cm. Smaller values are possible due to fragmentations, larger values are possible due to sintered agglomerates [106]. The distribution for PD hydraulic diameter in core region is set as uniform, with lower bound of 0.5 cm and upper bound of 2 cm.

In lower plenum region SOARCA value for hydraulic diameter is 2mm, based on FARO fragmented debris size [92], that show high percentages of melt fragmentation. Based on [107], lower plenum PD hydraulic diameter distribution is set as uniform with lower bound 2 mm, upper bound 5 mm.

VFALL: Debris is assumed to fall to the lower plenum with a user-specified velocity, VFALL, loosing heat to surrounding water. A uniform distribution is set for this input parameter, ranging from SOARCA recommended value of 0.01 m/s, to default MELCOR 2.1 users' guide value of 1 m/s [108].

PORDP: Debris porosity is defined on the PORDP. A normal distribution is used with mean at 0.4, sigma 0.04 (10% of mean value), lower bound 0.3, upper bound 0.5. Greater porosity cannot be considered structurally stable, and lesser porosity cannot reasonably achieved by random packing of solid debris particles.

HDBH2O: During debris relocation to lower plenum, a heat transfer coefficient from in-vessel falling debris to pool, HDBH2O, has to be set. This, together with falling velocity, are main parameters governing quenching of debris relocating into the lower plenum, influencing RPV thermal-hydraulic behaviour after core slumping. Review of FARO data shows that for fragmented particle sizes on the order of 5 mm, the HTC may be 1000 W/m^2-K [103]. SOARCA suggest 2000 W/m^2-K for debris size of 2 mm [56]. A uniform distribution is used with these two values as bounds.

HDBLH: The debris quenching model also affects the initial temperature response of debris in the lower plenum, and is therefore important for the subsequent calculations of RPV lower head response: once debris relocate to lower head, it increases its temperature based on debris-lower head heat transfer coefficient, input in MELCOR code as HDBLH. The default heat transfer coefficients are order-of-magnitude parameters that should be varied in sensitivity studies to determine their impact on lower head heat transfer and failure [56]. A uniform distribution is used, with bounds spanning from SOARCA recommended value of 100 W/m^2-K and default value of 1000 W/m^2-K.

A_SEAL: To better represent WW/DW pressure, recirculation pumps seals leak is assumed. Even if RCIC and HPCI operation have been set to better represent accident pressure and reactor liquid level, uncertain remains about them. A normal distribution is used with mean at 3.0E-5 m^2, sigma 3.0E-6 (10% of mean value).

9.4.7 Results of sensitivity and uncertainty analysis

Results have been statistically analysed through the RAVEN post-processor. A dynamic statistical analysis has been performed setting time as pivot parameter. To give a better visualization of uncertainty, the 0.05, 0.5 (median) and 0.95 quantiles have been selected, analysing the following figures-of-merits.

To describe the correlation between the variables, the Pearson's coefficient has been used. It is defined between -1 and 1 and measures the strength of the linear relationship between two variables. It has to be noted that all uncertain parameters selected are known to affect core degradation and subsequent consequence, so they don't influence accident progression till core degradation begins, at about 125000-160000s.

Area of recirculation pumps leak uncertainty instead, starts to affect accident progression from 22000s, when it was assumed to start.

9.4.7.1 Primary system pressure response

Shown in Figure 9.4.38 is the uncertainty range of predicted RPV pressure histories for the 197 MELCOR runs. The results of the calculated data coupled with the related uncertainty band envelope mostly of the TEPCO plant data available related to the rector pressure vessel pressure.

Area of recirculation pumps seal leak has main influence on RPV pressure behaviour: Figure 9.4.39 shown that Pearson coefficient is mostly negative in range of interest, that is from leak start to ADS actuation, meaning that an increase in leak area will cause a decrease in RPV pressure, as expected.

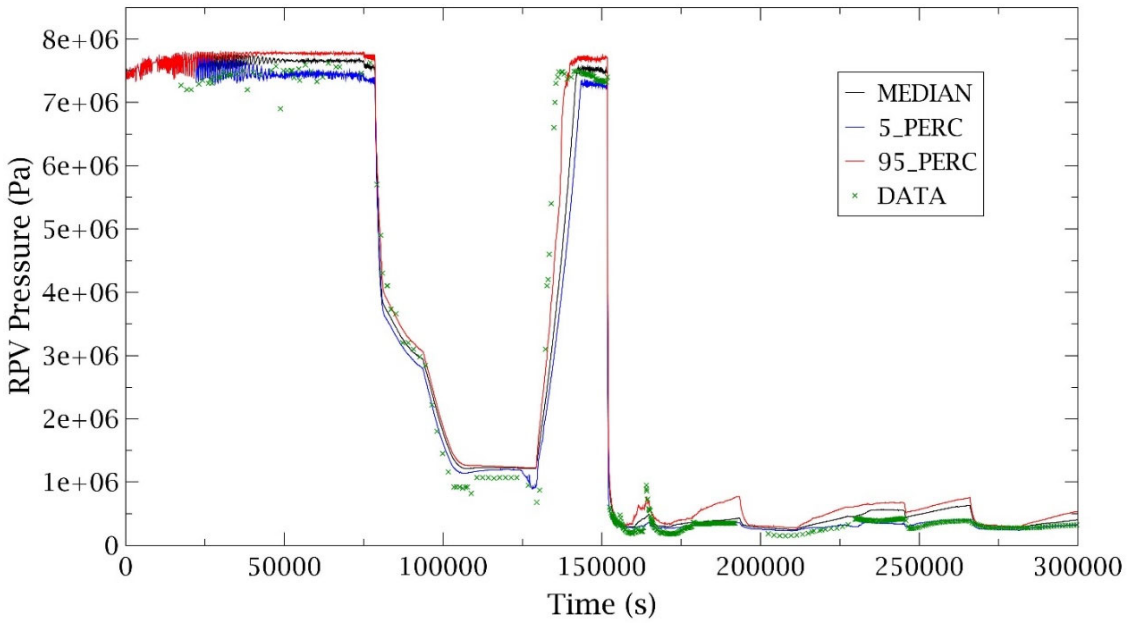

Figure 9.4.38 – RPV Pressure – Uncertainty analysis

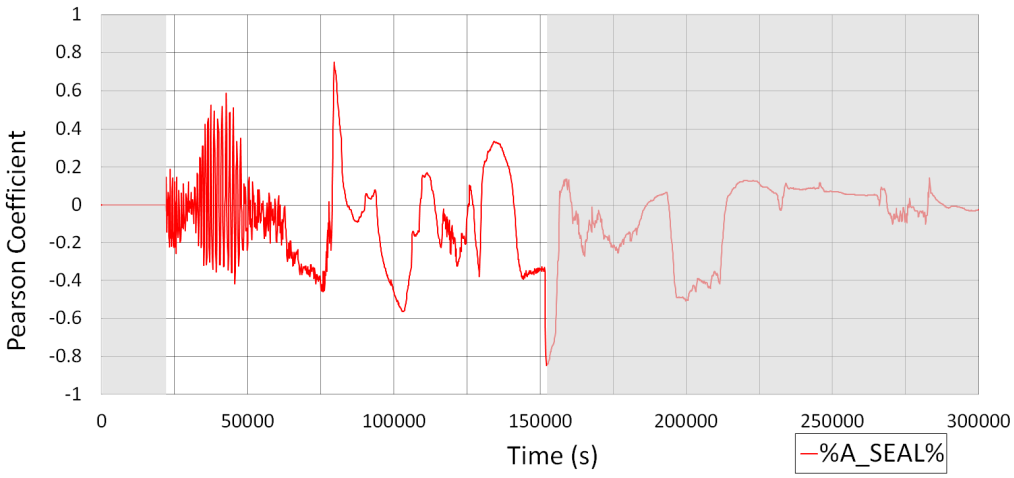

Figure 9.4.39 – RPV Pressure: A_SEAL Pearson coefficient

9.4.7.2 Core water level

The predicted reactor vessel water level is shown in Figure 9.4.40. From this figure we can see that median of MELCOR runs follow TEPCO data, with 95% and 5% quantiles band contain most of them, apart from later accident phase, where measurements of water level and alternative water injection by fire engine flow rate that reached core are uncertain.

Predicted core uncovery times fall in band between 130300-152300s with median of 151800s, with area of pumps leak that has strong influence on this phase: associated Pearson coefficient is strongly negative, as expected (Figure 9.4.41). For calculation comprised between median and 95%, water level drops under BAF at these time because of ADS actuation at 151750s, causing large pressure drop in RPV and subsequent flashing of water in the RPV, that cause in turn sudden sharp decrease in water level.

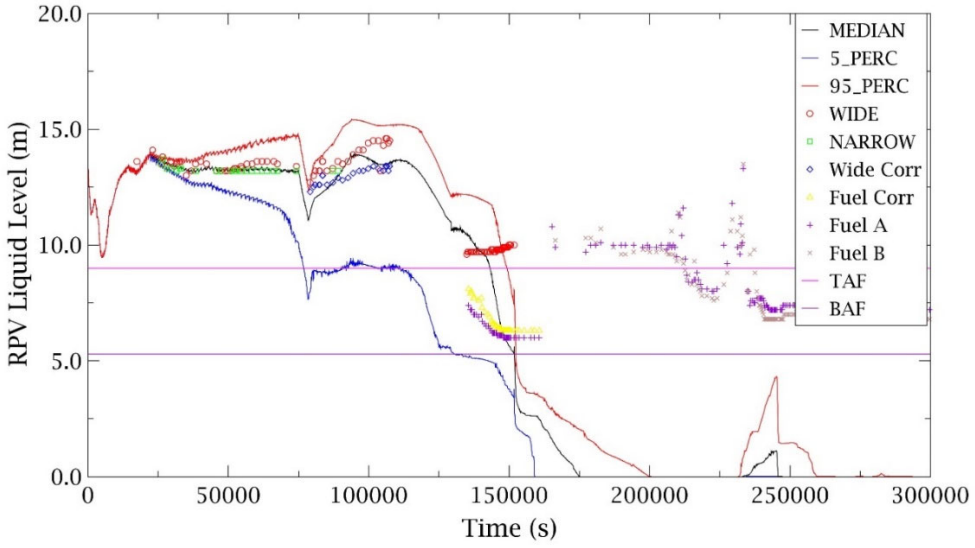

Figure 9.4.40 - RPV liquid level - Uncertainty analysis

Meantime as water level reaches the bottom of the core, a greater fraction of decay heat is retained in the fuel rods, causing heatup, onset of clad oxidation and hydrogen generation, with temperature that gradually exceed control blades and fuel rods collapse temperature. As results, core starts to fail and relocate, as discussed later. At core plate fail due to thermo-mechanical stresses, predicted between 145000s and 159000s, corium slumps in lower plenum region, producing high grade of vaporization,

with pressure spike in DW/WW/RPV and large water level drop, till lower plenum dryout predicted to falls in a band between 159000 s and 200000 s, with a median value of 175000s.

VFALL Pearson coefficients is positive during corium slumping. Higher velocity of falling debris, lesser time to exchange heat power from falling debris (that has greater total exchange surface respects to settled one) to lower plenum water, lesser vaporization relative to this aspect and higher water level.

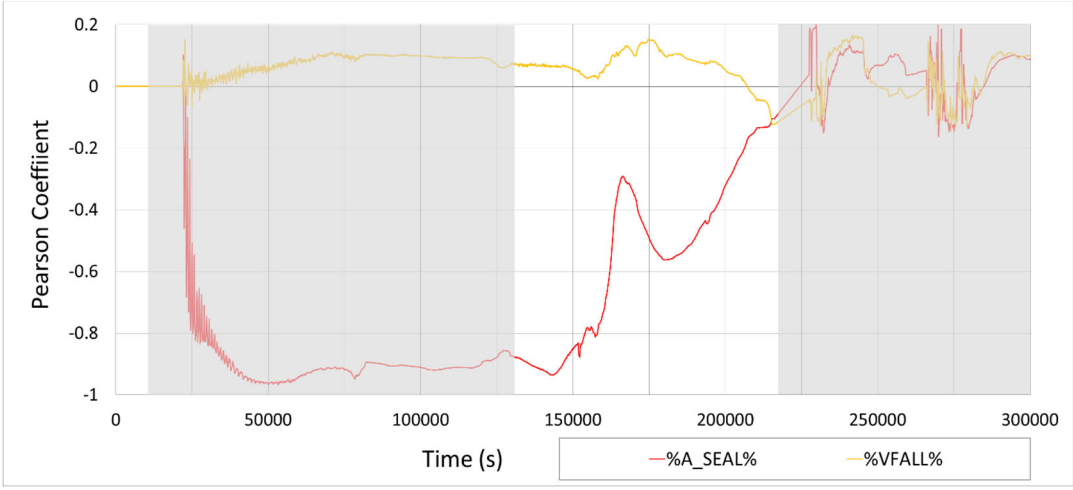

Figure 9.4.41 - RPV liquid level: A_SEAL, VFALL Pearson coefficients

9.4.7.3 Core degradation and ejection

The predicted fuel rods intact fraction is shown in

Figure 9.4.42 for median, 5% and 95% quantiles. Median of realizations suggests that some fuel assemblies remain intact, located on the outer ring of the core, where radial power factor are lowest. This is 26% of total mass, that is fuel mass located in ring 4 of MELCOR model.

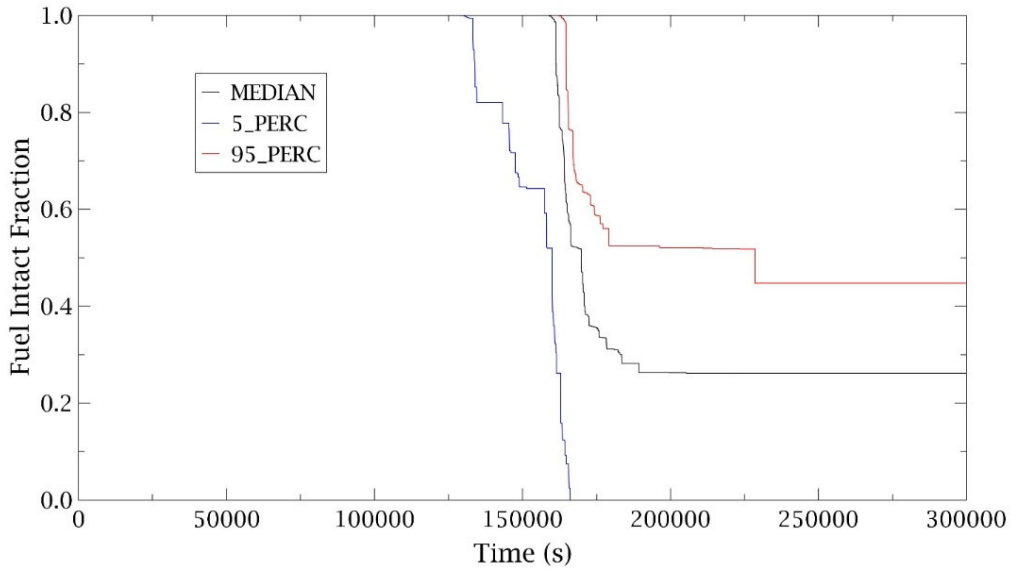

Figure 9.4.42 - Fuel Intact Fraction - Uncertainty analysis

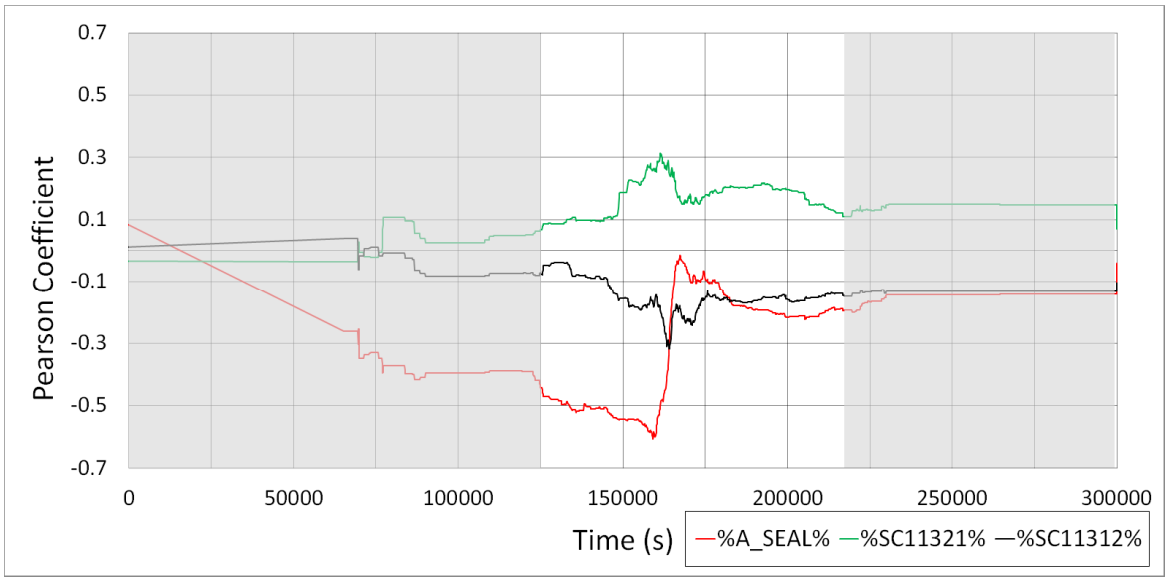

Figure 9.4.43 - Fuel Intact Fraction: A_SEAL, VFALL Pearson coefficients

Uncertain parameters that affects core degradation are: A_SEAL (area of pumps leakage), SC1132(1) (Effective temperature at which the eutectic formed from UO2 and ZrO2 melts) and SC1131(2) (break-through temperature):

- A_SEAL Pearson coefficient is strongly negative. Higher pumps leakage leads to faster core uncovery with faster onset of oxidation that in turn increases rate of fuel rods temperature raise, causing them fails once reaching MELCOR thresholds core degradation temperature, as expected. So, if A_SEAL rises, fuel intact fraction decreases over time faster, starting from 129000 s to 162000 s, with a median of 128940 s.
- SC1132(1) Pearson coefficient is positive. This sensitive coefficient of eutectic Zr-U-O melting temperature drives fuel rods fails. If this threshold temperature increases means that fuel rods can stands at higher temperature without fail, so fuel intact fraction increase at its increasing, as expected.
- SC1131(2) Pearson coefficient is negative. As described earlier, once molten Zr breaches oxide shell and candles down, oxidation reaction rate in that core cell decreases, lowering rate of increase of temperature, thus extending lifetime of that core zone. At higher breakout temperature corresponds higher fraction of oxidation degradation of local core zone, increasing rate of fuel rods failure, thus lowering fuel intact fraction.

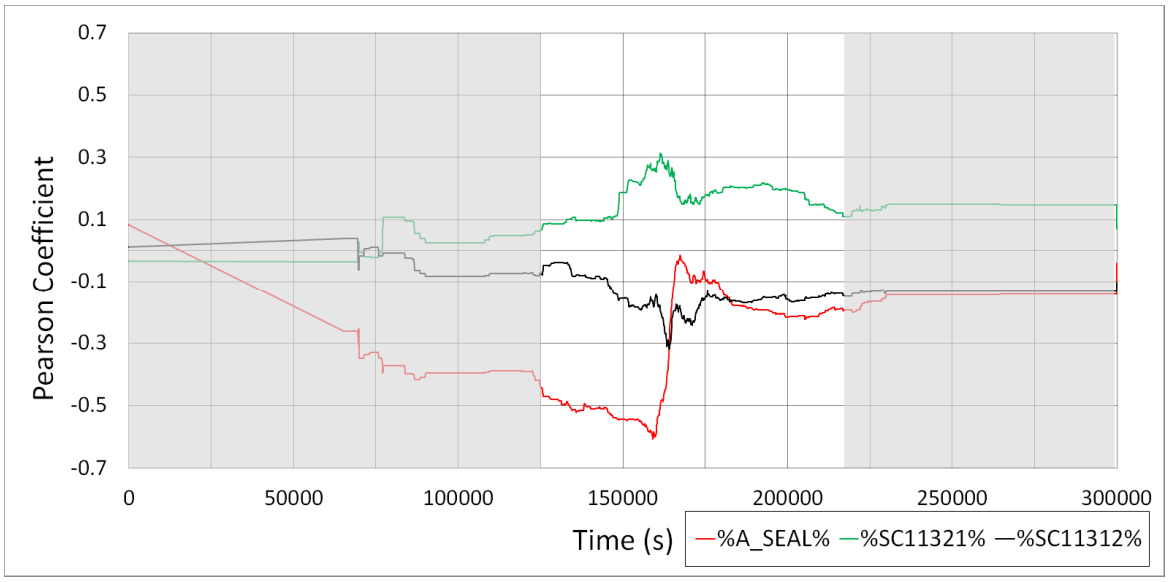

Figure 9.4.43 - Fuel Intact Fraction: A_SEAL, SC1132(1), SC1131(2) Pearson coefficients

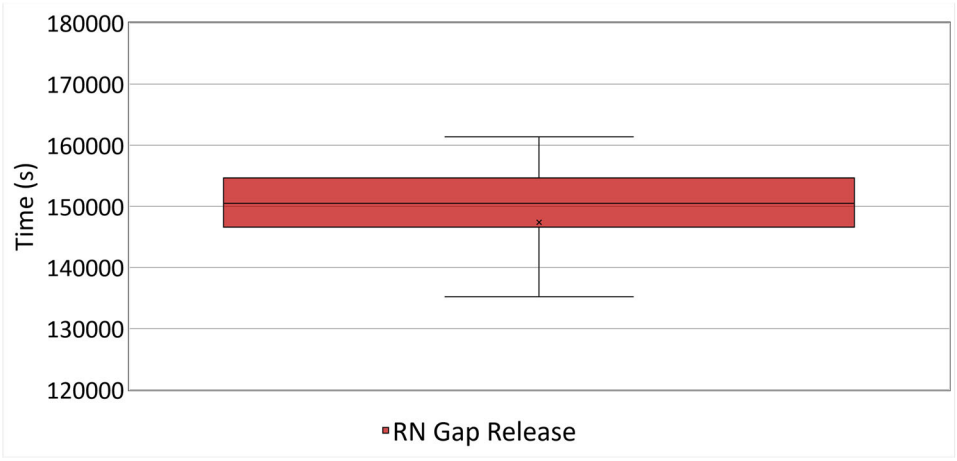

Figure 9.4.44 - Radionuclides gap release time - Uncertainty analysis

Figure 9.4.44 shows time of radionuclide gap release, happens at MELCOR default temperature threshold of 1173K. 150500s is mean of realizations, with time spans from 129300s of 5% quantile to 155000s of 95% quantile.

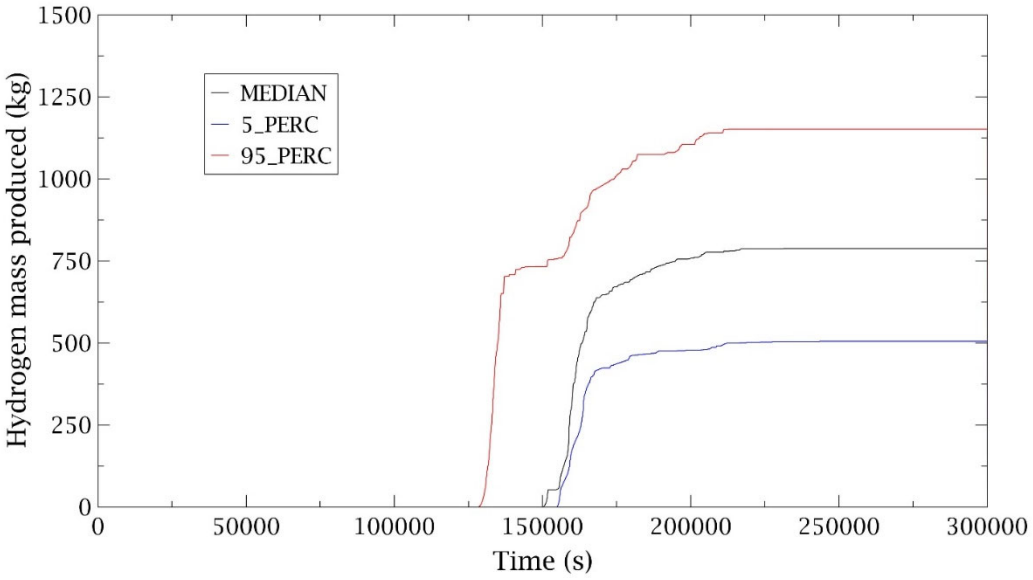

Figure 9.4.45 - Hydrogen mass produced - Uncertainty analysis

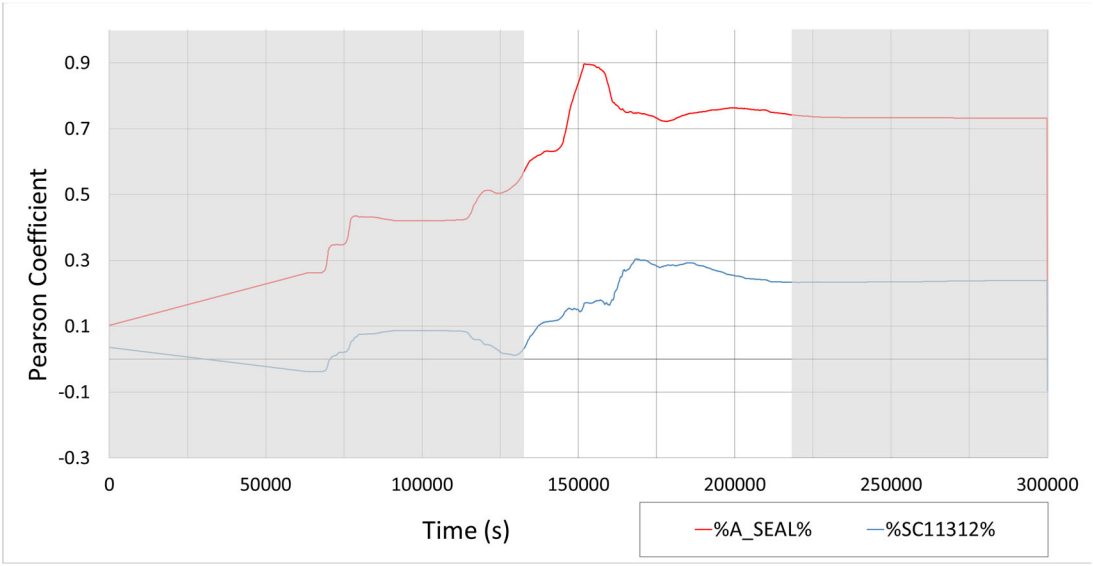

Figure 9.4.46 - H2 mass produced - A_SEAL, SC1131(2) Pearson coefficients

Figure 9.4.46 shows hydrogen mass generated. At the end of calculations, a median value of 788kg was produced, with a mass span from 505kg and 1152kg of quantiles. Main uncertain parameters that affects hydrogen generation are:

- A_SEAL: as expected, higher pumps leakage corresponds higher hydrogen mass, because of faster core uncover and clad temperature rise up, that causes faster onset of oxidation. Pearson coefficient is strongly positive.
- SC1131(2): in time range of interest, Zr breakout temperature Pearson coefficient is positive. As said, higher Zr breakout temperature means higher degree of local oxidation for more time. Furthermore, oxidation is an exponential function of temperature, so if oxidation can persist at higher temperature, more and more hydrogen is produced.

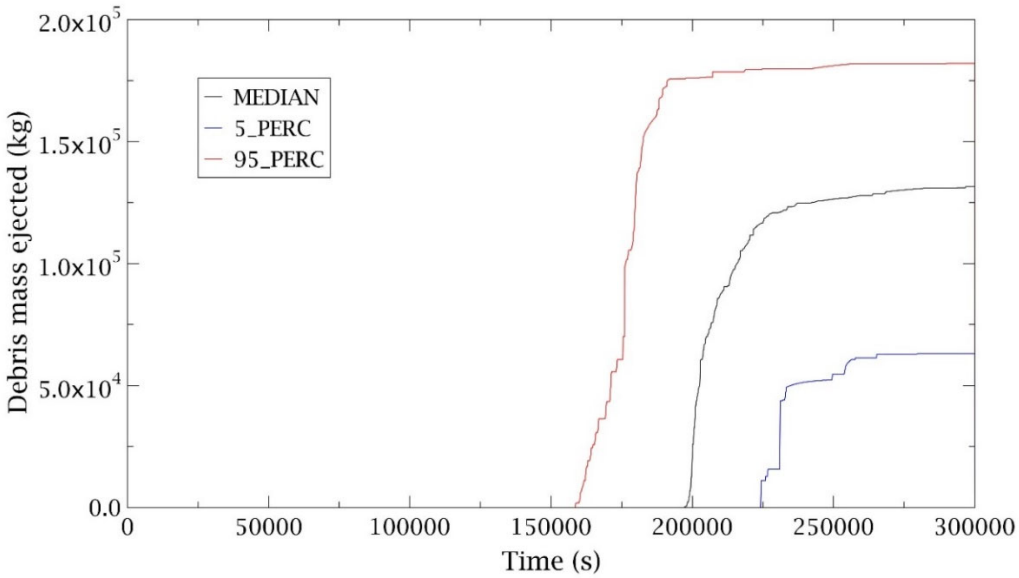

Figure 9.4.47 - Debris mass ejected - Uncertainty analysis

Total debris mass ejected at lower head fails (Figure 9.4.47) spans from 63000 kg to 182000 kg, with median value of 131500 kg. Median of time of failure (Figure 9.4.48) is 197000s, with a 5% quantile of 224000s and 95% of 158500s.

Lower head fails in all MELCOR runs.

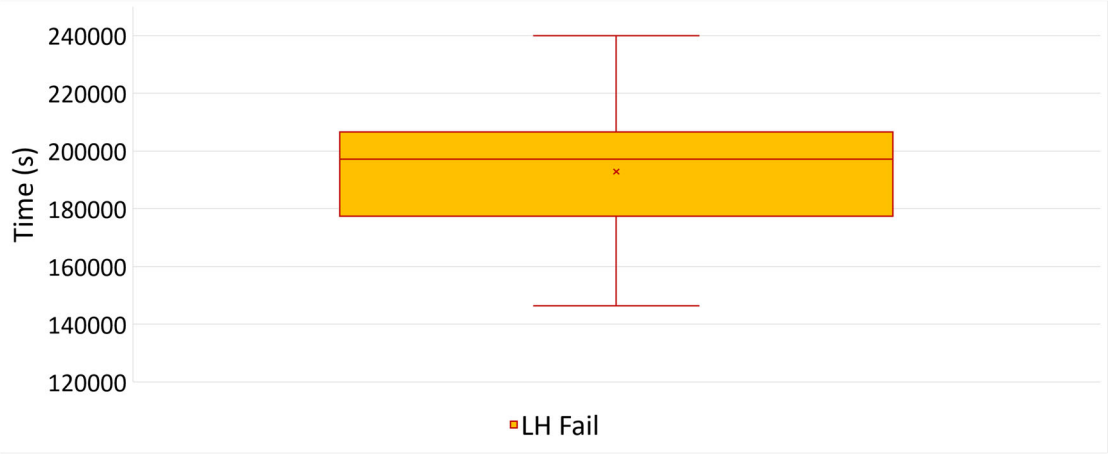

Figure 9.4.48 - Lower Head fail time - Uncertainty analysis

9.4.7.4 DryWell Pressure

Shown in Figure 9.4.49 is the spectrum of predicted DW pressure histories for the 197 MELCOR runs. The results of the calculated data coupled with the related uncertainty band envelope mostly of the TEPCO plant data available related to the drywell pressure.

Drywell and wetwell pressures response, follow same behavior after break of vacuum breaker, that is about at 23 mins. This pressure is important relative to environment source term, that is influenced by SRVs, pumps leakage, WW/DW sprays and RPV pressure after ADS actuation, thus also responsive to core degradation, water level, freshwater and seawater injection: it gives an almost complete view of the

accident progression. Like most of others main accident progression figure-of-merits, area of pumps leak influences DW pressure behavior (Figure 9.4.50).

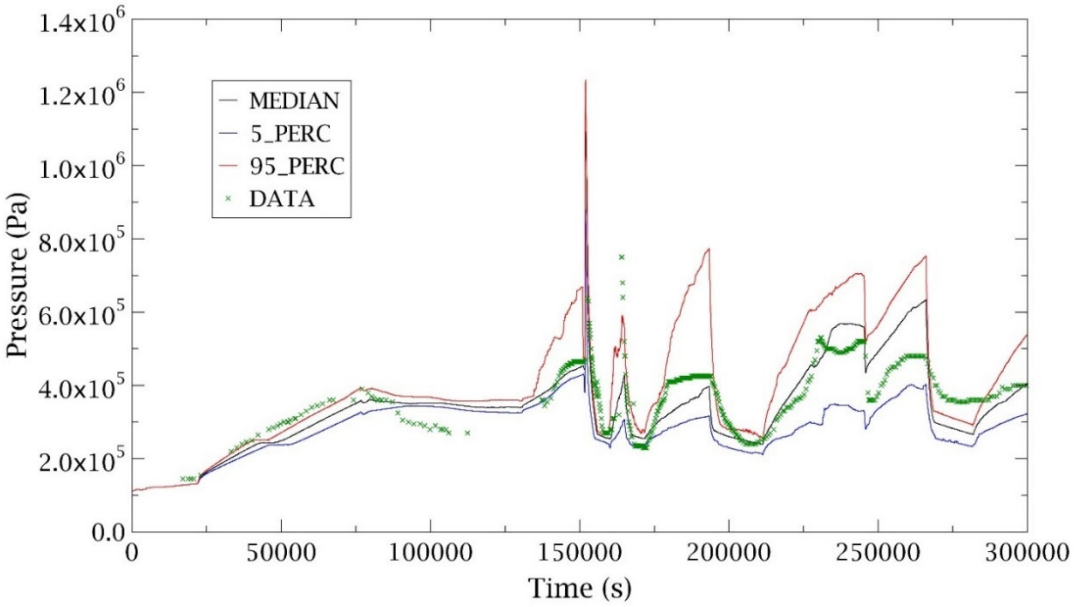

Figure 9.4.49 - DW pressure - Uncertainty analysis

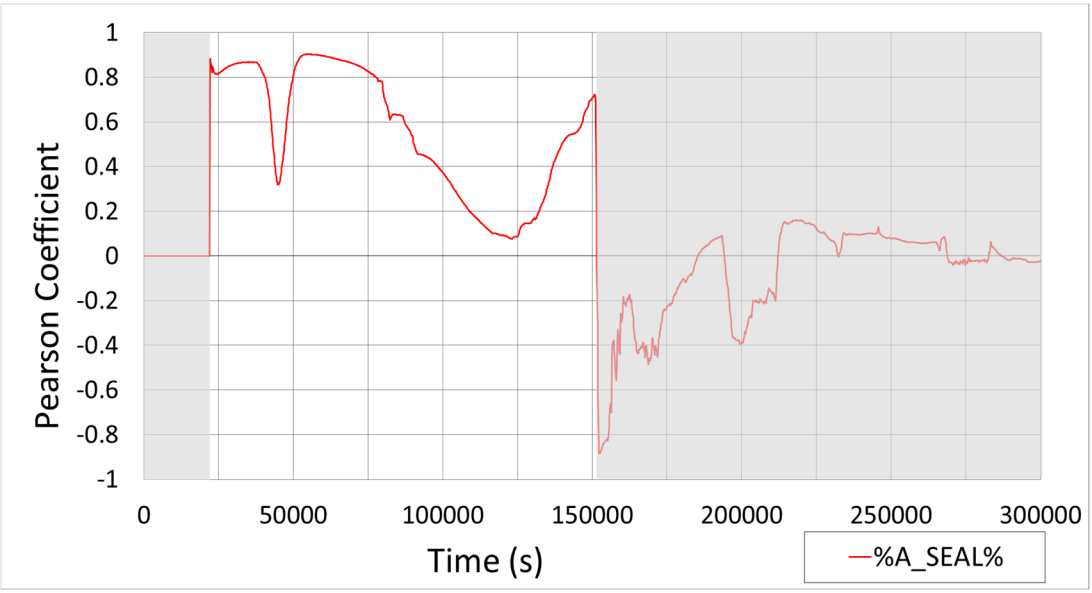

Figure 9.4.50 - DW Pressure: A_SEAL Pearson coefficient

Pumps seal leak to Pedestal, that is in communication with DW volume. So, more the leak, more the pressure increasing in DW, like Pearson coefficient describe with strong positive coefficient as expected.

At reactor depressurization, area of pumps leak uncertainty doesn't affect DW pressure directly, due to SRV kept open, but it's important regard past reactor accident behavior depending on them because it has affected core degradation, core water inventory etc.

For example, at core slumping, pressure peak is greater when leak area was been small, because of higher core water level that means more steam production and more hydrogen production. In fact, Pearson coefficient is negative.

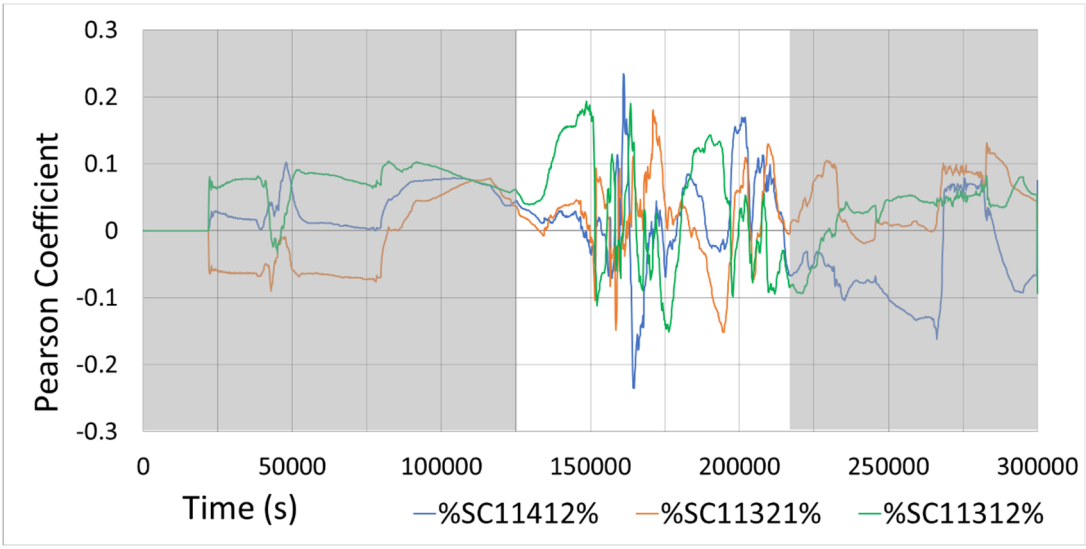

Figure 9.4.51 - DW Pressure: SC1141(2), SC1132(1), SC1131(2) Pearson coefficients

Focusing on core degradation time, that is from 129000 s, main uncertainty parameters that affects DW pressure behaviour are (Figure 9.4.51):

- Zircaloy breakout temperature (SC1131(2)) Pearson coefficient is positive during first phases of core degradation, till ADS activation. This is because influences hydrogen generation, thus reactor pressure, thus SRVs flow, thus WW pressure, thus DW pressure. As said before, higher Zr breakout temperature, means higher local core degradation and hydrogen generation, thus higher DW pressure.

- Maximum flow rate per unit surface width (kg/m-s) of molten Zr or molten pool (SC1141(2)) has a peak of its Pearson coefficient during second DW pressure peak, related to core plate fail and core slumping. Influencing falling molten pool behavior, has effects on heat transfer, steam production and so pressures.

- Temperature of eutectic Zr-U-O formation (SC1132(1)) influences most DW pressure after slumping. At this stage, corium settles in lower plenum and on its geometrical, physical and chemical characteristics depends later accident phases. If eutectic melt temperature is low, it's likely that molten pool will form, that is difficult to water cool. So, less heat power is transferred to water from molten corium that mean less steam produced and lower pressure. On contrary, at higher eutectic temperature formation, it's likely that corium exists as particulate debris, that is more effectively coolable by water, with consequences on DW pressure.

10 Conclusions and perspective

The work reported in this Ph.D. thesis has been performed during the period 20016-20019 within the nuclear engineering group of Sapienza University of Rome, mainly in the framework of the EUROfusion safety and environment work package activities.

The aim of this work was to investigate the safety and environmental performance of the EU DEMO WCLL concept design, studying the reactor response to some of the most severe possible accidents. The progression of the accident has been modeled following a conservative approach taking into consideration the passive and active accident mitigation capabilities of the plant.

The MELCOR code was used to assess the parameters (break flow rate, pressure and temperature in heat transfer loops, in the VV and in the pressure-suppression system, environmental releases of radioactive materials) associated with design basis accident and beyond design basis accidents.

A wide spectrum of design basis accidents, mainly LOCA, have been simulated to support the development of the safety-oriented design approach chosen for EU DEMO main components. Analyses of events "beyond the design basis", which are extremely unlikely to occur, was also performed to show the robustness of the design and to demonstrate an ultimate safety margin. A short summary of the main outcomes of the accident analysis is reported.

- A "double" in-vessel LOCA event characterized by the simultaneous failure of a BZ-PHTS feeding pipe and 262 FW channels, has been identified as a "worst case" scenario for the estimation of the needed flow area of VVPSS suppression pipework to limit the VV pressure below the limit imposed by safety. The results indicated that a total discharge area of 8.6 m^2 is required. Moreover, because limiters could be foreseen in a near future design of the EU DEMO reactor to prevent the plasma to touch the breeding blankets PFC, the same parametric study has been performed considering the single failure of a BZ-PHTS feeding pipe. In this case, the required discharge flow area is reduced to 7.1 m^2.

- Relatively to a simple in-vessel event involving the rupture of 10 first wall cooling pipes, two different simulation have been performed to evaluate downstream isolation valves effects in terms of radioactive releases and thermal hydraulic behavior of main DEMO components. In fact, the large number of downstream valves (isolation and SRVs) to be installed, will give rise to safety and reliability constraints. For such a reason it is important to properly evaluate if they are indeed necessary from a safety perspective. The results indicate the pressure increase in VV is very fast and the maximum pressure peak is 150 kPa. However, in both cases the intervention of VVPSS is enough to mitigate the transient and to keep the pressure well below the limit for the VV of 0.2 MPa. The pressure in VVPSS tanks remains below the containment pressure of 98.0 kPa ensuring very small off-site releases of radioactive materials. In fact, source term mobilization analysis demonstrated that large part of dust, ACP and HTO is entrained in the steam and is rapidly discharged from the VV to the VVPSS tanks. The closure of downstream isolation valves reduces the total amount of ACP entering the VV of about 30%, however because of the lower steam flow rate toward the VVPSS, the mobilization toward the suppression tanks is slower. In both the performed simulations about 620 g of hydrogen are produced, however the large amount of tungsten dust mobilized inside the VV-STs, for which the chemical reactivity has not been included in this study, could constitutes an additional source of hydrogen.

- Ex-vessel LOCA scenarios arising from failures in PHTS distributor rings demonstrated that some further efforts are still needed in the design of a suitable TCR for the EU DEMO WCLL concept.

Connections between different tokamak compartments should be foreseen to avoid pressure peaks over 5 bar and 10 bar in case of LOCA from FW-PHTS and BZ-PHTS, respectively. Moreover, if the connection between different TCR compartments will not be possible, overpressure mitigation systems (e.i. containment spray system, ice condenser etc.) shall be foreseen in the containment to avoid long term releases of tritiated water and activated products toward the environment.

- Despite the limitations imposed by safety codes a preliminary safety analyses of an in-box LOCA has been performed by means of a custom-developed Python script. Two separate models of water side and LiPb side have been developed and coupled through an external interface. Simulations for several chemical reaction rates demonstrated that both pressure peak and final pressure in the BZ remain below the design limits stated by design. However, large amounts of hydrogen could be produced during the accident sequence.

Concerning the BDBA, two different accident scenarios have been investigated to show the robustness of the defense in depth approach and demonstrating that no cliff edge effects occur in the safety analysis. The selected cases were an ex-vessel LOCA and a Loss of Flow Accident (LOFA) assuming in both the simulations the failure of active plasma shutdown system as aggravating event. Results demonstrated that for the LOVA, the main concern is the high pressure reachedf in-vessel components, which is strictly related to the number of failed FW channels and by the relief pressure set-point of SRVs. Instead, the ex-vessel LOCA simulation, demonstrated that some kilograms of tritiated water could be released toward the external environment.

In-box LOCAs, as well as other accidents involving a chemical reaction between hot steam and lead lithium, could led to the production of large amounts of hydrogen inside the tokamak vacuum chamber. In order to avoid that flammable concentrations could be achieved, the production of hydrogen must be limited and properly monitored. A preliminary concept of hydrogen mitigation system has been proposed with the aim to prevent that hydrogen concentration increases to levels that could produce large scale hydrogen deflagration or even detonations. The mitigation system consists of PARs installed in each tank of the VVPSS. Two different accident sequences have been performed to support this proposal. The first was an in-VV LOCA with steam suppression in tank A. In this case the HMS was able to remove about the 84.4% of the mass hydrogen inside the reactor. The second accident sequence was a LOFA without suppression of steam in tank A. At the end of the accident sequence the HMS was able to remove about the 60% of the mass hydrogen inside the reactor.

Sensitivity and uncertainty analyses performed for the EU DEMO reactor highlighted the temperature at which FW fails affects not only the mass of hydrogen produced, but also the overall VVPSS response. This study showed that if for FW melt temperature is higher than 1450 K the RDs are not triggered and the VVPSS function to retain the radioactive inventory is lost. Focusing the attention on hydrogen production, it is to underline that its uncertainty is mainly related to the temperature behavior of the FW, while the partial pressure of steam inside the VV has a low ranked influence for this accident scenario.

The safety analyses described in this work was carried out by following a deterministic approach, so conservative assumptions was employed to perform safety studies and worst enveloping scenarios was studied for each initiating event. These analyses will continue in the framework of the EUROfusion activities during the forthcoming years and will be funded by an EUROfusion Engineering Grant (Position ref. EEG-2019/08 DEMO Nuclear Safety Analyses). However, safety studies commonly aim also at obtaining an optimal nuclear power plant design and reactor operation, for this reason excess of conservatism sometimes should be avoided from the safety analyses. To obtain an in-depth safety assessment of the EU DEMO reactor, in the future, the deterministic analyses will be combined with

analyses implemented through a probabilistic approach. Moreover, probabilistic analysis might provide a useful tool to identify unforeseen vulnerabilities of the plant, unresolved issues and design needs.

11 Bibliography

[1] M. Ariola, A. Pironti, "*Magnetic Control of Tokamak Plasmas"*, Springer International, (10.1007/978-3-319-29890-0)

[2] Y. Song, W. Wu, S. Du et al., "*Tokamak Engineering Mechanics"*, Springer International, (10.1007/978-3-642-39575-8)

[3] F. Romanelli, et al., "*Fusion Electricity – A Roadmap to the Realization of Fusion Energy",* EFDA Report, ISBN 978-3-00-040720-8T, 2012

[4] Donné A. J. H., "*The European roadmap towards fusion electricity",* 377 Philosophical Transactions of the Royal Society A: Mathematical, Physical and Engineering Sciences http://doi.org/10.1098/rsta.2017.0432

[5] G. Federici, et al., *"Overview of the design approach and prioritization of R&D activities towards an EU DEMO"*, Fusion Eng. Des. 109–111 (2016) 1464–1474

[6] Stacey, W. M., "*Fusion plasma Physics*", 2005

[7] Stacey, W. M., "*An Introduction to the Physics and Technology of Magnetic Confinement Fusion"*, 1984

[8] IRSN Report 2017/199, "*Nuclear fusion Reactors: Safety and radiation protection considerations for demonstration reactors that follow the ITER facility"*, 2017

[9] Leslie C. Woods*, "Theory of Tokamak Transport: New Aspects for Nuclear Fusion Reactor Design",* WILEY-VCH

[10] J. Wesson, *"The Science of JET"*, (euro-fusionscipub.org/archives/jet-archive)

[11] J. Wesson, B.Balet, "*Abrupt Changes in Confinement in the JET Tokamak"*, (euro-fusionscipub.org/archives/jet-archive)

[12] I. Cook, G. Marbach, L. Di Pace, C. Girard, P. Rocco, N.P. Taylor, *"Results conclusions and implications of the SEAFP-programme"*, Fusion Engineering and Design 51-52 (2000) 409/417

[13] G. Caruso, *"Main components and issues of Tokamaks"*, Fusion Reactor technology, 2014

[14] G. Federici et al.,, "*European DEMO design strategy and consequences for materials",* Nucl. Fusion 57, 092002, 2017

[15] N.P. Taylor, "*Key issues for the safety and licensing of fusion",* Fusion Science and Technology, 47, 959, 2005

[16] N. Taylor, P. Cortes, *"Lessons learnt from ITER safety & licensing for DEMO and future nuclear fusion facilities", F*usion Engineering and Design 89, 1995-2000, 2014

[17] International Nuclear Safety Advisory Group, "*Basic Safety Principles for Nuclear Power Plants 75-INSAG-3*", Rev.1 (INSAG-12), IAEA Vienna, 1999

[18] International Nuclear Safety Advisory Group, "*Defence in Depth in Nuclear Safety"*, INSAG-10, International Atomic Energy Agency, Vienna 1996

[19] J. Johnston, *"Plant Safety Requirements Document"*, EUROfusion report EFDA_D_2MKFDY, V4.4, April 2019

[20] Porfiri M.T., Mazzini G.: *"DEMO BB Safety Data List (SDL)",* EUROfusion EFDA_D_2MF8KU, September 2018

[21] A. Del Nevo et al., *"Recent progress in developing a feasible and integrated conceptual design of the WCLL BB in EUROfusion project",* Fusion Eng. Des. 146 (2019), 1805-1809

[22] https://www.eurofusion.org/fileadmin/user_upload/Archive/wpcontent/uploads/2012/01/PPCS_overall_report_final.pdf

[23] L. Boisset, *"Note Technique: Chemical Reactions Inside the Torus Conclusions on Modelling."*, CEA, 1995

[24] G. R. Smolik, B. J. Merrill, and R. S. Wallace, *"Reaction of Porous Beryllium in Steam"*, EGG-FSP-10346, Idaho Natl. Eng. Lab., no. July, 1992

[25] DEMO, *"Generic Site Safety Report, Vol. III, Radiological and Energy Source Terms"* 2019

[26] A. Malizia, L. A. Poggi, J. F. Ciparisse, R. Rossi, C. Bellecci, and P. Gaudio, *"A review of dangerous dust in fusion reactors: From its creation to its resuspension in case of LOCA and LOVA Energies",* vol. 9, no. 8, 2016

[27] R. A. Pitts et al., *"Material erosion and migration in tokamaks",* Plasma Phys. Control. Fusion, vol. 47, no. 12 B, 2005

[28] G. Caruso, M. Nobili, L. Ferroni, *"Modelling of dust resuspension in Tokamak devices during an air inflow event"*, Journal of Fusion Energy, doi: 10.1007/s10894-015-9921-8

[29] L. Di Pace, L. Quintieri, *"Assessment of activated corrosion products for the DEMO WCLL",* Fusion Eng. Des. 136 (2018), 1168-1172

[30] Euratom-UKAEA Fusion Association, *"DEMO and the Route to Fusion Power"*, September 2009

[31] C. Gliss, *"DEMO Reference Configuration model",* IDM Ref. EFDA_D_2MUNPL, July 2017

[32] E Martelli et al, *"WCLL Design Report 2017",* EFDA_D_2MYHNE_v_1.1, July 2018

[33] C. Bachmann, *"Plant Description Document",* EFDA_D_2KVWQZ_v1_5, March 2019

[34] C. Bachmann, *"Load Specification for the DEMO Vacuum Vessel",* EFDA_D_2MBPN6_v1_6, August 2017

[35] C. Bachmann, *"Bioshield roof and cryostat top lid",* DCR-021, EFDA_D_2MRE2T_v1_1, 2017

[36] P. Marek, *"Design Description Document - Cryostat",* EFDA_2MWVNZ_v1_0, Dec. 2018

[37] L. Ciupinski*, "Structural analysis report of cryostat",* EFDA_D_2JPP5D_v1_1, March 2016

[38] B. Končar, M. Draksler, *"Initial Definition of DEMO Thermal shields concept"*, EFDA_D_2LFRFU_v1_1, February 2017

[39] B. Končar, O. C. Garrido, *"Development of DEMO Thermal shields concept and Analysis of Alternatives",* EFDA_D_2MD9WW_v1_0, March 2018

[40] G. Mazzone, V. Imbriani, U. Bonavolontà, D. Marzullo, *"DIV-1.1.1-T004-D001 AWP2017: Divertor cassette Design Description Document 2017",* EFDA_D_2MTEVX, July 2018

[41] J.H. You, G. Mazzone, E. Visca et al., *"Conceptual design studies for the European DEMO divertor: Rationale and first results",* Fus. Eng. Des. 109- 111 (2016) 1598-1603

[42] G. Mazzone, *"Divertor cassette Design Description Document 2018"*, EFDA_D_2NN3CP, June *2019*

[43] P A di Maio, et al., *"DEMO Divertor Thermo-hydraulic assessment report 2015",* EFDA_D_2MY45W_v1.0, February 2016

[44] G. Casini, *"A water cooled, lithium lead breeding blanket for a DEMO fusion reactor"*, 1991.

[45] Mohammad Mahdavi, Elham Asadi, *"Estimates of tritium Produced Ratio in the Blanket of Fusion Reactors",* December 2012

[46] Mater N., These K., Adiaharic K*., "Lthium-Lead Eutectic as breeding material in fusion reactors"*, 1985

[47] A. Del Nevo et al., *"Design Description Document 2015 for WCLL (update of DDD 2014)"*, EFDA_D_2MU9XC v1.1, June 2016

[48] P. Arena, et al., *"DDD for the consolidated design of WCLL – 2018"*, EFDA_D_2N6PT9 July 2019

[49] A. Del Nevo, *"DEMO BoP – WCLL BB PHTS and PCS preliminary design",* IDM Ref. EFDA_D_2MH7KC v1.2, May 2017

[50] A. Nevo, E. Martelli, F. Giannetti, *"WCLL BB DEMO Configuration with IHTS+ESS – BB/DIV/VV PHTS, IHTS, ESS and PCS Preliminary Design (DDD)",* EUROfusion deliverable WPBoP-2.2-T006-D001, IDM Ref. EFDA_D_2MV6DV v1.0, 2017

[51] C. Gliss et al., *"Integration of DEMO hazard piping into the tokamak building",* in proceeding of 14th International Symposium on Fusion Technology (ISFNT14), 2019

[52] S. Ciattaglia et al., *"EU DEMO Plant and Building Layout Criteria",* in proceeding of 14th International Symposium on Fusion Technology (ISFNT14), 2019

[53] S. Ciattaglia, *"DEMO Tokamak Building preliminary layout definition",* EFDA_D_2MQLTN, March 2016

[54] J. Johnston, *"Preliminary Assessment of Environmental Release Inventories for DEMO"*, EFDA_D_2MAT8C, 2018

[55] G. Caruso, F. Giannetti, *"Sizing of the Vacuum Vessel Pressure Suppression System of a Fusion Reactor Based on a Water-Cooled Blanket",* for the Purpose of the Preconceptual Design, Sci. Technol. Nucl. Install., Article No. 8719695. DOI:10.1155/2016/8719695

[56] Gauntt R O, *"MELCOR Computer Code Manuals, Vol. 1: Primer and Users Guide",* Sandia National Laboratories Albuquerque, NM 87185-0739, NUREG/CR-6119, 2005

[57] Gauntt R O, *"MELCOR Computer Code Manuals, Vol. 2: Reference Manual, Version 2.1.6840",* SAND 2015-6692 R, Sandia National Laboratories, August 2015

[58] B.J. Merrill, *"A recent version of MELCOR for fusion safety applications",* Fusion Eng. Des. 85 (2010) 1479-1483

[59] Merrill B. J., *"Recent development and application of a new safety analysis code for fusion reactors",* Fusion Engineering and Design 109-111 (2016) 970-974.

[60] T. Eade et al., *"Activation and decay heat analysis of the European DEMO blanket concepts",* Fusion Eng. Des. 124 (2017), 1241–1245

[61] C. Gliss, *"DEMO tokamak building 16 sectors configuration",* 2MYCRN, Apr. 2018

[62] DEMO*, "Generic Site Safety Report, Vol. VII, Analysis of accident scenarios within design basis and design extension conditions",* 2019

[63] T. Pinna et al., *"Identification of accident sequences for the DEMO plant",* Fusion Eng. Des. 124 (2017) 1277–1280

[64] Z Vizvary et al., *"European DEMO first wall shaping and limiters design and analysis status*", in proceeding of 14th International Symposium on Fusion Technology (ISFNT14), 2019

[65] G. R. Smolik, K. A. McCarthy, D. A. Petti, K. Coates, *"Hydrogen generation from steam reaction with tungsten",* J. Nucl. Mater., vol. 258–263, no. PART 2 B, pp. 1979–1984, 1998

[66] A. Del Nevo, et al., *"WCLL breeding blanket design and integration for DEMO 2015: status and perspectives",* Fusion Engineering and Design 124 (2017) 682-686.

[67] Ciampichetti, I. Ricapito, A. Aiello, G. Benamati: *"Water large leaks into liquid Pb-17Li: first experimental results on LIFUS 5 facility",* Fusion Engineering and Design 69 (2003) 563-567

[68] DEMO, *"Generic Site Safety Report, Vol. VIII, Analysis of beyond design basis events"*, 2019

[69] G. Caruso, *"Esercitazioni di impianti nucleari",* Aracne Ed., 2003

[70] M.T. Porfiri, *"Solutions to minimize in-vessel hydrogen and hydrogen/dust explosions: proposal and study"*, EFDA_D_2N458T, May 2018

[71] Jeongtae Cho, Gyunyoung Heo, Young-seok Lee, Hyuck Jong Kim, *"The Safety Implication of Hydrogen Production and Explosion for KFDP",* Transactions of the Korean Nuclear Society Spring Meeting Taebaek, Korea, May 26-27, 2011

[72] Kathryn Mccarthy, Boris Kolbasov, David Petti, Vladimir P. Shestakov, *"Beryllium interaction with steam or air in iter under accident conditions",* IAEA CN 69

[73] G.R. Smolik, K.A. McCarthy, D.A. Petti, K. Coates, *"Hydrogen generation from steam reaction with tungsten",* Journal of Nuclear Materials, Volumes 258–263, Part 2, October 1998, Pages 1979-1984

[74] S.J. Piet, A.Costley, G. Federici, F. Heckendorn, R. Littleb, *"ITER Tokamak Dust – Limits, Production, Removal, Surveying",* Fusion Engineering, 1997

[75] G. Caruso, F. Giannetti, M. D'Onorio, M. Frullini, *"Interim report on accident analyses: WCLL blanket in-box LOCA",* EFDA_D_2MND5X, January 2018

[76] M. D'Onorio, G.Mazzini, *"Solutions to minimize in-vessel hydrogen and hydrogen/dust explosions: proposal and study"*, EFDA_D_2MRHG6, July 2019

[77] J. Xiaoa, J.R. Travisb,W. Breitunga, T. Jordana, *"Numerical analysis of hydrogen risk mitigation measures for support of ITER licensing",* Fusion Engineering and Design, 85, 2010, pp. 205–214

[78] V. Chuyanov, L. Topilski, *"Prevention of hydrogen and dust explosion in ITER",* Fusion Engineering and Design, 81, 2006, pp. 1313–1319

[79] M. Adorni, G. Mazzini, et al., *"ETSON Presentation: Severe Accident Phenomenology",* ETSON Junior Staff Program, July 2013, Kaunas (LT)

[80] SARNET2/ENENIII, *"Materials of Short Course on Severe Accident analyses Phenomenology",* January 2011

[81] A. Denkevits, *"Study of In-Vessel Dust and Hydrogen Explosions",* EFDA WP13-SYS04 Task T04

[82] A. Alfonsi et al., *"RAVEN Theory Manual and User Guide",* Idaho National Laboratory, INL/EXT-16-38178

[83] C. Rabiti, A. Alfonsi, J. Cogliatti, D. Mandelli, and R. Kinoshita, *"Reactor Analysis and Virtual control ENVironment (RAVEN)",* FY12 REPORT," Tech. Rep. INL/EXT-12-27351, Idaho National Laboratory (INL) (2012).

[84] C. Rabit, A. Alfonsi, J. Cogliatti, D. Mandelli and R. Martieneau, *"RAVEN as Control Logic and Probabilistic Risk Assessment Driver for RELAP-7",* in proceeding of American Nuclear Society (ANS), San Diego (CA)," (2012), vol. 107, pp. 333–335

[85] A. Alfonsi et al., *"Raven as a tool for dynamic probabilistic risk assessment: Software overview",* in proceeding of M&C2013 International Topical Meeting on Mathematics and Computation

[86] M. D'Onorio, et al., *"Sensitivity Analysis for the Hydrogen Production During an Ex-Vessel LOCA without Plasma Shutdown for the EU DEMO WCLL Blanket Concept",* in proceeding of 14th International Symposium on Fusion Technology (ISFNT14), 2019

[87] Wilks S.S., *"Determination of Sample Sizes for Setting Tolerance Limits"*, Ann. Math. Stat., 12, pp. 91-96, 1941

[88] Gauntt, R., Kalinich, D., Cardoni, J., Phillips, J., Goldmann, A., Pickering, S., Francis, M., Robb, K., Ott, L., Wang, D., Smith, C., St. Germain, S., Schwieder, D., Phelan, Ch., 2012. *"FUKUSHIMA DAIICHI: ANS Committee Report, Fukushima Daiichi Accident Study (Status as of April 2012) SANDIA REPORT",* SAND2012-6173, Sandia National Laboratories, Albuquerque, New Mexico 87185 and Livermore, California 9455.

[89] TEPCO, Plant Specifications of Unit 3, 2013

[90] TEPCO, Measured Data, Unit 3, Pressure, 2012

[91] E.W.Coryell, F.P.Griffin, *"SCDAP/RELAP5 Lower core plate model",* 1999
[92] K. Ross, J. Phillips, R. O. Gauntt, K. C. Wagner, *"MELCOR Best Practices as Applied in the State-of-the-Art Reactor Consequence Analyses (SOARCA) Project*" NUREG/CR-7008, U.S. NRC, August 2014
[93] Steinbruck, M., *"Influence of boron carbide on core degradation during severe accidents in LWRs", 2014*
[94] TEPCO, *"Effects of the Earthquake and Tsunami on the Fukushima Daiichi and Daini Nuclear Power Stations",* 2011
[95] Hoshi, Harutaka, Ogino, Masao, Kawabe, Ryuhei, & Fukasawa, Masanori, *"Computational analysis on accident progression of Fukushima Dai-ichi NPS",* in proceedings of the PSAM topical conference in Tokyo (PSAM2013), (p. 532). Japan, 2013
[96] Sevón, T. (2015), *"A MELCOR model of Fukushima Daiichi Unit 3 accident",* Nuclear Engineering and Design, 284, 80-90.
[97] TEPCO, Unit 3 Shift Supervisor Task Handover Journal, 2011
[98] Pellegrini M., Suzuki H., Mizouchi H., Naitoh M., *"Early phase accident progression analysis of Fukushima Daiichi Unit 3 by the SAMPSON code",* (2014).
[99] Denman M., Brooks D., *"Fukushima Daiichi Unit 1 Uncertainty Analysis-Exploration of Core Melt Progression Uncertain Parameters-Volume II",* 2015
[100] IAEA, *"The Fukushima Daiichi Accident - Technical Volume 1/5 - Description and Context of the Accident",* 2013
[101] ICANPS, *"Interim Report-Committee on the Accident at Fukushima Nuclear Power Stations of Tokyo Electric Power",* 2011
[102] TEPCO, *"Major Event Sequence",* 2012
[103] *"Sequoyah Integrated Deterministic and Uncertainty Analyses",* SOARCA Project, Sandia National Laboratories
[104] Ross K. et al., *"Uncertainty Analysis of the Unmitigated Short-Term Station Blackout of the Surry Power Station"*, SOARCA Project, Sandia National Laboratories
[105] Cardoni J., Kalinich D., *"Fukushima Daiichi Unit 1 Uncertainty Analysis - Preliminary Selection of Uncertain Parameters and Analysis Methodology"*, SAND2014-1170, Sandia National Laboratories, 2014
[106] Pellegrini, M., Dolganov, K., Herranz Puebla, L.E., Bonneville, H., Luxat, D., Sonnenkalb, M., Ishikawa, J., Song, J.H., Gauntt, R.O., Fernandez Moguel, L., Payot, F., Nishi, Y., *"Benchmark Study of the Accident at the Fukushima Daiichi NPS: Best-Estimate Case Comparison",* Nucl. Technology, 2016
[107] Magallon D., *"Characteristics of corium debris bed generated in large-scale fuel-coolant interaction experiments",* Nuclear Engineering and Design Volume 236, Issues 19–21, , Pages 1998-2009, October 2006
[108] Denman M., Brooks D., *"Fukushima Daiichi Unit 1 Uncertainty Analysis-Exploration of Core Melt Progression Uncertain Parameters-Volume II",* 2015
[109] Fernandez-Moguel, L., Birchley, J., *"Analysis of the accident in the Fukushima Daiichi nuclear power station Unit 3 with MELCOR 2.1",* Ann. Nuclear Energy 2015 (83) 193–215